Charles University

Faculty of Science

Doctoral study program: Molecular and Cellular Biology, Genetics and Virology

Mgr. Jiří Pospíšil

Vnitrobuněčná a mezibuněčná regulace genové exprese u Gram-pozitivních bakterií

Intracellular and intercellular regulation of gene expression in Gram-positive bacteria

Doctoral Thesis

Supervisor: Doc. Mgr. Libor Krásný, PhD.

Department of Microbial Genetics and Gene Expression

Institute of Microbiology of the ASCR, v. v. i.

Prohlášení:

Prohlašuji, že jsem doktorskou práci zpracoval samostatně, a že jsem uvedl všechny použité informační zdroje a literaturu. Tato práce nebyla předložena k získání jiného nebo stejného akademického titulu.

Declaration:

I hereby declare that I am the author of this Doctoral Thesis and that I have cited all sources and literature. This Thesis has not been submitted elsewhere to obtain any other or the same degree.

November 2020, Prague

…….....

Mgr. Jiří Pospíšil

Acknowledgements

My biggest thanks belong to my supervisor Libor Krásný for his trust in me and my project. Without him, the Bacterial nanotubes project (and many other projects) could not be created and finished. It was his advice, and also the advice from my other colleagues (from Laboratory of Microbial Genetics and Gene Expression) that made me into the kind of scientist I am now. Next, I would like to thank my collaborators (friends) from other laboratories and Institutes, namely – Oldřich Benada (Inst Microbiol, Prague), Olga Kofroňová (Inst Microbiol, Prague), Imrich Barák (Inst Mol Biol, Bratislava), Katarina Muchová (Inst Mol Biol, Bratislava), Martin Hubálek (IOCB, Prague) and Martin Modrák (Inst Microbiol, Prague). It would not be possible to complete my projects without them. Finally, I thank my family and friends for their support.

Abstract

Bacteria, the most dominant organisms on Earth, are an everyday presence in our lives. Symbiotic bacteria, which are present in the digestive tract of animals, usually have a beneficial effect on the body. On the opposite side of the spectrum are pathogenic species that cause more or less serious diseases around the world. In order to fight pathogens effectively, it is necessary to learn as much as possible about the molecular mechanisms by which bacteria respond to their environment, and also about the types of communication within bacterial populations that allow them to react to environmental changes as “multicellular” organisms.

This Thesis consists of two main parts.

In the first part, selected aspects of bacterial gene expression are characterized, using *Bacillus subtilis* and *Mycobacterium smegmatis* as model organisms. DNA-dependent RNA polymerase (RNAP) is the enzyme that is responsible for transcription of DNA into RNA, and thus plays a key role in gene expression. This Thesis deals with the structure of bacterial RNAP and important auxiliary factors (proteins and RNA) that associate with this enzyme and modulate its function.

In the second part, the focus is on cell-to-cell communication, revealing which factors/mechanisms, including gene expression, affect this process in *B. subtilis*. Previously, it was believed that membranous protrusions of bacterial cells, the so-called nanotubes (NTs), could connect cells and function as channels to transport metabolites, mRNA, proteins, and even non-conjugative plasmids. This part of the Thesis identifies genetic determinants of NT formation and reveals that these structures emerge only from dead cells, excluding the possibility of transfer of cytoplasmic contents between cells by these structures.

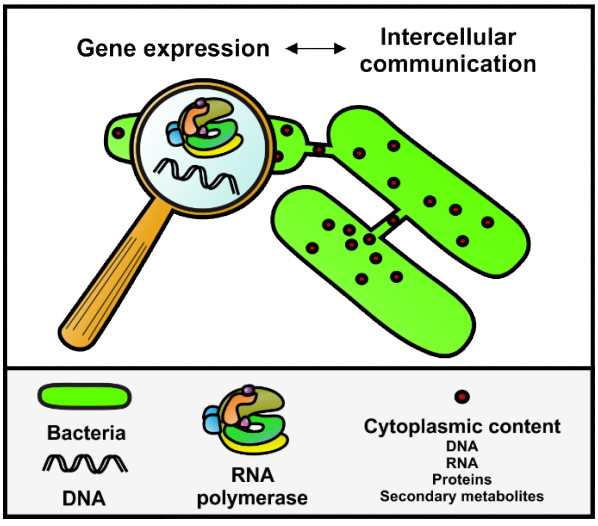

In summary, this Thesis reveals new information about the bacterial transcription apparatus, gene expression, and cell-to-cell communication, advancing thus our understanding and appreciation of the functioning of the bacterial cell.

Abstrakt

Bakterie patří mezi nejčetnější organismy na Zemi a jsou součástí našeho každodenního života. Symbiotické bakterie, které se nachází například v trávicím traktu živočichů, mají většinou příznivý vliv na organismus. Existují však také patogenní druhy bakterií, které jsou původci méně či více závažných onemocnění po celém světě. Abychom mohli s patogeny účinně bojovat, je zapotřebí co nejvíce pochopit strategie chování bakteriální populace a molekulární mechanismy, kterými tyto organismy reagují na okolní prostředí.

Práce je rozdělena na dvě hlavní části.

První část charakterizuje bakteriální genovou expresi v modelových organismech *Bacillus subtilis* a *Mycobacterium smegmatis*. DNA-dependentní RNA polymeráza (RNAP) je enzym zodpovědný za přepis nukleových kyselin (z DNA do RNA) a má tedy klíčovou roli v expresi genů. V Disertační práci je řešena struktura RNAP a důležité faktory (proteiny, nebo RNA), které s tímto enzymem asociují a ovlivňují jeho funkci.

Druhá část je zaměřena na bakteriální mezibuněčnou komunikaci a faktory/mechanismy (zahrnující genovou expresi), které tento proces ovlivňují. Jeden z typů bakteriální komunikace je označen jako bakteriální nanotrubičky (NT). NT byly v minulosti popsány jako mezibuněčné kanály, kterými si bakterie mohou předávat metabolity, mRNA, proteiny a dokonce nekonjugativní plazmidy. V této části práce jsou určeny geny, které jsou nezbytné pro vznik NT. Dále je zde odhalena skutečnost, že se NT vytváří pouze po bakteriální smrti jako projev buněčné lyze a je vyloučeno jejich zapojení v transportu nekonjugativních plazmidů.

V souhrnu tato práce poskytuje nové informace týkající se bakteriálního transkripčního aparátu, genové exprese a mezibuněčné komunikace. Tyto důležité poznatky tak významným způsobem přispívají k pochopení fyziologie bakteriální buňky.

Table of Contents

1 List of abbreviations

B. subtilis	*Bacillus subtilis*
C. acetobutylicum	*Clostridium acetobutylicum*
C. ljungdahlii	*Clostridium ljungdahlii*
C	Cytosol
CM	Cytoplasmic membrane
Cryo-EM	Cryogenic electron microscopy
CW	Cell wall
D. vulgaris	*Desulfovibrio vulgaris*
dsDNA	Double-stranded DNA
E. Coli	*Escherichia coli*
ECF	Extracytoplasmic σ factor
EX	Extracellular
M. smegmatis	*Mycobacterium smegmatis*
M. tuberculosis	*Mycobacterium tuberculosis*
M. xanthus	*Myxococcus xanthus*
mRNA	messenger RNA
MVs	Membrane vesicles
NCR	Non-conserved region
NMR	Nuclear magnetic resonance
NPs	Nanopods
nt	Nucleotide
NTs	Nanotubes
NWs	Nanowires

OM	Outer-membrane
OMTs	Outer-membrane tubes
OMV	Outer-membrane vesicles
PNPase	Polynucleotide Phosphorylase
qPCR	Quantitative PCR
QS	Quorum sensing
RNAP	RNA polymerase
RNAseq	RNA sequencing
RPc	Closed complex of RNA polymerase and promoter DNA
RPo	Open complex of RNA polymerase and promoter DNA
SEM	Scanning electron microscopy
SIM	Structured illumination microscopy
SLP	Surface layer protein
S. coelicolor	*Streptomyces coelicolor*
S. pneumoniae	*Streptococcus pneumoniae*
sRNA	Small RNA
ssDNA	Single-stranded DNA
TEM	Transmission electron microscopy
TNTs	Tunneling nanotubes
TSS	Transcription start site

2 Introduction

Two main aspects of bacterial physiology are addressed in this Doctoral Thesis – (i) gene expression (three sub-projects) and (ii) bacterial communication (one sub-project). The Thesis consists of four publications.

(i-a) The main enzyme of the transcription stage of gene expression is RNAP. Here we present the 3D structures of the RNAP core and holoenzyme (containing primary σ factor) forms of RNAP from *Mycobacterium smegmatis*. For this purpose, a heterologous expression system was created. Genes encoding RNAP core subunits and σ factor A from *M. smegmatis* were cloned into *Escherichia coli*. Subsequently, RNAP was purified in the two forms and their structures were determined by cryogenic electron microscopy (Cryo-EM) (**Publication I**).

(i-b) While RNAP itself is sufficient to carry out transcription, various interacting partners associate with RNAP during the transcription process and modulate its activity. Identification of these molecules and understanding of their effects on RNAP and the cell is a must in our quest to understand life. These molecules can be proteins or small RNAs (sRNA). A class of proteins important for RNAP function are σ factors. σ factors bind to RNAP and determine its specificity for promoter DNA. Alternative σ factor I from *B. subtilis* is described in this work. We identified genes that are regulated by this σ factor and described phenotypes of a *B. subtilis* mutant strain lacking the respective gene (**Publication II**).

(i-c) sRNA molecules can directly interact with RNAP and change its properties. In the last decade, our laboratory discovered Ms1, a sRNA from *M. smegmatis* that is present also in other mycobacteria (Arnvig et al., 2011). Ms1 binds to mycobacterial RNAP and its possible functions are addressed in this work (**Publication III**).

(ii) The last project is the pivotal project of this Thesis. It deals with one of the most exciting, yet controversial phenomena of the last decade in microbiology - bacterial nanotubes [(NTs) (Dubey et al., 2016; Dubey & Ben-Yehuda, 2011)]. We used *B. subtilis* as our main model organism for these studies. Originally, we had speculated that transcription factors could be transferred through NTs and one cell can affect gene expression in another cell. Throughout the course of the project, however, we came to a starkly different conclusion. In this project, we described how NTs are formed and

what genes are responsible for it. We discovered that NTs emerge only from dead cells when the cell integrity is compromised and the excess internal pressure causes their extrusion. Transfer of non-conjugative plasmids by NTs was used as a tool to demonstrate that NTs do not serve as conduits of cell-to-cell transfer. Finally, the physiological function of NTs is discussed and a comprehensive model of their formation and biological role(s) is presented. These results completely overwrite the current dogma about NTs (**Publication IV**).

Note: This Thesis contains images that were created by the author, based on original research publications that are cited in the Thesis.

3 Literature review

3.1 Bacterial populations and gene expression

As any other organisms, bacteria have to deal with various challenges during their life cycle. A highly sophisticated system of gene regulation allows bacteria to quickly react to environmental changes. In laboratory conditions, we can study bacteria in three major growth phases - (i) lag, (ii) exponential and (iii) stationary phase (**Fig. 1**). In lag phase, bacteria must adapt to the environment that is now rich in nutrients (*e. g.* they must identify carbon sources, sense amino acid availability, *etc*.) and activate the adequate pathways of the gene expression machinery (Rolfe et al., 2012). Exponential phase is characterized by massive growth of the bacterial population. During this phase, cells are literally like small factories for ribosome biosynthesis and the three processes, representing the three major pillars of the molecular biology dogma (replication, transcription and translation), are unstoppable (Watanabe et al., 2015). In stationary phase, when nutrients are exhausted, bacteria must adapt to the poor nutritional/environmental conditions. During this phase, some bacteria become "selfish" and cannibalize their kin. An ultimate form of adaptation are dormant cells, spores, that can survive in hostile environments for millions years (Höfler et al., 2016; Nakamura et al., 2006; Shleeva et al., 2011; Vreeland et al., 2000). All these adaptations hinge on correct changes in gene expression – in time and in magnitude. Thus, during the bacterial life, gene expression has to constantly respond to environmental signals.

Bacteria can also collaborate and form colonies. Within and also outside of colonies, bacteria communicate with each other, the signals that they receive (small peptides, proteins, metabolites, genetic information) from other cells modulate their gene expression (Rösch & Graumann, 2015; Wolf et al., 2015; Yang Yang et al., 2013).

Figure 1. Phases of bacterial growth

A schematic chart showing all bacterial growth phases in laboratory conditions. The y axis represents the number of cells in logarithmic scale. The x axis represents time. Blue line indicates bacterial growth curve; Green dashed line indicates the level of nutrients in the environment. Events which occur during specific phase are described and schematically sketched below the chart. Green cells - viable bacteria; Red cells - stationary phase bacteria, or dormant cells; Circles - spores; Grey cells - dead cells.

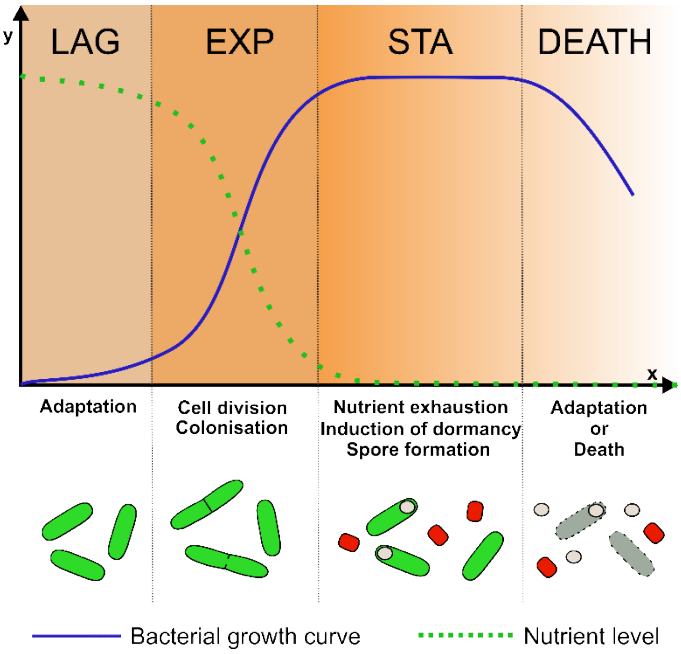

3.2 Transcription

Transcription is the very first step of gene expression. The multi-subunit enzyme, RNAP, is responsible for catalysis of this reaction and copying of DNA into RNA. The transcription process can be divided into three stages – initiation, elongation and termination. In the first stage (initiation), the RNAP core binds a σ factor to form the holoenzyme. The σ factor helps RNAP to recognize and bind to a specific sequence on DNA (promoter) that is typically localized upstream of genes. This binding results in the so called closed complex (RPc), in which the DNA is still double stranded. Subsequently, the double stranded DNA in the promoter region (ca 13-14 bp) is unwound and the transcription "bubble" is formed, resulting in the open complex (RPo) (J. Chen et al., 2020). After binding the first two nucleoside triphosphates, the first bond is catalyzed by RNAP, and RNA synthesis thus begins. The σ factor is released after transcription of ca 15 nt and RNAP then moves along the DNA template and synthetizes the RNA transcript [(elongation)(Kainz & Roberts, 1992; Zuo et al., 2020)]. The elongating RNAP must be stopped (termination) at the end of the gene. Therefore, a termination sequence (terminator) is localized in this region. Some terminators require the presence of the Rho protein, whereas others work independently of Rho (Brennan et al., 1987). Rho-independent terminators consist GC enriched palindromic

site followed by 7-9 thymines (de Hoon et al., 2005). RNAP is destabilized by the stem-loop structure that is created on mRNA upon transcription of the terminator and this leads to dissociation of RNAP from DNA [(**Fig. 2**)(Wilson & Von Hippel, 1995)]. There are many factors (proteins, sRNAs or small ligands) that regulate transcription during the various stages of transcription. Promoter sequences and selected factors that are in direct contact with RNAP are discussed in following chapters.

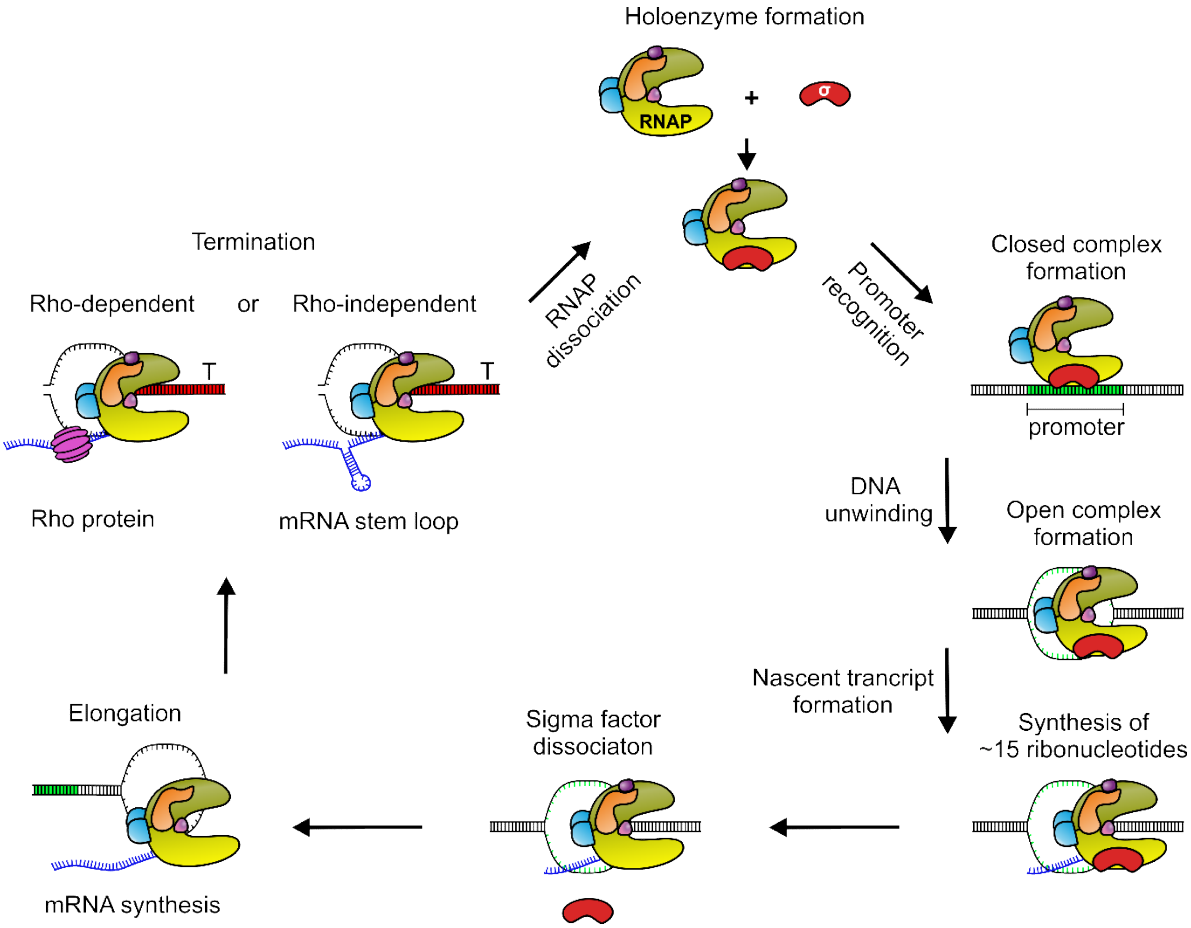

Figure 2. A scheme of bacterial transcription

Transcription starts with holoenzyme formation (RNAP binds σ factor). This is followed by promoter (green) recognition and binding. Subsequent reorganization of the promoter-RNAP complex leads to the formation of the open complex and, after transcription of several nts, σ factor dissociation. RNAP initiates transcription of DNA template strand and synthesis of mRNA (blue). When a terminator sequence (marked as T or colored red) is transcribed, the Rho protein (magenta) binds to mRNA and dislodges the elongation complex (Rho-dependent termination) or a stem loop structure is formed in mRNA and the elongation complex is destabilized without Rho (Rho-independent termination). RNAP is released and the whole process can be repeated.

3.2.1 Promoter sequence

Promoter sequence is a specific combination of nucleotides in dsDNA that is recognized by an RNAP holoenzyme containing an appropriate σ factor. σ factors are dedicated proteins, dissociable subunits of RNAP, specifically recognizing promoters. Several types of σ factors exist and each of them recognizes its own specific sequence. Most promoters contain two main regions, -10 and -35, located upstream of the transcription start site (TSS). The sequence and length of the spacer that is located between -10 and -35 regions may also play important role in the proper promoter function (Hook-Barnard & Hinton, 2009; H. Liu & Ganta, 2019). The -10 element recognized by the primary σ factor (responsible for transcription of housekeeping genes) is often called the Pribnow or TATA box. Based on research conducted with *E. coli* σ^{70}, the Pribnow box was defined to consist of a TA-rich consensus sequence ($T_{-12}A_{-11}T_{-10}A_{-9}A_{-8}T_{-7}$ – the numbers represent distance in nt from TSS) and it is the most conserved and essential promoter motif across all bacterial species [(**Fig. 3**) (Hook-Barnard & Hinton, 2007; Shultzaberger et al., 2007)]. Consistently, in *Actinomycetes* (*Mycobacteriaceae*, *Streptomycetes*), it was shown that promoters do not even need the -35 region, suggesting that the -10 region is the most important part in majority of promoters (Cortes et al., 2013; Šmídová et al., 2019; Y. Zhu et al., 2017). Nevertheless, the activities of promoters are also controlled by other specific sequences localized around or overlapping the promoter.

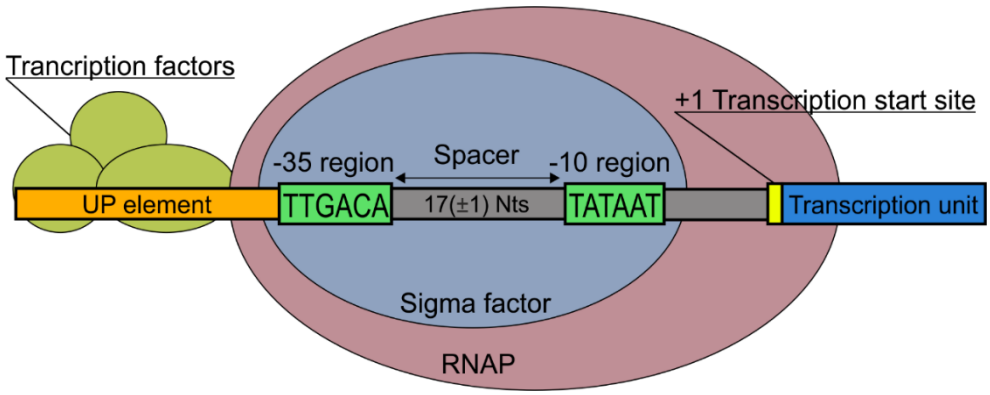

Figure 3. A scheme of bacterial promoter

Promoter consensus sequence (-10 and -35 regions-the core promoter) is localized upstream of the transcription start site and is recognized by the σ factor (here, the consensus sequences for the primary σ factor are shown). Spacer between -10 and -35 regions often contains important sequence motifs that enhance transcription effectivity. So called UP element is localized upstream of the core promoter and can bind the C-terminal domains of alpha subunits of RNAP, thereby increasing the affinity of RNAP for the promoter (Gaal et al., 1996).

Those sequences are binding motifs for transcription factors (proteins). Transcription factors contain a DNA binding domain and bind around/over the promoter and regulate (activate or repress) gene expression depending on the environmental conditions, metabolic requirements or stress response, and, of course, the exact positon of binding of the transcription factor to DNA with respect to the promoter region (Moreno-Campuzano et al., 2006; Sanchez et al., 2020).

3.2.2 RNA polymerase

RNAP is a multi-subunit enzyme. Its core is generally composed of α dimer, β, β′ and ω subunits that form a ~400 kDa complex. The first structural study of bacterial RNAP was done by electron microscopy in the late 80's (Darst et al., 1989). Nevertheless, researchers obtained a better structure resolution of *Thermus aquaticus* core RNAP by X-Ray crystallography in 1999 (G. Zhang et al., 1999). Recently, however, the Cryo-EM approach has become the technique of choice to solve RNAP structures and its complexes as it allows to observe proteins in their native states without fixation procedures and (as opposed to nuclear magnetic resonance) is suitable for relatively large molecules (Glyde et al., 2017; Liu et al., 2017; Narayanan et al., 2018). RNAPs display a "*crab claw*" shape where the two pincers are formed by β and β′ subunits. The active site is localized inside (at the bottom) of the "*crab claw*" (Sutherland & Murakami, 2018; G. Zhang et al., 1999). The α dimer is located on the β and β′ interface and has many functions: proper RNAP core assembly, interaction with AT-rich DNA sequence upstream from promoter (UP element), interaction with transcription factors (Gourse et al., 2000; Murakami et al., 1996; Ross et al., 1993). The ω subunit is the smallest (7.62 kDa) subunit of RNAP. It is bound to the β' subunit and prevents β′ aggregation during RNAP core assembly [(**Fig. 4A**) (Ghosh et al., 2001; Minakhin et al., 2001; G. Zhang et al., 1999)]. Moreover, subsequent studies revealed an impact of the ω subunit on transcriptional specificity of RNAP (Gunnelius et al., 2014; Weiss et al., 2017) and the ability of *E. coli* RNAP to bind and respond to ppGpp, an alarmone made in the cell at times of stress (Bhardwaj et al., 2018). RNAP forms a stable holoenzyme with a σ factor that is necessary for promoter recognition (**Fig. 4B**). The σ factors are discussed in the following chapter.

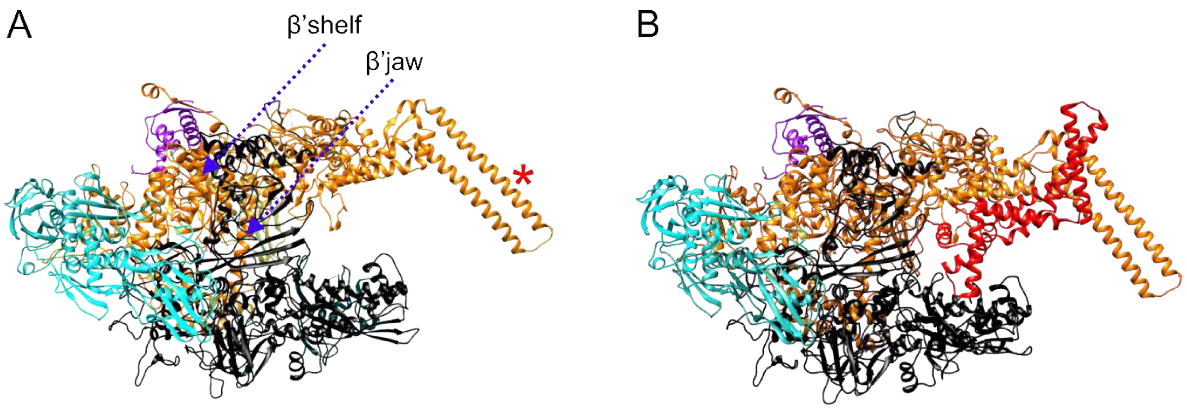

Figure 4. Structure of *M. smegmatis* RNAP

The Cryo-EM structure of *M. smegmatis* RNAP shows the typical crab's claw shape (Kouba et al., 2019).

A Structure of the RNAP core. Red asterisk indicates the double helical structure (β′i1 domain), which is unique for mycobacteria. Blue dashed arrows indicate important structure modules of β′ that are necessary for δ subunit binding in *B. subtilis*.

B Structure of the RNAP holoenzyme consisting primary σ factor A (red).

Subunit color code: 2α (cyan), ω (magenta), β′ (orange), β (black).

Compared to RNAPs from Gram-negative bacteria, such as *E. coli*, it was reported that RNAPs from Gram-positive *Firmicutes* contain small accessory subunits, termed as ε and δ. The 3D structure of the ε subunit was determined by X-ray crystallography. Previous studies suggested that ε is bound to the β′ subunit around the secondary channel. As ε shares homology with a known structure of the Gp2 phage protein that binds to RNAP in Gram-negative *E. coli*, it was suggested that ε blocks binding of similar, hypothetical proteins to RNAP in Gram-positive species, functioning as an immunity protein (Bae et al., 2013; Delumeau et al., 2011; James et al., 2012; Keller et al., 2014).

The δ subunit is a similarly enigmatic subunit of RNAP. The direct position of δ on RNAP was discovered only very recently in *Mycoplasma pneumonia* and *B. subtilis*. In both cases, δ was localized between the β' shelf and jaw with a potential to interact with ribosomal proteins in the transcribing-translating complex [(localizations of β' shelf and jaw are shown in **Fig. 5A**)(O'Reilly et al., 2020; Wahl et al., 2020)]. The structure of δ was determined by Nuclear magnetic resonance (NMR) already several years ago. The δ subunit possesses two distinct regions, N-terminal and C-terminal parts. The N-

terminus is structured and allows δ to interact with RNAP, whilst the negatively charged, unstructured C-terminus is predicted to interfere with non-specific RNAP-DNA interactions (Motáčková et al., 2010; Papoušková et al., 2013).

Unlike α, β, β′, the ω, ε and δ proteins are not essential subunits of RNAP. Bacteria can live without these small accessory subunits but there is evidence that absence of ω or δ cause defects in biofilm formation, morphology differentiation, adaption to, and survival during stress (Santos-Beneit et al., 2011; Weiss et al., 2017; Xue et al., 2010, 2012).

3.2.3 σ factors

σ factors are key players in transcription initiation. They bind to the catalytic RNAP core, recognize the specific consensus promoter sequence and are involved in promoter opening. The number of σ factors varies between bacterial species. For example, *B. subtilis* encodes 19 σ factors, *M. smegmatis* 26 and *E. coli* "only" 7 (Cho et al., 2014; Nicolas et al., 2012; Waagmeester et al., 2005). The largest number of σ factors in one species was discovered in *Sorangium cellulosum,* which contains 109 different σ factors (Han et al., 2013) Generally, σ factors are divided into 4 groups according to their structure. The groups differ by the presence or absence of one (or more) of the 4 structural domains. Each of the domains is further divided into subdomains [(**Domains (D):** subdomains - **D1:** 1.1, **D2:** 1.2-2.4, **D3:** 3.0-3.2 and **D4:** 4.1-4.2)(Campbell et al., 2002; Paget & Helmann, 2003)]. Specific domains bind to specific parts of the promoter sequence except for domain 1.1, which is unique for σ factors belonging to group 1. Domain 1.1 prevents non-specific binding of σ factors to promoter sequence in the absence of RNAP, by blocking the specific interaction domains (2 and 4) in σ (Dombroski et al., 1993).

Finally, σ^{54} factors represent a separate group of alternative σ factors that recognize promoters consisting of -12 and -24 elements (L. Wang et al., 1999; Yun Yang et al., 2015). σ^{54} was discovered in *E. coli* and its homologues are intensively studied in other (Gram-positive or negative) bacterial species. σ^{54}-like factors are responsible for transcription of important regulatory genes involved in flagellar biosynthesis, nitrogen metabolism, virulence or stress response (Brahmachary et al., 2004; Francke et al., 2011; Lloyd et al., 2017; Wiegeshoff et al., 2006). Unlike the RNAP–σ^{70}, the RNAP-σ^{54}

holoenzyme forms a transcriptionally inactive RPc complex which is unable to access template DNA. Formation of the RPo complex is possible only after ATP hydrolysis by activator proteins binding to the enhancer-like sequence upstream of the promoter (Bordes et al., 2004; Bose et al., 2008; Wedel et al., 1990).

σ factor domain comparisons and their binding to promoters and the RNAP core are summarized in **Figure 5**.

3.2.3.1 Group 1 σ factors

Group 1 consists of primary (housekeeping) σ factors (*e. g.* σ^{70} and σ^{A}) that contain all domains (D1-D4). Primary σ factors are essential for transcription of housekeeping genes and have the largest regulons of all σ factors (Ramaniuk et al., 2017). The *E. coli* primary σ factor is termed σ^{70} according its molecular weight (70 kDa). In other bacteria, the primary σ factors are typically referred to as σ^{A} (*B. subtilis*, *M. smegmatis*) although other names also appear, such as HrdB [(*S. coelicolor*)(Gomez et al., 1998; Ramaniuk et al., 2017; Shiina et al., 1991)].

3.2.3.2 Group 2-4 σ factors

σ factors, besides housekeeping σ factors, are termed as alternative σ factors. A subclass of alternative σ factors are extracytoplasmic function (ECF) σ factors as they are related to extracellular stress responses (Helmann, 2002).

The alternative σ factors are smaller (~30 kDa) than primary σ factors and lack some of the structural domains. Alternative σ factors recognize promoter consensus sequences different from those of primary σ factors. Thus, they are responsible for transcription of gene subsets with specific functions. It allows bacteria to mount quick responses to environmental changes. An example is the cascade of σ factors (σ^{H}, σ^{F}, σ^{E}, σ^{G}, σ^{K}) that regulates sporulation in *B. subtilis* or σ^{D} that preferentially controls genes for motility (Cozy & Kearns, 2010; Kroos et al., 1999). Alternative σ factors are mostly regulated by anti-σ factors and in some cases also with anti-anti-σ factors (Dufour & Haldenwang, 1994). Anti-σ factors regulate functions of σ factors by their inactivation upon binding. The σ /anti-σ complex is very stable and incompatible with

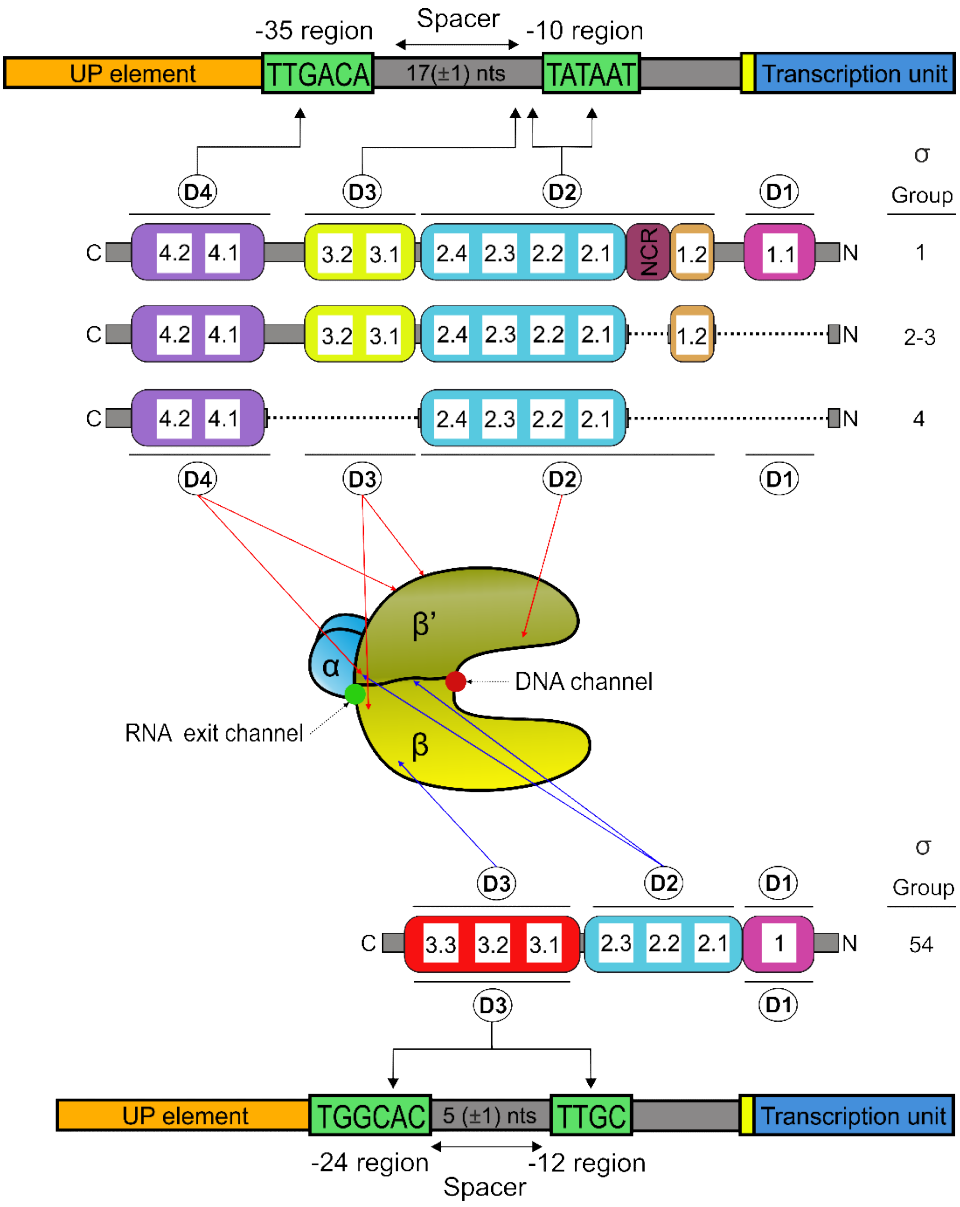

Figure 5. Groups of σ factors and their binding to RNAP and promoters

The upper part of the Figure shows a schematic alignment of σ factor groups 1-4. σ factors belonging to group 1 contain the whole set of domains (D1-D4) including the non-conserved region (NCR). σ factors of groups 2-4 are known as alternative σ factors and lack some of the domains (dashed lines). Black arrows represent binding of specific σ domains to the promoter sequences. Red arrows represent binding of the σ domains to RNAP core. The bottom part of the Figure shows the scheme for the group of σ^{54} factors. σ^{54} factors recognize a different promoter sequence than σ factors of groups 1-4. In the literature, domains of σ^{54} factors are described as Regions I-III. Regions I-III share few functional and structural homologies with domains of other σ factors but definitely they are not homologues. Nevertheless, I refer to RI-RIII as D1-D3 for simplify comparisons with other σ factors. Binding to a promoter (σ^{A} dependent) and the RNAP core is shown by black and blue arrows respectively.

RNAP binding (Sorenson & Darst, 2006). For example, the anti-σ factors regulating ECF σs are often localized in the cell membrane and consist of sensory/signaling domain that responds to signals outside of cell (*e. g.* presence of some stressors or lack of nutrients). In response to the signal, the anti-σ factor is processed (by specific proteases) and the σ factor is released and becomes active [(**Fig. 6**)(Ellermeier & Losick, 2006; Ho et al., 2011)].

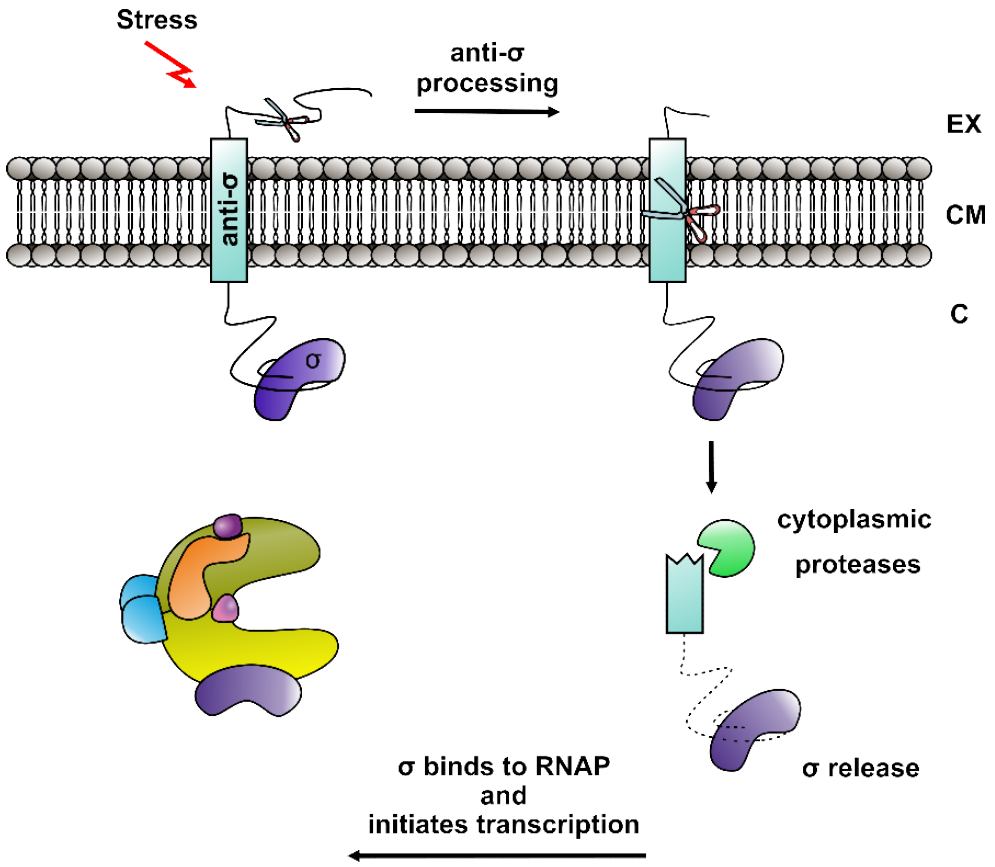

Figure 6. Regulation of alternative σ factors by anti-σ.

The most of alternative σ factors are bound to their anti-σ factors that are localized on the cytoplasmic membrane (CM). The anti-σ factor sensor domain is exposed to the extracellular environment (EX) and receives environmental signals. According to these signals, the anti-σ factor changes its structure and is released from CM to cytosol (C), where is degraded by a specific protease. Thus, the σ factor is liberated from its anti-σ and can bind to RNAP and initiate transcription of a specific subset of genes.

3.2.4 Other interaction partners of RNAP

Many molecules (RNA, proteins) influence transcription by their interactions with RNAP. In the following chapter I discuss small RNAs (sRNAs) that directly interact with RNAP and change its activity.

3.2.4.1 Small RNA (sRNA)

sRNAs are non-coding (they are not translated to proteins) RNA molecules with regulation functions. Each sRNA displays a unique secondary structure playing important roles in its function. Moreover, the secondary structure of sRNAs is also a useful tool for their identification in various organisms by computational approaches (Schwarz et al., 2020). Typically, sRNAs regulate gene expression post-transcriptionally and with respect to their target, they are encoded either in *cis* or *trans*. Both *cis*- and *trans*-encoded sRNAs bind to mRNA molecules, modify their secondary structures and thus influence translatability or stability of mRNAs (Li et al., 2012). Another group of sRNA binds to proteins and can change their activities. An example of these sRNAs are those that bind to RNAP and are directly involved in transcription regulation.

3.2.4.1.1 6S RNA

In 1960', the first sRNA was discovered in *E. coli* and termed 6S RNA (Hindley, 1967). Its function and binding partner had been enigmatic for several decades. Only in 2000 it was discovered that 6S RNA binds to RNAP and regulates its activity (Wassarman & Storz, 2000). In *E. coli*, 6S RNA is expressed in stationary phase of bacterial growth and binds to the RNAP holoenzyme containing the primary σ factor, σ^{70}. This interaction is possible due to the secondary structure of 6S RNA that mimics a promoter open complex, for which RNAP has a great affinity. Binding of 6S RNA to RNAP prevents transcription from σ^{70}-dependent promoters during stationary phase (J. Chen et al., 2017; Trotochaud & Wassarman, 2005; Wassarman & Storz, 2000). This is beneficial for the cell because in stationary phase when bacteria are not dividing as the nutrients are depleted, the holoenzyme is not required in large amounts, and is "stored" in the complex with 6S RNA in an inactive form (Wada et al., 2000). However, when environmental conditions improve, the holoenzyme is released from 6S RNA by transcription of its several nucleotides [(this transcript is termed as pRNA)(Cavanagh et al., 2012)]. Thus, the holoenzyme is free and active again, ready to transcribe its

target genes. This represents one of the most elegant bacterial strategies for regulation of gene expression.

6S RNA was subsequently also discovered and intensively studied in Gram-positive *B. subtilis*. *B. subtilis* contains two different 6S RNAs termed 6S-1 and 6S-2 RNA and both of them bind to the RNAP holoenzyme containing the main σ factor A (Burenina et al., 2014). However, expression profiles of the two *B. subtilis* 6S RNAs are different from each other and thus probably regulate different sets of genes (Ando et al., 2002; Barrick et al., 2005; Beckmann et al., 2011; Thüring et al., 2020). An analysis of a *B. subtilis* strain lacking its 6S RNAs revealed some phenotypic abnormalities. One of them is the lower optical density of mutant cells which is probably caused by more rapid nutrient consumption resulting from RNAP-σ^{70} holoenzyme deregulation (Hoch et al., 2015).

3.2.4.1.2 Ms1

Some bacteria lack the 6S RNA-encoding gene. One such an example is *M. smegmatis* where a 6S RNA was not identified according by computational predictions. However, subsequent research of our laboratory revealed another sRNA that binds to

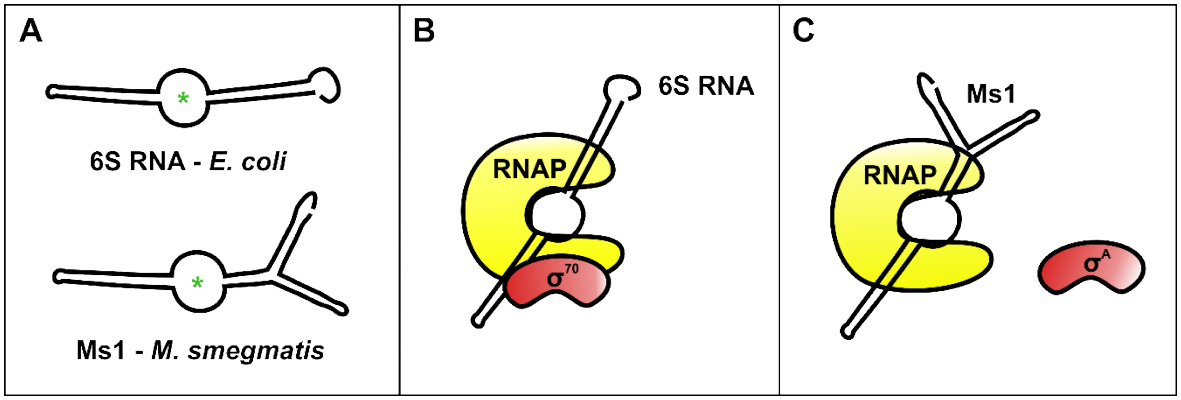

Figure 7. 6S vs Ms1 sRNAs

A A scheme of sRNAs of *E. coli* (6S RNA) and *M. smegmatis* (Ms1). Both, 6S RNA and Ms1, share structural similarities. One of them is the central unpaired region (marked with green asterisk) that mimics the transcription bubble to which RNAP readily binds.

B 6S RNA binds to RNAP containing σ^{70}. It leads to transcription inhibition of σ 70-dependent genes in stationary phase.

C Ms1 binds to RNAP without σ factor. The binding occurs in stationary phase. The nature of this binding is not yet known.

RNAP in Mycobacteria. This sRNA is expressed during stationary phase and is termed Ms1. Computational modeling and subsequent experiments revealed that Ms1 forms secondary structure very similar to that in 6S RNA (Pánek et al., 2011). Ms1, in contrast to 6S RNA, binds to the RNAP core (without primary σ factor) and its function is probably different from 6S RNA [(**Fig. 7**)(Hnilicová et al., 2014)]. Homologues of Ms1 were biocomputationaly predicted also in other *Actinomycetes* (*Rhodococcocales, Streptomycetes*) and experimentally proved in pathogenic bacteria such as *Mycobacterium tuberculosis* [(in *M. tuberculosis* the respective gene is termed MTS2823)(Arnvig et al., 2011; Pánek et al., 2011)].

3.3 Bacterial intercellular communication

As in other organisms, bacteria rely on intercellular communication to control population expansion. This communication involves every single cell, both in colonies and in cell suspensions. This communication is mediated by secretion of various signals (effectors) whose manufacture depends on gene expression (the basic principles of gene expression are described in preceding Chapters) of appropriate molecules. These effectors could be metabolites, pheromones, proteins, or nucleic acids (DNA, RNA). Bacteria have developed a wide number of mechanisms by which these effectors are delivered to target cells. In principle, these mechanisms could be divided into two classes: (i) contact independent and (ii) contact dependent mechanisms, and they are described in the following chapters.

3.3.1 Contact independent cell-cell communication

Bacteria can send signals across long distances. Communication by these systems does not require a direct contact between two bacterial cells.

3.3.1.1 Quorum sensing

Quorum sensing (QS) is one of the best-studied communication pathways. QS involves secretion of signals (termed autoinducers) that are recognized by other bacteria in the population. The concentration of the autoinducer increases with cell density, thereby providing information about the number of cells in the available space (*i. e.* their concentration). Cells in the population then change their gene expression

according to the concentration of the extracellular autoinducer. By this mechanism, bacteria control physiological processes in response to cell density.

In *B. subtilis*, QS is maintained by the ComQXPA proteins (Mandic-Mulec et al., 2003; Tortosa et al., 2001). ComX is a pheromone functioning as the autoinducer, which is recognized by ComP (sensor protein kinase) that is localized on the cytoplasmic membrane (Magnuson et al., 1994). ComQ is involved in maturation and secretion of ComX (Weinrauch et al., 1991). Binding of ComX to ComP leads to phosphorylation of ComA, which is a transcription regulator targeting specific subsets of genes [(**Fig. 8**) (*e. g.* genes for biofilm formation or natural competence – see next Chapter: 3.3.1.2 Natural competence)(Weinrauch et al., 1989)]. Moreover, many pathogenic bacteria also regulate their virulence by QS when they reach the host (Pearson et al., 2000).

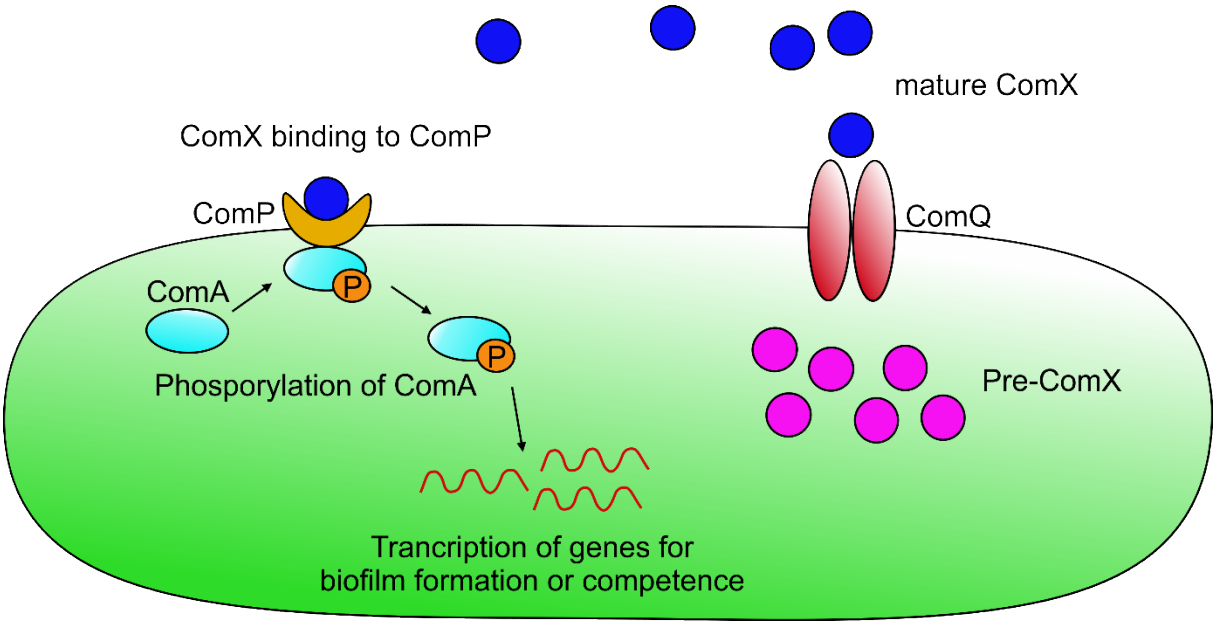

Figure 8. Quorum sensing in *B. subtilis*

The scheme shows a situation when optical density of a bacterial population is high. This leads to an increased concentration of the autoinducer ComX in the extracellular environment. ComX is matured from its precursor, pre-ComX, and exported by ComQ, which is localized on the cytoplasmic membrane. ComX binds to its respective sensor protein, ComP (localized on the cytoplasmic membrane). Subsequently, cytosolic ComA is phosphorylated and functions as a transcription factor for biofilm or competence genes.

3.3.1.2 Natural competence

Some bacteria are able to receive “naked” exogenous DNA from the environment and incorporate it into their genomes. This process is called natural competence (Anagnostopoulos & Spizizen, 1961). In *B. subtilis*, genes required for this process are under control of the transcriptional regulator ComK (van Sinderen et al., 1994). Natural competence is strictly connected to QS because a small protein, ComS, produced as a result of signaling by QS, triggers the release of ComK from its repressor, MecA (Ogura et al., 1999). Subsequently, ComK binds as a dimer to three AT-rich boxes (UP element, see Chapter 3.2.1 Promoter sequence) upstream of the regulated promoters. Binding of ComK results in DNA bending and stabilization of the RNAP-promoter complex (Hamoen et al., 1998; Susanna et al., 2004). Deletion of ComK or ComS leads to a total loss of natural competence (Hamoen et al., 1995; van Sinderen et al., 1995). Competence in Gram-positive bacteria is maintained by structures called Type IV pili. A Type IV pilus is a retractile protein structure that consists of the ComGC protein polymer. This polymer binds to extracellular dsDNA and pull it across the cell wall to the cytoplasmic membrane. ComEA, ComEC, and EndA (Endonuclease A) proteins, localized on the membrane, subsequently arrange transport of ssDNA to the cytosol (**Fig. 9**). This mechanism was nicely described for Gram-positive *Streptococcus pneumoniae* [(*S. pneumonia*)(Muschiol et al., 2015, 2017)]. *B. subtilis* also harbors an operon of pilin-like genes (*comG* operon), which are even homologues to those in *S. pneumoniae*. Moreover, there is an evidence that the Com proteins form a macromolecular complex in *B. subtilis*; however unlike *S. pneumoniae*, no such structure had been directly visualized by microscopy (I. Chen et al., 2006). Nevertheless, a loss of the *B. subtilis comG* operon leads to the uncompetent phenotype, suggesting the importance of these proteins for DNA uptake (Breitling & Dubnau, 1990). Bacterial competence system is a powerful tool of bacterial gene diversity. By using this tool, bacteria can obtain various genes that can be decisive in their evolutionary struggle for survival [(*e. g.* resistance against antibiotics *etc.*) (Domingues et al., 2012)].

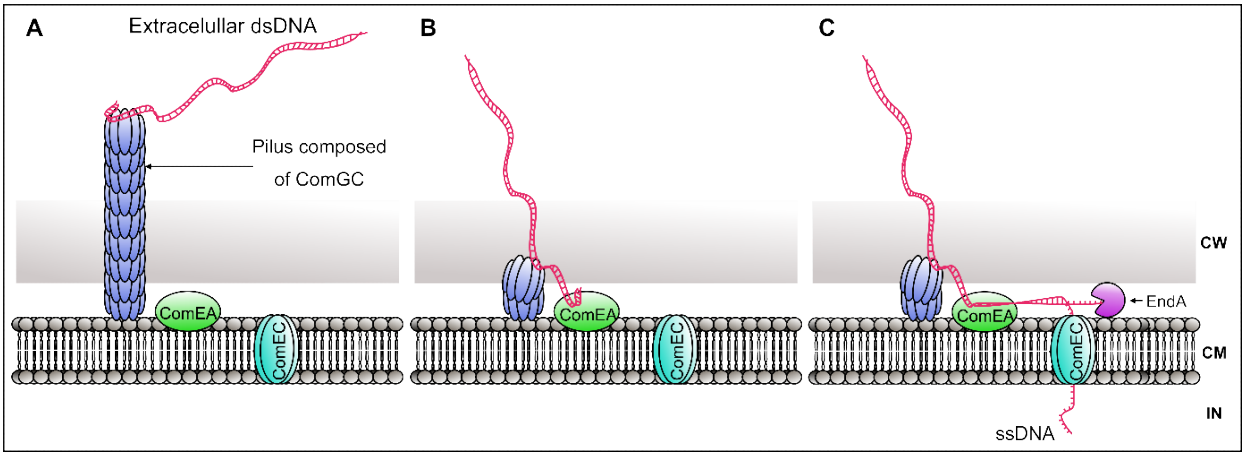

Figure 9 DNA uptake mechanism

A ComGC protein polymer is synthetized across the cell wall (CW) and forms Type IV pilus structure that binds to extracellular dsDNA.

B Type IV pilus is retracted by rapid degradation of ComGC proteins. It leads to pull-in of dsDNA to cytoplasmic membrane (CM) where is bound to ComEA protein.

C Subsequently, endonuclease A (EndA) degrades one strand of dsDNA whereas second strand is transferred to the cell by ComEC protein.

3.3.1.3 Membrane vesicles

Membrane vesicles (MVs) are usually considered as part of the cell-to-cell molecular traffic, functioning as carriers for various cargo. Their formation was (and still is) intensively studied especially in Gram-negative bacteria, where they are composed from the outer-membrane and therefore termed as outer-membrane vesicles [(OMVs) (Schwechheimer & Kuehn, 2015)]. Published articles showed that basically every molecule, inside of the Gram-negative cell, could be found in OMVs (Altindis et al., 2014; Bitto et al., 2017; Koeppen et al., 2016). Interestingly, stress conditions such as treatment with cell wall-directed compounds (polymyxin B and d-cycloserine) or heat shock massively induce OMVs formation (de Jonge et al., 2020; MacDonald & Kuehna, 2013) .

In the case of Gram-positive bacteria, research of membrane vesicles was historically slow to get going but the situation has significantly improved over the past several years. Unlike Gram-negative bacteria, Gram-positive bacteria possess a thick cell wall, and, therefore, the formation of vesicles was considered to be impossible in these

organisms. However, some publications exist, reporting MVs formation by Gram-positive bacteria (E. Y. Lee et al., 2009; Rivera et al., 2010). MVs of Gram-positive bacteria contain, as well as OMVs, a majority of cell cytoplasmic molecules and some laboratories consider formation of MVs as an active metabolic process (Brown et al., 2014; Liao et al., 2014; Prados-Rosales et al., 2011).

3.3.2 Contact dependent cell-cell communication

Unlike QS, competence or vesicular transfer, this type of communication requires two cells in a close or relatively close distance. Two main mechanisms of such communication, which are most related to my PhD thesis, are described in the following Chapters. However, also other mechanisms exist, mediating DNA or protein transfer. One of them that needs to be at least mentioned here is called conjugation where donor cells establish a connection with recipient cells by a structure called the F-pilus. By retraction of the F pilus, the recipient cell is attracted to the donor and the conjugative plasmid is exchanged (Goessweiner-Mohr et al., 2015; Kohler et al., 2019). Biogenesis of conjugative pili is dependent on the bacterial Type IV secretion system. This system can also mediate molecular exchange between bacteria and eukaryotic hosts (Goessweiner-Mohr et al., 2013).

3.3.2.1 Direct cell to cell transfer

The first evidence of this phenomenon was described in the Gram-negative bacterium *Myxococcus xanthus* (*M. xanthus*). The authors revealed outer-membrane (OM) protein transfer between two *M. xanthus* cells while their outer membranes were literally fused. The direct contact and presence of both TraA and TraB proteins was necessary for sufficient protein transport. Moreover, both proteins had to be expressed simultaneously by donor and recipient cells. The TraA protein is highly similar to flocculins (cell surface adhesins) that mediate cell-to-cell interaction in yeast. Function of the TraB protein remains unknown (Pathak et al., 2012; Veelders et al., 2010; X. Wei et al., 2011). Some of the cells become motile after membrane fusion which leads to formation of an OM tube between donor and recipient cells (Ducret et al., 2013).

A similar interaction to that one observed in *M. xanthus* was showed in co-cultivation experiments of *Desulfovibrio vulgaris* (*D. vulgaris*) and *Clostridium acetobutylicum* (*C. acetobutylicum*). This time, it was a communication between Gram-positive and Gram-negative bacteria and, therefore, it was even more fascinating. In addition, the

communication occurred only during nutritional stress where transfer of small molecules and even proteins was detected. The results showed that *D. vulgaris* survived in hostile environment only through its interaction with *C. acetobutylicum* (Benomar et al., 2015).

Finally, direct cell-to-cell contact dependent communication was very recently reported between two Gram-positive bacterial species, *C. acetobutylicum* and *C. ljungdahlii* . The authors demonstrated both membrane and cell wall fusions by Transmission Electron Microscopy (TEM) and electron tomography. Their results suggested that proteins or RNA can be transferred via these envelope fusions (Charubin et al., 2020).

3.3.2.2 Membranous tubular structures

In the last decade, another system of bacterial communication was described. This apparatus consists of membranous tubular structures that connect bacteria and are termed bacterial nanotubes (NTs). NTs were discovered in *B. subtilis* but similar tubular structures were observed also in *E. coli* cells under stress and named NTs as well [(**Fig. 10**)(Dubey & Ben-Yehuda, 2011; Pande et al., 2015)]. During the last decade, two types of *B. subtilis* NTs were identified - intercellular and extending NTs - both in exponential phase of bacterial growth. It was also shown that cytoplasmic molecules such as plasmids, proteins (including toxins) and amino acids could be transferred via NTs. Moreover, the transfer can occur between the same or different bacterial species and even between bacteria and eukaryotic cells (Dubey & Ben-Yehuda, 2011; Pal et al., 2019; Stempler et al., 2017). Nanotube morphology was determined by Cryo-EM, revealing a continuous lumen encased in the cell cytoplasmic membrane. The mechanism of NT formation, however, was still unknown at this time (Dubey et al., 2016). A recent study reported the importance of autolysins (enzymes that are involved in the cell wall synthesis and degradation) in NT formation and their penetration (attachment) to other cells (Baidya et al., 2020). In addition, a few other proteins had been identified to associate with NTs/to be important for their formation. One is YmdB, a phosphodiesterase (Diethmaier et al., 2014), and the other proteins are flagellar basal body proteins (Bhattacharya et al., 2019; Dubey et al., 2016).

The NT-like structures have been found also in other bacterial species, but they are called differently. An example are tubular membranous structures, termed nanowires

(NWs), which were observed in *Shewanella oneidensis* MR-1, and contain lipids, proteins, and periplasm (but there is no evidence about cytosolic proteins inside of NWs). NWs are rapidly formed under limiting oxygen conditions, and their outer-membrane contains cytochromes MtrC and OmcA needed for extracellular electron transfer. Thus, it is believed that NWs serve as an outer-membrane extension

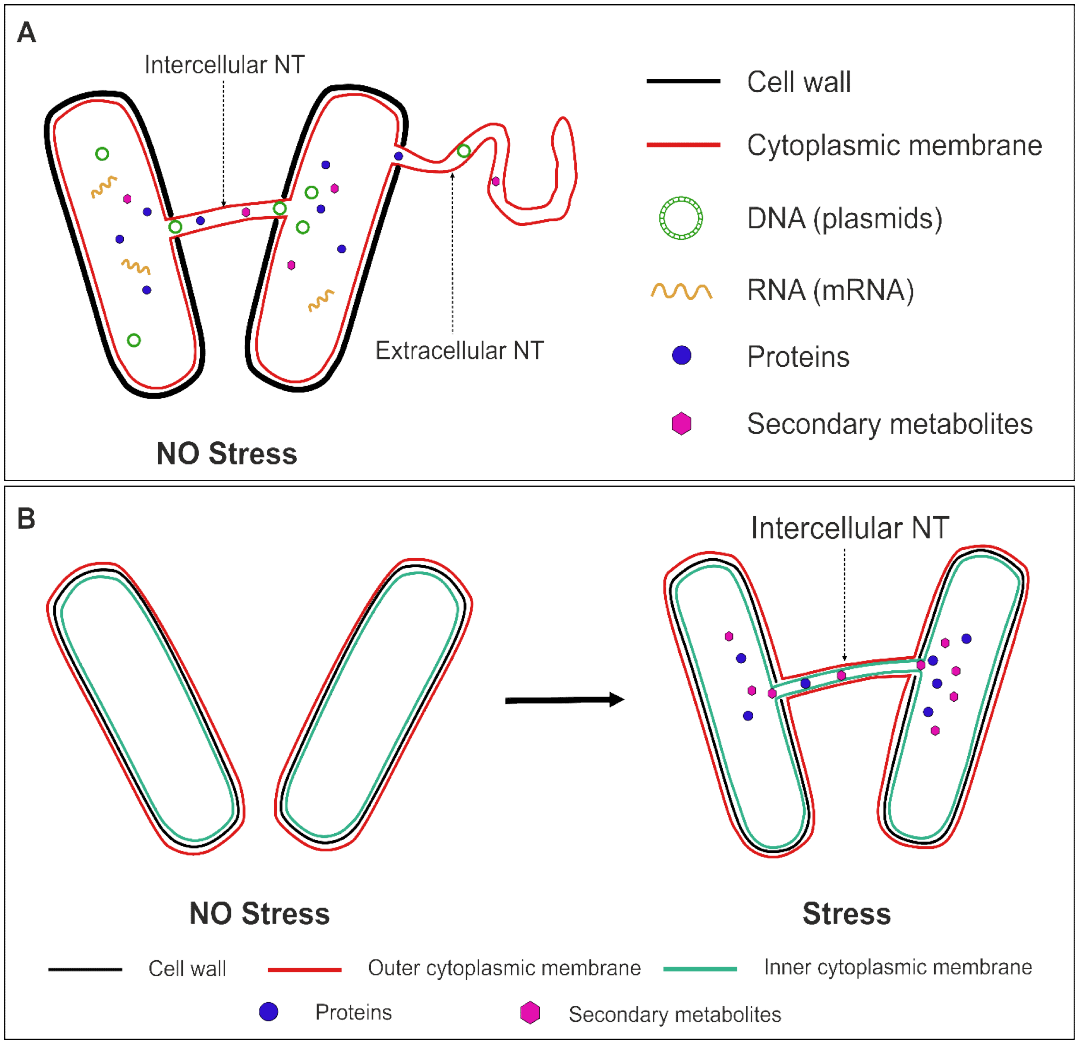

Figure 10. Formation of NTs and molecular transfer in *B. subtilis* and *E. coli*.

A Scheme of intercellular and extracellular NTs that were described in *B. subtilis*. It was described that NT formation in *B. subtilis* occurs in normal growth conditions (without accessory stress). Those NTs predominantly serve like channels for transfer of various cytoplasmic material between bacterial cells.

B Scheme of intercellular NTs of *E. coli* which formation is coupled with amino-acids starvation (stress). There is evidence that *E. coli* NTs are composed from membranes. However, structural data are missing and, thus, it is not clear whether those NTs are formed from outer or inner cytoplasmic membrane (or both).

transporting electrons (Barchinger et al., 2016; Pirbadian et al., 2014; Subramanian et al., 2018).

So called nanopods (NPs) were discovered in Gram-negative *Delfitia* sp. Cs1-4 and in hyperthermophilic archaea of the genus *Thermococcus*. NPs consist of strings of OMVs, encased within a tubular sheath of a novel glycosylated surface layer protein (SLP), termed Nanopod Protein A (NpdA). NP formation is induced by growth on polycyclic aromatic hydrocarbon phenanthrene and it is considered that they are related to phenanthrene degradation (Shetty et al., 2011; Shetty & Hickey, 2014; Soler et al., 2008).

Outer-membrane tubes (OMTs) were studied in *M. xanthus*. The presence of OM proteins and lipids in OMTs was proved, but the presence of cytosolic material was not confirmed. Subsequently, it was revealed that the number of OMTs was increased when cells were placed in liquid medium without agitation. Importantly, the massive OMTs production blocked the TraAB dependent transfer of OM proteins. Moreover, the number of OMTs was not changed after the addition of metabolic inhibitors, suggesting that OMTs could be a by-product of outer membrane dynamics caused by membrane stress under specific conditions (X. Wei et al., 2014). OMTs were also found in pathogens *Francisella novidica* and *Francisella tularensis*. Here, OMTs were again stimulated by stress conditions, namely by amino acid deprivation or during macrophage infection respectively (McCaig et al., 2013; Sampath et al., 2018). Thus, except for *B. subtilis*, formation of nanotubular structures in bacteria was induced under stress conditions.

This brings the following question: Is *B. subtilis* NTs production an active process driven by bacteria or by occasional events during some stress?

All membranous tubular structures described in this Chapter are schematically shown in **Table 1**.

	Composition			Transfer				Formation conditions	
	Membrane	Cell wall	S-layer	DNA	RNA	Proteins	Metabolites	Coupling with stress	Independent on stress
Bsu NTs	+	-	-	+	+	+	+	?	+
Eco NTs	+	?	-	-	?	+	+	+	-
Son NWs	+	-	-	?	?	?	?	+	+
Mxa OMTs	+	-	-	?	?	-	?	+	-
Fno OMTs	+	-	-	?	?	?	?	+	-
Dac NPs	+	?	+	?	?	?	?	?	+
Tga NPs	+	?	+	?	?	?	?	?	+
The NTs	+	?	+	?	?	?	?	?	+

Table 1. Comparison of tubular structures formed by different bacterial species.

Summary of bacterial nanotubular structures based on published research. Information was extracted from the literature. + or green color represents *True*, - or red color represents *False* and question mark or light grey columns represent unknown or insufficiently proved facts. Strains: *Bsu* - *B. subtilis*; *Eco* - *E.coli*; *Son* - *S.oneidensis*; *Mxa* - *M. xanthus*; *Fno* - *F. novidica*; *Dac* - *D.acidovorans*; *Tga* - *T. gammatolerans*; *The* - *Thermococcus*.

4 Aims

This work addresses two topics that overlap in their requirement for more detailed understanding of gene expression and its regulation.

(**1**) The first project focuses on bacterial RNAP and its interacting factors (σ factor, sRNA) in Gram-positive *M. smegmatis* and *B. subtilis*.

Questions to be answered:

- What are the structures of the mycobacterial RNAP core and holoenzyme?
- What is the function of Ms1, a sRNA interacting with mycobacterial RNAP?
- Which genes are regulated by alternative σ factor I (σ^I) in *B. subtilis*?

(**2**) The Second project focuses on bacterial nanotubes in *B. subtilis*.

Questions to be answered:

- Which genes (or σ factors) are responsible for NT formation?
- How are NTs formed (conditions, mechanism)?
- What is the biological role of NTs?

5 Materials and Methods

The research was conducted with Gram-positive organism *B. subtilis* and *M. smegmatis* mc^2 155. *E. coli* strains (DH5α and DE3) were used for DNA and protein purification.

List of methods:

Bacterial cultivation

- cultivation of bacteria on solid or in liquid media
- co-cultivation assays of various bacterial species (*in vivo* DNA transfer assay)

Bacterial strain construction

- PCR
- cloning
- transformation

DNA and protein purification

- Ni^{+II} affinity chromatography (His-tag)
- heparin based protein purification
- plasmid isolation
- chromosomal DNA isolation

In vitro multiple-round transcription

Microscopy

- Various sample preparations and fixations for SEM
- Conventional fluorescence microscopy
- Structured illumination microscopy (SIM)

6 List of publications

During my PhD studies, I (co-)authored a total of 8 publications (see my CV). Some publications were on different topics than this Thesis [(*e. g.* antibacterial compounds) (Seydlová et al., 2017)]; some publications were on related topics but their inclusion would make this Thesis unnecessarily long (Kouba et al., 2020; Pospíšil, et al., 2020; Šmídová et al., 2019). Therefore, this Thesis contains a selection of the most prominent results with a special focus on nanotubes.

Individual selected publications are appended to the end of this Thesis.

Publication I

The Core and Holoenzyme Forms of RNA Polymerase from *Mycobacterium smegmatis*.

Kouba T, Pospíšil J, Hnilicová J, Šanderová H, Barvík I, Krásný L.

J Bacteriol. 2019 Jan 28;201(4):e00583-18.

PMID: 30478083

IF_{2019}: 3.004

The contribution of the author: 40 %, I cloned the genes encoding the subunits of RNAP from *M. smegmatis* into a plasmid that allows their expression in *E. coli*. I performed *in vitro* multiple-round transcription assays with the purified enzyme.

Publication II

σ^I from *Bacillus subtilis*: Impact on Gene Expression and Characterization of σ^I-Dependent Transcription That Requires New Types of Promoters with Extended -35 and -10 Elements.

Ramaniuk O, Převorovský M, Pospíšil J, Vítovská D, Kofroňová O, Benada O, Schwarz M, Šanderová H, Hnilicová J, Krásný L.

J Bacteriol. 2018 Aug 10;200(17):e00251-18.

PMID: 29914988

IF_{2018}: 3.234

IF_{2019}: 3.004

The contribution of the author: 15 %, I characterized the phenotype of the *B. subtilis* mutant lacking σ^I under the microscope (Light microscopy, preparation of samples for SEM).

Publication III

Ms1 RNA increases the amount of RNA polymerase in *Mycobacterium smegmatis*.

Šiková M, Janoušková M, Ramaniuk O, Páleníková P, Pospíšil J, Bartl P, Suder A, Pajer P, Kubičková P, Pavliš O, Hradilová M, Vítovská D, Šanderová H, Převorovský M, Hnilicová J, Krásný L.

Mol Microbiol. 2019 Feb;111(2):354-372.

PMID: 30427073

IF_{2019}: 3.418

The contribution of the author: 10 %, I initiated a collaboration with colleagues from the Faculty of Nuclear Science and Physical Engineering where these colleagues and I tested the ability of *M. smegmatis* wt and ΔMs1 strains to survive under chronic irradiation.

Publication IV

Bacterial nanotubes as a manifestation of cell death.

Pospíšil J, Vítovská D, Kofroňová O, Muchová K, Šanderová H, Hubálek M, Šiková M, Modrák M, Benada O, Barák I, Krásný L.

Nat Commun. 2020 Oct 2;11(1):4963.

PMID: 33009406

IF_{2019}: 12.298

The contribution of the author: 80 %, I conceived the project and designed/performed most of the experiments (constructions of bacterial strains, DNA transfer assays, fluorescence microscopy, sample preparation for Mass spectrometry and SEM, data processing).

I confirm that this Doctoral Thesis was written by Jiří Pospíšil and it is based on published data generated during his Ph.D. study in between 2014-2020. I hereby declare that his contribution described above is based on truth.

Supervisor: Doc. Mgr. Libor Krásný, PhD.

7 Summary of publications

Publication I

The Core and Holoenzyme Forms of RNA Polymerase from *Mycobacterium smegmatis*.

In this publication, we cloned all core subunits (α, β, β′, ω) of the *M. smegmatis* RNAP enzyme into an *E. coli* expression strain. These core subunits were expressed from a single plasmid and purified by His-tag affinity chromatography. Primary σ factor A (σ^A) from *M. smegmatis* was prepared in the same manner. After protein purification, the activity of the reconstituted RNAP-σ^A holoenzyme was successfully tested on a mycobacterial σ^A-dependent promoter by *in vitro* multiple-round transcription assay. By Cryo-EM analysis, we then solved the 3D structures of two main forms of RNAP: RNAP core and RNAP-σ^A holoenzyme. Interestingly, both forms were observed in two different conformations (termed Core1, Core2 and Holo1, Holo2). All conformations represented open forms (independently of the presence of σ^A) of RNAP which is suitable with DNA binding. Nevertheless, the structures differed in the degree of the crab claw opening (open or extremely open). It suggested a flexibility of RNAP β and β′ pincers in the open state. All data obtained by Cryo-EM had a resolution of ~4 Å. Subsequently, atomic modeling was performed, based on known RNAP structures and our data. Subsequently, we characterized the movement of the double helical structure of the β′ N- terminal domain (β′i1), which is unique for mycobacteria. We observed that β′i1 is markedly swung outwards relative to the β domain in core and holoenzyme forms of RNAP. This conformation widens the passage between β′i1 and β domain and promotes a steric funneling toward the DNA binding channel. Finally, we identified a position of the σ^A 1.1 domain on RNAP. It is localized in primary DNA channel inside of RNAP claw which is consistent with 1.1 domain of *E. coli* primary σ factor 70.

Publication II

σ^I from *Bacillus subtilis*: Impact on Gene Expression and Characterization of σ^I-Dependent Transcription That Requires New Types of Promoters with Extended -35 and -10 Elements.

In this study we demonstrated the impact of alternative σ^I on growth and gene expression in *B. subtilis*. Strains lacking both *sigI* and *rsgI* (anti-σ factor I) or only *rsgI* genes were created (Δ*sigI-rsgI* and Δ*rsgI*, respectively). Phenotypic assays were conducted with the strains in comparison with the wt strain. A phenotype was observed only when the Δ*sigI-rsgI* strain was grown at elevated temperature (52 °C). This was further confirmed by SEM where the Δ*sigI-rsgI* strain displayed altered cell morphology at 52 °C. Wt and Δ*sigI-rsgI* strains were then grown at different temperatures (37 °C and 52 °C) and their gene expressions were analyzed by RNA sequencing (RNAseq). RNAseq analysis then revealed ∼130 genes that were affected by the absence of σ^I. In total, 62 and 69 genes were positively or negatively regulated, respectively, across both tested temperatures in the Δ*sigI-rsgI* strain. Proteins encoded by these genes are involved in transcription, translation, cell wall metabolism and coping with stress. One interesting group of genes were those regulating cell iron metabolism that were downregulated in the Δ*sigI-rsgI* strain. This fact was further confirmed by phenotypic assays. However, among the ∼130 RNAseq identified genes, only a small fraction belongs to the real σ^I regulon as the most of genes seem to be influenced by secondary effects caused by the σ^I deletion. We demonstrated this by testing of 22 putative newly identified promoters (based on RNAseq data) of the Δ*sigI-rsgI* downregulated genes by *in vitro* transcription and found that only 3 of them were recognized by RNAP in complex with σ^I. Some of these promoters are responsible for transcription of operons which resulted in a total of 16 genes that are confirmed as bona fide members of the σ^I regulon. Thus, the regulon is small but important as it includes genes that are critical for maintaining iron homeostasis. Finally, the consensus sequence of σ^I-dependent promoter was defined. This sequence is, compared to sequences of promoters of other alternative σ factors, unusually complex.

Publication III

Ms1 RNA increases the amount of RNA polymerase in *Mycobacterium smegmatis*.

This publication describes a mycobacterial sRNA, Ms1. Based on RNAseq data, we showed that Ms1 belongs to the most upregulated *M. smegmatis* genes in stationary phase. Next, using promoter-lacZ fusions, β-galactosidase assays and reverse transcription quantitative PCR (RT-qPCR), we identified the promoter of the Ms1 gene *in vivo*. Moreover, we characterized the activity of the core of the Ms1 promoter as well as its upstream region that strongly enhances transcription. Subsequent experiments (also done with promoter-lacZ fusion) revealed that the Ms1 gene is upregulated in ethanol stressed cells. Next, our data showed that Ms1 is more stable in stationary phase when its half-life is ca 8 hours, much longer than the 8 minutes in exponential phase and this, together with an increased activity of the Ms1 promoter, contributes to the pronounce accumulation of Ms1 in stationary phase. *In vivo* and *in vitro* experiments then showed that Polynucleotide Phosphorylase (PNPase) is, in part, responsible for Ms1 degradation in exponential phase. Furthermore, a Ms1 deletion strain (Δ*Ms1*) was constructed. It revealed that Ms1 is not essential for *M. smegmatis*. However, stationary Δ*Ms1* cells failed to survive in chronic gamma radiation and displayed impaired outgrowth after dilution into the fresh medium (compared to wt). Finally, RNAseq of Δ*Ms1* and wt strains were performed. Results showed downregulation of 14 genes in the Δ*Ms1* strain during stationary phase including genes for β and β′ subunits of RNAP. This downregulation was further confirmed on RNA and protein levels by RT-qPCR and Western blot assay, respectively.

Publication IV

Bacterial nanotubes as a manifestation of cell death.

In this study we have uncovered the true nature of *B. subtilis* NTs.

First, we set out to determine/confirm whether these structures existed and to distinguish them from flagella in bacterial populations, using SEM and SIM approaches. We discovered that under normal laboratory growth conditions (rich medium, 37 °C) flagella were much more numerous than NTs. However, the number of NTs did not reach the previously reported numbers, the difference being several orders of magnitude. Nevertheless, we established at this point that NTs existed.

To follow up, we performed a systematic screen of *B. subtilis* mutants lacking genes for σ factors to identify regulons/genes responsible for their formation. We identified σ factor D (σ^D) as a regulator that is responsible for NT production. By mass spectrometry analysis, we further identified autolysins LytE and LytF (LytF belongs to σ^D regulon) as necessary proteins for NT formation. However, the NTs we had observed were still very rare during the normal *B. subtilis* cultivation.

To find conditions where NTs were more numerous, we tested several sample preparation methods that are commonly used for fluorescence microscopy. This allowed us to identify conditions/sample preparation method where the majority of bacterial cells formed NTs. It was the sample preparation in which external pressure was applied on the coverslip. This led to extrusion of NTs from almost every cell. Importantly, we noticed that cells forming nanotubes were typically visible as grey cells by phase contrast microscopy and we referred to them as ghost cells. Such cells might indicate cell death. This prompted us to test whether these cells might be dead or otherwise significantly compromised. For this purpose, we used SYTOX green staining that penetrates only into dead cells with impaired membranes. Using this staining, we were able to accurately determine the moment of bacterial cell death. Thus, we determined that NTs were formed exclusively from dead cells (after SYTOX green penetration). Moreover, time-lapse experiments showed that the material for NTs (cytoplasmic membrane) was cannibalized from the cell membrane. Importantly, other stressors such as antibiotics also induced NT formation (although to various degrees, depending on the antibiotic). External pressure was subsequently also applied to other bacterial species (*Bacillus megaterium*, *Escherichia coli*, *Deinococcus radiodurans*)

where the same postmortem formation of membrane structures occurred. Finally, we tested DNA transfer via NTs. In this experiment we used a donor strain containing plasmid with the resistance gene against chloramphenicol and a recipient strain harboring the macrolides resistance gene in genome. The results showed that plasmid transfer was strictly dependent on the natural competence system and not on NTs. In summary, NTs are manifestation of bacterial death and appear to have no physiological function.

8 Discussion

This Thesis advances our understanding of transcription and cell-to-cell communication in Gram-positive bacteria. The first part of the Thesis solves the structure of RNAP and addresses the functions of its two interacting partners [(Ms1 and σ^{I})(Kouba et al., 2019; Ramaniuk et al., 2018; Šiková et al., 2019)]. The second part deals with intercellular communication via bacterial NTs, and reveals how σ factors affect their formation (Pospíšil et al., 2020).

8.1 RNAP core and holoenzyme prefer open conformation

We determined structures of RNAP core and RNAP-σ^{A} holoenzyme from *M. smegmatis*. Previously published papers showed that the RNAP clamp, formed by β and β′ subunits, is predominantly open in the free *E. coli* RNAP core and RPc complex but closed in RPo and during elongation (Chakraborty et al., 2012; Duchi et al., 2018). We did not use promoter DNA in our experiments, and consistently, we observed predominantly open conformation of both forms of RNAP (core and holoenzyme). According to our data and published observations, opening and closing of the RNAP clamp is not dependent on presence of σ^{A} but on promoter DNA and other interacting factors during transcription initiation (Chakraborty et al., 2012; Vassylyev et al., 2007).

8.2 β′i1, the enigmatic part of mycobacterial RNAP

Previous studies offered more than one hypothesis of the β′i1 function. Lin et al. showed that β′i1 interacts with the N-terminal region of housekeeping σ^{A} (σ^{A}_{N}) and deletion of β′i1 or σ^{A}_{N} destabilized RPo formation in *M. tuberculosis* (Lin et al., 2017). Another study claimed that β′i1 cooperates with σ^{A}_{N} to impede promoter DNA entry into the primary channel (Hubin, Lilic, et al., 2017). Our structural results are more consistent with the first hypothesis. We observed a significantly swung out β′i1 (in RNAP core and holoenzyme), which is desirable for DNA binding and its accommodation in the primary channel.

8.3 Interaction of the RNAP with σ^{A}

In our study, we obtained only partial information about binding of the entire σ^{A} to RNAP. Our RNAP holoenzyme structure lacked signal densities for σ^{A} domains 3 and 4 that are reported to be localized around the RNA exit channel region of RNAP (Hubin, Fay, et al., 2017). On the other hand, we obtained clear information about the σ^{A} 1.1

domain (N-terminal domain). The *E. coli* σ^{70} 1.1 domain was previously identified in the primary channel of RNAP but the exact position of mycobacterial σ^{A} 1.1 was still unclear (Bae et al., 2013). There are two opposite proposals of how σ^{A} 1.1 interacts with RNAP in mycobacteria. One of them claims that σ^{A} 1.1 is not localized in active site of the primary channel whereas the second proposal claims the opposite (Hubin, Lilic, et al., 2017; Lin et al., 2017). We described that σ^{A} 1.1 is localized within the primary channel in the open-clamp holoenzyme structure. However, this σ^{A} 1.1 binding does not allow RNAP to bind to DNA. Therefore, σ^{A} 1.1 domain must be displaced from the active site to permit conformational changes during RPo formation.

8.4 Mycobacterial sRNA, Ms1, affects cellular level of RNAP

Until now, the role of Ms1 was entirely enigmatic. Our RNAseq data from *M. smegmatis* wt and Δ*Ms1* strains showed that only a few genes were affected by the absence of Ms1. This was surprising because Ms1 binds directly to the RNAP core and, therefore, we expected a more pronounced effect of the Ms1 deletion. However, genes for RNAP itself were downregulated in the Δ*Ms1* strain. Thus, Ms1 must somehow affect the stability or expression of *rpoB* (β) and *rpoC* (β′) mRNAs. The *rpoB* and *rpoC* genes are localized in an operon (*rpoBC*) and regulated by two promoters. Regulation of *rpoBC* expression was previously described in *M. tuberculosis* where addition of rifampicin led to *rpoBC* overexpression. Moreover, transcription from the upstream promoter was stopped and only the downstream promoter was active during rifampicin treatment (J. H. Zhu et al., 2018). Why and how is Ms1 connected with expression of *rpoBC* must be further investigated.

8.5 Ms1 is possibly important for mycobacterial virulence

Downregulation of *rpoBC* genes in the Δ*Ms1* strain leads to a decrease of the RNAP reservoir and this is probably the cause of the impaired growth under the gamma irradiation and other stresses. Gamma irradiation creates reactive oxygen species (ROS) that cause oxidative stress. Mycobacteria must deal with such stress inside of macrophages during host infection (Akaki et al., 2000; Nathan & Shiloh, 2000; Paziak-Domańska et al., 2000; Yu et al., 1999). Moreover, it was reported that MTS2823, a *M. tuberculosis* homologue of Ms1, was upregulated during host infection (Arnvig et al., 2011). We propose that the smaller pool of available functional RNAPs in the Δ*Ms1*

strain hinders the ability of the cell to defend itself against the stress. In other words, Ms1 helps to protect the cell.

8.6 Ms1 is degraded by PNPase

The Ms1-encoding gene appears to be under the control of a single σ^A-dependent (according to its consensus sequence) promoter and further by yet unidentified transcription factors binding to the region upstream of the promoter. Our data showed that Ms1 is degraded by PNPase during exponential phase. PNPase is a critical enzyme in RNA metabolism that functions in most organisms as a 3' to 5' exoribonuclease or as a polynucleotide or poly(A) polymerase (Leszczyniecka et al., 2004; Mohanty & Kushner, 2000; Yehudai-Resheff et al., 2001). Moreover, PNPase was identified as a binding partner of Ms1 in previously published co-immunoprecipitation experiment (Hnilicová et al., 2014). Interestingly and contrarily, the amount of MTS2823 in *M. tuberculosis* decreases after PNPase depletion (Płociński et al., 2019). In comparison with Ms1, the *E. coli* 6S RNA level is regulated by RNase BN (exo- and endoribonuclease), which is known to participate in tRNA maturation. RNase BN deletion in *E. coli* led to a two-fold accumulation of 6S RNA in exponential phase. Moreover, it was shown that the 6S RNA:pRNA duplex is the most favorable substrate for RNase BH and only the endoribonuclease activity is required for 6S RNA degradation (H. Chen et al., 2016). Furthermore, *E. coli* also contains PNPase but its deletion had no effect on the 6S RNA level (Pobre et al., 2019). Therefore, the mechanisms of Ms1 and 6S RNA degradations (the respective RNase) are most likely quite different.

8.7 *B. subtilis* σ^I regulates cell iron homeostasis and stress response

Beside of sRNAs, we characterized also the most important protein partners of RNAP, σ factors. In our study, we examined the function of alternative σ^I in *B. subtilis* belonging to σ factor classes 3-4. Phenotypic tests of a Δ*sigI-rsgI* strain confirmed already published data showing that σ^I has an impact on growth at elevated temperature (Schirner & Errington, 2009; Zuber et al., 2001). Although previous studies

partially characterized σ^I regulon, no systematic identification of the regulon had been performed (Tseng et al., 2011; Tseng & Shaw, 2008).

Therefore, by RNAseq we conducted transcriptomic analyses of Δ*sigI-rsgI* and wt strains grown at two different temperatures (37 °C and 52 °C). As a result, we identified 131 genes that were deregulated in the Δ*sigI-rsgI* strain, including five from the seven already known genes of the σ^I regulon [(namely, *lytE*, *sigI*, *rsgI*, *mreBH*, *ykpC*)(Tseng et al., 2011; Tseng & Shaw, 2008)]. LytE is an autolysin that localizes at cell poles and septa and allows proliferation of cells and cell wall turnover (Hashimoto et al., 2012). MreBH is a homologue and interacts with LytE during cell morphogenesis (Carballido-López et al., 2006). Downregulation of these two proteins in the Δ*sigI-rsgI* strain probably caused defective cell morphology at elevated temperature. Our *in vitro* experiments showed that not all of the 131 genes that had been identified by RNAseq were regulated directly by σ^I. We tested 22 putative new promoter regions by *in vitro* transcription assay but only three of them were active. However, those three promoters regulate operons containing 9 genes (*dhbACEBF*; *ykuNOP*; and *fabI*). The *dhbACEBF* and *ykuNOP* operons contain bacillibactin and flavodoxin synthesis genes respectively. Those genes are responsible for iron cell homeostasis and are necessary during iron starvation or biofilm formation (Baichoo et al., 2002; Pisithkul et al., 2019; Qin et al., 2019). Accordingly, we observed a growth defect of the Δ*sigI-rsgI* strain in a medium without iron. Finally, although the regulon of *B. subtilis* σ^I is small, it seems to be very important for adaptation to stress conditions and for iron utilization.

8.8 Promoter spacer sequence is crucial for σ^I-dependent transcription

We used the identified σ^I-dependent promoters to create a promoter consensus sequence logo. Besides the -10 and -35 elements, sequences of spacers shared significant similarities. Moreover, earlier studies already reported that the spacer sequence can modulate strength of prokaryotic promoters (Gaballa et al., 2018; Hook-Barnard & Hinton, 2009; Jensen & Hammer, 1998). For that reasons, we mutated the spacer of σ^I-dependent promoter and tested its activity by *in vitro* transcription. Results showed that mutations inside the spacer decreased or even abolished transcription. A homologue of σ^I was studied by another group in Gram-positive *Clostridium spp*. The σ^I-dependent promoter consensus in *Clostridium* is very similar to the one observed in

Bacillus (Muñoz-Gutiérrez et al., 2016). The mechanism of the RNAP-σ^I holoenzyme binding to this specific promoter must be addressed further. However, it is clear that σ^I is very specific σ factor. σ^I is classified as group 3 σ factor but contains only domain 2 (D2), which binds to -10 promoter region and C-terminal domains that do not share homology with other known proteins (Z. Wei et al., 2019). C-terminal domain is still enigmatic and could play an important role in σ^I binding.

8.9 σ factor that allows formation of NTs in *B. subtilis*

Next, we examined the influence of σ factors on *B. subtilis* NT formation. We tested deletions of 10 alternative σ factors [(out of the 19 present in *B. subtilis*)(Burton et al., 2019; Gaballa et al., 2018; Nicolas et al., 2012)] and observed that only the σ^D deletion strain (Δ*sigD*) did not form NTs. This was consistent with the known involvement of the CORE element (containing σ^D-dependent genes) in NT formation (Bhattacharya et al., 2019). Moreover, it is known that σ^D is the master regulator of motility, chemotaxis and cell separation genes (Marquez et al., 1990; Phillips et al., 2015; Serizawa et al., 2004). Therefore, the Δ*sigD* strain did not form flagella and this mutant grew as non-separated bacterial chains without any tubular structures.

Bacterial NTs are composed of cytoplasmic membranes and we, therefore, compared membrane fractions of wt and Δ*sigD* (strain non-forming NTs) by mass spectrometry. The results showed dramatic changes in membrane protein composition. This, among other things, suggested a large impact of σ^D on *B. subtilis* membrane proteins. Furthermore, only in the wt membrane fraction we detected autolysins LytF (σ^D-dependent) and LytE (σ^I-dependent). Autolysins are peptidoglycan hydrolases that degrade the peptidoglycan net and allow the insertion of newly synthesized material during cell division and separation (Hashimoto et al., 2018). Thus, we hypothesized that LytF and LytE could play an important role in the very first step of NTs formation by opening the thick Gram-positive cell wall. Further, we constructed a double deletion strain of these autolysins (Δ*lytEF*) and tested whether this strain is able to form NTs. Consistently with our hypothesis, the Δ*lytEF* cells displayed the same disorder of NTs formation as Δ*sigD*. This was consistent with recently published data showing an influence of autolysins LytB and LytC (which both are also σ^D-dependent) on NTs formation (Baidya et al., 2020; R. Chen et al., 2009).

8.10 Conditions where NTs are formed

Initially, we observed NTs as highly infrequently occurring structures in the bacterial population. It was contrary to published reports where the majority of cells contained NTs in normal growth conditions. Importantly, most of the NT quantifications, in the published reports, were done by SEM which does not allow to discriminate NTs from other tube-like structures [(*e.g.* bundles of polysaccharides)(Bhattacharya et al., 2019; Dubey & Ben-Yehuda, 2011)]. Therefore, we chose several methods of sample preparation and quantified NTs by membrane staining and fluorescence microscopy. Each method induced different production of bacterial NTs and the largest amount of NTs was surprisingly observed with the conventional method of microscopic sample preparation. Here, bacterial culture suspension was spotted on a glass slide and covered with a coverslip. Subsequently, mechanical pressure (~80 kPa) was applied to the coverslip to obtain a monolayer of bacterial cells. In this case, we observed NTs in the majority of bacterial cells which finally corresponded with the published numbers (Bhattacharya et al., 2019; Dubey & Ben-Yehuda, 2011). Importantly, under these conditions, NTs emanated preferentially from the cell poles and septa. Furthermore, we showed that Δ*sigD* and Δ*lytEF* strains did not form NTs under pressure during the time window of the experiment. It was consistent with our previous observations about the importance of autolysins LytE and LytF for NT formation as these proteins are localized to cell poles (Yamamoto et al., 2003).

8.11 NTs are a postmortem phenomenon

Thus fur, we had identified conditions where NTs were formed. However, after more detailed examination of fluorescence microscope images, we realized that cells forming NTs were mostly grey in the phase contrast channel. Changes in phase contrast intensity are due to the efflux of cytoplasmic contents and this is associated with cell death (S. Lee et al., 2011; Mohamed & Valvano, 2014). Subsequently, our time-lapse fluorescence microscopy using SYTOX green (staining cells with impaired membrane – dead cells) revealed that NTs were typically formed within seconds after cell death and that the cytoplasmic membrane was consumed for NT building. The same approach was used previously for *B. subtilis* membrane vesicle research where similar results were obtained. The authors described that MVs were formed through holes in the cell wall that were caused by the action of prophage-encoded endolysin.

However, the ensuing loss of membrane integrity during MV formation led to cell death (Toyofuku et al., 2017). This model is consistent with the conspicuous absence of even a single report showing time-lapse experiments with living bacteria (Gram-negative or -positive) that form MVs and are still alive.

Importantly, in Δ*sigD* and Δ*lytEF* we finally also observed NTs formation but with a long delay (90 minutes) after cell death. Therefore, the absence of autolysins and other proteins (from σ^D regulon) affected the kinetics of cell lysis (Smith et al., 2000).

The finding that NTs are a manifestation of bacterial death was entirely unexpected and a big surprise for us. To convince ourselves, we performed time-lapse fluorescence microscopy with *B. subtilis* that was spotted on LB agar and covered with a coverslip that was held by a frame. Under these conditions no pressure was exerted on the bacteria and they could divide. Importantly, under these conditions, no NTs were detected in live cells which is consistent with published live cell time-lapse experiments of *B. subtilis* stained by membrane staining (Eswaramoorthy et al., 2011; Gregory et al., 2008). However, when we added an antibiotic, *e. g.* ampicillin, the cells began to die and form NTs because ampicillin inhibits the transpeptidase that is involved in bacterial cell wall biosynthesis (Izaki et al., 1968). Thus, some holes in peptidoglycan could be formed, thereby creating space for NT protrusion.

8.12 NTs formation in other organisms

Furthermore, we were curious whether other bacterial species form NT-like structures under the pressure. For this, we chose Gram-negative *E. coli* and Gram-positive *B. megaterium* and *D. radiodurans*. Time-lapse experiments with SYTOX-stained dead cells revealed postmortem formation of NTs or other membrane blebs in all above mentioned organisms. Thus, we believe that bacterial NT-like membranous structures that were reported by previous studies are likely also manifestations of cell death (Bhattacharya et al., 2019; Pande et al., 2015; Shetty & Hickey, 2014; Stempler et al., 2017; Subramanian et al., 2018; X. Wei et al., 2014).

Nanotubes were discovered also in eukaryotic cells and termed as Tunneling nanotubes (TNTs). TNT formation was reported in several types of cells (epithelial, neuronal, macrophages etc.) with a potential to transport cytoplasmic molecules and even organelles (Dupont et al., 2018). TNTs can be formed by two mechanisms: (i) Cells are initially in contact and a TNT is established when they separate from each

other; (ii) Cell forms filopodia that are converted to TNTs after reaching the neighboring cell (Gerdes et al., 2013; Kimura et al., 2012). The first mentioned mechanism seems to be very similar to *M. xanthus* OMT formation reported by Ducret and colleagues (Ducret et al., 2013). TNTs, unlike NTs, are supported by actin backbone and can contain microtubules (X. Wang et al., 2012). Nevertheless, there is a lot of evidence that TNT formation is also coupled with stress or even apoptosis (Desir et al., 2016; Kretschmer et al., 2019; Y. Wang et al., 2011; D. Zhu et al., 2005).

8.13 DNA is transferred by natural competence

Although we did not detect any NTs associated with live cells, we wanted to be sure that some, by us undetected live cells, do not form connecting NT and do not *e. g.* transfer non-conjugative plasmids (Baidya et al., 2020; Bhattacharya et al., 2019; Dubey et al., 2016; Dubey & Ben-Yehuda, 2011). So, we set up a final test, screening for cells that acquired non-conjugative plasmids. Our screen revealed that plasmid transfer was totally abolished in a Δ*comK* strain or in the presence of DNase I. It showed that plasmid transfer was exclusively dependent on the cell ability to take up exogenous DNA by natural competence. Moreover, the competence of the Δ*sigD* strain was also slightly decreased. As we further showed, this decrease was caused by downregulation of the *comK* gene in the Δ*sigD* strain. Consistently, impaired competence was also described in a *B. subtilis* mutant lacking strictly σ^D-dependent gene *hag* [(coding structural subunit of flagella)(Hölscher et al., 2018)]. In the light of the evidence, NTs do not serve as channels for DNA transfer and are postmortem phenomena that do not have any known physiological function. Whether or not they have a potential in vaccination, similarly as proposed for OMVs that are able to induce a strong protective immunity in animals (Choi et al., 2015; W. H. Lee et al., 2015; Q. Liu et al., 2016; X. Zhang et al., 2018), is a question for the future.

In Summary, considering the fact that the membranous tubular structures (NTs, NWs, OMTs or NPs) are often formed by other bacteria under stressful conditions, it is, at best, questionable whether they are formed by active cell process and not as a consequence of postmortem events (Barchinger et al., 2016; Dubey et al., 2016; Pande et al., 2015; Shetty et al., 2011; X. Wei et al., 2014).

9 Conclusions

In my Doctoral Thesis, gene expression and its influence on bacterial intercellular communication is addressed in Gram-positive bacteria. First, we characterized the core and the holoenzyme structures of mycobacterial RNAP, and our analysis revealed important structural aspects of this enzyme. Moreover, the creation of the recombinant *M. smegmatis* RNAP provided us with a tool for future studies of interactions of this enzyme with its other molecules.

One such an interaction partner is the mycobacterial small RNA, Ms1. Ms1 is bound to the mycobacterial RNAP core in stationary phase where it probably forms a reservoir of inactive RNAPs, waiting to be utilized when conditions improve. We further showed that the cellular level of Ms1 is, in part, regulated by the PNPase enzyme that can degrade Ms1. Determination of the RNAP-Ms1 structure would provide further important information in the future about the interaction and function of this sRNA, which appears to be critical for mycobacterial virulence.

Next, we described the function of the alternative σ factor I from the gram-positive bacterium *B. subtilis*. This factor differs from other σ factors in its domain composition and consequently also in the mechanism of binding to the recognized promoter sequence. In this work, we defined sequence determinants of σ^I-dependent promoters and the effect of σ^I on bacterial growth.

The key project then uncovered the origin and function of bacterial nanotubes. Here we discovered that NTs are not channels for transport of cytoplasmic material as previously claimed. NTs are a manifestation of bacterial death and likely have no physiological function, analogous in this respect to rigor mortis. In our work, we further showed that also other bacterial species can form NTs and these NTs were likewise induced by stress conditions and occurred after cell death. Similar structures, which have been observed in other bacteria so far, should be examined with great care, considering the possibility that they might be a similar post-mortem phenomenon.

10 References

Akaki, T., Tomioka, H., Shimizu, T., Dekio, S., & Sato, K. (2000). Comparative roles of free fatty acids with reactive nitrogen intermediates and reactive oxygen intermediates in expression of the anti-microbial activity of macrophages against Mycobacterium tuberculosis. *Clinical and Experimental Immunology*. https://doi.org/10.1046/j.1365-2249.2000.01298.x

Altindis, E., Fu, Y., & Mekalanos, J. J. (2014). Proteomic analysis of Vibrio cholerae outer membrane vesicles. *Proceedings of the National Academy of Sciences of the United States of America*. https://doi.org/10.1073/pnas.1403683111

Anagnostopoulos, C., & Spizizen, J. (1961). REQUIREMENTS FOR TRANSFORMATION IN BACILLUS SUBTILIS1. *Journal of Bacteriology*. https://doi.org/10.1128/jb.81.5.741-746.1961

Ando, Y., Asari, S., Suzuma, S., Yamane, K., & Nakamura, K. (2002). Expression of a small RNA, BS203 RNA, from the yocI-yocJ intergenic region of Bacillus subtilis genome. *FEMS Microbiology Letters*. https://doi.org/10.1016/S0378-1097(01)00551-1

Arnvig, K. B., Comas, I., Thomson, N. R., Houghton, J., Boshoff, H. I., Croucher, N. J., Rose, G., Perkins, T. T., Parkhill, J., Dougan, G., & Young, D. B. (2011). Sequence-based analysis uncovers an abundance of non-coding RNA in the total transcriptome of Mycobacterium tuberculosis. *PLoS Pathogens*. https://doi.org/10.1371/journal.ppat.1002342

Bae, B., Davis, E., Brown, D., Campbell, E. A., Wigneshweraraj, S., & Darst, S. A. (2013). Phage T7 Gp2 inhibition of Escherichia coli RNA polymerase involves misappropriation of σ70 domain 1.1. *Proceedings of the National Academy of Sciences of the United States of America*, *110*(49), 19772–19777. https://doi.org/10.1073/pnas.1314576110

Baichoo, N., Wang, T., Ye, R., & Helmann, J. D. (2002). Global analysis of the Bacillus subtilis fur regulon and the iron starvation stimulon. *Molecular Microbiology*. https://doi.org/10.1046/j.1365-2958.2002.03113.x

Baidya, A. K., Rosenshine, I., & Ben-Yehuda, S. (2020). Donor-delivered cell wall hydrolases facilitate nanotube penetration into recipient bacteria. *Nature Communications*. https://doi.org/10.1038/s41467-020-15605-1

Barchinger, S. E., Pirbadian, S., Sambles, C., Baker, C. S., Leung, K. M., Burroughs, N. J., El-Naggar, M. Y., & Golbeck, J. H. (2016). Regulation of gene expression in Shewanella oneidensis MR-1 during electron acceptor limitation and bacterial nanowire formation. *Applied and Environmental Microbiology*. https://doi.org/10.1128/AEM.01615-16

Barrick, J. E., Sudarsan, N., Weinberg, Z., Ruzzo, W. L., & Breaker, R. R. (2005). 6S RNA is a widespread regulator of eubacterial RNA polymerase that resembles an open promoter. *RNA*. https://doi.org/10.1261/rna.7286705

Beckmann, B. M., Burenina, O. Y., Hoch, P. G., Kubareva, E. A., Sharma, C. M., & Hartmann, R. K. (2011). In vivo and in vitro analysis of 6S RNA-templated short transcripts in Bacillus subtilis. *RNA Biology*. https://doi.org/10.4161/rna.8.5.16151

Benomar, S., Ranava, D., Cárdenas, M. L., Trably, E., Rafrafi, Y., Ducret, A., Hamelin, J., Lojou, E., Steyer, J. P., & Giudici-Orticoni, M. T. (2015). Nutritional stress induces exchange of cell material and energetic coupling between bacterial species. *Nature Communications*. https://doi.org/10.1038/ncomms7283

Bhardwaj, N., Syal, K., & Chatterji, D. (2018). The role of ω-subunit of Escherichia coli RNA polymerase in stress response. *Genes to Cells*. https://doi.org/10.1111/gtc.12577

Bhattacharya, S., Baidya, A. K., Pal, R. R., Mamou, G., Gatt, Y. E., Margalit, H., Rosenshine, I., & Ben-Yehuda, S. (2019). A Ubiquitous Platform for Bacterial Nanotube Biogenesis. *Cell Reports*. https://doi.org/10.1016/j.celrep.2019.02.055

Bitto, N. J., Chapman, R., Pidot, S., Costin, A., Lo, C., Choi, J., D'Cruze, T., Reynolds, E. C., Dashper, S. G., Turnbull, L., Whitchurch, C. B., Stinear, T. P., Stacey, K. J., & Ferrero, R. L. (2017). Bacterial membrane vesicles transport their DNA cargo into host cells. *Scientific Reports*. https://doi.org/10.1038/s41598-017-07288-4

Bordes, P., Wigneshweraraj, S. R., Chaney, M., Dago, A. E., Morett, E., & Buck, M. (2004). Communication between Eσ54, promoter DNA and the conserved threonine residue in the GAFTGA motif of the PspF σ54- dependent activator during transcription activation. *Molecular Microbiology*. https://doi.org/10.1111/j.1365-2958.2004.04280.x

Bose, D., Pape, T., Burrows, P. C., Rappas, M., Wigneshweraraj, S. R., Buck, M., & Zhang, X. (2008). Organization of an Activator-Bound RNA Polymerase Holoenzyme. *Molecular Cell*. https://doi.org/10.1016/j.molcel.2008.09.015

Brahmachary, P., Dashti, M. G., Olson, J. W., & Hoover, T. R. (2004). Helicobacter pylori FlgR is an enhancer-independent activator of σ54-RNA polymerase holoenzyme. *Journal of Bacteriology*. https://doi.org/10.1128/JB.186.14.4535-4542.2004

Breitling, R., & Dubnau, D. (1990). A membrane protein with similarity to N-methylphenylalanine pilins is essential for DNA binding by competent Bacillus subtilis. *Journal of Bacteriology*. https://doi.org/10.1128/jb.172.3.1499-1508.1990

Brennan, C. A., Dombroski, A. J., & Platt, T. (1987). Transcription termination factor rho is an RNA-DNA helicase. *Cell*, *48*(6), 945–952. https://doi.org/10.1016/0092-8674(87)90703-3

Brown, L., Kessler, A., Cabezas-Sanchez, P., Luque-Garcia, J. L., & Casadevall, A. (2014). Extracellular vesicles produced by the Gram-positive bacterium Bacillus subtilis are disrupted by the lipopeptide surfactin. *Molecular Microbiology*. https://doi.org/10.1111/mmi.12650

Burenina, O. Y., Hoch, P. G., Damm, K., Salas, M., Zatsepin, T. S., Lechner, M., Oretskaya, T. S., A. Kubareva, E., & Hartmann, R. K. (2014). Mechanistic comparison of Bacillus subtilis 6S-1 and 6S-2 RNAs-commonalities and differences. *RNA*. https://doi.org/10.1261/rna.042077.113

Burton, A. T., DeLoughery, A., Li, G. W., & Kearns, D. B. (2019). Transcriptional regulation and mechanism of sigN (ZpdN), a pBS32-encoded sigma factor in bacillus subtilis. *MBio*. https://doi.org/10.1128/mBio.01899-19

Campbell, E. A., Muzzin, O., Chlenov, M., Sun, J. L., Olson, C. A., Weinman, O., Trester-Zedlitz, M. L., & Darst, S. A. (2002). Structure of the bacterial RNA polymerase promoter specificity σ subunit. *Molecular Cell*, *9*(3), 527–539. https://doi.org/10.1016/S1097-2765(02)00470-7

Carballido-López, R., Formstone, A., Li, Y., Ehrlich, S. D., Noirot, P., & Errington, J. (2006). Actin Homolog MreBH Governs Cell Morphogenesis by Localization of the Cell Wall Hydrolase LytE. *Developmental Cell*. https://doi.org/10.1016/j.devcel.2006.07.017

Cavanagh, A. T., Sperger, J. M., & Wassarman, K. M. (2012). Regulation of 6S RNA by pRNA synthesis is required for efficient recovery from stationary phase in E. coli and B. subtilis. *Nucleic Acids Research*. https://doi.org/10.1093/nar/gkr1003

Chakraborty, A., Wang, D., Ebright, Y. W., Korlann, Y., Kortkhonjia, E., Kim, T., Chowdhury, S., Wigneshweraraj, S., Irschik, H., Jansen, R., Nixon, B. T., Knight, J., Weiss, S., & Ebright, R. H. (2012). Opening and closing of the bacterial RNA polymerase clamp. *Science*. https://doi.org/10.1126/science.1218716

Charubin, K., Modla, S., Caplan, J. L., & Papoutsakis, E. T. (2020). Interspecies Microbial Fusion and Large-Scale Exchange of Cytoplasmic Proteins and RNA in a Syntrophic Clostridium Coculture. *MBio*. https://doi.org/10.1128/mBio.02030-20

Chen, H., Dutta, T., & Deutscher, M. P. (2016). Growth phase-dependent variation of RNase BN/Z affects small RNAs. *Journal of Biological Chemistry*. https://doi.org/10.1074/jbc.M116.757450

Chen, I., Provvedi, R., & Dubnau, D. (2006). A macromolecular complex formed by a pilin-like protein in competent Bacillus subtilis. *Journal of Biological Chemistry*. https://doi.org/10.1074/jbc.M604071200

Chen, J., Chiu, C., Gopalkrishnan, S., Chen, A. Y., Olinares, P. D. B., Saecker, R. M., Winkelman, J. T., Maloney, M. F., Chait, B. T., Ross, W., Gourse, R. L., Campbell, E. A., & Darst, S. A. (2020). Stepwise Promoter Melting by Bacterial RNA Polymerase. *Molecular Cell*, 1–14. https://doi.org/10.1016/j.molcel.2020.02.017

Chen, J., Wassarman, K. M., Feng, S., Leon, K., Feklistov, A., Winkelman, J. T., Li, Z., Walz, T., Campbell, E. A., & Darst, S. A. (2017). 6S RNA Mimics B-Form DNA to Regulate Escherichia coli RNA Polymerase. *Molecular Cell*. https://doi.org/10.1016/j.molcel.2017.09.006

Chen, R., Guttenplan, S. B., Blair, K. M., & Kearns, D. B. (2009). Role of the σD-dependent autolysins in Bacillus subtilis population heterogeneity. *Journal of Bacteriology*. https://doi.org/10.1128/JB.00521-09

Cho, B. K., Kim, D., Knight, E. M., Zengler, K., & Palsson, B. O. (2014). Genome-scale reconstruction of the sigma factor network in Escherichia coli: Topology and functional states. *BMC Biology*. https://doi.org/10.1186/1741-7007-12-4

Choi, S. J., Kim, M. H., Jeon, J., Kim, O. Y., Choi, Y., Seo, J., Hong, S. W., Lee, W. H., Jeon, S. G., Gho, Y. S., Jee, Y. K., & Kim, Y. K. (2015). Active immunization with extracellular vesicles derived from Staphylococcus aureus effectively protects against staphylococcal lung infections, mainly via Th1 cell-mediated immunity. *PLoS ONE*. https://doi.org/10.1371/journal.pone.0136021

Cortes, T., Schubert, O. T., Rose, G., Arnvig, K. B., Comas, I., Aebersold, R., & Young, D. B. (2013). Genome-wide Mapping of Transcriptional Start Sites Defines an Extensive Leaderless Transcriptome in Mycobacterium tuberculosis. *Cell Reports*. https://doi.org/10.1016/j.celrep.2013.10.031

Cozy, L. M., & Kearns, D. B. (2010). Gene position in a long operon governs motility development in Bacillus subtilis. *Molecular Microbiology*. https://doi.org/10.1111/j.1365-2958.2010.07112.x

Darst, S. A., Kubalek, E. W., & Kornberg, R. D. (1989). Three-dimensional structure of Escherichia coli RNA polymerase holoenzyme determined by electron crystallography. *Nature*. https://doi.org/10.1038/340730a0

de Hoon, M. J. L., Makita, Y., Nakai, K., & Miyano, S. (2005). Prediction of Transcriptional Terminators in Bacillus subtilis and Related Species. *PLoS Computational Biology*, *1*(3), e25. https://doi.org/10.1371/journal.pcbi.0010025

de Jonge, E. F., Balhuizen, M. D., van Boxtel, R., Wu, J., Haagsman, H. P., & Tommassen, J. (2020). Heat shock enhances outer-membrane vesicle release in Bordetella spp. *Current Research in Microbial Sciences*. https://doi.org/10.1016/j.crmicr.2020.100009

Delumeau, O., Lecointe, F., Muntel, J., Guillot, A., Guédon, E., Monnet, V., Hecker, M., Becher, D., Polard, P., & Noirot, P. (2011). The dynamic protein partnership of RNA polymerase inBacillus subtilis. *Proteomics*, *11*(15), 2992–3001. https://doi.org/10.1002/pmic.201000790

Desir, S., Dickson, E. L., Vogel, R. I., Thayanithy, V., Wong, P., Teoh, D., Geller, M. A., Steer, C. J., Subramanian, S., & Lou, E. (2016). Tunneling nanotube formation is stimulated by hypoxia in ovarian cancer cells. *Oncotarget*. https://doi.org/10.18632/oncotarget.9504

Diethmaier, C., Newman, J. A., Kovács, Á. T., Kaever, V., Herzberg, C., Rodrigues, C., Boonstra, M., Kuipers, O. P., Lewis, R. J., & Stülke, J. (2014). The YmdB phosphodiesterase is a global regulator of late adaptive responses in bacillus subtilis. *Journal of Bacteriology*. https://doi.org/10.1128/JB.00826-13

Dombroski, A. J., Walter, W. A., & Gross, C. A. (1993). Amino-terminal amino acids modulate σ-factor DNA-binding activity. *Genes and Development*. https://doi.org/10.1101/gad.7.12a.2446

Domingues, S., Nielsen, K. M., & da Silva, G. J. (2012). Various pathways leading to the acquisition of antibiotic resistance by natural transformation. *Mobile Genetic Elements*. https://doi.org/10.4161/mge.23089

Dubey, G. P., & Ben-Yehuda, S. (2011). Intercellular nanotubes mediate bacterial communication. *Cell*. https://doi.org/10.1016/j.cell.2011.01.015

Dubey, G. P., Malli Mohan, G. B., Dubrovsky, A., Amen, T., Tsipshtein, S., Rouvinski, A., Rosenberg, A., Kaganovich, D., Sherman, E., Medalia, O., & Ben-Yehuda, S. (2016). Architecture and Characteristics of Bacterial Nanotubes. *Developmental Cell*. https://doi.org/10.1016/j.devcel.2016.01.013

Duchi, D., Mazumder, A., Malinen, A. M., Ebright, R. H., & Kapanidis, A. N. (2018). The RNA polymerase clamp interconverts dynamically among three states and is stabilized in a partly closed state by ppGpp. *Nucleic Acids Research*. https://doi.org/10.1093/nar/gky482

Ducret, A., Fleuchot, B., Bergam, P., & Mignot, T. (2013). Direct live imaging of cell-cell protein transfer by transient outer membrane fusion in Myxococcus xanthus. *ELife*. https://doi.org/10.7554/eLife.00868

Dufour, A., & Haldenwang, W. G. (1994). Interactions between a Bacillus subtilis anti-σ factor (RsbW) and its antagonist (RsbV). *Journal of Bacteriology*, *176*(7), 1813–1820. https://doi.org/10.1128/jb.176.7.1813-1820.1994

Dupont, M., Souriant, S., Lugo-Villarino, G., Maridonneau-Parini, I., & Vérollet, C. (2018). Tunneling nanotubes: Intimate communication between myeloid cells. In *Frontiers in Immunology*. https://doi.org/10.3389/fimmu.2018.00043

Ellermeier, C. D., & Losick, R. (2006). Evidence for a novel protease governing regulated intramembrane proteolysis and resistance to antimicrobial peptides in Bacillus subtilis. *Genes and Development*. https://doi.org/10.1101/gad.1440606

Eswaramoorthy, P., Erb, M. L., Gregory, J. A., Silverman, J., Pogliano, K., Pogliano, J., & Ramamurthi, K. S. (2011). Cellular architecture mediates DivIVA ultrastructure and regulates min activity in Bacillus subtilis. *MBio*. https://doi.org/10.1128/mBio.00257-11

Francke, C., Groot Kormelink, T., Hagemeijer, Y., Overmars, L., Sluijter, V., Moezelaar, R., & Siezen, R. J. (2011). Comparative analyses imply that the enigmatic sigma factor 54 is a central controller of the bacterial exterior. *BMC Genomics*. https://doi.org/10.1186/1471-2164-12-385

Gaal, T., Ross, W., Blatter, E. E., Tang, H., Jia, X., Krishnan, V. V., Assa-Munt, N., Ebright, R. H., & Gourse, R. L. (1996). DNA-binding determinants of the α subunit of RNA polymerase: Novel DNA-binding domain architecture. *Genes and Development*. https://doi.org/10.1101/gad.10.1.16

Gaballa, A., Guariglia-Oropeza, V., Dürr, F., Butcher, B. G., Chen, A. Y., Chandrangsu, P., & Helmann, J. D. (2018). Modulation of extracytoplasmic function (ECF) sigma factor promoter selectivity by spacer region sequence. *Nucleic Acids Research*. https://doi.org/10.1093/nar/gkx953

Gerdes, H. H., Rustom, A., & Wang, X. (2013). Tunneling nanotubes, an emerging intercellular communication route in development. In *Mechanisms of Development*. https://doi.org/10.1016/j.mod.2012.11.006

Ghosh, P., Ishihama, A., & Chatterji, D. (2001). Escherichia coli RNA polymerase subunit ω and its N-terminal domain bind full-length β′ to facilitate incorporation into the α2β subassembly. *European Journal of Biochemistry*. https://doi.org/10.1046/j.1432-1327.2001.02381.x

Glyde, R., Ye, F., Darbari, V. C., Zhang, N., Buck, M., & Zhang, X. (2017). Structures of RNA Polymerase Closed and Intermediate Complexes Reveal Mechanisms of DNA Opening and Transcription Initiation. *Molecular Cell*, *67*(1), 106-116.e4. https://doi.org/10.1016/j.molcel.2017.05.010

Goessweiner-Mohr, N., Arends, K., Keller, W., & Grohmann, E. (2013). Conjugative type IV secretion systems in Gram-positive bacteria. In *Plasmid*. https://doi.org/10.1016/j.plasmid.2013.09.005

Goessweiner-Mohr, N., Arends, K., Keller, W., & Grohmann, E. (2015). Conjugation in Gram-Positive Bacteria. In *Plasmids*. https://doi.org/10.1128/9781555818982.ch14

Gomez, M., Doukhan, L., Nair, G., & Smith, I. (1998). SigA is an essential gene in Mycobacterium smegmatis. *Molecular Microbiology*. https://doi.org/10.1046/j.1365-2958.1998.00960.x

Gourse, R. L., Ross, W., & Gaal, T. (2000). UPs and downs in bacterial transcription initiation: The role of the alpha subunit of RNA polymerase in promoter recognition. In *Molecular Microbiology*. https://doi.org/10.1046/j.1365-2958.2000.01972.x

Gregory, J. A., Becker, E. C., & Pogliano, K. (2008). Bacillus subtilis MinC destabilizes FtsZ-rings at new cell poles and contributes to the timing of cell division. *Genes and Development*. https://doi.org/10.1101/gad.1732408

Gunnelius, L., Hakkila, K., Kurkela, J., Wada, H., Tyystjärvi, E., & Tyystjärvi, T. (2014). The omega subunit of the RNA polymerase core directs transcription efficiency in cyanobacteria. *Nucleic Acids Research*, *42*(7), 4606–4614. https://doi.org/10.1093/nar/gku084

Hamoen, L. W., Eshuis, H., Jongbloed, J., Venema, G., & van Sinderen, D. (1995). A small gene, designated comS, located within the coding region of the fourth amino acid-activation domain of srfA, is required for competence development in Bacillus subtilis. *Molecular Microbiology*. https://doi.org/10.1111/j.1365-2958.1995.tb02220.x

Hamoen, L. W., Van Werkhoven, A. F., Bijlsma, J. J. E., Dubnau, D., & Venema, G. (1998). The competence transcription factor of Bacillus subtilis recognizes short A/T-rich sequences arranged in a unique, flexible pattern along the DNA helix. *Genes and Development*, *12*(10), 1539–1550. https://doi.org/10.1101/gad.12.10.1539

Han, K., Li, Z. F., Peng, R., Zhu, L. P., Zhou, T., Wang, L. G., Li, S. G., Zhang, X. B., Hu, W., Wu, Z. H., Qin, N., & Li, Y. Z. (2013). Extraordinary expansion of a Sorangium cellulosum genome from an alkaline milieu. *Scientific Reports*. https://doi.org/10.1038/srep02101

Hashimoto, M., Matsushima, H., Putu Suparthana, I., Ogasawara, H., Yamamoto, H., Teng, C., & Sekiguchi, J. (2018). Digestion of peptidoglycan near the cross-link is necessary for the growth of bacillus subtilis. *Microbiology (United Kingdom)*. https://doi.org/10.1099/mic.0.000614

Hashimoto, M., Ooiwa, S., & Sekiguchi, J. (2012). Synthetic lethality of the lytE cwlO genotype in Bacillus subtilis is caused by lack of D, L-endopeptidase activity at the lateral cell wall. *Journal of Bacteriology*. https://doi.org/10.1128/JB.05569-11

Helmann, J. D. (2002). The extracytoplasmic function (ECF) sigma factors. In *Advances in Microbial Physiology*. https://doi.org/10.1016/S0065-2911(02)46002-X

Hindley, J. (1967). Fractionation of 32P-labelled ribonucleic acids on polyacrylamide gels and their characterization by fingerprinting. *Journal of Molecular Biology*, *30*(1), 125–136. https://doi.org/10.1016/0022-2836(67)90248-3

Hnilicová, J., Jirát Matějčková, J., Šiková, M., Pospíšil, J., Halada, P., Pánek, J., & Krásný, L. (2014). Ms1, a novel sRNA interacting with the RNA polymerase core in mycobacteria. *Nucleic Acids Research*, *42*(18), 11763–11776. https://doi.org/10.1093/nar/gku793

Ho, T. D., Hastie, J. L., Intile, P. J., & Ellermeier, C. D. (2011). The Bacillus subtilis extracytoplasmic function σ factor σ v is induced by lysozyme and provides resistance to lysozyme. *Journal of Bacteriology*, *193*(22), 6215–6222. https://doi.org/10.1128/JB.05467-11

Hoch, P. G., Burenina, O. Y., Weber, M. H. W., Elkina, D. A., Nesterchuk, M. V., Sergiev, P. V., Hartmann, R. K., & Kubareva, E. A. (2015). Phenotypic characterization and complementation analysis of Bacillus subtilis 6S RNA single and double deletion mutants. *Biochimie*. https://doi.org/10.1016/j.biochi.2014.12.019

Höfler, C., Heckmann, J., Fritsch, A., Popp, P., Gebhard, S., Fritz, G., & Mascher, T. (2016). Cannibalism stress response in Bacillus subtilis. *Microbiology (United Kingdom)*, *162*(1), 164–176. https://doi.org/10.1099/mic.0.000176

Hölscher, T., Schiklang, T., Dragoš, A., Dietel, A. K., Kost, C., & Kovács, Á. T. (2018). Impaired competence in flagellar mutants of Bacillus subtilis is connected to the regulatory network governed by DegU. *Environmental Microbiology Reports*. https://doi.org/10.1111/1758-2229.12601

Hook-Barnard, I. G., & Hinton, D. M. (2007). Transcription Initiation by Mix and Match Elements: Flexibility for Polymerase Binding to Bacterial Promoters. *Gene Regulation and Systems Biology*. https://doi.org/10.1177/117762500700100020

Hook-Barnard, I. G., & Hinton, D. M. (2009). The promoter spacer influences transcription initiation via σ70 region 1.1 of Escherichia coli RNA polymerase. *Proceedings of the National Academy of Sciences of the United States of America*, *106*(3), 737–742. https://doi.org/10.1073/pnas.0808133106

Hubin, E. A., Fay, A., Xu, C., Bean, J. M., Saecker, R. M., Glickman, M. S., Darst, S. A., & Campbell, E. A. (2017). Structure and function of the mycobacterial transcription initiation complex with the essential regulator RbpA. *ELife*. https://doi.org/10.7554/eLife.22520

Hubin, E. A., Lilic, M., Darst, S. A., & Campbell, E. A. (2017). Structural insights into the mycobacteria transcription initiation complex from analysis of X-ray crystal structures. *Nature Communications*. https://doi.org/10.1038/ncomms16072

Izaki, K., Matsuhashi, M., & Strominger, J. L. (1968). Biosynthesis of the peptidoglycan of bacterial cell walls. 8. Peptidoglycan transpeptidase and D-alanine carboxypeptidase: penicillin-sensitive enzymatic reaction in strains of Escherichia coli. *Journal of Biological Chemistry*.

James, E., Liu, M., Sheppard, C., Mekler, V., Cámara, B., Liu, B., Simpson, P., Cota, E., Severinov, K., Matthews, S., & Wigneshweraraj, S. (2012). Structural and Mechanistic Basis for the Inhibition of Escherichia coli RNA Polymerase by T7 Gp2. *Molecular Cell*, *47*(5), 755–766. https://doi.org/10.1016/j.molcel.2012.06.013

Jensen, P. R., & Hammer, K. (1998). The sequence of spacers between the consensus sequences modulates the strength of prokaryotic promoters. *Applied and Environmental Microbiology*. https://doi.org/10.1128/aem.64.1.82-87.1998

Kainz, M., & Roberts, J. (1992). Structure of transcription elongation complexes in vivo. *Science*. https://doi.org/10.1126/science.1536008

Keller, A. N., Yang, X., Wiedermannova´, J., Delumeau, O., Kra´sny´, L., & Lewis, P. J. (2014). ε, a new subunit of RNA polymerase found in gram-positive bacteria. *Journal of Bacteriology*, *196*(20), 3622–3632. https://doi.org/10.1128/JB.02020-14

Kimura, S., Hase, K., & Ohno, H. (2012). Tunneling nanotubes: Emerging view of their molecular components and formation mechanisms. *Experimental Cell Research*. https://doi.org/10.1016/j.yexcr.2012.05.013

Koeppen, K., Hampton, T. H., Jarek, M., Scharfe, M., Gerber, S. A., Mielcarz, D. W., Demers, E. G., Dolben, E. L., Hammond, J. H., Hogan, D. A., & Stanton, B. A. (2016). A Novel Mechanism of Host-Pathogen Interaction through sRNA in Bacterial Outer Membrane Vesicles. *PLoS Pathogens*. https://doi.org/10.1371/journal.ppat.1005672

Kohler, V., Keller, W., & Grohmann, E. (2019). Regulation of gram-positive conjugation. In *Frontiers in Microbiology*. https://doi.org/10.3389/fmicb.2019.01134

Kouba, T., Koval', T., Sudzinová, P., Pospíšil, J., Brezovská, B., Hnilicová, J., Šanderová, H., Janoušková, M., Šiková, M., Halada, P., Sýkora, M., Barvík, I., Nováček, J., Trundová, M., Dušková, J., Skálová, T., Chon, Ur., Murakami, K. S., Dohnálek, J., & Krásný, L. (2020). Mycobacterial HelD is a nucleic acids-clearing factor for RNA polymerase. *Nature Communications*, *Preprint*.

Kouba, T., Pospíšil, J., Hnilicová, J., Šanderová, H., Barvík, I., & Krásný, L. (2019). The core and holoenzyme forms of RNA polymerase from mycobacterium smegmatis. *Journal of Bacteriology*, *201*(4). https://doi.org/10.1128/JB.00583-18

Kretschmer, A., Zhang, F., Somasekharan, S. P., Tse, C., Leachman, L., Gleave, A., Li, B., Asmaro, I., Huang, T., Kotula, L., Sorensen, P. H., & Gleave, M. E. (2019). Stress-induced tunneling nanotubes support treatment adaptation in prostate cancer. *Scientific Reports*. https://doi.org/10.1038/s41598-019-44346-5

Kroos, L., Zhang, B., Ichikawa, H., & Yu, Y. T. N. (1999). Control of σ factor activity during Bacillus subtilis sporulation. In *Molecular Microbiology*. https://doi.org/10.1046/j.1365-2958.1999.01214.x

Lee, E. Y., Choi, D. Y., Kim, D. K., Kim, J. W., Park, J. O., Kim, S., Kim, S. H., Desiderio, D. M., Kim, Y. K., Kim, K. P., & Gho, Y. S. (2009). Gram-positive bacteria produce membrane vesicles: Proteomics-based characterization of Staphylococcus aureus-derived membrane vesicles. *Proteomics*. https://doi.org/10.1002/pmic.200900338

Lee, S., Kim, Y. R., Lee, J. Y., Rhee, J. H., Park, C.-S., & Kim, D. Y. (2011). Dynamic analysis of pathogen-infected host cells using quantitative phase microscopy. *Journal of Biomedical Optics*. https://doi.org/10.1117/1.3548882

Lee, W. H., Choi, H. Il, Hong, S. W., Kim, K. S., Gho, Y. S., & Jeon, S. G. (2015). Vaccination with Klebsiella pneumoniae-derived extracellular vesicles protects against bacteria-induced lethality via both humoral and cellular immunity. *Experimental and Molecular Medicine*. https://doi.org/10.1038/emm.2015.59

Leszczyniecka, M., DeSalle, R., Kang, D. C., & Fisher, P. B. (2004). The origin of polynucleotide phosphorylase domains. *Molecular Phylogenetics and Evolution*. https://doi.org/10.1016/j.ympev.2003.07.012

Li, W., Ying, X., Lu, Q., & Chen, L. (2012). Predicting sRNAs and Their Targets in Bacteria. In *Genomics, Proteomics and Bioinformatics*. https://doi.org/10.1016/j.gpb.2012.09.004

Liao, S., Klein, M. I., Heim, K. P., Fan, Y., Bitoun, J. P., Ahn, S. J., Burne, R. A., Koo, H., Brady, L. J., & Wen, Z. T. (2014). Streptococcus mutans extracellular DNA is upregulated during growth in biofilms, actively released via membrane vesicles, and influenced by components of the protein secretion machinery. *Journal of Bacteriology*. https://doi.org/10.1128/JB.01493-14

Lin, W., Mandal, S., Degen, D., Liu, Y., Ebright, Y. W., Li, S., Feng, Y., Zhang, Y., Mandal, S., Jiang, Y., Liu, S., Gigliotti, M., Talaue, M., Connell, N., Das, K., Arnold, E., & Ebright, R. H. (2017). Structural Basis of Mycobacterium tuberculosis Transcription and Transcription Inhibition. *Molecular Cell*. https://doi.org/10.1016/j.molcel.2017.03.001

Liu, B., Hong, C., Huang, R. K., & Yu, Z. (2017). Transcription Activation. *Research*, *951*(November), 947–951.

Liu, H., & Ganta, R. R. (2019). Sequence Determinants Spanning −10 Motif and Spacer Region Implicated in Unique Ehrlichia chaffeensis Sigma 32-Dependent Promoter Activity of dnaK Gene. *Frontiers in Microbiology*. https://doi.org/10.3389/fmicb.2019.01772

Liu, Q., Liu, Q., Yi, J., Liang, K., Liu, T., Roland, K. L., Jiang, Y., & Kong, Q. (2016). Outer membrane vesicles derived from Salmonella Typhimurium mutants with truncated LPS induce cross-protective immune responses against infection of Salmonella enterica serovars in the mouse model. *International Journal of Medical Microbiology*. https://doi.org/10.1016/j.ijmm.2016.08.004

Lloyd, M. G., Lundgren, B. R., Hall, C. W., Gagnon, L. B. P., Mah, T. F., Moffat, J. F., & Nomura, C. T. (2017). Targeting the alternative sigma factor RpoN to combat virulence in Pseudomonas aeruginosa. *Scientific Reports*. https://doi.org/10.1038/s41598-017-12667-y

MacDonald, I. A., & Kuehna, M. J. (2013). Stress-induced outer membrane vesicle production by Pseudomonas aeruginosa. *Journal of Bacteriology*. https://doi.org/10.1128/JB.02267-12

Magnuson, R., Solomon, J., & Grossman, A. D. (1994). Biochemical and genetic characterization of a competence pheromone from B. subtilis. *Cell*. https://doi.org/10.1016/0092-8674(94)90313-1

Mandic-Mulec, I., Kraigher, B., Cepon, U., & Mahne, I. (2003). Variability of the quorum sensing system in natural isolates of Bacillus sp. In *Food Technology and Biotechnology*.

Marquez, L. M., Helmann, J. D., Ferrari, E., Parker, H. M., Ordal, G. W., & Chamberlin, M. J. (1990). Studies of σ(D)-dependent functions in bacillus subtilis. *Journal of Bacteriology*. https://doi.org/10.1128/jb.172.6.3435-3443.1990

McCaig, W. D., Koller, A., & Thanassi, D. G. (2013). Production of outer membrane vesicles and outer membrane tubes by Francisella novicida. *Journal of Bacteriology*. https://doi.org/10.1128/JB.02007-12

Minakhin, L., Bhagat, S., Brunning, A., Campbell, E. A., Darst, S. A., Ebright, R. H., & Severinov, K. (2001). Bacterial RNA polymerase subunit ω and eukaryotic polymerase subunit RPB6 are sequence, structural, and functional homologs and promote RNA polymerase assembly. *Proceedings of the National Academy of Sciences of the United States of America*. https://doi.org/10.1073/pnas.98.3.892

Mohamed, Y. F., & Valvano, M. A. (2014). A burkholderia cenocepacia murJ (MviN) homolog is essential for cell wall peptidoglycan synthesis and bacterial viability. *Glycobiology*. https://doi.org/10.1093/glycob/cwu025

Mohanty, B. K., & Kushner, S. R. (2000). Polynucleotide phosphorylase functions both as a 3' → 5' exonuclease and a poly(A) polymerase in Escherichia coli. *Proceedings of the National Academy of Sciences of the United States of America*. https://doi.org/10.1073/pnas.220295997

Moreno-Campuzano, S., Janga, S. C., & Pérez-Rueda, E. (2006). Identification and analysis of DNA-binding transcription factors in Bacillus subtilis and other Firmicutes - A genomic approach. *BMC Genomics*, *7*, 1–10. https://doi.org/10.1186/1471-2164-7-147

Motáčková, V., Šanderová, H., Zídek, L., Nováček, J., Padrta, P., Švenková, A., Korelusová, J., Jonák, J., Krásný, L., & Sklenář, V. (2010). Solution structure of the N-terminal domain in of Bacillus subtilis δ subunit of RNA polymerase ana its classification based on structural homologs. *Proteins: Structure, Function and Bioinformatics*, *78*(7), 1807–1810. https://doi.org/10.1002/prot.22708

Muñoz-Gutiérrez, I., De Ora, L. O., Grinberg, I. R., Garty, Y., Bayer, E. A., Shoham, Y., Lamed, R., & Borovok, I. (2016). Decoding biomass-sensing regulons of clostridium thermocellum alternative sigma-I factors in a heterologous bacillus subtilis host system. *PLoS ONE*. https://doi.org/10.1371/journal.pone.0146316

Murakami, K., Fujita, N., & Ishihama, A. (1996). Transcription factor recognition surface on the RNA polymerase alpha subunit is involved in contact with the DNA enhancer element. *The EMBO Journal*. https://doi.org/10.1002/j.1460-2075.1996.tb00809.x

Muschiol, S., Balaban, M., Normark, S., & Henriques-Normark, B. (2015). Uptake of extracellular DNA: Competence induced pili in natural transformation of Streptococcus pneumoniae. *BioEssays*. https://doi.org/10.1002/bies.201400125

Muschiol, S., Erlendsson, S., Aschtgen, M. S., Oliveira, V., Schmieder, P., De Lichtenberg, C., Teilum, K., Boesen, T., Akbey, U., & Henriques-Normark, B. (2017). Structure of the competence pilus major pilin ComGC in Streptococcus pneumoniae. *Journal of Biological Chemistry*. https://doi.org/10.1074/jbc.M117.787671

Nakamura, M. M., Liew, S. Y., Cummings, C. A., Brinig, M. M., Dieterich, C., & Relman, D. A. (2006). Growth phase- and nutrient limitation-associated transcript abundance regulation in Bordetella pertussis. *Infection and Immunity*. https://doi.org/10.1128/IAI.00781-06

Narayanan, A., Vago, F. S., Li, K., Qayyum, M. Z., Yernool, D., Jiang, W., & Murakami, K. S. (2018). Cryo-EM structure of Escherichia coli 70 RNA polymerase and promoter DNA complex revealed a role of non-conserved region during the open complex formation. *Journal of Biological Chemistry*, *293*(19), 7367–7375. https://doi.org/10.1074/jbc.RA118.002161

Nathan, C., & Shiloh, M. U. (2000). Reactive oxygen and nitrogen intermediates in the relationship between mammalian hosts and microbial pathogens. *Proceedings of the National Academy of Sciences of the United States of America*. https://doi.org/10.1073/pnas.97.16.8841

Nicolas, P., Mäder, U., Dervyn, E., Rochat, T., Leduc, A., Pigeonneau, N., Bidnenko, E., Marchadier, E., Hoebeke, M., Aymerich, S., Becher, D., Bisicchia, P., Botella, E., Delumeau, O., Doherty, G., Denham, E. L., Fogg, M. J., Fromion, V., Goelzer, A., … Noirot, P. (2012). Condition-dependent transcriptome reveals high-level regulatory architecture in Bacillus subtilis. *Science*. https://doi.org/10.1126/science.1206848

O'Reilly, F. J., Xue, L., Graziadei, A., Sinn, L., Lenz, S., Tegunov, D., Blötz, C., Singh, N., Hagen, W. J. H., Cramer, P., Stülke, J., Mahamid, J., & Rappsilber, J. (2020). In-cell architecture of an actively transcribing-translating expressome. *Science*. https://doi.org/10.1126/science.abb3758

Ogura, M., Liu, L., LaCelle, M., Nakano, M. M., & Zuber, P. (1999). Mutational analysis of ComS: Evidence for the interaction of ComS and MecA in the regulation of competence development in Bacillus subtilis. *Molecular Microbiology*. https://doi.org/10.1046/j.1365-2958.1999.01399.x

Paget, M. S. B., & Helmann, J. D. (2003). The sigma70 family of sigma factors. *Genome Biology*.

Pal, R. R., Baidya, A. K., Mamou, G., Bhattacharya, S., Socol, Y., Kobi, S., Katsowich, N., Ben-Yehuda, S., & Rosenshine, I. (2019). Pathogenic E. coli Extracts Nutrients from Infected Host Cells Utilizing Injectisome Components. *Cell*. https://doi.org/10.1016/j.cell.2019.02.022

Pande, S., Shitut, S., Freund, L., Westermann, M., Bertels, F., Colesie, C., Bischofs, I. B., & Kost, C. (2015). Metabolic cross-feeding via intercellular nanotubes among bacteria. *Nature Communications*. https://doi.org/10.1038/ncomms7238

Pánek, J., Krásný, L., Bobek, J., Ježková, E., Korelusová, J., & Vohradský, J. (2011). The suboptimal structures find the optimal RNAs: Homology search for bacterial non-coding RNAs using suboptimal RNA structures. *Nucleic Acids Research*. https://doi.org/10.1093/nar/gkq1186

Papoušková, V., Kadeřávek, P., Otrusinová, O., Rabatinová, A., Šanderová, H., Nováček, J., Krásný, L., Sklenář, V., & Žídek, L. (2013). Structural study of the partially disordered full-length δ subunit of RNA polymerase from bacillus subtilis. *ChemBioChem*, *14*(14), 1772–1779. https://doi.org/10.1002/cbic.201300226

Pathak, D. T., Wei, X., Bucuvalas, A., Haft, D. H., Gerloff, D. L., & Wall, D. (2012). Cell contact-dependent outer membrane exchange in myxobacteria: Genetic determinants and mechanism. *PLoS Genetics*. https://doi.org/10.1371/journal.pgen.1002626

Paziak-Domańska, B., Klink, M., Jurkiewicz, M., & Rudnicka, W. (2000). Production of reactive nitrogen and oxygen intermediates in human granulocytes and monocytes during internalization of live BCG bacilli. *Medycyna Doświadczalna i Mikrobiologia*.

Pearson, J. P., Feldman, M., Iglewski, B. H., & Prince, A. (2000). Pseudomonas aeruginosa cell-to-cell signaling is required for virulence in a model of acute pulmonary infection. *Infection and Immunity*. https://doi.org/10.1128/IAI.68.7.4331-4334.2000

Phillips, A. M., Calvo, R. A., & Kearns, D. B. (2015). Functional Activation of the Flagellar Type III Secretion Export Apparatus. *PLoS Genetics*. https://doi.org/10.1371/journal.pgen.1005443

Pirbadian, S., Barchinger, S. E., Leung, K. M., Byun, H. S., Jangir, Y., Bouhenni, R. A., Reed, S. B., Romine, M. F., Saffarini, D. A., Shi, L., Gorby, Y. A., Golbeck, J. H., & El-Naggar, M. Y. (2014). Shewanella oneidensis MR-1 nanowires are outer membrane and periplasmic extensions of the extracellular electron transport components. *Proceedings of the National Academy of Sciences of the United States of America*. https://doi.org/10.1073/pnas.1410551111

Pisithkul, T., Schroeder, J. W., Trujillo, E. A., Yeesin, P., Stevenson, D. M., Chaiamarit, T., Coon, J. J., Wang, J. D., & Amador-Noguez, D. (2019). Metabolic remodeling during biofilm development of bacillus subtilis. *MBio*. https://doi.org/10.1128/mBio.00623-19

Płociński, P., Maclos, M., Houghton, J., Niemiec, E., Płocińska, R., Brzostek, A., Słomka, M., Dziadek, J., Young, D., & Dziembowski, A. (2019). Proteomic and transcriptomic experiments reveal an essential role of RNA degradosome complexes in shaping the transcriptome of Mycobacterium tuberculosis. *Nucleic Acids Research*. https://doi.org/10.1093/nar/gkz251

Pobre, V., Barahona, S., Dobrzanski, T., Steffens, M. B. R., & Arraiano, C. M. (2019). Defining the impact of exoribonucleases in the shift between exponential and stationary phases. *Scientific Reports*. https://doi.org/10.1038/s41598-019-52453-6

Pospíšil, J., Strunin, D., Ziková, A., Hubálek, M., & Vohradský, J. (2020). A Comparison of Protein and mRNA Expression during Development of the Soil Dwelling Prokaryote (S. coelicolor). *PROTEOMICS*. https://doi.org/10.1002/pmic.202070135

Pospíšil, J., Vítovská, D., Kofroňová, O., Muchová, K., Šanderová, H., Hubálek, M., Šiková, M., Modrák, M., Benada, O., Barák, I., & Krásný, L. (2020). Bacterial nanotubes as a manifestation of cell death. *Nature Communications*. https://doi.org/10.1038/s41467-020-18800-2

Prados-Rosales, R., Baena, A., Martinez, L. R., Luque-Garcia, J., Kalscheuer, R., Veeraraghavan, U., Camara, C., Nosanchuk, J. D., Besra, G. S., Chen, B., Jimenez, J., Glatman-Freedman, A., Jacobs, W. R., Porcelli, S. A., & Casadevall, A. (2011). Mycobacteria release active membrane vesicles that modulate immune responses in a TLR2-dependent manner in mice. *Journal of Clinical Investigation*. https://doi.org/10.1172/JCI44261

Qin, Y., He, Y., She, Q., Larese-Casanova, P., Li, P., & Chai, Y. (2019). Heterogeneity in respiratory electron transfer and adaptive iron utilization in a bacterial biofilm. *Nature Communications*. https://doi.org/10.1038/s41467-019-11681-0

Ramaniuk, O., Černý, M., Krásný, L., & Vohradský, J. (2017). Kinetic modelling and meta-analysis of the B. subtilis SigA regulatory network during spore germination and outgrowth. *Biochimica et Biophysica Acta - Gene Regulatory Mechanisms*. https://doi.org/10.1016/j.bbagrm.2017.06.003

Ramaniuk, O., Převorovský, M., Pospíšil, J., Vítovská, D., Kofroňová, O., Benada, O., Schwarz, M., Šanderová, H., Hnilicová, J., & Krásný, L. (2018). σI from Bacillus subtilis : Impact on Gene Expression and Characterization of σI -Dependent Transcription That Requires. *Journal of Bacteriology*, *200*(17), 1–15.

Rivera, J., Cordero, R. J. B., Nakouzi, A. S., Frases, S., Nicola, A., & Casadevall, A. (2010). Bacillus anthracis produces membrane-derived vesicles containing biologically active toxins. *Proceedings of the National Academy of Sciences of the United States of America*. https://doi.org/10.1073/pnas.1008843107

Rolfe, M. D., Rice, C. J., Lucchini, S., Pin, C., Thompson, A., Cameron, A. D. S., Alston, M., Stringer, M. F., Betts, R. P., Baranyi, J., Peck, M. W., & Hinton, J. C. D. (2012). Lag phase is a distinct growth phase that prepares bacteria for exponential growth and involves transient metal accumulation. *Journal of Bacteriology*. https://doi.org/10.1128/JB.06112-11

Rösch, T. C., & Graumann, P. L. (2015). Induction of plasmid conjugation in Bacillus subtilis is bistable and driven by a direct interaction of a Rap/Phr quorum-sensing system with a master repressor. *Journal of Biological Chemistry*, *290*(33), 20221–20232. https://doi.org/10.1074/jbc.M115.664110

Ross, W., Gosink, K. K., Salomon, J., Igarashi, K., Zou, C., Ishihama, A., Severinov, K., & Gourse, R. L. (1993). A third recognition element in bacterial promoters: DNA binding by the α subunit of RNA polymerase. *Science*. https://doi.org/10.1126/science.8248780

Sampath, V., McCaig, W. D., & Thanassi, D. G. (2018). Amino acid deprivation and central carbon metabolism regulate the production of outer membrane vesicles and tubes by Francisella. *Molecular Microbiology*. https://doi.org/10.1111/mmi.13897

Sanchez, I., Hernandez-Guerrero, R., Mendez-Monroy, P. E., Martinez-Nuñez, M. A., Ibarra, J. A., & Pérez-Rueda, E. (2020). Evaluation of the abundance of DNA-binding transcription factors in Prokaryotes. *Genes*. https://doi.org/10.3390/genes11010052

Santos-Beneit, F., Barriuso-Iglesias, M., Fernández-Martínez, L. T., Martínez-Castro, M., Sola-Landa, A., Rodríguez-García, A., & Martín, J. F. (2011). The RNA polymerase omega factor rpoZ is regulated by phop and has an important role in antibiotic biosynthesis and morphological differentiation in Streptomyces coelicolor. *Applied and Environmental Microbiology*. https://doi.org/10.1128/AEM.00465-11

Schirner, K., & Errington, J. (2009). The cell wall regulator σI specifically suppresses the lethal phenotype of mbl mutants in Bacillus subtilis. *Journal of Bacteriology*. https://doi.org/10.1128/JB.01497-08

Schwarz, M., Vohradský, J., Modrák, M., & Pánek, J. (2020). rboAnalyzer: A Software to Improve Characterization of Non-coding RNAs From Sequence Database Search Output. *Frontiers in Genetics*. https://doi.org/10.3389/fgene.2020.00675

Schwechheimer, C., & Kuehn, M. J. (2015). Outer-membrane vesicles from Gram-negative bacteria: Biogenesis and functions. In *Nature Reviews Microbiology*. https://doi.org/10.1038/nrmicro3525

Serizawa, M., Yamamoto, H., Yamaguchi, H., Fujita, Y., Kobayashi, K., Ogasawara, N., & Sekiguchi, J. (2004). Systematic analysis of SigD-regulated genes in Bacillus subtilis by DNA microarray and Northern blotting analyses. *Gene*. https://doi.org/10.1016/j.gene.2003.12.024

Seydlová, G., Pohl, R., Zborníková, E., Ehn, M., Šimák, O., Panova, N., Kolář, M., Bogdanová, K., Večeřová, R., Fišer, R., Šanderová, H., Vítovská, D., Sudzinová, P., Pospíšil, J., Benada, O., Křížek, T., Sedlák, D., Bartůněk, P., Krásný, L., & Rejman, D. (2017). Lipophosphonoxins II: Design, Synthesis, and Properties of Novel Broad Spectrum Antibacterial Agents. *Journal of Medicinal Chemistry*, *60*(14), 6098–6118. https://doi.org/10.1021/acs.jmedchem.7b00355

Shetty, A., Chen, S., Tocheva, E. I., Jensen, G. J., & Hickey, W. J. (2011). Nanopods: A new bacterial structure and mechanism for deployment of outer membrane vesicles. *PLoS ONE*. https://doi.org/10.1371/journal.pone.0020725

Shetty, A., & Hickey, W. J. (2014). Effects of outer membrane vesicle formation, surface-layer production and Nanopod development on the metabolism of phenanthrene by Delftia acidovorans Cs1-4. *PLoS ONE*. https://doi.org/10.1371/journal.pone.0092143

Shiina, T., Tanaka, K., & Takahashi, H. (1991). Sequence of hrdB, an essential gene encoding sigma-like transcription factor of Streptomyces coelicolor A3(2): homology to principal sigma factors. *Gene*.

Shleeva, M. O., Kudykina, Y. K., Vostroknutova, G. N., Suzina, N. E., Mulyukin, A. L., & Kaprelyants, A. S. (2011). Dormant ovoid cells of Mycobacterium tuberculosis are formed in response to gradual external acidification. *Tuberculosis*, *91*(2), 146–154. https://doi.org/10.1016/j.tube.2010.12.006

Shultzaberger, R. K., Chen, Z., Lewis, K. A., & Schneider, T. D. (2007). Anatomy of Escherichia coli σ70 promoters. *Nucleic Acids Research*. https://doi.org/10.1093/nar/gkl956

Šiková, M., Janoušková, M., Ramaniuk, O., Páleníková, P., Pospíšil, J., Bartl, P., Suder, A., Pajer, P., Kubičková, P., Pavliš, O., Hradilová, M., Vítovská, D., Šanderová, H., Převorovský, M., Hnilicová, J., & Krásný, L. (2019). Ms1 RNA increases the amount of RNA polymerase in Mycobacterium smegmatis. *Molecular Microbiology*, *111*(2), 354–372. https://doi.org/10.1111/mmi.14159

Šmídová, K., Ziková, A., Pospíšil, J., Schwarz, M., Bobek, J., & Vohradsky, J. (2019). DNA mapping and kinetic modeling of the HrdB regulon in Streptomyces coelicolor. *Nucleic Acids Research*, *47*(2), 621–633. https://doi.org/10.1093/nar/gky1018

Smith, T. J., Blackman, S. A., & Foster, S. J. (2000). Autolysins of Bacillus subtilis: Multiple enzymes with multiple functions. In *Microbiology*. https://doi.org/10.1099/00221287-146-2-249

Soler, N., Marguet, E., Verbavatz, J. M., & Forterre, P. (2008). Virus-like vesicles and extracellular DNA produced by hyperthermophilic archaea of the order Thermococcales. *Research in Microbiology*. https://doi.org/10.1016/j.resmic.2008.04.015

Sorenson, M. K., & Darst, S. A. (2006). Disulfide cross-linking indicates that FIgM-bound and free σ28 adopt similar conformations. *Proceedings of the National Academy of Sciences of the United States of America*, *103*(45), 16722–16727. https://doi.org/10.1073/pnas.0606482103

Stempler, O., Baidya, A. K., Bhattacharya, S., Malli Mohan, G. B., Tzipilevich, E., Sinai, L., Mamou, G., & Ben-Yehuda, S. (2017). Interspecies nutrient extraction and toxin delivery between bacteria. *Nature Communications*. https://doi.org/10.1038/s41467-017-00344-7

Subramanian, P., Pirbadian, S., El-Naggar, M. Y., & Jensen, G. J. (2018). Ultrastructure of Shewanella oneidensis MR-1 nanowires revealed by electron cryotomography. *Proceedings of the National Academy of Sciences of the United States of America*. https://doi.org/10.1073/pnas.1718810115

Susanna, K. A., Van Der Werff, A. F., Den Hengst, C. D., Calles, B., Salas, M., Venema, G., Hamoen, L. W., & Kuipers, O. P. (2004). Mechanism of Transcription Activation at the comG Promoter by the Competence Transcription Factor ComK of Bacillus subtilis. *Journal of Bacteriology*, *186*(4), 1120–1128. https://doi.org/10.1128/JB.186.4.1120-1128.2004

Sutherland, C., & Murakami, K. S. (2018). An Introduction to the Structure and Function of the Catalytic Core Enzyme of Escherichia coli RNA Polymerase. *EcoSal Plus*. https://doi.org/10.1128/ecosalplus.esp-0004-2018

Thüring, M., Ganapathy, S., Schlüter, M. A. C., Lechner, M., & Hartmann, R. K. (2020). 6S-2 RNA deletion in the undomesticated B. subtilis strain NCIB 3610 causes a biofilm derepression phenotype. *RNA Biology*. https://doi.org/10.1080/15476286.2020.1795408

Tortosa, P., Logsdon, L., Kraigher, B., Itoh, Y., Mandic-Mulec, I., & Dubnau, D. (2001). Specificity and genetic polymorphism of the Bacillus competence quorum-sensing system. *Journal of Bacteriology*. https://doi.org/10.1128/JB.183.2.451-460.2001

Toyofuku, M., Cárcamo-Oyarce, G., Yamamoto, T., Eisenstein, F., Hsiao, C. C., Kurosawa, M., Gademann, K., Pilhofer, M., Nomura, N., & Eberl, L. (2017). Prophage-triggered membrane vesicle formation through peptidoglycan damage in Bacillus subtilis. *Nature Communications*. https://doi.org/10.1038/s41467-017-00492-w

Trotochaud, A. E., & Wassarman, K. M. (2005). A highly conserved 6S RNA structure is required for regulation of transcription. *Nature Structural and Molecular Biology*. https://doi.org/10.1038/nsmb917

Tseng, C. L., Chen, J. T., Lin, J. H., Huang, W. Z., & Shaw, G. C. (2011). Genetic evidence for involvement of the alternative sigma factor SigI in controlling expression of the cell wall hydrolase gene lytE and contribution of LytE to heat survival of Bacillus subtilis. *Archives of Microbiology*. https://doi.org/10.1007/s00203-011-0710-0

Tseng, C. L., & Shaw, G. C. (2008). Genetic evidence for the actin homolog gene mreBH and the bacitracin resistance gene bcrC as targets of the alternative sigma factor SigI of Bacillus subtilis. *Journal of Bacteriology*. https://doi.org/10.1128/JB.01497-07

van Sinderen, D., Luttinger, A., Kong, L., Dubnau, D., Venema, G., & Hamoen, L. (1995). comK encodes the competence transcription factor, the key regulatory protein for competence development in Bacillus subtilis. *Molecular Microbiology*. https://doi.org/10.1111/j.1365-2958.1995.tb02259.x

van Sinderen, D., ten Berge, A., Hayema, B. J., Hamoen, L., & Venema, G. (1994). Molecular cloning and sequence of comK, a gene required for genetic competence in Bacillus subtilis. *Molecular Microbiology*. https://doi.org/10.1111/j.1365-2958.1994.tb00347.x

Vassylyev, D. G., Vassylyeva, M. N., Perederina, A., Tahirov, T. H., & Artsimovitch, I. (2007). Structural basis for transcription elongation by bacterial RNA polymerase. *Nature*. https://doi.org/10.1038/nature05932

Veelders, M., Brückner, S., Ott, D., Unverzagt, C., Mösch, H. U., & Essen, L. O. (2010). Structural basis of flocculin-mediated social behavior in yeast. *Proceedings of the National Academy of Sciences of the United States of America*. https://doi.org/10.1073/pnas.1013210108

Vreeland, R. H., Rosenzweig, W. D., & Powers, D. W. (2000). Isolation of a 250 million-year-old halotolerant bacterium from a primary salt crystal. *Nature*, *407*(6806), 897–900. https://doi.org/10.1038/35038060

Waagmeester, A., Thompson, J., & Reyrat, J. M. (2005). Identifying sigma factors in Mycobacterium smegmatis by comparative genomic analysis. In *Trends in Microbiology*. https://doi.org/10.1016/j.tim.2005.08.009

Wada, A., Mikkola, R., Kurland, C. G., & Ishihama, A. (2000). Growth phase-coupled changes of the ribosome profile in natural isolates and laboratory strains of Escherichia coli. *Journal of Bacteriology*. https://doi.org/10.1128/JB.182.10.2893-2899.2000

Wahl, M., Pei, H.-H., Hilal, T., Chen, Z., Huang, Y.-H., Gao, Y., Said, N., Loll, B., Rappsilber, J., Belogurov, G., & Artsimovitch, I. (2020). An energy charge sensor for balancing RNA polymerase recycling and hibernation. *Nature Communications*, *Preprint*. https://doi.org/10.21203/rs.3.rs-40617/v1

Wang, L., Guo, Y., & Gralla, J. D. (1999). Regulation of sigma 54-dependent transcription by core promoter sequences: Role of -12 region nucleotides. *Journal of Bacteriology*. https://doi.org/10.1128/jb.181.24.7558-7565.1999

Wang, X., Bukoreshtliev, N. V., & Gerdes, H. H. (2012). Developing Neurons Form Transient Nanotubes Facilitating Electrical Coupling and Calcium Signaling with Distant Astrocytes. *PLoS ONE*. https://doi.org/10.1371/journal.pone.0047429

Wang, Y., Cui, J., Sun, X., & Zhang, Y. (2011). Tunneling-nanotube development in astrocytes depends on p53 activation. *Cell Death and Differentiation*. https://doi.org/10.1038/cdd.2010.147

Wassarman, K. M., & Storz, G. (2000). 6S RNA regulates E. coli RNA polymerase activity. *Cell*. https://doi.org/10.1016/S0092-8674(00)80873-9

Watanabe, S., Ohbayashi, R., Kanesaki, Y., Saito, N., Chibazakura, T., Soga, T., & Yoshikawa, H. (2015). Intensive DNA replication and metabolism during the lag phase in Cyanobacteria. *PLoS ONE*, *10*(9), 1–16. https://doi.org/10.1371/journal.pone.0136800

Wedel, A., Weiss, D. S., Popham, D., Dröge, P., & Kustu, S. (1990). A bacterial enhancer functions to tether a transcriptional activator near a promoter. *Science*. https://doi.org/10.1126/science.1970441

Wei, X., Pathak, D. T., & Wall, D. (2011). Heterologous protein transfer within structured myxobacteria biofilms. *Molecular Microbiology*. https://doi.org/10.1111/j.1365-2958.2011.07710.x

Wei, X., Vassallo, C. N., Pathak, D. T., & Wall, D. (2014). Myxobacteria produce outer membrane-enclosed tubes in unstructured environments. *Journal of Bacteriology*. https://doi.org/10.1128/JB.00850-13

Wei, Z., Chen, C., Liu, Y. J., Dong, S., Li, J., Qi, K., Liu, S., Ding, X., De Ora, L. O., Munoz-Gutíerrez, I., Li, Y., Yao, H., Lamed, R., Bayer, E. A., Cui, Q., & Feng, Y. (2019). Alternative σi/anti-σI factors represent a unique form of bacterial σ/anti-σ complex. *Nucleic Acids Research*. https://doi.org/10.1093/nar/gkz355

Weinrauch, Y., Guillen, N., & Dubnau, D. A. (1989). Sequence and transcription mapping of Bacillus subtilis competence genes comB and comA, one of which is related to a family of bacterial regulatory determinants. *Journal of Bacteriology*. https://doi.org/10.1128/jb.171.10.5362-5375.1989

Weinrauch, Y., Msadek, T., Kunst, F., & Dubnau, D. (1991). Sequence and properties of comQ, a new competence regulatory gene of Bacillus subtilis. *Journal of Bacteriology*. https://doi.org/10.1128/jb.173.18.5685-5693.1991

Weiss, A., Moore, B. D., Tremblay, M. H. J., Chaput, D., Kremer, A., & Shaw, L. N. (2017). The Omega Subunit Governs RNA Polymerase Stability and Transcriptional Specificity in Staphylococcus aureus. *Journal of Bacteriology*, *199*(2), 1–16.

Wiegeshoff, F., Beckering, C. L., Debarbouille, M., & Marahiel, M. A. (2006). Sigma L is important for cold shock adaptation of Bacillus subtilis. *Journal of Bacteriology*. https://doi.org/10.1128/JB.188.8.3130-3133.2006

Wilson, K. S., & Von Hippel, P. H. (1995). Transcription termination at intrinsic terminators: The role of the RNA hairpin. *Proceedings of the National Academy of Sciences of the United States of America*, *92*(19), 8793–8797. https://doi.org/10.1073/pnas.92.19.8793

Wolf, D., Rippa, V., Mobarec, J. C., Sauer, P., Adlung, L., Kolb, P., & Bischofs, I. B. (2015). The quorum-sensing regulator ComA from Bacillus subtilis activates transcription using topologically distinct DNA motifs. *Nucleic Acids Research*, *44*(5), 2160–2172. https://doi.org/10.1093/nar/gkv1242

Xue, X., Li, J., Wang, W., Sztajer, H., & Wagner-Döbler, I. (2012). The global impact of the delta subunit RpoE of the RNA polymerase on the proteome of Streptococcus mutans. *Microbiology*. https://doi.org/10.1099/mic.0.047936-0

Xue, X., Tomasch, J., Sztajer, H., & Wagner-Döbler, I. (2010). The delta subunit of RNA polymerase, RpoE, is a global modulator of Streptococcus mutans environmental adaptation. *Journal of Bacteriology*. https://doi.org/10.1128/JB.00653-10

Yamamoto, H., Kurosawa, S. I., & Sekiguchi, J. (2003). Localization of the Vegetative Cell Wall Hydrolases LytC, LytE, and LytF on the Bacillus subtilis Cell Surface and Stability of These Enzymes to Cell Wall-Bound or Extracellular Proteases. *Journal of Bacteriology*. https://doi.org/10.1128/JB.185.22.6666-6677.2003

Yang, Yang, Yao, F., Zhou, M., Zhu, J., Zhang, X., Bao, W., Wu, S., Hardwidge, P. R., & Zhu, G. (2013). F18ab Escherichia coli flagella expression is regulated by acyl-homoserine lactone and contributes to bacterial virulence. *Veterinary Microbiology*, *165*(3–4), 378–383. https://doi.org/10.1016/j.vetmic.2013.04.020

Yang, Yun, Darbari, V. C., Zhang, N., Lu, D., Glyde, R., Wang, Y. P., Winkelman, J. T., Gourse, R. L., Murakami, K. S., Buck, M., & Zhang, X. (2015). Structures of the RNA polymerase-σ54 reveal new and conserved regulatory strategies. *Science*. https://doi.org/10.1126/science.aab1478

Yehudai-Resheff, S., Hirsh, M., & Schuster, G. (2001). Polynucleotide Phosphorylase Functions as Both an Exonuclease and a Poly(A) Polymerase in Spinach Chloroplasts. *Molecular and Cellular Biology*. https://doi.org/10.1128/mcb.21.16.5408-5416.2001

Yu, K., Mitchell, C., Xing, Y., Magliozzo, R. S., Bloom, B. R., & Chan, J. (1999). Toxicity of nitrogen oxides and related oxidants on mycobacteria: M. tuberculosis is resistant to peroxynitrite anion. *Tubercle and Lung Disease*. https://doi.org/10.1054/tuld.1998.0203

Zhang, G., Campbell, E. A., Minakhin, L., Richter, C., Severinov, K., & Darst, S. A. (1999). Crystal structure of thermus aquaticus core RNA polymerase at 3.3 å resolution. *Cell*. https://doi.org/10.1016/S0092-8674(00)81515-9

Zhang, X., Yang, F., Zou, J., Wu, W., Jing, H., Gou, Q., Li, H., Gu, J., Zou, Q., & Zhang, J. (2018). Immunization with Pseudomonas aeruginosa outer membrane vesicles stimulates protective immunity in mice. *Vaccine*. https://doi.org/10.1016/j.vaccine.2018.01.034

Zhu, D., Tan, K. S., Zhang, X., Sun, A. Y., Sun, G. Y., & Lee, J. C. M. (2005). Hydrogen peroxide alters membrane and cytoskeleton properties and increases intercellular connections in astrocytes. *Journal of Cell Science*. https://doi.org/10.1242/jcs.02507

Zhu, J. H., Wang, B. W., Pan, M., Zeng, Y. N., Rego, H., & Javid, B. (2018). Rifampicin can induce antibiotic tolerance in mycobacteria via paradoxical changes in rpoB transcription. *Nature Communications*. https://doi.org/10.1038/s41467-018-06667-3

Zhu, Y., Mao, C., Ge, X., Wang, Z., Lu, P., Zhang, Y., Chen, S., & Hu, Y. (2017). Characterization of a minimal type of promoter containing the -10 element and a guanine at the -14 or -13 position in mycobacteria. *Journal of Bacteriology*. https://doi.org/10.1128/JB.00385-17

Zuber, U., Drzewiecki, K., & Hecker, M. (2001). Putative sigma factor sigI (ykoZ) of Bacillus subtilis is induced by heat shock. *Journal of Bacteriology*. https://doi.org/10.1128/JB.183.4.1472-1475.2001

Zuo, Y., De, S., Feng, Y., & Steitz, T. A. (2020). Structural Insights into Transcription Initiation from De Novo RNA Synthesis to Transitioning into Elongation. *IScience*. https://doi.org/10.1016/j.isci.2020.101445

AMERICAN SOCIETY FOR MICROBIOLOGY | Journal of Bacteriology®

RESEARCH ARTICLE

The Core and Holoenzyme Forms of RNA Polymerase from *Mycobacterium smegmatis*

Tomáš Kouba,[a]* Jiří Pospíšil,[b,c] Jarmila Hnilicová,[b] Hana Šanderová,[b] Ivan Barvík,[d] Libor Krásný[b]

[a]MRC Laboratory of Molecular Biology, Cambridge, United Kingdom
[b]Laboratory of Microbial Genetics and Gene Expression, Institute of Microbiology, Academy of Sciences of the Czech Republic, Prague, Czech Republic
[c]Department of Genetics and Microbiology, Faculty of Science, Charles University in Prague, Prague, Czech Republic
[d]Division of Biomolecular Physics, Institute of Physics, Faculty of Mathematics and Physics, Charles University in Prague, Prague, Czech Republic

ABSTRACT Bacterial RNA polymerase (RNAP) is essential for gene expression and as such is a valid drug target. Hence, it is imperative to know its structure and dynamics. Here, we present two as-yet-unreported forms of *Mycobacterium smegmatis* RNAP: core and holoenzyme containing σ^A but no other factors. Each form was detected by cryo-electron microscopy in two major conformations. Comparisons of these structures with known structures of other RNAPs reveal a high degree of conformational flexibility of the mycobacterial enzyme and confirm that region 1.1 of σ^A is directed into the primary channel of RNAP. Taken together, we describe the conformational changes of unrestrained mycobacterial RNAP.

IMPORTANCE We describe here three-dimensional structures of core and holoenzyme forms of mycobacterial RNA polymerase (RNAP) solved by cryo-electron microscopy. These structures fill the thus-far-empty spots in the gallery of the pivotal forms of mycobacterial RNAP and illuminate the extent of conformational dynamics of this enzyme. The presented findings may facilitate future designs of antimycobacterial drugs targeting RNAP.

KEYWORDS RNA polymerase, bacterial transcription, conformational change, cryo-electron microscopy, mycobacteria, protein structure, transcription initiation factor

Mycobacteria are a group of medicinally important bacteria with a number of species that cause serious human and animal diseases, such as tuberculosis, which ranks among the top 10 causes of death worldwide according to the World Health Organization. Understanding the molecular machinery of these organisms is necessary to combat these pathogens.

RNA polymerase (RNAP) is a central enzyme of gene expression and, as such, it is an attractive drug target. Rifampin, an antibiotic binding to RNAP, has been used to treat tuberculosis since the late 1960s, but mycobacteria are able to gain resistance due to point mutations of amino acids in the rifampin-binding cavity (1). Detailed knowledge of the RNAP structure and dynamics is thus fundamental for the rational design of new RNAP inhibitors (2).

RNAP is a multisubunit enzyme consisting of an α dimer and β, β', and ω subunits (3). This RNAP core is catalytically active, but to initiate transcription it needs a sigma factor. σ^A is the principal sigma factor responsible for transcription of housekeeping genes (4). Eventually, other subunits, in particular, various transcription activators such as CarD (5) or RpbA (6, 7), may be associated with the RNAP holoenzyme.

σ^A (σ^{70} in *Escherichia coli*) is composed of domains 1 to 4, some of which are further subdivided (4). Interestingly, region 1.1 of σ^A is still somewhat elusive even after almost two decades of structural studies. It is usually partly or fully missing in the bacterial RNAP crystal structures. A notable exception is $\sigma^A{}_{1.1}$ from *E. coli*, which was solved by

Citation Kouba T, Pospíšil J, Hnilicová J, Šanderová H, Barvík I, Krásný L. 2019. The core and holoenzyme forms of RNA polymerase from *Mycobacterium smegmatis*. J Bacteriol 201:e00583-18. https://doi.org/10.1128/JB.00583-18.

Editor Ann M. Stock, Rutgers University-Robert Wood Johnson Medical School

Address correspondence to Tomáš Kouba, tkouba@embl.fr, or Libor Krásný, krasny@biomed.cas.cz.

* Present address: Tomáš Kouba, EMBL Grenoble, Grenoble, France.

Received 20 September 2018
Accepted 20 November 2018
Accepted manuscript posted online 26 November 2018
Published 28 January 2019

crystallography in complex with RNAP, where it is positioned in the primary channel of RNAP (8), from which it must be displaced by DNA during transcription initiation. Otherwise, only isolated structures of $\sigma^{A}_{1.1}$ from *Thermotoga maritima* and *Bacillus subtilis* were determined by using nuclear magnetic resonance (9, 10).

The 1.1 domains from all these organisms are playing the same roles. They prevent binding of the σ^{A} free form to promoter DNA. Further, they prevent access of DNA to the active site of RNAP prior to formation of the catalytically competent transcription initiation complex. However, the structural details between 1.1 domains from different organisms vary widely. Currently, three types of known structures of this domain exist: (i) the highly similar structures, as solved for *B. subtilis* and *E. coli*, consisting of three helices (HI to HIII) packed in antiparallel manner (8, 10); (ii) the structure from *T. maritima*, where HI packs perpendicularly to HII and HIII (9); and (iii) the possibly disordered and flexible structure from mycobacteria with only the $\sigma^{A}_{\text{N-helix}}$ discernible (11–14).

Transcription initiation is a highly dynamic process and conformational changes of RNAP are required for it to happen (15, 16). RNAP first forms the closed complex (RP_C) with promoter DNA, in which the two DNA strands are still together; subsequently, the complex isomerizes through a kinetic intermediate(s) to the open complex (RP_O), where the DNA is opened from positions −10 to +2 (relative to +1, the transcription start) (17–19). In mycobacteria, the conformational change from RP_C to RP_O is greatly stimulated by the presence of transcriptional factors RpbA and CarD in a cooperative manner (12, 20). RP_O is also stabilized by the presence of nucleoside triphosphates (NTPs) complementary to the +1 and, to a lesser degree, the +2 transcription positions of the template strand (10, 21).

Historically, the established structural models of bacterial transcription were based on studies of RNAP from *Thermus aquaticus*, *Thermus thermophilus*, and *Escherichia coli*. However, even alignments of amino acids of individual subunits from various species reveal significant differences between these enzymes and studies addressing this variety have now only just begun (22). Hence, structural studies were recently published, focusing on specific transcription systems, especially those from, or related to pathogenic species, such as *Mycobacterium tuberculosis* (11, 14, 23) and *Mycobacterium smegmatis* (12, 13).

Currently, cryo-electron microscopy (cryo-EM) structures are available for *M. tuberculosis* RNAP σ^{A} in complexes (see Table 1) with RbpA (PDB entry 6C05 [11]), fidaxomicin (PDB entry 6FBV [23]), or both (PDB entry 6C06 [11]) and with RbpA and double-fork DNA (PDB entry 6C04 [11]) or RbpA, fidaxomicin, and upstream-fork DNA (PDB entry 6BZO [11]). Moreover, crystal structures have been reported for *M. smegmatis* RNAP σ^{A} in complex with RbpA and upstream fork DNA (PDB entry 5VI8 [12]), RP_O with RbpA (PDB entry 5VI5 [13]), the *M. tuberculosis* RNAP σ^{A} holoenzyme with downstream fork DNA and with various inhibitors (including rifampin and *N*-α-aroyl-*N*-aryl-phenylalaninamides) and short fragments (2 to 4 nucleotides [nt]) of RNA (PDB entries 5UHA, 5UHB, 5UHE, 5UHF, 5UHG, 5UH7, 5UH9, 5UH5, 5UH8, 5UH6, 5UHC, and 5UHD [14]) (see Table 1).

Compared to previously known structures of RNAPs from other organisms, the mycobacterial RNAPs contain a prominent feature, a long α-helical coiled-coil domain protruding from the β' clamp (β'il), and the models also depict the position of a part of the N-terminal segment of the σ^{A} factor. Both of these elements are involved in specific mechanisms of transcription initiation. It was proposed that the taxon-specific mycobacterial RNAP structural features might help stabilize the very labile mycobacterial RP_O (14), but the mechanistic details are still debated (12). Furthermore, the cryo-EM three-dimensional (3D) structures, which are captured in almost native states, hint at the importance of the β' clamp dynamics during transition from RP_C to RP_O.

Here, using cryo-EM, we describe the as-yet-unreported *M. smegmatis* RNAP core and holoenzyme structures containing σ^{A} but no other factors. The structural information presented here provides further details on the taxon-specific nonconserved extension, β'i1, in the β' subunit of RNAP, as well as the N-terminal part of the σ^{A} factor

(region 1.1). In summary, the RNAP core and RNAP σ^A structures, combined with the published models of *M. smegmatis* and *M. tuberculosis* RNAPs (see Tables 1 and 2), reveal the extent of conformational changes of mycobacterial RNAP and complete the gallery of the pivotal forms of the enzyme.

RESULTS AND DISCUSSION

Cryo-EM microscopy of *M. smegmatis* RNAP. We cloned all the *M. smegmatis* RNAP core subunits into a plasmid (see Fig. S1A in the supplemental material), overexpressed in *E. coli*, and purified. The purification procedure consisted of affinity tag purification, followed by high-salt washes and size exclusion chromatography (Fig. S1B). The elution peak included a fractional shoulder, suggesting a minor heterogeneity of the sample. We also found that intermediate ion exchange cleaning steps induced a loss of the ω subunit and therefore were excluded from the purification procedure. Also, we prepared *M. smegmatis* σ^A (for details, see Materials and Methods). Subsequently, we used these recombinant proteins to reconstitute the *M. smegmatis* RNAP σ^A holoenzyme (Fig. S1B). We verified its enzymatic activity in an *in vitro* transcription assay using a DNA template with a native ribosomal promoter (Fig. S1C).

Several vitrification conditions were tested to prepare cryo-EM specimens of the *M. smegmatis* RNAP σ^A holoenzyme. Free standing vitreous ice conditions introduced a strong preferred orientation of RNAP molecules and were limited to a single view, and, consequently, unsuited for 3D reconstructions. To circumvent this problem, we used graphene oxide supports, which allowed a much broader distribution of RNAP orientations (for details see Materials and Methods and Fig. S2A, B, and E). However, the graphene oxide support required a relatively low protein concentration (~110 nM) in the vitreous specimen, and the low protein concentration caused a partial dissociation of the RNAP holoenzyme (σ^A binds to the RNAP core with a K_d of ~90 nM, as measured by isothermal titration calorimetry [data not shown]).

In total, we imaged ~500,000 single-particle images of RNAP molecules. Several rounds of unsupervised 3D particle classifications to high degree of angular accuracy (for details, see Materials and Methods) separated all presented structural species and produced cryo-EM densities for each of them (Fig. S2C and D). Primarily, we targeted the *M. smegmatis* RNAP σ^A holoenzyme, but as a result of the low protein concentration in the cryo-EM specimens, we also identified RNAP core particles in the data set.

Hence, two main forms of *M. smegmatis* RNAP were identified: core and holoenzyme. Moreover, both of them were detected in two major conformations. These conformations were represented by the two most abundant 3D classes of each form, and they were clearly distinguishable by the correlation coefficient of fit in the map tool in Chimera (for the number of particles in each class, see Fig. S2C). The remaining minor 3D classes were not analyzed. The resolutions of the cryo-EM density maps for the most abundant 3D classes of the *M. smegmatis* RNAP core (here referred to as Core1) and RNAP σ^A holoenzyme (here referred to as Holo1) were estimated at 3.8 and 4.2 Å at the 0.143 gold standard Fourier shell correlation (FSC) cutoff (Fig. S2F). The resolutions of the cryo-EM density maps for the second most abundant 3D classes, here referred to as Core2 and Holo2, were estimated at 4.3 and 4.9 Å, respectively (Fig. S2F). Local resolution calculations (Fig. S3) indicated that the central part of the complexes was more defined than the peripheries. A particle orientation efficiency score (24) of ~0.47 (Table S1) suggested a minor Fourier space gap in the 3D electron densities volumes and probably slightly hampered the final resolution (a particle orientation efficiency score of >0.6 is reported to be optimal [18]), but no 3D deformation related to poor particle distribution was observed.

Construction of atomic models of *M. smegmatis* RNAP. The protein chains of *M. smegmatis* RNAP were fitted into the produced cryo-EM densities. Atomic models of core and holoenzyme were generated (Fig. 1; see also Fig. S3 and S4) using the crystal structure of *M. smegmatis* transcription initiation complex (TIC) and RP_O as the templates (PDB entries 5VI8 and 5VI5 [12, 13]). For further details, see Materials and Methods.

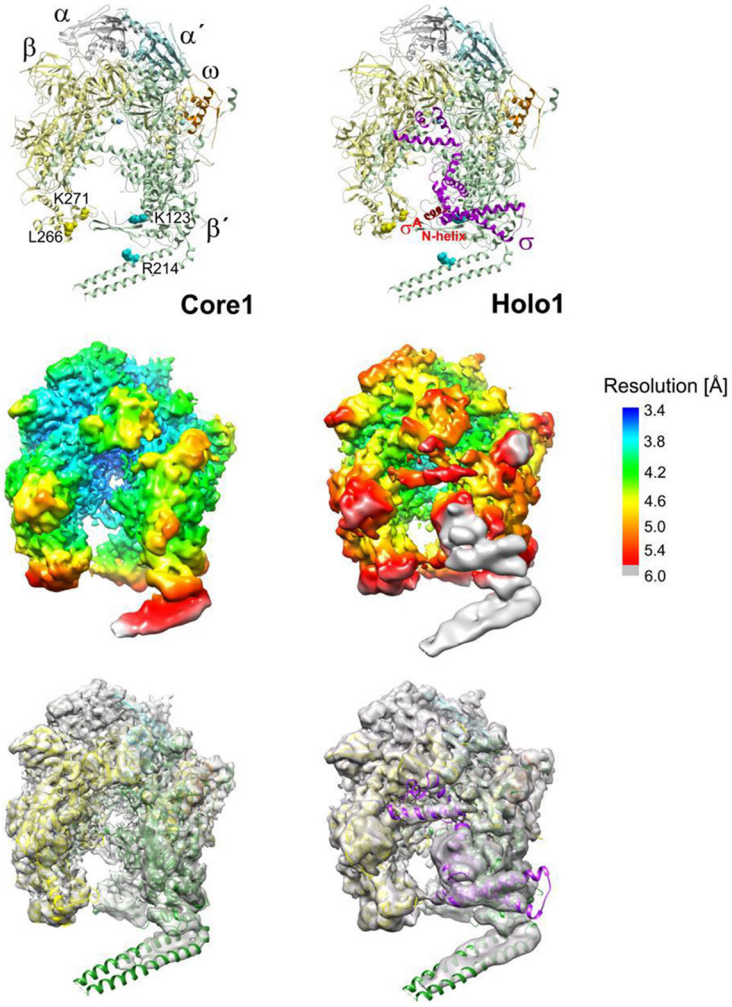

FIG 1 Cryo-EM structure determinations of *M. smegmatis* RNAP complexes. (Top row) Secondary structures of two forms of RNAP from *M. smegmatis* as observed in the experimental cryo-EM densities: core (left) and holoenzyme (right, RNAP in complex with primary sigma factor, σ^A). Subunits are colored as follows: β, yellow; β', green; α, gray; α', cyan; ω, orange; σ^A, magenta. (Middle row) Cryo-EM maps are filtered and colored according to local resolution calculated with the RELION software package (see Fig. S3 for more detail). (Bottom row) Cryo-EM maps, together with fit of secondary structure models of *M. smegmatis* RNAP complexes. Maps are visualized as 0.5 transparent at 0.08 volume threshold in Chimera (see Fig. S4 for more detail). Color coding is as described for the top row.

Next, we superimposed the obtained models over the other recent X-ray and cryo-EM structures and this provided three main insights into the structure of *M. smegmatis* RNAP: (i) structural arrangement of the primary channel, the binding site for the downstream DNA (dwDNA) in the RNAP core; (ii) movements of the nonconserved coiled-coil domain β'i1 that is specific for mycobacteria; and (iii) interaction of the RNAP core with σ^A, including the position of the structured part of the σ^A region 1.1 in the holoenzyme. This information contributes to the recent discussion of how these two latter elements influence the transcription initiation and especially the formation of RP_O, as they virtually block passage of DNA template into the active site of RNAP.

(i) Conformational changes of conserved parts of the *M. smegmatis* RNAP primary channel. The overall shape of RNAP resembles a crab claw with the two pincers (the clamp consisting of parts of β and β' subunits) forming the primary channel. In the primary channel, RNAP interacts with 14 bp of the DNA downstream of the active site (25). This interaction causes changes in the positions of the two pincers along the defined molecular hinges of switch regions (Table S2) (26). It was shown that the RNAP clamp is predominantly open in the free RNAP core form and RP_C, but closed

TABLE 1 Distances between the β and β' subunits at the narrowest point of the dwDNA entrance: βLys271Cα and β'Lys123Cα (*M. smegmatis*) and βLys280Cα and β'Lys123Cα (*M. tuberculosis*)[a]

RNAP complex	Organism	Distance (Å)	Residues	PDB entry	Source or reference
Core1	*M. smegmatis*	28.0	K271-K123	6F6W[EM]	This study
Core2	*M. smegmatis*	32.2	K271-K123	NA	This study
Holo1	*M. smegmatis*	29.4	K271-K123	6EYD[EM]	This study
Holo2	*M. smegmatis*	33.6	K271-K123	NA	This study
holo + RbpA	*M. tuberculosis*	29.9	K280-K123	6C05[EM]	11
holo + LpM	*M. tuberculosis*	34.2	K280-K123	6FBV[EM]	23
holo + RbpA + Fdx	*M. tuberculosis*	33.6	K280-K123	6C06[EM]	11
holo + RbpA + Fdx + up	*M. tuberculosis*	32.3	K280-K123	6BZO[EM]	11
holo + RbpA + up + down	*M. tuberculosis*	19	K280-K123	6C04[EM]	11
holo + down	*M. tuberculosis*	18.7	K280-K123	5UHA[XR]	14
holo + down + Rif	*M. tuberculosis*	18.8	K280-K123	5UHB[XR]	14
holo + down + D-AAP1	*M. tuberculosis*	18.7	K280-K123	5UHE[XR]	14
holo + down + D-IX336	*M. tuberculosis*	18.3	K280-K123	5UHF[XR]	14
holo + down + Rif + D-AAP1	*M. tuberculosis*	18.3	K280-K123	5UHG[XR]	14
holo + RbpA + up	*M. smegmatis*	17.8	K271-K123	5VI8[XR]	12
RP_O + RbpA	*M. smegmatis*	20.0	K271-K123	5VI5[XR]	13
holo + down + 2 nt RNA	*M. tuberculosis*	18.3	K280-K123	5UH9[XR]	14
holo + down + 3 nt RNA	*M. tuberculosis*	18.5	K280-K123	5UH5[XR]	14
holo + down + 4 nt RNA	*M. tuberculosis*	18.4	K280-K123	5UH8[XR]	14
holo + down + Rif + 2 nt RNA	*M. tuberculosis*	18.7	K280-K123	5UH6[XR]	14
holo + down + Rif + 3 nt RNA	*M. tuberculosis*	18.2	K280-K123	5UHC[XR]	14
holo + down + Rif + 4 nt RNA	*M. tuberculosis*	18.5	K280-K123	5UHD[XR]	14

[a]"up" stands for DNA upstream fork; "down" stands for DNA downstream fork. nt, nucleotide(s); holo, holoenzyme; Fdx, fidaxomicin; LpM, lipiarmycin A3; Rif, rifampin; D-AAP1, *N*-α-(benzenecarbonyl)-*N*-(2-methylphenyl)-D-phenylalaninamide; D-IX336, *N*-(2-methylphenyl)-*N*-α-(selenophene-2-carbonyl)-D-phenylalaninamide; NA, not applicable. Superscripts: XR, X-ray; EM, Cryo-EM.

in RP_O, initial transcribing complexes (RP_{ITC}), and a transcription elongation complex (EC) (15, 27).

We quantitated the extent of these conformational changes (Table 1 and Fig. 2; see also Fig. S5) between various forms of the mycobacterial enzyme by measuring the distance between the β and β' subunits at the narrowest point of the dwDNA entrance (i.e., distance between βLys271Cα and β'Lys123Cα). This distance is only approximately 17.8 to 20 Å (Table 1) in the closed dwDNA primary channel-occupied structures, as well as in structures containing RbpA and upstream fork DNA 5VI8 (12) that securely hold DNA. On the other hand, it is approximately 28.0 to 34.2 Å (Table 1) in the case of the open core and holoenzyme structures, which would allow a double-stranded dwDNA to enter the primary channel. The open conformation seems to be an intrinsic feature of the RNAP core itself, as observed for both the Core1 and Core2, and is not dependent on the presence the σ factor, a finding consistent with previous observations (15). We also confirm that the mycobacterial holoenzyme favors the open state (11, 15, 23, 27), since the Holo1 conformation is similar to the relaxed open state of the RNAP Holo/RbpA (11), and the Holo2 conformation is similar to the one in the extreme open form trapped by fidaxomicin (11, 23). This in agreement with the observation that the conformational change toward the close state occurs only after binding of dwDNA.

(ii) RNAP core and holoenzyme structures reveal a new position of the non-conserved domain β'i1 of *M. smegmatis* RNAP. Even though the local resolution of β'i1 is relatively low (Fig. S4), we were able to localize its position according to the fit of secondary structures (Fig. S5 and S6). β'i1 was previously reported to hold its extended coiled-coil fold independently (14), and thus even the incomplete density may determine its full position. However, the lack of cryo-EM density in the area where the tip of the domain would be predicted suggests that this region displays some degree of flexibility relative to the rest of the domain.

Contrary to the previously characterized X-ray and cryo-EM closed-clamp structures containing dwDNA (Table 1) (11–14), but similar to the recent open-clamp holoenzyme complexes with RbpA and/or fidaxomicin determined by cryo-EM (Table 1) (11, 23), the position of the β'i1 domain in both our open-clamp RNAP core and holoenzyme structures is markedly swung outwards relative to the β domain 2 (Fig. 2). This

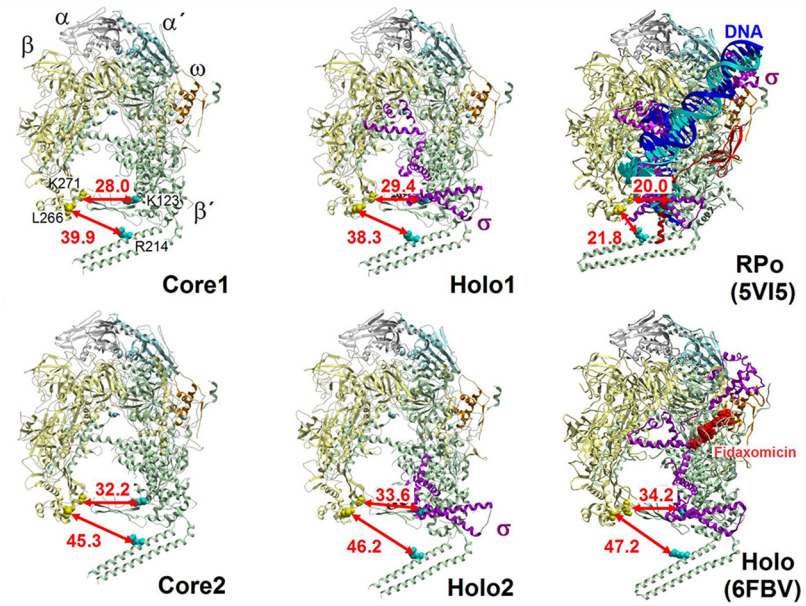

FIG 2 *M. smegmatis* RNAP exhibits conformational dynamics. Conformational dynamics are illustrated by distances (arrows) between the β and β' subunits at the narrowest point of the dwDNA entrance (distance between βGly271Cα and β'Lys123Cα) and by positioning of the nonconserved domain β'i1 (distances between βLeu266Cα and β'Arg214Cα) in the main conformation of *M. smegmatis* RNAP. Core1/Core2 and Holo1/Holo2 represent the two most represented conformations of respective forms of *M. smegmatis* RNAP. Closed RNAP conformations of *M. smegmatis* RPo (PDB entry 5VI5) and *M. tuberculosis* holoenzyme in complex with the antibacterial compound fidaxomicin (PDB entry 6FBV) that traps the open conformation of the pincer are shown for comparison. RNAP subunits and nucleic acids chains are colored as follows: β, yellow; β', green; α, gray; α', cyan; ω, orange; σA, magenta; DNA duplex, blue and cyan.

displacement increases further from the rotational axis defined by the switch regions (Table S2), and the central part of the β'i1, which is the closest to the β domain 2 (Table S2), is relocated up to ~25 Å (in terms of the βLeu266Cα – β'Arg214Cα distance) (Table 2 and Fig. 2; see also Fig. S5 and S6). This conformation also widens the passage between β'i1 and β domain 2 to around 30 Å and at the same time promotes a steric funneling toward the primary channel.

Lin et al. (14) suggested that β'i1 could rotate with respect to the rest of the β' clamp (β'1-133 and β'255-404) around a presumed hinge in-between these two domains. This, then, should allow opening of the DNA passageway toward the primary channel. Therefore, we analyzed the location of β'i1 with respect to the rest of the β' clamp in all variants of *M. smegmatis* RNAP complexes. The mutual orientations of these two domains stay rigid, and thus we conclude that there is no molecular hinge between these domains that would allow β'i1 any substantial movements with respect to the rest of the β' clamp. Nevertheless, the lack of any cryo-EM density for the β'il RNAP-distal part (the tip) then suggests that the tip may display some flexibility relative to the RNAP-proximal part of this domain. This flexibility may play a role in accommodation of DNA in the primary channel. Together, this confirms that solely the molecular hinge of the β' switch regions allows for flexible arrangement of the β' clamp and the adjacent β'il, and this opens the enzyme pincer enough to let double-stranded DNA pass through and accommodate it into the primary channel and the active site, similar to what has been recently reported for *E. coli* RNAP with a partially loaded DNA promoter (18, 19). It should be noted that in the case of the holoenzyme, part of the primary channel might be occupied by the sigma factor and thus reduce the actual space available for DNA. This might be a reason why RNAP molecules exhibit conformations where the pincer is splayed to around 30 Å.

(iii) Interaction of the RNAP core with σ^A and movement of $\sigma^A{}_{1.1}$. Our cryo-EM structure of the *M. smegmatis* holoenzyme lacks cryo-EM densities for the $\sigma^A{}_{3.2}$ and $\sigma^A{}_4$

TABLE 2 Positioning of the nonconserved domain β′i1 of *M. smegmatis* RNAP: distances between βLeu266Cα and β′Arg214Cα (*M. smegmatis*) and βLeu275Cα and β′Arg214Cα (*M. tuberculosis*)[a]

RNAP complex	Organism	Distance (Å)	Residues	PDB entry	Source or reference
Core1	*M. smegmatis*	39.9	L266-R214	6F6W[EM]	This study
Core2	*M. smegmatis*	45.3	L266-R214	NA	This study
Holo1	*M. smegmatis*	38.3	L266-R214	6EYD[EM]	This study
Holo2	*M. smegmatis*	46.2	L266-R214	NA	This study
holo + RbpA	*M. tuberculosis*	38.7	L275-R214	6C05[EM]	11
holo + LpM	*M. tuberculosis*	47.2	L275-R214	6FBV[EM]	23
holo + RbpA + Fdx	*M. tuberculosis*	45.3	L275-R214	6C06[EM]	11
holo + RbpA + Fdx + up	*M. tuberculosis*	43.3	L275-R214	6BZO[EM]	11
holo + RbpA + up + down	*M. tuberculosis*	23.7	L275-R214	6C04[EM]	11
holo + down	*M. tuberculosis*	21.9	L275-R214	5UHA[XR]	14
holo + down + Rif	*M. tuberculosis*	22	L275-R214	5UHB[XR]	14
holo + down + D-AAP1	*M. tuberculosis*	21.4	L275-R214	5UHE[XR]	14
holo + down + D-IX336	*M. tuberculosis*	21.7	L275-R214	5UHF[XR]	14
holo + down + Rif + D-AAP1	*M. tuberculosis*	21.2	L275-R214	5UHG[XR]	14
holo + RbpA + up	*M. smegmatis*	21.4	L266-R214	5VI8[XR]	12
RP_O + RbpA	*M. smegmatis*	21.8	L266-R214	5VI5[XR]	13
holo + down + 2 nt RNA	*M. tuberculosis*	22.2	L275-R214	5UH9[XR]	14
holo + down + 3 nt RNA	*M. tuberculosis*	22.2	L275-R214	5UH5[XR]	14
holo + down + 4 nt RNA	*M. tuberculosis*	22.1	L275-R214	5UH8[XR]	14
holo + down + Rif + 2 nt RNA	*M. tuberculosis*	22.5	L275-R214	5UH6[XR]	14
holo + down + Rif + 3 nt RNA	*M. tuberculosis*	22.1	L275-R214	5UHC[XR]	14
holo + down + Rif + 4 nt RNA	*M. tuberculosis*	21.9	L275-R214	5UHD[XR]	14

[a]"up" stands for DNA upstream fork; "down" stands for DNA downstream fork. nt, nucleotide(s); Fdx, fidaxomicin; LpM, lipiarmycin A3; Rif, rifampin; D-AAP1, *N*-α-(benzenecarbonyl)-*N*-(2-methylphenyl)-D-phenylalaninamide; D-IX336, *N*-(2-methylphenyl)-*N*-α-(selenophene-2-carbonyl)-D-phenylalaninamide; NA, not applicable. Superscripts: XR, X-ray; EM, cryo-EM.

C-terminal regions (Fig. 3), which usually protrude through RNA exit channel in holoenzyme structures of bacterial polymerases (12). The constituents of the RNA exit channel cleft, the region of the β′ flap, are generally not very well defined in the presented electron microscopic structures, and the β-flap tip (β 802 to 822) is missing entirely. The RNA exit cleft itself is wider compared to holoenzymes with a defined $\sigma_{3.2-4}$ region. This may be a consequence of the absence of other factors (like RpbA and/or antibacterial compounds) that were present in previous mycobacterial holoenzyme structures (11, 23).

A major difference exists in sequence and structure between *E. coli* $\sigma^{70}_{1.1}$ (including its preceding linker) and the equivalent N-terminal part of the σ^A region (σ^A_N) from mycobacteria, and this is reflected in interactions of this region with RNAP (Fig. 3). Whereas the *E. coli* $\sigma^{70}_{1.1}$ was identified in the primary channel in the RNAP holoenzyme (8), it still remained unclear whether mycobacterial σ^A_N was directed outside by its $\sigma^A_{N\text{-helix}}$ (12, 14).

In previously published mycobacterial RNAP closed conformation structures (i.e., PDB entries 5VI8 [12]; 5VI5 [13]; 5UHA, 5UHB, 5UHE, 5UHF, 5UHG, 5UH9, 5UH5, 5UH8, 5UH6, 5UHC, and 5UHD [14]; and 6C04 [11]), the σ^A region 1.1 appeared to be mostly unstructured with only the $\sigma^A_{N\text{-helix}}$ (σ^A 149 to 162) well defined and positioned outside the RNAP active site cleft on periphery in between the β and β′ subunit claws, parallel to the taxon-specific β′i1 finger (Fig. 3, middle). Two different proposals have been made regarding the position of mycobacterial σ^A_N in RNAP holoenzyme: first, it was proposed that, that unlike *E. coli* $\sigma^{70}_{1.1}$, *M. smegmatis* σ^A_N may never reside in the RNAP active-site cleft (12), whereas it was previously proposed that, like Eco *E. coli* $\sigma^{70}_{1.1}$, mycobacterial σ^A_N resides in the active-site cleft in RNAP holoenzyme (14).

Consistent with the second model (14), the *M. tuberculosis* $\sigma^A_{N\text{-helix}}$ (defined by residues σ^A 207 to 225 that is preceded by a short defined loop [σ^A 202 to 206], which is buttressed by β domain 2) was directed into the RNAP active-site cleft in several recent open-clamp conformation structures of *M. tuberculosis* RNAP (PDB entries 6C05, 6C06, and 6BZO [11] and in cryo-EM density EMDataBank [EMD] entry EMD-4230 [23]). However, this interesting fact was not mentioned (11, 23).

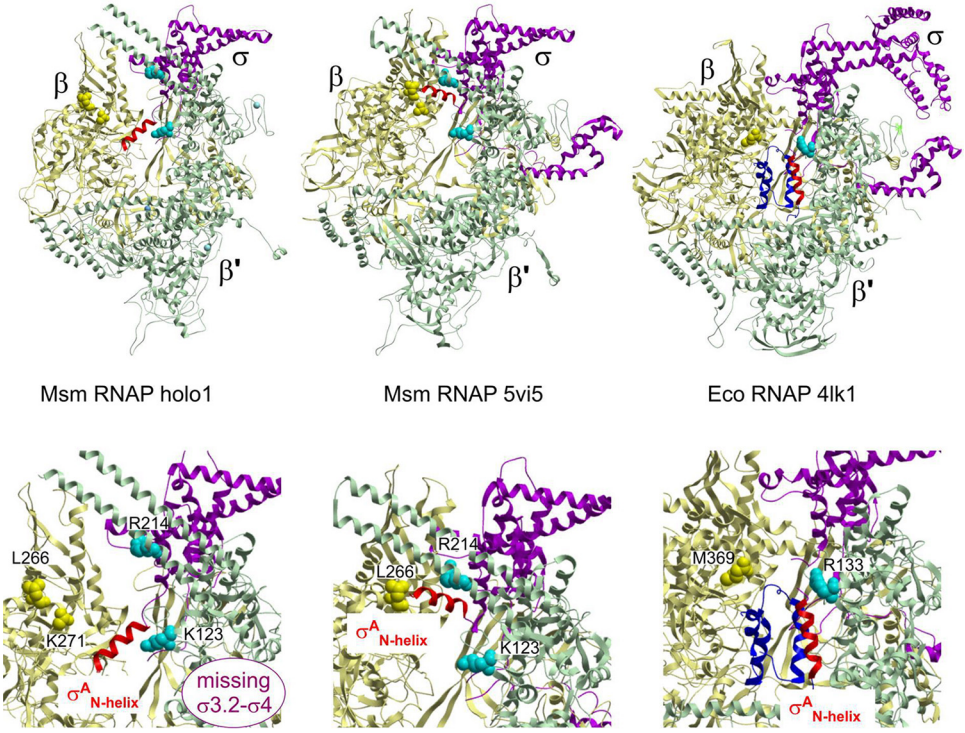

FIG 3 The σAN-helix changes position within the RNAP. (Top left) The N-terminal α-helix (red) of σA (amino acids [aa] 149 to 162) is located within the primary channel of the *M. smegmatis* open-conformation holoenzyme RNAP. The σAN-helix is positioned between the β′ coiled-coil and the inner edge of β domain 2 (Table S2) and oriented perpendicular to the nonconserved domain (NCD) β′i1 finger. (Top middle) The N-terminal α-helix (red) of σA (aa 149 to 162) in the closed-conformation mycobacterial RNAP structures (12) is positioned on the periphery in between the β and σ′ subunit claws, parallel to the NCD β′i1 finger. (Top right) σ701.1 from *E. coli* in complex with RNAP positioned in the primary channel of RNAP (8). RNAP subunits are colored as follows: β, yellow; β′, green; α, gray; α′, cyan; ω, orange; σA/70, magenta; the N-terminal part of σA/70, dark blue; σAN-helix, red. (Bottom row) Detailed views of the respective σA/70N helix regions from the structures in the upper row.

We here describe here that in the open-clamp holoenzyme structure the $\sigma^{A}_{N\text{-helix}}$ is present within the primary channel (Fig. 3, left; see Fig. S7). There, the $\sigma^{A}_{N\text{-helix}}$ (namely, amino acids Ala149-Ala161) is positioned between the β and β′ subunit claws, spanning from the β′ coiled-coil to the inner edge of β domain 2 (Table S2) and perpendicular to β′i1. The $\sigma^{A}_{N\text{-helix}}$ must be displaced from this position in between the RNAP claw to permit a conformational change during RP_O formation, since it would clash with incoming or even already loaded DNA. This is in agreement with the observation that deletion of the 1.1 region influences the stability of mycobacterial RP_O (14). The rest of the 1.1 region is not defined, but it is clear the *M. smegmatis* $\sigma^{A}_{N\text{-helix}}$ plays a pivotal role in positioning of the N-terminal part of the σ^{A} protein and, in the case of the holoenzyme the $\sigma^{A}_{N\text{-helix}}$, probably directs at least a part of it into the downstream region of the primary channel.

The positioning and movement of region 1.1 must also depend on the net negative charge within the σ^{A}_{N} disordered part (12) that likely drives its positioning in between the positively charged inner surface of the clamp and β′i1. On the other hand, the positively charged first part of σ^{A}_{N} might interact with the negatively charged surface of RNAP and the outer side of β′i1. A potential functional role of this directional charge arrangement needs to be further clarified.

To conclude, the mycobacterial RNAP core and holoenzyme structures presented here, combined with other reported structures of mycobacterial RNAP, complete the overall picture of the main conformational forms of this enzyme.

MATERIALS AND METHODS

Bacterial strains and plasmids. Vector pAC22 (a pET28a derivative, a gift from Bob Landick Lab) containing *Mycobacterium bovis* RNAP core subunit genes was used as a template to create an analogous

vector containing *M. smegmatis* RNAP core genes. *rpoA*, *rpoZ*, *rpoB*, and *rpoC* were amplified by PCR using primers listed in Table S3 in the supplemental material and genomic DNA of *Mycobacterium smegmatis* mc²155 as a template. The *M. smegmatis rpoA* gene was inserted to the pAC22 vector via XbaI and PacI restriction sites. The *rpoC* gene was assembled from two amplified fragments via the KpnI restriction site, and the complete gene, containing an 8×His tag on the 3′ end, was then inserted into the pAC22 vector via BamHI and AscI restriction sites. The *rpoB* gene was inserted together with a 9-amino-acid polylinker via NotI and AscI restriction sites and connected in frame to *rpoC*. Finally, the *rpoZ* gene was inserted into the pAC22 vector via the PacI and NotI restriction sites. The final vector, pRMS4, encodes a polycistronic transcript for expression of all five RNAP core subunits (Fig. S1A). It contains a β' C-terminal 8×His tag for affinity purification. Expression is driven from a T7 RNAP-dependent promoter.

pSigA-His6 encoding *M. smegmatis* Sigma A factor was prepared as follows. The *mysA* gene was cloned into the pET22b+ expression vector via EcoRI and XhoI restriction sites. The *mysA* gene thus obtained a 6×His tag at the 3′ end.

***M. smegmatis* RNAP core purification.** *E. coli* strain BL21(DE3) was transformed with the pRMS4(kanR) plasmid. To express and purify *M. smegmatis* RNAP, cultures were incubated at 37°C until reaching an optical density at 600 nm (OD_{600}) of ~0.8; expression was induced with 500 μM IPTG (isopropyl-β-D-thiogalactopyranoside) at 17°C for 16 h. Cells were lysed using sonication by Sonic dismembrator model 705 (Fisher Scientific) in a lysis buffer containing 50 mM NaH_2PO_4-Na_2HPO_4 (pH 8; 4°C), 300 mM NaCl, 2.5 mM $MgCl_2$, 30 mM imidazole, 5 mM β-mercaptoethanol, EDTA-free protease inhibitor cocktail (Roche), RNase A (Sigma), DNase I (Sigma), and lysozyme (Sigma). Clarified lysate was loaded onto a HisTrap FF crude column (GE Healthcare), and proteins were eluted with a linear gradient of imidazole to a final concentration of 400 mM over 20 column volumes. The *M. smegmatis* RNAP core elution fractions were pooled and dialyzed to 20 mM Tris-HCl (pH 8; 4°C), 1 M NaCl, 5% (vol/vol) glycerol, and 4 mM dithiothreitol (DTT) for 20 h. The protein was further purified on a XK 26/70 Superose 6-pg column (GE Healthcare) equilibrated in 20 mM Tris-HCl (pH 8; 4°C), 300 mM NaCl, 5% (vol/vol) glycerol, and 4 mM DTT. The final *M. smegmatis* RNAP core fractions were eluted at 6 μM, aliquoted, flash-frozen in liquid nitrogen, and then stored at −80°C.

SigA (σ^A) factor purification. *E. coli* strain BL21(DE3) was transformed with pET22b+(ampR) plasmid derivative encoding the *M. smegmatis* σ^A factor fusion with a C-terminal 8×His tag, transcribed from a T7 promoter. To express and purify σ^A, the culture was incubated at 37°C until the OD_{600} reached ~0.8; expression was induced with 500 μM IPTG at 17°C for 16 h. Cells were lysed using sonication by Sonic dismembrator model 705 (Fisher Scientific) in a lysis buffer containing 50 mM NaH_2PO_4-Na_2HPO_4 (pH 8; 4°C), 300 mM NaCl, 2.5 mM $MgCl_2$, 30 mM imidazole, 5 mM β-mercaptoethanol, EDTA-free protease inhibitor cocktail (Roche), RNase A (Sigma), DNase I (Sigma), and lysozyme (Sigma). Clarified lysate was loaded onto a HisTrap FF crude column (GE Healthcare), and proteins were eluted with a linear gradient of imidazole to the final concentration of 400 mM over 20 column volumes. Fractions containing σ^A were pooled and dialyzed for 20 h against the dialysis buffer containing 20 mM Tris-HCl (pH 8; 4°C), 200 mM NaCl, 5% (vol/vol) glycerol, and 4 mM DTT and then loaded onto a HiTrap heparin HP column (GE Healthcare), followed by column equilibration in dialysis buffer containing 350 mM NaCl. The protein was then eluted in one step with dialysis buffer containing 450 mM NaCl. Finally, the elution fractions were directly subjected to a size exclusion chromatography using a Superdex 75 column (GE Healthcare) equilibrated in 20 mM Tris-HCl (pH 8; 4°C), 300 mM NaCl, 5% (vol/vol) glycerol, and 4 mM DTT. The σ^A protein was eluted at 66 μM, aliquoted, flash-frozen in liquid nitrogen, and then stored at −80°C.

***In vitro* transcription assay.** *In vitro* transcriptions were performed with two σ^A-dependent promoters: P*veg*, a *B. subtilis* vegetative promoter (28), and P*rrnAPCL1*, a *M. smegmatis* ribosomal promoter (29). Multiple-round transcription assays were carried out as described previously (29). Briefly, the RNAP core was reconstituted with σ^A for 15 min at 37°C in 1× standard transcription buffer [STB; 5 mM Tris-HCl (pH 8.0), 1 mM $Mg(C_2H_3O_2)_2$, 20 μM DTT, 10 mM KCl, and 50 μg/ml bovine serum albumin] to form holoenzyme at a ratio of 1:5 (RNAP to σ^A). Subsequently, a mixture of promoter (final concentration, 50 nM) and NTPs (the ATP, CTP, and GTP concentrations were 200 μM; the UTP concentration was 10 μM plus 2 μM radiolabeled [α-^{32}P]UTP) in STB was prepared. Finally, transcription reactions were initiated with holoenzyme (final concentration, 200 nM). All transcriptions were allowed to proceed for 15 min at 37°C. After 15 min, transcription was stopped by the addition of 1× stop solution (95% formamide, 20 mM EDTA [pH 8.0], 0.05% bromophenol blue, 0.05% xylene cyanol). Samples were loaded onto a 7% polyacrylamide gel and electrophoresed. The gels were scanned by using a a Molecular Imager_FX (Bio-Rad). Data were analyzed with QuantityOne software (Bio-Rad).

RNAP core and σ^A factor *in vitro* reconstitution for cryo-EM. To assemble the holoenzyme consisting of the RNAP core and σ^A, the individual proteins were mixed at a molar ratio of 1:3, respectively. The *in vitro* reconstitutions were carried out at 4°C, and the reconstitution mixture was incubated for 15 min. Then, 50 μl of the reconstitution mixture was injected onto a Superose 6 Increase 3.2/300 column (GE Healthcare) equilibrated in 20 mM Tris-HCl (pH 7.8; 4°C), 150 mM NaCl, 10 mM $MgCl_2$, and 2 mM DTT. Next, 50-μl fractions were collected, and the protein was eluted at 1.5 μM (~17-fold above the estimated K_d). The RNAP core and RNAP σ^A comigrated in size exclusion chromatography (SEC) in a single peak (Fig. S1B).

Electron microscopy. Reconstituted complexes were processed immediately after the last size exclusion chromatography step. Complexes were diluted to ~110 nM, and aliquots of 3 μl were applied to Quantifoil R1.2/1.3 Au 300 mesh grids coated with graphene oxide (Graphene Supermarket). The grids were incubated for 30 s at 4°C and 100% humidity, blotted for 2 s, and then plunged into liquid ethane using an FEI Vitrobot IV. The grids were loaded into an FEI Tecnai Polara electron microscope operated at an accelerating voltage of 300 kV and equipped with a Falcon III direct detector. Micrographs were

taken using EPU software (FEI) at a nominal magnification of ×78,000, yielding a pixel size of 1.34 Å per pixel at the specimen level.

Each image was exposed for 1.8 or 2 s at dose rate of around 36 or 26 electrons/Å²/s, respectively. The beam used was larger (ca. 1.6 μm in diameter) than the Quantifoil hole, illuminating the carbon all around the hole. Defocus range was set at −1.8 to −3.8 μm. An in-house built system was used to intercept videos from the detector, and 56 (1.8-s exposure) or 62 (2-s exposure) movie frames were recorded for each image (30).

Image processing. Movie frames were first aligned by the MotionCor2 (31) program before subsequent processing. First three movie frames of total dose of approximately 3 electrons/Å² were discarded, mimicking a preexposure. The rest of the frames were aligned using a dose-weighting scheme of MotionCor2 program. The total dose used was 52 electrons/Å² (2-s exposure) or 64 electrons/Å² (1.8-s exposure), which equals around 1 electron/Å² in one movie frame. Contrast transfer function parameters were calculated with Gctf (32) from the motion-corrected and not dose-weighted images. Initially, particles (in 208 × 208 pixels box size) were selected automatically by Gautomatch (provided in-house by Kai Zhang [http://www.mrc-lmb.cam.ac.uk/kzhang]) from a small portion of the data set (~200 micrographs [see Fig. S2A]). The relatively high dose enabled sufficient contrast to allow particle picking even in low defocused micrographs. After 2D classification using RELION 2.0 (30), eight images in different views were selected from the 2D averages and used as reference for automatic particle picking for the whole data set by RELION 2.0 or Gautomatch.

The following procedures were performed in RELION to exclude bad particles from the final reconstruction. First, particles in each micrograph were displayed and manually screened to delete wrongly picked areas. Second, 2D classification was performed iteratively to obtain the accuracy of the rotations of most of the 2D classes of ~2.6°. Particles in bad classes with poor structural features were removed.

The resultant particles (~540 thousands) were then used for 3D classifications. The first round of 3D classification restricted to eight classes was performed using X-ray crystal structure of *E. coli* RNA polymerase σ^{70} holoenzyme (PDB entry 4YG2) as a 60-Å low-pass filtered initial model. Classification was done during three rounds of 25 iterations each, using the regularization parameter T=4 and restricted to 12 classes. During the second and third rounds, local angular searches were performed to 3.5° and 1.8° to clearly separate structural species. Most abundant classes were pooled, and a second round of classification was performed, again restricted to eight classes. The final accuracy of the rotational alignment was ~2°, and the translational alignment accuracy was 0.7 pixels. Distinguishable species of RNAP core and σ^{A}-bound holoenzyme were identified and further classified separately. A summary of particles used for final refinements is listed in Table S1. We used statistical movie processing in RELION (30) to estimate the per-particle beam induced movement for all movie frames with running averages of five movie frames and a standard deviation of 1 pixel for the translational alignments. For each class independently, we used a particle-polishing step (30), which includes B-factor weighting to estimate the dose- and resolution-dependent radiation damage for each movie frame. In this step, the signal from the very late frames, with very high radiation damage, was damped. The final particle sets were 3D autorefined and postprocessed in RELION. The local resolution (Fig. S3) was calculated using the RELION software package. The angular distribution of particles was calculated using the cryoEF software package (24).

Model building and refinement. Atomic models of protein parts of *M. smegmatis* RNAP species (Fig. 1 and 2) were generated according to the recent crystal structure of *M. smegmatis* RP_O and TIC (PDB entries 5VI5 and 5VI8). Protein chains of the whole complexes were first rigid-body fit into cryo-EM density by Molrep (33). Individual subdomains of *M. smegmatis* RNAP were then assigned according to the rigid modules previously described in *T. thermophilus* (26) (Table S2) and fit into the cryo-EM density by JiggleFit tool (34) in Coot (35). Best fits of the subdomains from both 5VI5 and 5VI8 were chosen according to a correlation coefficient in the JiggleFit tool. The atomic models building for the second most abundant conformation forms of RNAP core and holoenzyme were stopped at this point.

The models were then iteratively improved by manual building in Coot and refinement in Refmac (36). For the Refmac refinement, the model atomic distance were restrained according to the crystal structure of *M. smegmatis* RP_O (5VI5) in ProSMART (37). The criterion for refinement completion was a stabilized R factor and low RMS of bond angles and lengths (Table S1).

Accession number(s). The EM maps and atomic coordinates of *M. smegmatis* RNA polymerase core (PDB entry 6F6W and EMD entry EMD-4192) and holoenzyme (PDB entry 6EYD and EMD entry EMD-3983) have been deposited in the Protein Data Bank (http://wwpdb.org) and the EMDataBank (http://emdatabank.org/).

SUPPLEMENTAL MATERIAL

Supplemental material for this article may be found at https://doi.org/10.1128/JB.00583-18.

SUPPLEMENTAL FILE 1, PDF file, 1.4 MB.

ACKNOWLEDGMENTS

We thank Alan Roy Fersht for material and scientific support of this work in his laboratory. We also thank Xiaochen Bai and Kai Zhang for advice with cryo-EM data processing and Christos Savva and Greg McMullan for help with the data collection. We

thank Jake Grimmett and Toby Darling for assistance with the Laboratory of Molecular Biology, MRC, computing cluster.

This study was funded by the Czech Science Foundation grants 17-03419S (to L.K.) and 13-27150P (to J.H.) and by grant GAUK 794317 (to J.P.).

We declare that we have no conflicts of interest with the contents of this article.

T.K. expressed and purified proteins, reconstituted the RNAP complexes, prepared cryo-EM grids, collected EM data, performed image processing and reconstruction, built models, made figures, and wrote the manuscript. J.P. and J.H. cloned the expression vectors, expressed and purified proteins, and performed the transcription assays. J.H. and H.Š. developed expression and purification protocols. I.B. prepared the figures and wrote the manuscript. L.K. conceived the project, organized the collaboration, and wrote the manuscript.

REFERENCES

1. Molodtsov V, Scharf NT, Stefan MA, Garcia GA, Murakami KS. 2017. Structural basis for rifamycin resistance of bacterial RNA polymerase by the three most clinically important RpoB mutations found in *Mycobacterium tuberculosis*. Mol Microbiol 103:1034–1045. https://doi.org/10.1111/mmi.13606.
2. Ma C, Yang X, Lewis PJ. 2016. Bacterial transcription as a target for antibacterial drug development. Microbiol Mol Biol Rev 80:139–160. https://doi.org/10.1128/MMBR.00055-15.
3. Sutherland C, Murakami KS. 2018. An introduction to the structure and function of the catalytic core enzyme of *Escherichia coli* RNA polymerase. EcoSal Plus 8. https://doi.org/10.1128/ecosalplus.ESP-0004-2018.
4. Paget MS. 2015. Bacterial sigma factors and anti-sigma factors: structure, function and distribution. Biomolecules 5:1245–1265. https://doi.org/10.3390/biom5031245.
5. Bae B, Chen J, Davis E, Leon K, Darst SA, Campbell EA. 2015. CarD uses a minor groove wedge mechanism to stabilize the RNA polymerase open promoter complex. Elife 4:e08505. https://doi.org/10.7554/eLife.08505.001.
6. Hu Y, Morichaud Z, Perumal AS, Roquet-Baneres F, Brodolin K. 2014. Mycobacterium RbpA cooperates with the stress-response sigmaB subunit of RNA polymerase in promoter DNA unwinding. Nucleic Acids Res 42:10399–10408. https://doi.org/10.1093/nar/gku742.
7. Sudalaiyadum Perumal A, Vishwakarma RK, Hu Y, Morichaud Z, Brodolin K. 2018. RbpA relaxes promoter selectivity of *Mycobacterium tuberculosis* RNA polymerase. Nucleic Acids Res 46:10106–10118. https://doi.org/10.1093/nar/gky714.
8. Bae B, Davis E, Brown D, Campbell EA, Wigneshweraraj S, Darst SA. 2013. Phage T7 Gp2 inhibition of *Escherichia coli* RNA polymerase involves misappropriation of sigma70 domain 1.1. Proc Natl Acad Sci U S A 110:19772–19777. https://doi.org/10.1073/pnas.1314576110.
9. Schwartz EC, Shekhtman A, Dutta K, Pratt MR, Cowburn D, Darst S, Muir TW. 2008. A full-length group 1 bacterial sigma factor adopts a compact structure incompatible with DNA binding. Chem Biol 15:1091–1103. https://doi.org/10.1016/j.chembiol.2008.09.008.
10. Zachrdla M, Padrta P, Rabatinova A, Sanderova H, Barvik I, Krasny L, Zidek L. 2017. Solution structure of domain 1.1 of the sigma(A) factor from *Bacillus subtilis* is preformed for binding to the RNA polymerase core. J Biol Chem 292:11610–11617. https://doi.org/10.1074/jbc.M117.784074.
11. Boyaci H, Chen J, Lilic M, Palka M, Mooney RA, Landick R, Darst SA, Campbell EA. 2018. Fidaxomicin jams *Mycobacterium tuberculosis* RNA polymerase motions needed for initiation via RbpA contacts. Elife 7:e34823. https://doi.org/10.7554/eLife.34823.
12. Hubin EA, Fay A, Xu C, Bean JM, Saecker RM, Glickman MS, Darst SA, Campbell EA. 2017. Structure and function of the mycobacterial transcription initiation complex with the essential regulator RbpA. Elife 6:e22520. https://doi.org/10.7554/eLife.22520.
13. Hubin EA, Lilic M, Darst SA, Campbell EA. 2017. Structural insights into the mycobacteria transcription initiation complex from analysis of X-ray crystal structures. Nat Commun 8:16072. https://doi.org/10.1038/ncomms16072.
14. Lin W, Mandal S, Degen D, Liu Y, Ebright YW, Li S, Feng Y, Zhang Y, Mandal S, Jiang Y, Liu S, Gigliotti M, Talaue M, Connell N, Das K, Arnold E, Ebright RH. 2017. Structural basis of *Mycobacterium tuberculosis* transcription and transcription inhibition. Mol Cell 66:169–179. https://doi.org/10.1016/j.molcel.2017.03.001.
15. Chakraborty A, Wang D, Ebright YW, Korlann Y, Kortkhonjia E, Kim T, Chowdhury S, Wigneshweraraj S, Irschik H, Jansen R, Nixon BT, Knight J, Weiss S, Ebright RH. 2012. Opening and closing of the bacterial RNA polymerase clamp. Science 337:591–595. https://doi.org/10.1126/science.1218716.
16. Darst SA, Opalka N, Chacon P, Polyakov A, Richter C, Zhang G, Wriggers W. 2002. Conformational flexibility of bacterial RNA polymerase. Proc Natl Acad Sci U S A 99:4296–4301. https://doi.org/10.1073/pnas.052054099.
17. Ruff EF, Drennan AC, Capp MW, Poulos MA, Artsimovitch I, Record MT, Jr. 2015. *E. coli* RNA polymerase determinants of open complex lifetime and structure. J Mol Biol 427:2435–2450. https://doi.org/10.1016/j.jmb.2015.05.024.
18. Glyde R, Ye F, Jovanovic M, Kotta-Loizou I, Buck M, Zhang X. 2018. Structures of Bacterial RNA polymerase complexes reveal the mechanism of DNA loading and transcription initiation. Mol Cell 70:1111–1120. https://doi.org/10.1016/j.molcel.2018.05.021.
19. Glyde R, Ye F, Darbari VC, Zhang N, Buck M, Zhang X. 2017. Structures of RNA polymerase closed and intermediate complexes reveal mechanisms of DNA opening and transcription initiation. Mol Cell 67:106–116. https://doi.org/10.1016/j.molcel.2017.05.010.
20. Browning DF, Busby SJ. 2016. Local and global regulation of transcription initiation in bacteria. Nat Rev Microbiol 14:638–650. https://doi.org/10.1038/nrmicro.2016.103.
21. Krasny L, Tiserova H, Jonak J, Rejman D, Sanderova H. 2008. The identity of the transcription +1 position is crucial for changes in gene expression in response to amino acid starvation in *Bacillus subtilis*. Mol Microbiol 69:42–54. https://doi.org/10.1111/j.1365-2958.2008.06256.x.
22. Lane WJ, Darst SA. 2010. Molecular evolution of multisubunit RNA polymerases: sequence analysis. J Mol Biol 395:671–685. https://doi.org/10.1016/j.jmb.2009.10.062.
23. Lin W, Das K, Degen D, Mazumder A, Duchi D, Wang D, Ebright YW, Ebright RY, Sineva E, Gigliotti M, Srivastava A, Mandal S, Jiang Y, Liu Y, Yin R, Zhang Z, Eng ET, Thomas D, Donadio S, Zhang H, Zhang C, Kapanidis AN, Ebright RH. 2018. Structural basis of transcription inhibition by fidaxomicin (lipiarmycin A3). Mol Cell 70:60–71. https://doi.org/10.1016/j.molcel.2018.02.026.
24. Naydenova K, Russo CJ. 2017. Measuring the effects of particle orientation to improve the efficiency of electron cryomicroscopy. Nat Commun 8:629. https://doi.org/10.1038/s41467-017-00782-3.
25. Vassylyev DG, Vassylyeva MN, Perederina A, Tahirov TH, Artsimovitch I. 2007. Structural basis for transcription elongation by bacterial RNA polymerase. Nature 448:157–162. https://doi.org/10.1038/nature05932.
26. Tagami S, Sekine S, Kumarevel T, Hino N, Murayama Y, Kamegamori S, Yamamoto M, Sakamoto K, Yokoyama S. 2010. Crystal structure of bacterial RNA polymerase bound with a transcription inhibitor protein. Nature 468:978–982. https://doi.org/10.1038/nature09573.
27. Duchi D, Mazumder A, Malinen AM, Ebright RH, Kapanidis AN. 2018. The RNA polymerase clamp interconverts dynamically among three states and is stabilized in a partly closed state by ppGpp. Nucleic Acids Res 46:7284–7295. https://doi.org/10.1093/nar/gky482.
28. Sojka L, Kouba T, Barvik I, Sanderova H, Maderova Z, Jonak J, Krasny

L. 2011. Rapid changes in gene expression: DNA determinants of promoter regulation by the concentration of the transcription initiating NTP in *Bacillus subtilis*. Nucleic Acids Res 39:4598–4611. https://doi.org/10.1093/nar/gkr032.
29. China A, Tare P, Nagaraja V. 2010. Comparison of promoter-specific events during transcription initiation in mycobacteria. Microbiology 156:1942–1952. https://doi.org/10.1099/mic.0.038620-0.
30. Scheres SH. 2012. A Bayesian view on cryo-EM structure determination. J Mol Biol 415:406–418. https://doi.org/10.1016/j.jmb.2011.11.010.
31. Zheng SQ, Palovcak E, Armache JP, Verba KA, Cheng Y, Agard DA. 2017. MotionCor2: anisotropic correction of beam-induced motion for improved cryo-electron microscopy. Nat Methods 14:331–332. https://doi.org/10.1038/nmeth.4193.
32. Zhang K. 2016. Gctf: real-time CTF determination and correction. J Struct Biol 193:1–12. https://doi.org/10.1016/j.jsb.2015.11.003.
33. Vagin A, Teplyakov A. 2010. Molecular replacement with MOLREP. Acta Crystallogr D Biol Crystallogr 66:22–25. https://doi.org/10.1107/S0907444909042589.
34. Brown A, Long F, Nicholls RA, Toots J, Emsley P, Murshudov G. 2015. Tools for macromolecular model building and refinement into electron cryo-microscopy reconstructions. Acta Crystallogr D Biol Crystallogr 71:136–153. https://doi.org/10.1107/S1399004714021683.
35. Emsley P, Lohkamp B, Scott WG, Cowtan K. 2010. Features and development of Coot. Acta Crystallogr D Biol Crystallogr 66:486–501. https://doi.org/10.1107/S0907444910007493.
36. Murshudov GN, Skubak P, Lebedev AA, Pannu NS, Steiner RA, Nicholls RA, Winn MD, Long F, Vagin AA. 2011. REFMAC5 for the refinement of macromolecular crystal structures. Acta Crystallogr D Biol Crystallogr 67:355–367. https://doi.org/10.1107/S0907444911001314.
37. Nicholls RA, Long F, Murshudov GN. 2012. Low-resolution refinement tools in REFMAC5. Acta Crystallogr D Biol Crystallogr 68:404–417. https://doi.org/10.1107/S090744491105606X.

The Core and Holoenzyme forms of RNA Polymerase from *Mycobacterium smegmatis*

Tomáš Kouba[1,2], Jiří Pospíšil[3,4], Jarmila Hnilicová[3], Hana Šanderová[3], Ivan Barvík[5], and Libor Krásný[3]

From the [1]MRC Laboratory of Molecular Biology, Cambridge CB2 0QH, United Kingdom; [2]Present address: EMBL Grenoble, 71 avenue des Martyrs, CS 90181, 38042 Grenoble Cedex 9, France [3]Department of Molecular Genetics of Bacteria, Institute of Microbiology, Academy of Sciences of the Czech Republic, CZ-14220 Prague 4, Czech Republic; [4]Department of Genetics and Microbiology, Faculty of Science, Charles University, Viničná 5, 128 43 Prague 2, Czech Republic; [5]Division of Biomolecular Physics, Institute of Physics, Faculty of Mathematics and Physics, Charles University in Prague, Ke Karlovu 5, 121 16 Prague 2, Czech Republic

To whom correspondence should be addressed: Tomas Kouba, EMBL Grenoble, 71 avenue des Martyrs, CS 90181, 38042 Grenoble Cedex 9, France, Telephone: +33 476 209 478, E-mail: tkouba@embl.fr and Libor Krásný, Laboratory of Microbial Genetics and Gene Expression, Institute of Microbiology, The Czech Academy of Sciences, CZ-14220 Prague 4, Czech Republic, Telephone: +420 241 063 208, E-mail: krasny@biomed.cas.cz

Keywords: bacterial transcription, protein structure, RNA polymerase, transcription initiation factor, conformational change, drug target, cryo-electron microscopy

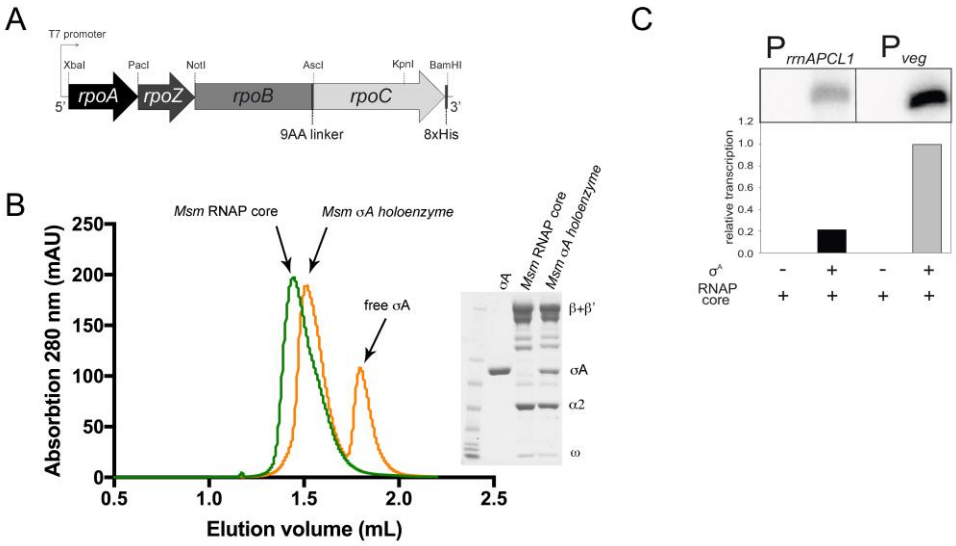

Figure S1: Reconstitution of RNAP holoenzyme. Related to Figure 1
A) Schematics of expression vector for a polycistronic transcript of all five *Msm* RNAP core subunits **B)** SEC analysis of RNAP core alone (green line). SEC analysis of protein sample after reconstitution of RNAP core with σ^A factor at a 1:3 ratio (yellow line). The first yellow peak (from left) is the σ^A reconstituted holoenzyme, the second, lower peak is free σ^A. 20 µg protein samples of peak fractions were loaded onto analytical SDS-PAGE. **C)** Multiple round *in vitro* transcription assays of *Msm* RNAP with/without σ^A. Mycobacterial ribosomal *PrrnAPCL1* (1) and *B. subtilis* vegetative *Pveg* (2) were used as promoters.

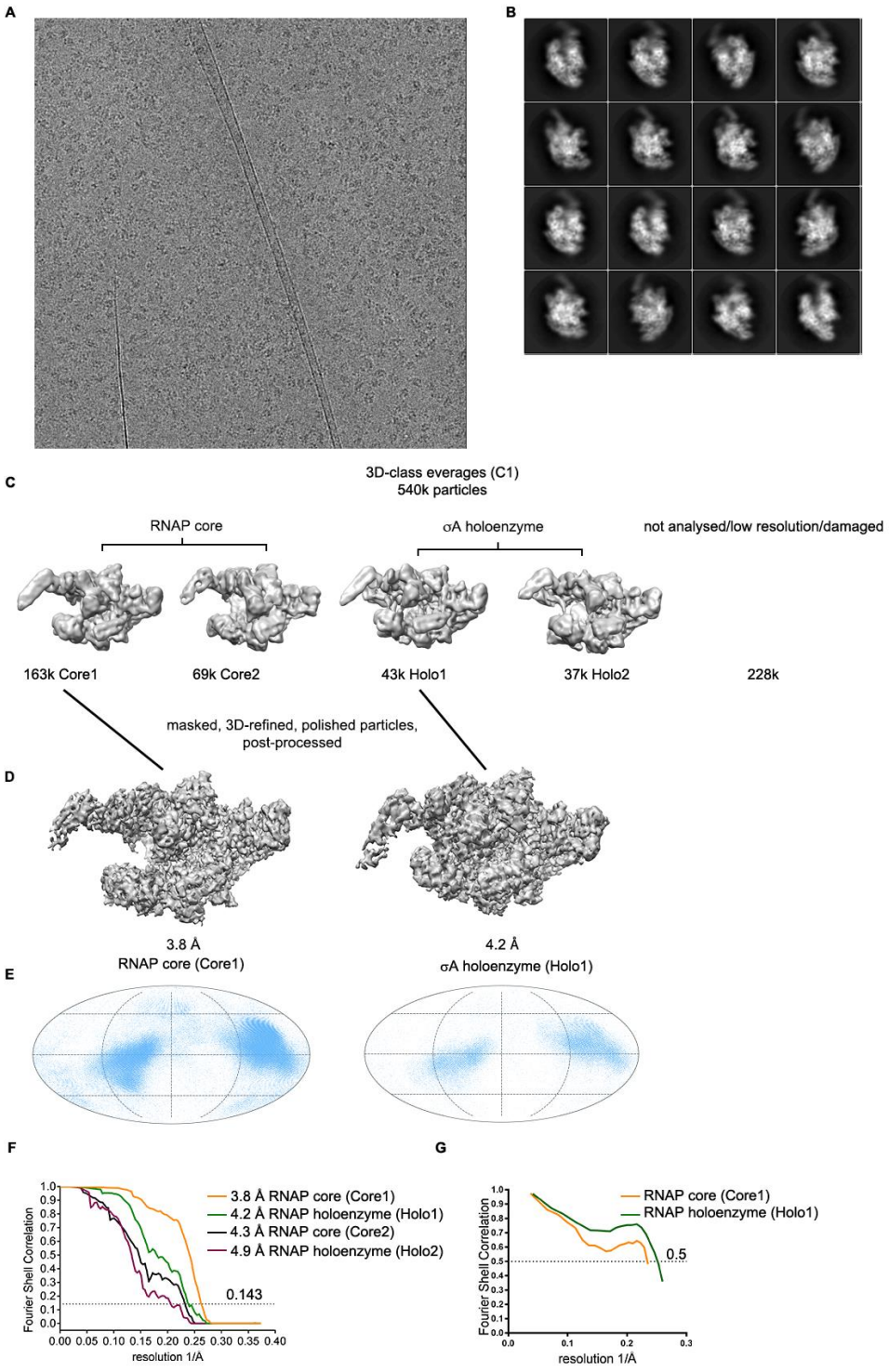

Figure S2: Electron microscopy and image processing. Related to Figure 1
A) Representative micrograph **B)** 2D-class averages **C-D)** Summary of the cryo-EM 3D classification and refinement of *Msm* RNAP structures. In total of 540k particles was classified into distinct 3D-classes (upper lane in grey, number of particles in each class is indicated in thousands) representing the RNAP core and σ_A bound RNAP. Heterogeneous, low resolution and damaged particle classes were excluded from data analysis. Most prominent 3D-class from each species was further 3D-refined and post-processed in RELION **E)** Angular distribution

for particle projections was calculated by cryoEF (3) and plotted on a globe like plane. The particle orientation efficiency score (3) of ~ 0.47 (Table 1S1) suggests a minor Fourier space gap in the 3D electron densities volumes, but was sufficient for 3D reconstructions. **F)** FSC curves for the observed reconstructions. FSC between two independently refined half-maps plots showing the overall resolution of the *Msm* RNAP maps reconstructed in this study. Gold-standard FSC 0.143 cutoff criteria is indicated. **G)** Fourier Shell Correlation (FSC) between the *Msm* RNAP models and EM density maps. FSC 0.5 cutoff criteria is indicated.

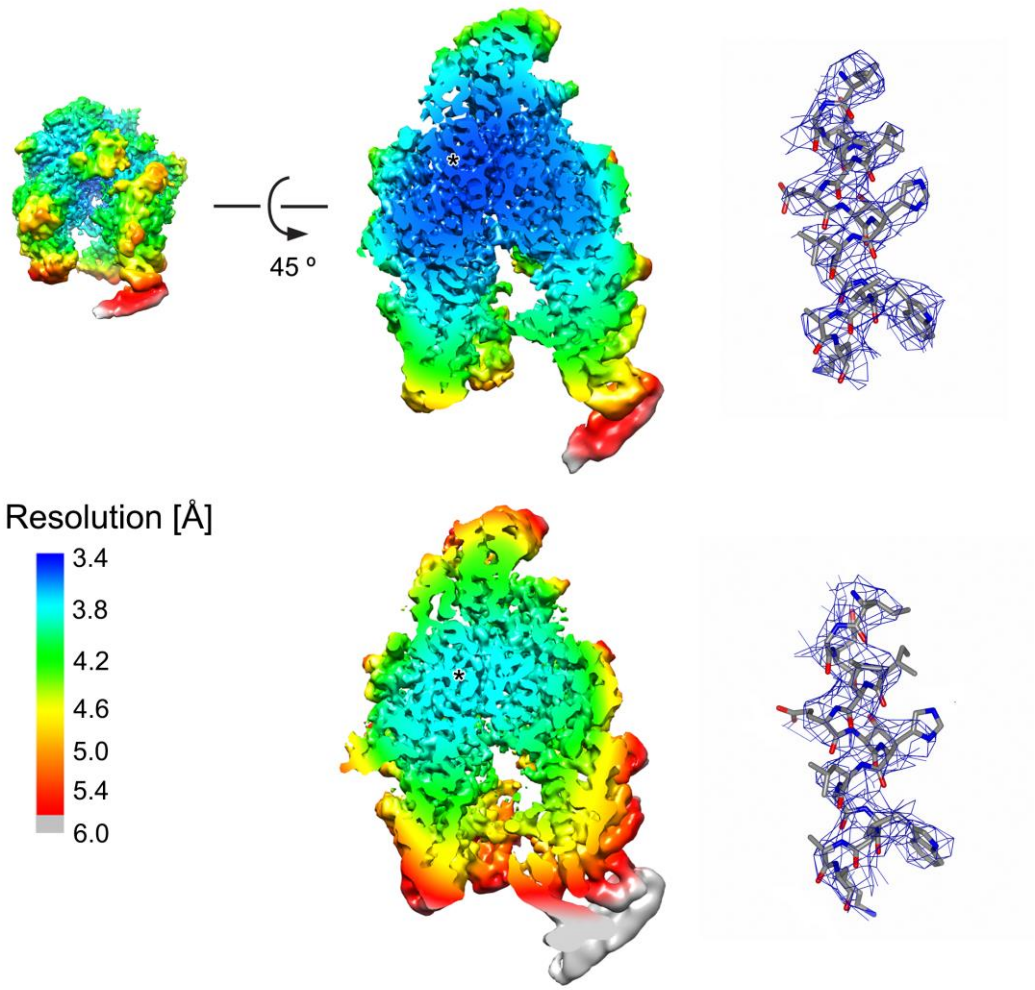

Figure S3: Local resolution of cryo-EM maps. Related to figure S2
Slices through cryo-EM maps of (**Top**) Core1 and (**Bottom**) Holo1 rotated by ~45° degrees in respect to Figure 1, together with representative fits of atomic models into the generated cryo-EM electron densities (**Right column**). Maps are colored according to local resolution calculated within RELION software package. Resolution is as indicated in the resolution color bar. The resolution decreases towards the peripheries of the complexes and remarkably towards the tip of the β' clamp and β domain 2. This phenomenon is in agreement with the pronounced swing motion of both of these features further from the rotational axis defined by the switch regions (see chapter Results (i)).
Fit of helix residues β 919-932 of the central part (**Right column**). marked by asterisks in the local resolution map) of (**Top**) Core1 and (**Bottom**) Holo1 RNAP molecules into the cryo-EM electron densities low pass filtered at 3.8 Å and 4.2 Å gold standard FSC resolution respectively. Bulky side chain residues of β His 926 and Trp 929 are visible in the electron density.

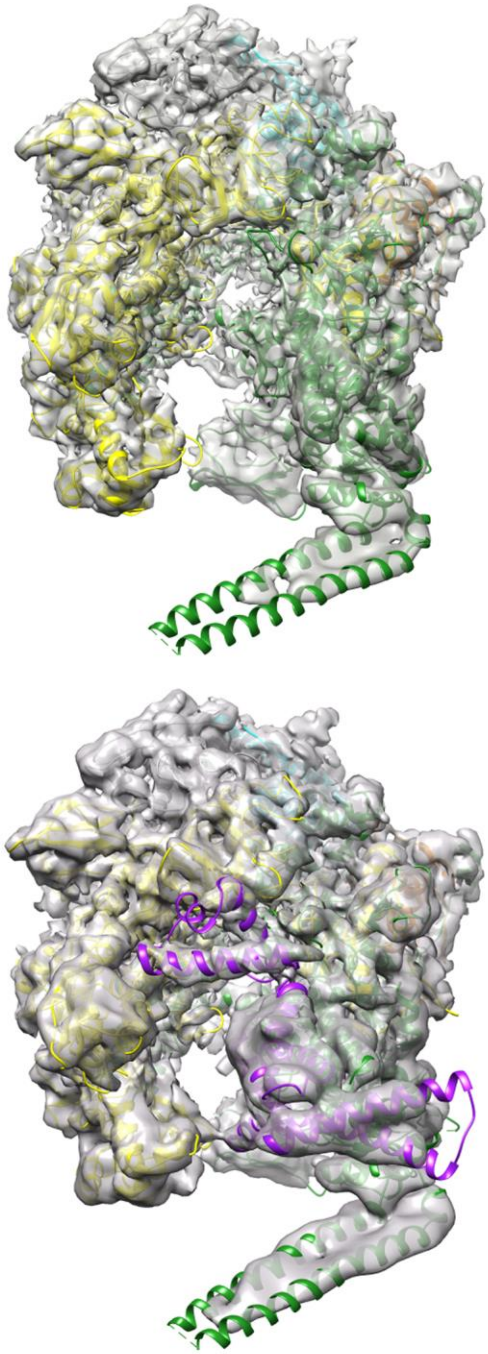

Figure S4: Cryo-EM maps and models of *Msm* RNAP complexes. Related to Figure S2
Cryo-EM maps of (**Top**) Core1 and (**Bottom**) Holo1 low pass filtered at local resolution according to Figure S4. Maps are visualized as 0.5 transparent at 0.08 volume threshold in Chimera. Secondary structures of RNAP subunits and nucleic acids chains are colored as follows: β – yellow, β'– green, α – grey, α' – cyan, ω – orange.

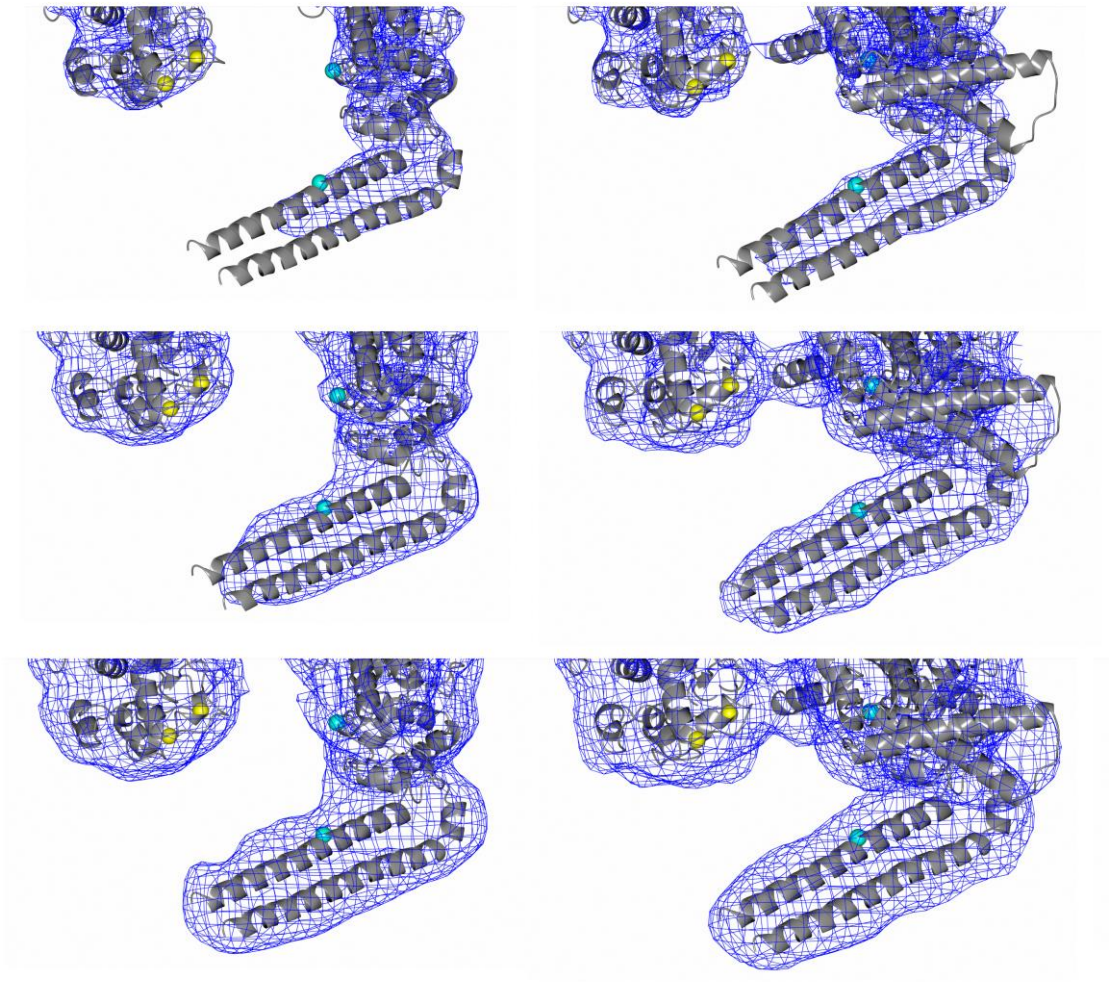

Figure S5: Structure feature of the β'i1. Related to Figure 2
Fits of secondary structure of β'i1 together with part of β' clamp and β domain 2 into 8 Å resolution low pass filtered cryo-EM electron densities of (**Left column**) Core1 and (**Right column**) Holo1 oriented as in Figure 2. The densities are visualized at 0.08, 0.04 and 0.02 (**Top**, **middle** and **bottom row** respectively) density volume threshold (in ccp4mg image software) to emphasize density for β'i1. The very tip of β'i1 (residues β' 186-191) is not defined even at very low density threshold and was excluded from the model in case of RNAP core and holoenzyme. The spheres represent the Cα atoms of residues used for distance measurement in Table 1 and 2 (yellow – β Leu 266 Cα and β Gly 271 Cα, and cyan – β' Lys 123 Cα and β' Arg 214 Cα). The residues are positioned in an area with well-defined cryo-EM electron density (**Top row**)

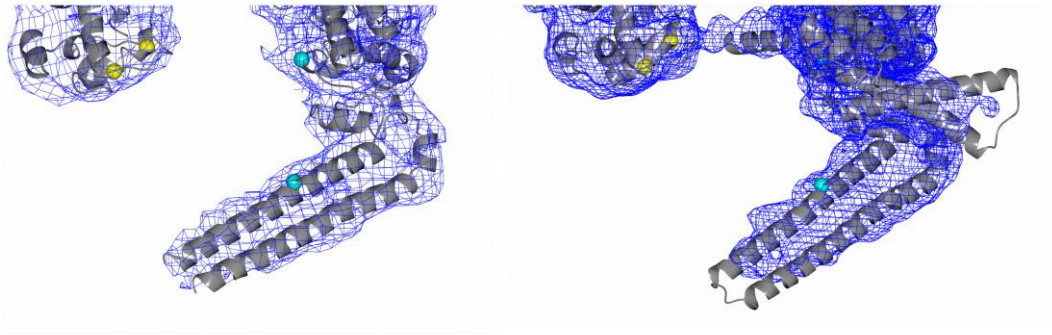

Figure S6: Structure feature of the β'i1 in the second most abundant 3D classes of RNAP core and holoenzyme

Fits of secondary structure of β'i1 together with part of β' clamp and β domain 2 into 8 Å resolution low pass filtered cryo-EM electron densities of (**Left**) Core2 and (**Right**) Holo2 second most abundant 3D classes oriented as in Figure 2. The densities are visualized at 0.04 density volume threshold (in ccp4mg image software) to emphasize density for β'i1. The spheres represent the Cα atoms of residues used for distance measurement in Table 1 and 2 (yellow – β Leu 266 Cα and β Gly 271 Cα, and cyan – β' Lys 123 Cα and β' Arg 214 Cα). The residues are positioned in an area with well-defined cryo-EM electron density.

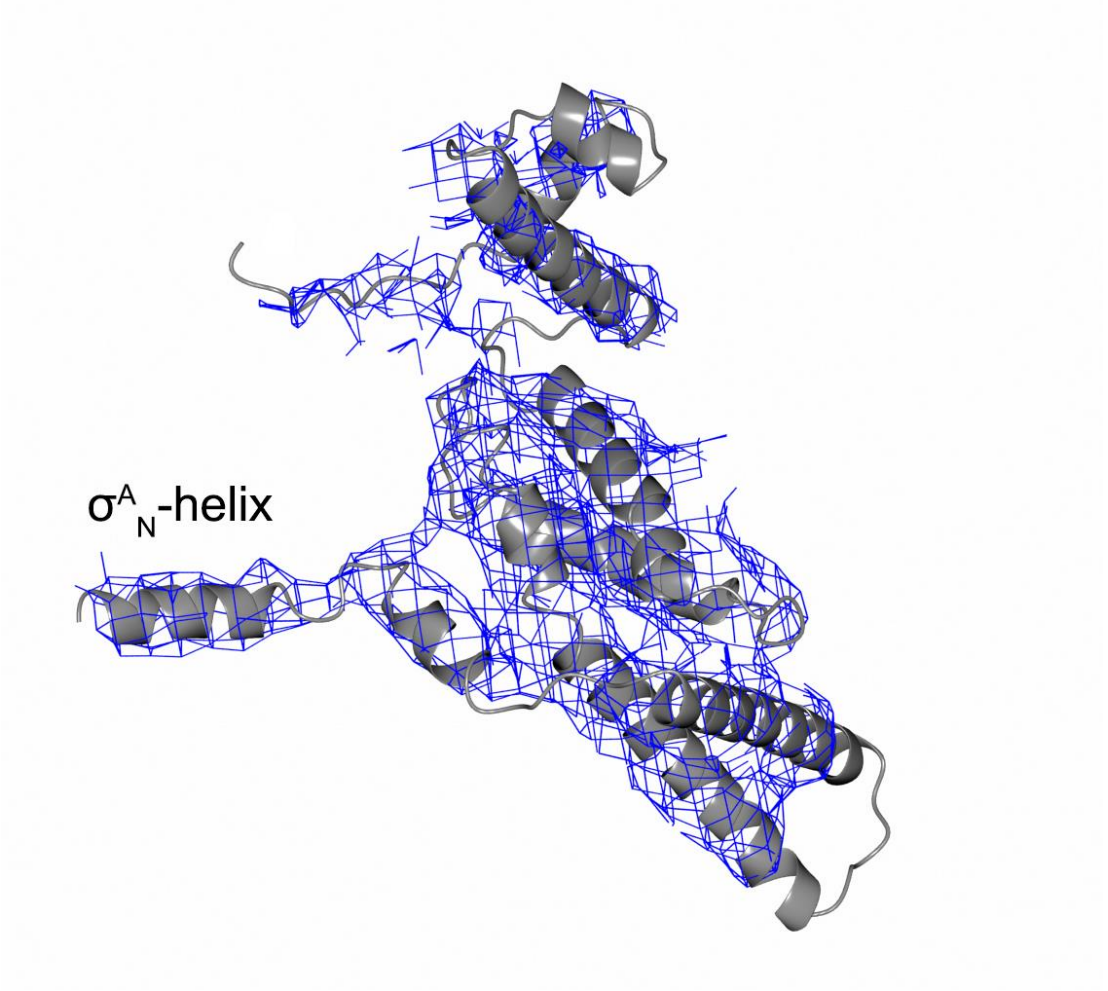

Figure S7: Structure features of the σ^A subunit in *Msm* RNAP
A) Fit of σ^A subunit secondary structure into cryo-EM electron density of *Msm* holoenzyme low pass filtered at 5 Å resolution according to the local resolution estimation (Figure S4). Secondary structure features are visible in the map for most of the protein chain and $\sigma^A_{N\text{-helix}}$.

Table S1: EM data refinement and refined atomic models statistics

	RNAP core (Core1)	σ^A holoenzyme (Holo1)
Final particles	163 000	43 000
Particle orientation efficiency score [a]	0.46	0.48
Overall resolution (Å)[b]	3.81	4.22
EMD	EMD-4192	EMD-3983
Ramachandran outliers	1.20 %	0.82 %
Ramachandran favoured	89.53 %	91.81 %
Model average FSC	0.68	0.63
RMS bond angles (º)	1.278	1.309
RMS bond lengths (Å)	0.0027	0.0033
Molprobity score	1.81	1.69
Clashscore (all atoms)	2.59	2.65
PDB ID	6F6W	6EYD

[a] (3)

[b] Gold-standard FSC 0.143 cutoff criteria (Figure S2F)

Table S2: *Msm* RNA polymerase rigid body alignment

Module	Subunit	Residues in *Msm* RNAP	Residues in *Tt* RNAP
Shelf module	β subunit	1030:1098	1006:1071
	β' subunit	420:573 881:1218 1260:1307	621:778 1103:1432 1473:1520
	ω subunit	all	all
Bridge helix	β' subunit	848:880	1070:1102
Hinge loop	β' subunit	574:578	779:782
Core module	2 α subunits	all	all
	β subunit	21-44 430:738 870:1024	1:17 394:700 833:997
	β' subunit	579:847	783:1069
Clamp	β subunit	1110:1141	1083:1112
	β' subunit	1:133 255:404 1231:1255	1:131 455:605 1444:1468
β' NCD	β' subunit	134:254	132:454
β domain 1	β subunit	44-171 368:429	18:142 332:393
β domain 2	β subunit	172:367	143:331
β flap domain	β subunit	739:869	701:832
Switch 1	β' subunit	1218:1230	1431:1443
Switch 2	β' subunit	405:419	606:620
Switch 3	β subunit	1025:1029	998:1005
Switch 4	β subunit	1099:1109	1072:1082
Switch 5	β' subunit	1256:1259	1469:1472
Trigger loop	β' subunit	1009:1028	1236:1255
Secondary channel coiled coil	β' subunit	739:793	958:1014

Table S3: Primers used for PCR

mysA	
LK1155	GGAATTCCCATATGGTGGCAGCGACAAAGGCA
LK1156	CCGCTCGAGGTCCAGGTAGTCGCGCAG
rpoA	
LK1922	CCCCTCTAGAGTTTAAACTTTAAGAAGGAGATATACTCATGCTGATCTCTCA GCGTCCCACC
LK1923	GGGTTAATTAAGTTAAAGCTGCTCGGTCTCGGCGTA
rpoZ	
LK1924	CCCTTAATTAAGCAATTAACACAATATAAGAGGAGGTCCCAGTCGTGAGCAC CCCGCACGCCGATGCG
LK1925	GGGGCGGCCGCTTATTCGCCTTCGGTGTGCTCGAG
rpoB	
LK1900	CCCCGCGGCCGCTTTAAGAAGGAGATATATCTATGCTGGAAGGATGCATC
LK1996	GGGGGGCGCGCCAGCGCGAGATCCTCGACGGACGCGGATTCG
rpoC	
LK1902	CCCCGGCGCGCCACGGTGGCTCGGGTGCAATGCTAGACGTCAACTTC
LK1915	GCGGTAATCCGAGTAGCCGTAGTCGTCCAGCGG
LK1903	CGCGGGATCCCTAGTGATGGTGATGGTGATGGTGATGGCGGTAATCCGAGTA GC
LK1914	ATGCTAGACGTCAACTTCTTCGATGAACTCCGC

References

1. Flentie K, Garner AL, Stallings CL. 2016. Mycobacterium tuberculosis Transcription Machinery: Ready To Respond to Host Attacks. J Bacteriol 198:1360-73.
2. Sojka L, Kouba T, Barvik I, Sanderova H, Maderova Z, Jonak J, Krasny L. 2011. Rapid changes in gene expression: DNA determinants of promoter regulation by the concentration of the transcription initiating NTP in Bacillus subtilis. Nucleic Acids Res 39:4598-611.
3. Naydenova K, Russo CJ. 2017. Measuring the effects of particle orientation to improve the efficiency of electron cryomicroscopy. Nat Commun 8:629.

AMERICAN SOCIETY FOR MICROBIOLOGY | Journal of Bacteriology®

RESEARCH ARTICLE

σ^I from *Bacillus subtilis*: Impact on Gene Expression and Characterization of σ^I-Dependent Transcription That Requires New Types of Promoters with Extended −35 and −10 Elements

Olga Ramaniuk,[a,b] Martin Převorovský,[c] Jiří Pospíšil,[a] Dragana Vítovská,[a] Olga Kofroňová,[d] Oldřich Benada,[d] Marek Schwarz,[e] Hana Šanderová,[a] Jarmila Hnilicová,[a] Libor Krásný[a]

[a]Laboratory of Microbial Genetics and Gene Expression, Institute of Microbiology of the Czech Academy of Sciences, Prague, Czech Republic

[b]Department of Genetics and Microbiology, Faculty of Science, Charles University, Prague, Czech Republic

[c]Department of Cell Biology, Faculty of Science, Charles University, Prague, Czech Republic

[d]Laboratory of Molecular Structure Characterization, Institute of Microbiology of the Czech Academy of Sciences, Prague, Czech Republic

[e]Laboratory of Bioinformatics, Institute of Microbiology of the Czech Academy of Sciences, Prague, Czech Republic

ABSTRACT The σ^I sigma factor from *Bacillus subtilis* is a σ factor associated with RNA polymerase (RNAP) that was previously implicated in adaptation of the cell to elevated temperature. Here, we provide a comprehensive characterization of this transcriptional regulator. By transcriptome sequencing (RNA-seq) of wild-type (wt) and σ^I-null strains at 37°C and 52°C, we identified ~130 genes affected by the absence of σ^I. Further analysis revealed that the majority of these genes were affected indirectly by σ^I. The σ^I regulon, i.e., the genes directly regulated by σ^I, consists of 16 genes, of which eight (the *dhb* and *yku* operons) are involved in iron metabolism. The involvement of σ^I in iron metabolism was confirmed phenotypically. Next, we set up an *in vitro* transcription system and defined and experimentally validated the promoter sequence logo that, in addition to −35 and −10 regions, also contains extended −35 and −10 motifs. Thus, σ^I-dependent promoters are relatively information rich in comparison with most other promoters. In summary, this study supplies information about the least-explored σ factor from the industrially important model organism *B. subtilis*.

IMPORTANCE In bacteria, σ factors are essential for transcription initiation. Knowledge about their regulons (i.e., genes transcribed from promoters dependent on these σ factors) is the key for understanding how bacteria cope with the changing environment and could be instrumental for biotechnologically motivated rewiring of gene expression. Here, we characterize the σ^I regulon from the industrially important model Gram-positive bacterium *Bacillus subtilis*. We reveal that σ^I affects expression of ~130 genes, of which 16 are directly regulated by σ^I, including genes encoding proteins involved in iron homeostasis. Detailed analysis of promoter elements then identifies unique sequences important for σ^I-dependent transcription. This study thus provides a comprehensive view on this underexplored component of the *B. subtilis* transcription machinery.

KEYWORDS RNAP, RNA-seq, iron metabolism, promoter, sigma factor

Bacillus subtilis is a Gram-positive microorganism that belongs to the bacterial phylum *Firmicutes*. Its main habitat is soil, but it is also found in the gastrointestinal microbiomes of many organisms, including that of humans. In these habitats, *B. subtilis*

Received 26 April 2018 **Accepted** 9 June 2018

Accepted manuscript posted online 18 June 2018

Citation Ramaniuk O, Převorovský M, Pospíšil J, Vítovská D, Kofroňová O, Benada O, Schwarz M, Šanderová H, Hnilicová J, Krásný L. 2018. σ^I from *Bacillus subtilis*: impact on gene expression and characterization of σ^I-dependent transcription that requires new types of promoters with extended −35 and −10 elements. J Bacteriol 200:e00251-18. https://doi.org/10.1128/JB.00251-18.

Editor Tina M. Henkin, Ohio State University

Address correspondence to Libor Krásný, krasny@biomed.cas.cz.

encounters a wide range of conditions. Adaptation to these conditions depends on changes in gene expression. The first step in gene expression is transcription of DNA into RNA, which is mediated by RNA polymerase (RNAP) (1). The bacterial RNAP ($\alpha_2\beta\beta'\omega$) consists of several subunits. The α dimer holds together β and β', which form the catalytic center. The small ω subunit mainly binds to the C-terminal part of β' and helps with assembly and structural integrity of the enzyme (2, 3). Furthermore, in *Firmicutes* RNAP associates with additional small proteins, δ and ε, which are considered to be additional subunits, although the role of δ has recently been debated (4–6). The core enzyme ($\alpha_2\beta\beta'\omega\delta\varepsilon$) must associate with a σ factor to initiate transcription. σ factors endow RNAP with the ability to recognize promoters—specific sequences in DNA where transcription initiates. Depending on diverse environmental signals, bacterial gene expression is controlled by various σ factors that control different sets of genes (7, 8).

B. subtilis has one primary σ factor, σ^A, responsible for transcription of housekeeping genes. The σ^A factor consists of four domains, of which domain 1.1 autoinhibits this factor in free form, preventing its binding to promoter DNA (9, 10). Furthermore, *B. subtilis* has 17 alternative σ factors and one σ-like factor (11–14). While most *B. subtilis* σ factors have been systematically studied, σ^I remains poorly characterized, with a nearly unknown regulon.

The σ^I factor was discovered in 2001 by Zuber and colleagues (15). It is encoded by the nonessential gene *sigI* (*ykoZ*) that is cotranscribed with *rsgI*, which encodes the cognate anti-σ factor RsgI. Transcription of the *sigI-rsgI* operon is driven by a σ^I-dependent promoter (16) and also by a σ^A-dependent promoter (17). The predicted molecular weight of σ^I is 29.04 kDa, and it has a theoretical isoelectric point of 8.31. RsgI is a transmembrane protein that sequesters σ^I under favorable growth conditions and releases it when appropriate stimuli—for example, heat shock—appear (16). Degradation of RsgI by proteases ClpC and ClpP then provides a posttranslational layer of regulation of σ^I activity (18).

A σ^I deletion strain was reported to be unable to grow on agar plates at 54° to 55°C (15). This temperature-sensitive phenotype of strains lacking σ^I was also implied in other studies (16, 19–21). Moreover, it was shown that, along with heat shock response, σ^I was involved in cold shock response (20).

Currently, there are only seven genes, organized in five operons known to be σ^I dependent in *B. subtilis*: the *sigI-rsgI* operon itself (16), *bcrC*, the *mreBH-ykpC* operon (21), *lytE* (22), and *gsiB* (15). Expression of some of these genes was shown to be stimulated by WalR. WalR is the response regulator of the WalRK two-component system that controls cell wall metabolism (23).

BcrC helps protect the cell against bacitracin (24) and paraquat (25), and it is also needed for production of the carrier lipid for cell wall synthesis (26). MreBH participates in formation of straight rod-shaped cells, and its depletion or overexpression in *B. subtilis* leads to the appearance of malformed cells (27–30). Moreover, MreBH is required for the lytic activity of a cell wall hydrolase, LytE, that is important for cell elongation and separation (31–33). The function of the *ykpC* gene, which is located in the same operon as the *mreBH* gene, is still unknown. GsiB is a general stress protein that prevents inactivation of cellular enzymes upon freeze-thaw treatments and is involved in responses to nutrient deprivation (34, 35).

In summary, information concerning σ^I in *B. subtilis* is still fragmentary and incomplete. As *B. subtilis* is an extensively studied and industrially important organism, we decided to fill this gap in our knowledge. In this report, we use transcriptome sequencing (RNA-seq) to reveal the impact of *B. subtilis* σ^I on gene expression. Based on the transcriptomic data, we subsequently demonstrate that σ^I is involved in iron metabolism. Finally, using recombinant σ^I, we set up a σ^I-dependent *in vitro* transcription system to describe its promoter specificity, as well as to test the promoter regions of selected genes for their dependence on σ^I.

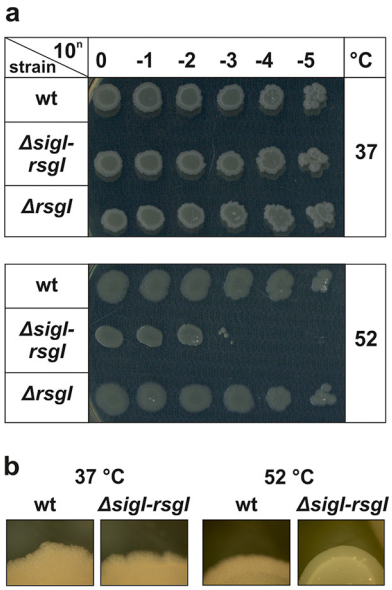

FIG 1 Spot assays of *B. subtilis* wt, Δ*sigI-rsgI*, and Δ*rsgI* strains on agar plates at 37°C and 52°C. (a) Serial dilutions of mid-logarithmic phase cultures (OD_{600}, ~0.45) of wt, Δ*sigI-rsgI*, and Δ*rsgI* strains were spotted on LB agar plates and incubated at 37°C and 52°C for 40 h. The experiment was repeated three times with the same result. (b) Colony morphology of wt and Δ*sigI-rsgI* strains.

RESULTS

The σ^I factor is important for growth at elevated temperature. We used *B. subtilis* 168 trp+ (BaSysBio) as the genetic background to create Δ*sigI-rsgI* and Δ*rsgI* strains (for details, see Materials and Methods). Under standard conditions (aerobic cultivation in LB broth at 37°C), Δ*sigI-rsgI* and Δ*rsgI* strain growth was indistinguishable from that of the wild-type (wt) strain (see Fig. S1 in the supplemental material).

Subsequently, we determined whether the Δ*sigI-rsgI* strain was sensitive to elevated temperature. We grew Δ*sigI-rsgI*, Δ*rsgI*, and wt strains in LB at 37°C, spotted serial dilutions of cell suspensions on agar plates, and let them incubate at 37°C and 52°C for 40 h (Fig. 1). All three strains displayed the same pattern of growth when cultivated at 37°C. In contrast, the Δ*sigI-rsgI* strain displayed impaired growth at 52°C, while wt and Δ*rsgI* strains cultivated at this temperature had the same pattern of growth as that at 37°C. Thus, σ^I was essential for efficient growth when the cells were chronically exposed to elevated temperature. This result was in agreement with previously published observations (15, 16, 34).

Deletion of σ^I changes cell morphology during heat stress. During the spot assays described above, we noticed that the Δ*sigI-rsgI* colonies grown at 52°C displayed different morphology in comparison to that of the wt and Δ*rsgI* strains (Fig. 1b). Hence, we looked at the cells in close detail by scanning electron microscopy (SEM) of mid-logarithmic phase Δ*sigI-rsgI*, Δ*rsgI*, and wt strains cultivated at 37°C and 52°C (Fig. 2). The results correlated with those of the spot assays; cells of all three strains grown at 37°C had the typical rod shape of *B. subtilis*. In contrast, the Δ*sigI-rsgI* cells grown at 52°C displayed a previously unreported phenotype; that is, cells were bent and their shape was irregular even compared to that of the same cells grown at 37°C, as well as to that of Δ*rsgI* and wt cells grown at 37°C and 52°C. Finally, we tested whether the loss of MreBH expression could be responsible for the growth defect at 52°C. We performed the same type of experiment as in Fig. 1 using a Δ*mreBH* strain. The absence of *mreBH* did not result in impaired growth at any temperature tested when the cells were cultivated on LB agar plates (see Fig. S2 in the supplemental material).

σ^I influences expression of 131 genes. To identify the genes regulated by σ^I, we used Δ*sigI-rsgI* and wt strains and RNA-seq as the first approach. We cultivated the strains at 37°C and 52°C to mid-logarithmic phase and performed Illumina-based

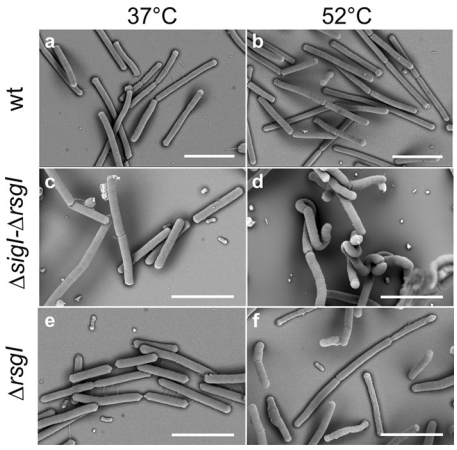

FIG 2 Cell shapes of the *B. subtilis* wt, Δ*sigI-rsgI*, and Δ*rsgI* cells imaged by scanning electron microscopy (SEM). (a) wt cells grown in LB at 37°C. (b) wt cells grown in LB at 52°C. (c) Δ*sigI-rsgI* cells grown in LB at 37°C. (d) Δ*sigI-rsgI* cells grown in LB at 52°C. (e) Δ*rsgI* cells grown in LB at 37°C. (f) Δ*regI* cells grown in LB at 52°C. The experiment was performed twice with identical results. Bars, 5 μm.

RNA-seq, with subsequent comparison of the Δ*sigI-rsgI* and wt transcriptomes to identify differentially expressed genes (DEGs).

First, we identified DEGs between Δ*sigI-rsgI* and wt cells grown at 37°C (>1.5-fold difference, <5% false discovery rate). Expression of 13 genes was decreased in the Δ*sigI-rsgI* strain relative to that of the wt (Fig. 3a, blue circle [i.e., genes positively regulated by σ^I]). Proteins encoded by these genes are mainly involved in transcription, translation, and coping with stress (see Fig. S3 and Table S2 in the supplemental material). Moreover, expression of 63 genes was increased (upregulated) in the Δ*sigI-rsgI* strain (Fig. 3b, blue circle [i.e., genes negatively regulated by σ^I]). They are mainly involved in the regulation of cell metabolism and in coping with stress (Fig. S3 and Table S2). Thus, at 37°C, σ^I positively affects 13 genes and negatively affects 63 genes.

Second, at 52°C we detected 55 downregulated and eight upregulated genes in the Δ*sigI-rsgI* strain compared to in the wt (Fig. 3, red circles). The majority of the affected genes are involved in the regulation of the cell metabolism (e.g., iron metabolism). In addition, upregulated genes included those involved in cell wall turnover (see Fig. S4 and Tables S4 and S5 in the supplemental material). Thus, at 52°C, σ^I positively affected 55 genes and negatively affected eight genes. A considerable portion of these genes encoded membrane-associated proteins (Fig. S3 and S4).

Six genes were downregulated at both temperatures, namely, *lytE*, *sigI*, *rsgI*, *mreBH*, *ykpC* (previously known to be σ^I dependent), and *spoVD*. Two genes—*ykrP*

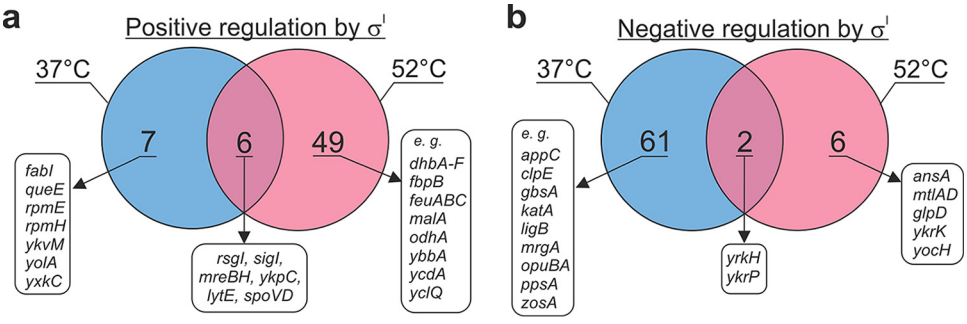

FIG 3 Genes in *B. subtilis* affected by σ^I. *B. subtilis* Δ*sigI-rsgI* and wt strains were grown at 37°C and 52°C in LB broth to an OD_{600} of ~0.45. RNA was extracted and libraries were prepared for transcriptome sequencing (RNA-seq). (a) Genes positively regulated by σ^I. These genes were downregulated in the Δ*sigI-rsgI* strain compared to in the wt strain. (b) Genes negatively regulated by σ^I. These genes were upregulated in Δ*sigI-rsgI* compared to wt.

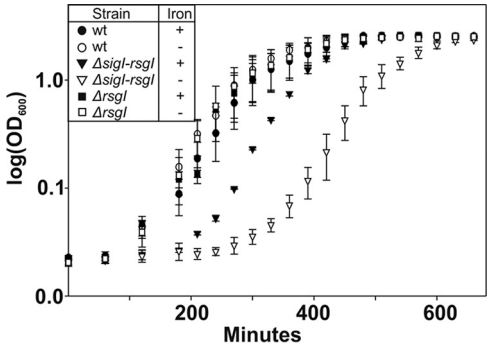

FIG 4 The σ^I factor is involved in iron metabolism in *B. subtilis*. Growth curves of the Δ*sigI-rsgI* (triangles), Δ*rsgI* (squares), and wt (circles) strains grown in defined MOPS medium at 37°C in the presence (filled shapes) or absence (empty shapes) of $FeCl_3$. The experiment was repeated three times. The error bars show ± standard deviation (SD).

and *yrkH*—were upregulated at both temperatures in the Δ*sigI-rsgI* strain compared to those in the wt.

Taking these results together, based on the RNA-seq data, we find that σ^I affected expression of 131 genes organized in 90 operons (Fig. 3; see also Tables S2 to S5 in the supplemental material). We note here that the identified DEGs could be regulated by σ^I either directly (the bona fide σ^I regulon) or indirectly.

Genes affected by σ^I in the context of the heat stimulon. To assess the importance of σ^I for the cell, we compared genes affected by σ^I with the genes stimulated by heat in wt (52°C versus 37°C) and investigated where among these genes the σ^I-affected genes ranked (see Fig. S5 and Tables S6 and S7 in the supplemental material). According to our RNA-seq data, the wt heat stimulon contained >370 genes (DEGs, >2-fold difference). Seven genes that were stimulated by σ^I (either directly or indirectly) belonged among the top 10% of the heat-stimulated genes (e.g., *malA*, carbon metabolism; *mreBH*, cell shape; and *dhb* genes, iron metabolism). We concluded that σ^I was involved in the regulation of expression of genes whose stimulation was prominent at elevated temperature.

σ^I is involved in iron metabolism. The RNA-seq data revealed that a significant number of genes influenced by σ^I (23 genes organized in 11 operons) were involved in iron metabolism (see Tables S3 and S4 in the supplemental material). Two of these genes were misregulated at 37°C and 21 genes were misregulated at 52°C.

The absence of σ^I increased expression of *zosA* (*pfeT*) [Fe(II) efflux pump] and *mrgA* (iron storage protein) at 37°C. We speculated that a combination of increased iron efflux and increased iron retention by MrgA in the Δ*sigI-rsgI* strain could affect iron homeostasis under limiting iron conditions. To test this hypothesis, we cultivated wt, Δ*sigI-rsgI*, and Δ*rsgI* strains in a defined 3-(*N*-morpholino)propanesulfonic acid (MOPS) medium containing or lacking iron. While the doubling time of all strains was comparable, the results repeatedly showed that at 37°C, the Δ*sigI-rsgI* strain had a markedly prolonged lag phase in the absence of iron (Fig. 4).

The presence of σ^I increased expression of 21 genes associated with iron metabolism at 52°C (Table S4), including genes involved in iron uptake (e.g., enzymes participating in siderophore [iron-chelating compound] synthesis and ABC transporters of siderophores). However, the Δ*sigI-rsgI* strain did not grow at 52°C in the defined MOPS medium, regardless of the presence or absence of iron (see Fig. S6 in the supplemental material).

The σ^I regulon is small. To start distinguishing between direct and indirect effects of σ^I, we cloned and purified recombinant σ^I by nickel affinity chromatography via the introduced C-terminal His tag (see Fig. S9 in the supplemental material). Next, we set up an *in vitro* transcription system to assess the ability of σ^I to directly regulate selected genes. We used 25 promoter regions identified in our RNA-seq analysis (including three

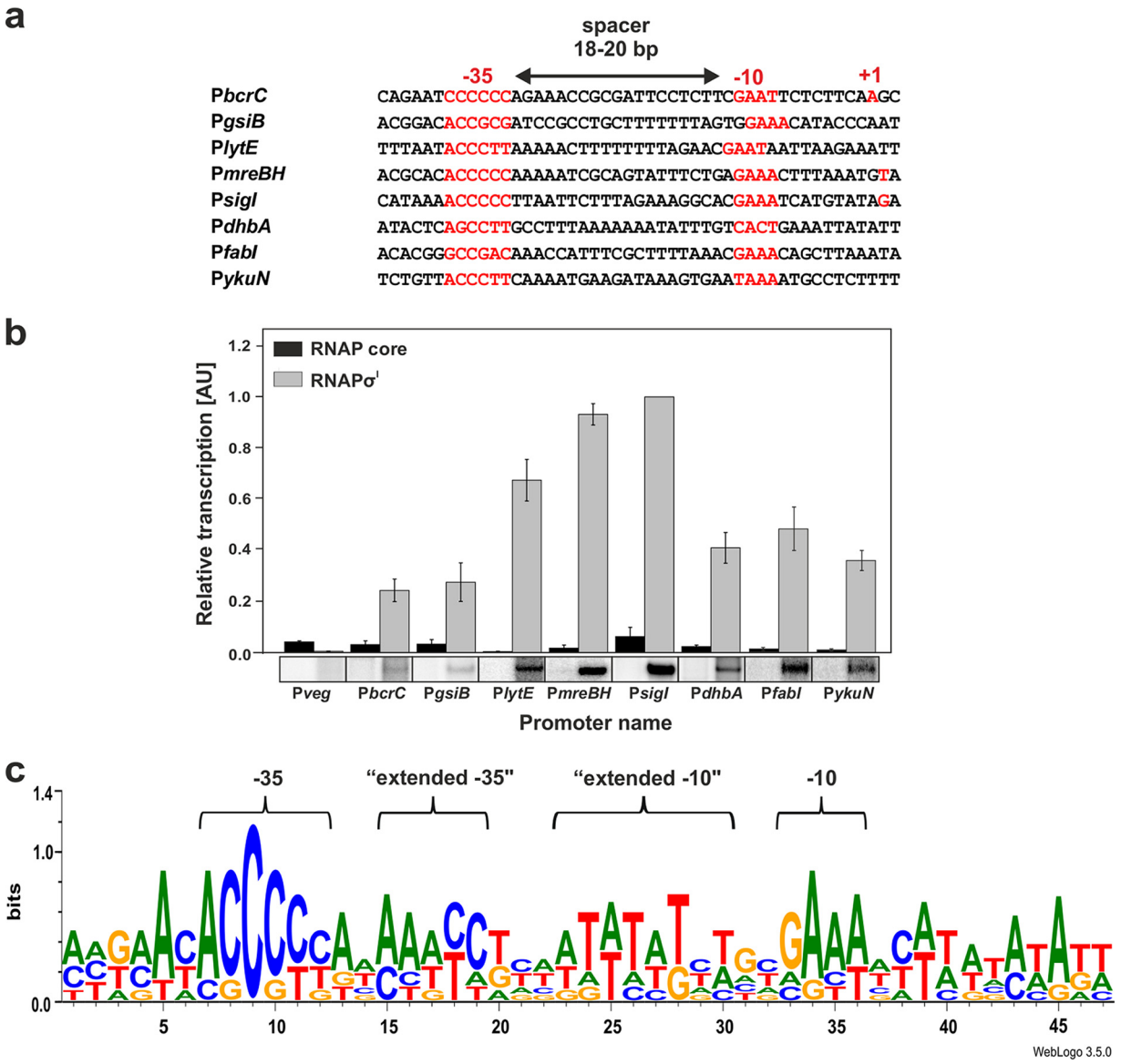

FIG 5 Multiple-round *in vitro* transcription assays with promoter regions of σ^I-regulated genes and RNAPσ^I. (a) Alignment of σ^I-dependent promoters. The −10 and −35 elements and +1 position for P*sigI* (16), P*mreBH*, and P*bcrC* (21) are in red. (b) Transcription was performed with the RNAPσ^I holoenzyme and the RNAP core. Transcription with the RNAP core was used to assess potential contamination of the RNAP core with σ factors. Promoter P*sigI* was used as a control and its transcription was set as 1. P*veg* (σ^A dependent) was used as a negative control for RNAPσ^I. Primary data (radioactively labeled transcripts resolved on polyacrylamide [PAA] gels) are shown below the graph. The error bars show averages from three independent experiments ± SD. (c) The σ^I consensus logo was created from the 8 promoter sequences shown in panel a. Conserved promoter elements are indicated above the logo.

promoter regions of genes previously demonstrated to be σ^I dependent) and the promoter regions of *bcrC* and *gsiB*, which were previously shown to be affected by σ^I but which did not appear in our transcriptomic screen (27 promoter regions in total). We performed transcription assays with these templates both with RNAPσ^A (see Fig. S7 in the supplemental material) and with RNAPσ^I (Fig. 5). RNAPσ^A was active on P*veg* (positive control) and also on promoter regions of the *lytE*, *sigI*, and *dhb* operon. These genes were previously known to contain σ^A-dependent promoters; our results confirmed these findings (Fig. S7). The experiments were done at 37°C. In addition, we also performed experiments with RNAPσ^I at 52°C, and the results were similar to those obtained at 37°C (data not shown).

RNAPσ^I was active on eight out of the 27 tested promoter regions, namely, *bcrC*, *gsiB*, *sigI-rsgI*, *lytE*, *mreBH-ykpC*, *dhb*, *yku*, and *fabI*. The first five promoter regions

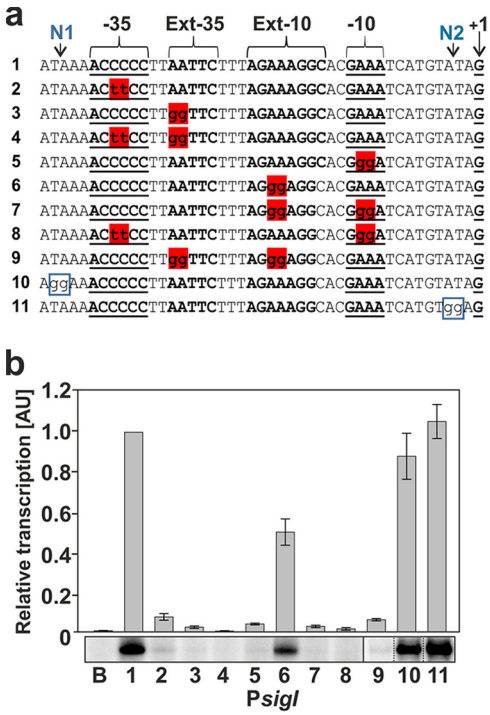

FIG 6 Multiple-round *in vitro* transcription assays with mutated P*sigI* promoter region. (a) Fragments of the P*sigI* promoter region used for evaluating the importance of the identified sequence elements. Fragment 1 contains the native P*sigI* promoter region. Fragments 2 to 9 contain mutations in −10, −35, extended −35 (Ext −35), extended −10 (Ext −10) elements, and their combinations. Mutations are highlighted in red. Fragments 10 and 11 contain control neutral (N) mutations highlighted in blue boxes. The −10 and −35 regions and +1 position are in bold and underlined. Extended elements are in bold. (b) *In vitro* transcription with specific double substitutions in P*sigI* −10 and −35 σ^I binding sites, extended −10, and extended −35 elements. Transcription was performed with the RNAP core (lane B, blank assay) and RNAPσ^I holoenzyme on PCR products as a template. The blank assay was used to demonstrate that the RNAP core was devoid of contaminating σ factors. Primary data (radioactively labeled transcripts resolved on PAA gel) are shown below the quantification graph; the vertical black line indicates the border between two PAA gels used for illustration. The dotted lines indicate lanes from the same gel electronically positioned next to each other. Error bars show averages from three independent experiments ± SD.

corresponded to genes/operons known to be regulated by σ^I. Thus, among the newly identified putative 22 promoter regions, RNAPσ^I was active on only three of them (promoter regions of *dhb* and *yku* operons and the *fabI* gene). Although we did not test the remaining 37 promoter regions that were positively affected by σ^I according to RNA-seq, this result strongly implied that the σ^I regulon is small.

Characterization of the σ^I promoter sequence. We aligned all of the known and newly identified σ^I promoter regions and created a σ^I promoter sequence logo (Fig. 5a and c). In comparison with the previously published σ^I promoter logo created from σ^I-dependent promoter regions from *Bacillales* (21, 36), in addition to the −10, −35 and "extended −35" elements, we also identified an "extended −10" element, which was dissimilar to the well-studied extended −10 element of σ^A-dependent promoters (37). A bioinformatic search for the σ^I consensus sequence among promoter regions of the σ^I-affected genes yielded no obvious additional hits.

As the σ^I logo was information rich (compared to that of, e.g., σ^A), we wished to determine the importance of the individual sequence elements for promoter activity. For this purpose, we used the P*sigI* promoter and systematically mutated these elements (Fig. 6). The results showed that double substitutions in −35 and −10 elements drastically reduced transcription (constructs 2 and 5, by ~90% and ~97%, respectively), and their combination (construct 8) virtually abolished transcription. Interestingly, the experiments revealed that the extended −35 element is highly

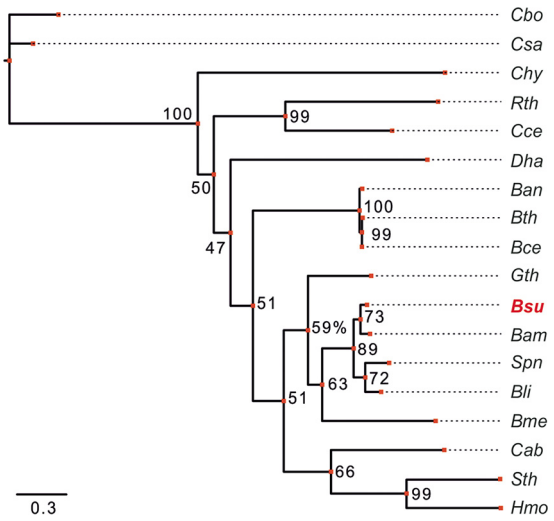

FIG 7 Phylogenetic tree of *B. subtilis* σ^I homologs. The list of the homologs is in Fig. S8 in the supplemental material. The phylogenetic tree was inferred with RAxML, and the best-scoring maximum likelihood tree is shown. Numbers denote bootstrap values (percent), as reported by RAxML. The scale bar represents expected number of substitutions per site. Cbo, *Clostridium botulinum*; Csa, *Clostridium saccharobutylicum*; Chy, *Carboxydothermus hydrogenoformans*; Rth, *Rumuniclostridium thermocellum*; Cce, *Clostridium cellulolyticum*; Dha, *Desulfitobacterium hafniense*; Ban, *Bacillus anthracis*; Bth, *Bacillus thuringiensis*; Bce, *Bacillus cereus*; Gth, *Geobacillus thermodenitrificans*; Bsu, *Bacillus subtilis*; Bam, *Bacillus amyloliquefaciens*; Spn, *Streptococcus pneumoniae*; Bli, *Bacillus licheniformis*; Bme, *Bacillus megaterium*; Cab, *Chlamydia abortus*; Sth, *Symbiobacterium thermophilum*; Hmo, *Heliobacterium modesticaldum*.

important, as its mutation almost completely canceled transcription (construct 3). The extended −10 element then led to an approximately 40% decrease in transcription activity (construct 6), suggesting that it is still required for optimal performance of the promoter (Fig. 6). Control "neutral" mutations without expected large effects on transcription confirmed that the "extended" elements are bona fide promoter regulatory sequences that are involved in σ^I-dependent transcription (Fig. 6b, constructs 10 and 11).

σ^I in different bacterial species. Finally, to identify σ^I homologs in other bacterial species, we performed BLAST (38) searches and created a phylogenetic tree (Fig. 7) from the most related amino acid sequences (see Fig. S8 in the supplemental material). The closest relatives of *B. subtilis* σ^I were proteins from *Bacillus amyloliquefaciens*, a putative σ^I from *Streptococcus pneumoniae*, and σ^I from *Bacillus licheniformis*.

DISCUSSION

In this study, we performed a comprehensive characterization of σ^I from *B. subtilis*. We determined the effect of its presence/absence on gene expression during exponential growth in a rich medium at 37°C and 52°C, identified its involvement in iron metabolism, and defined its transcriptional properties.

Effect of σ^I on gene expression. The σ^I factor affected expression of 131 genes. Nevertheless, the majority of these genes appear to be indirectly affected by σ^I. Of the seven genes that had been known or proposed to be regulated by σ^I, we identified five by RNA-seq, which gave us confidence in the credibility of the transcriptomic data. We also demonstrated the direct ability of RNAPσ^I to initiate transcription from upstream regions of these genes. In addition, we detected σ^I-dependent promoter activity for the *bcrC* and *gsiB* genes *in vitro*. However, we did not identify these genes in our RNA-seq analysis. This could be due to the very weak transcriptional activity of the σ^I-dependent promoters of these genes (Fig. 5b) and, perhaps, to the specific experimental conditions used; i.e., chronic heat stress (this study) versus temperature shift (15, 21).

Out of the 22 tested putative new promoter regions, *in vitro* transcription analysis revealed three σ^I-dependent promoters driving transcription of nine genes (*dhbA-dhbC-dhbE-dhbB-dhbF*, *ykuN-ykuO-ykuP*, and *fabI*). The first two operons are involved in

iron metabolism. The *dhb* operon is involved in bacillibactin siderophore synthesis (39). The *yku* operon encodes flavodoxins that replace ferredoxin under conditions of iron limitation and catalyze the O_2-dependent desaturation of the acyl chain of membrane phospholipids (40). In our transcriptomic data (in SigI-null relative to wt), we observed decreased expression of *ykuO* and *ykuP* genes at 52°C, but their σ^I-dependent promoter was identified in *in vitro* transcription within a DNA fragment preceding the first gene of the operon, *ykuN*. Careful inspection of the RNA-seq data revealed that also the *ykuN* gene was affected ($\sim 2\times \downarrow$) by the absence of σ^I in the same way as *ykuO* and *ykuP*, but this change in expression was not deemed significant by the DESeq2 algorithm, due to the low level of *ykuN* expression. The product of the *fabI* gene is enoyl-acyl carrier protein reductase, which participates in fatty acid biosynthesis (41). Expression of the *fabI* gene was affected at 37°C, suggesting that this effect is heat shock independent.

In summary, the σ^I regulon, as of now, is one of the smallest known *B. subtilis* regulons, currently containing 16 genes. A search for σ^I promoter sequences within the upstream regions of genes that did not function in *in vitro* transcriptions revealed, in all cases but one (*feuA*), the −10 GAAA motif and the absence of −35 regions. Hence, it is possible that some of these genes are still regulated by σ^I, and the presence of an unknown regulator is required. Moreover, as there are still 37 promoter regions with putative activation by σ^I untested, a few more genes may be added to the list in the future.

σ^I-dependent promoters. We used all eight known promoter regions to create the σ^I promoter sequence logo (Fig. 5). Our logo revealed that σ^I-dependent promoters are information rich in the spacer region; besides −35 and −10 elements, extended −35 and −10 elements were identified. Importantly, functional analysis of extended −35 and −10 elements demonstrated their significance for the promoter activity (Fig. 6). The importance of the spacer region sequence for efficient promoter utilization was demonstrated in a number of previous studies. In Gram-negative *Escherichia coli*, it was shown that an AT-rich spacer could both stimulate and inhibit transcription initiation, depending on the promoter (42, 76). In Gram-positive *B. subtilis* it was demonstrated for extracytoplasmic function (ECF) σ factor-dependent promoters that the homopolymeric T-tract motif, proximal to the −35 element, functioned in combination with the core promoter sequences to determine selectivity of ECF σ factors (43). This homopolymeric T-tract is reminiscent of, and might be analogous to, the σ^I extended −35 element described here. The sequence and position of the σ^I extended −10 element then differs from the TRTGn motif that was described for $\sigma^{A/70}$-dependent promoters (44), where it precedes the −10 element by 2 to 5 bp and interacts with domain 3 of $\sigma^{A/70}$ (45, 46). The extended −10 element of σ^I, however, is positioned 7 to 8 bp upstream of the −10 element, and may thus not interact with domain 3. It is possible that the A·T pairs within the "extended" promoter elements increase conformational flexibility (47, 48) of the relatively long spacer (18 to 20 bp; compared to ~17-bp σ^A promoters [49]) and thus contribute to promoter accommodation onto RNAP and to proper interactions of −35 and −10 elements with σ^I. Future studies will be required to address the detailed roles of the extended elements in recognition of these promoters by RNAP.

Cellular role of σ^I. Despite the relatively small number of genes directly regulated and indirectly affected by σ^I, this σ factor is important for proper functioning of the cell. No single gene directly regulated by σ^I is likely to be solely responsible for the growth defect at elevated temperature. Nevertheless, some of the indirectly affected genes could be responsible for this phenotype. The growth defect might be, at least in part, due to downregulation of genes involved in carbon uptake and central metabolism, such as *malA*, which encodes NAD(H)-dependent phospho-α-1,4-glucosidase (50) (the 3rd most upregulated gene in wt 37°C→52°C), and *odhA*, which encodes 2-oxoglutarate dehydrogenase, an essential enzyme of the tricarboxylic acid (TCA) cycle (51).

TABLE 1 List of strains and plasmids

Strain or plasmid	Relevant characteristics[a]	Source or reference
B. subtilis		
LK#1432 (BSB1)	BaSysBio wt 168 trp+	13
LK#1550	Δ*sigI-rsgI*::*spc*, BaSysBio	This work
MGNA-A781 (LK#1435)	Δ*rsgI*::MLS	72
LK#1456	Δ*rsgI*::MLS, BaSysBio	This work
MH5636 (LK#1275)	Bsu RNAP *rpoC*-10×His	66
DK5247 (LK#2181)	Δ*mreBH*::*kan*	73; gift from D. Kearns
LK#2191	Δ*mreBH*::*kan*, BaSysBio	This work
Escherichia coli		
LK#278	pET-22b, DH5α	This work
LK#475	pGEX-5X-3	This work
LK#1242	BL21/pSigI-6×His, BL21(DE3)	This work
LK#805 (LK22)	pCD2/Bsu_sigA, BL21(DE3)	67
LK#180 (pRLG770)	pRLG770, DH5α	74
LK#1177 (LK7558)	pRLG770 with P*veg* (−38/+1, +1G), DH5α	75
LK#1236	pRLG770 with P*bcrC*, DH5α	This work
LK#1230	pRLG770 with P*gsiB*, DH5α	This work
LK#1238	pRLG770 with P*lytE*, DH5α	This work
LK#1453	pRLG770 with P*mreBH*, DH5α	This work
LK#1452	pRLG770 with P*sigI*, DH5α	This work
LK#1766	pRLG770 with P*dhbA*, DH5α	This work

[a]MLS, macrolide-lincosamide-streptogramin B resistance; *kan*, kanamycin resistance gene; *spc*, spectinomycin resistance gene.

Furthermore, we observed a previously unreported malformed cell shape of Δ*sigI-rsgI* at 52°C. This malformation might be attributed to pronounced downregulation of *mreBH* and *lytE*, as it was previously demonstrated that both MreBH and LytE were required for proper cell shape (27, 52). Moreover, these two proteins were shown to interact in the cell (19, 27). The downregulation of both *mreBH* and *lytE* in the Δ*sigI-rsgI* strain at 52°C was quite pronounced (~16× ↓ for both genes), whereas at 37°C it was rather moderate (~3× ↓ for both genes), suggesting why the change in cell morphology was observed only at the higher temperature. The downregulation of *mreBH* alone, then, was not responsible for the impaired growth, as a Δ*mreBH* strain did not display this growth phenotype in spot assays (Fig. S2). In addition, *yfiY* and *yjeA*, which are involved in cell wall metabolism, were also downregulated, and this might have contributed to the distorted cell shape.

A significant fraction of the affected genes in the Δ*sigI* mutant were genes involved in iron metabolism. Accordingly, a growth defect, prolonged lag phase, was observed in the absence of iron at 37°C (Fig. 4). This could be due to altered iron homeostasis, as iron uptake during the lag phase is important for preparing the cell for subsequent exponential growth (53).

Finally, homologs of σ^I from *B. subtilis* exist in other *Bacillus* and *Clostridium* spp., as well as in some other species, such as *Heliobacterium* spp. and *Geobacillus* spp. (54). A phylogenetic tree of σ^I factor homologs is shown in Fig. 7. Interestingly, in different organisms, these factors regulate divergent sets of genes (thermotolerance [15, 22], virulence [55], and polysaccharide sensing [36]), although the promoter consensus sequences, at least between *Bacillus* and *Clostridium* species, are similar (36), illustrating, analogously to, e.g., eukaryotic Tcf7l1 (56), how different species tailored the use of a transcription factor to their specific needs.

MATERIALS AND METHODS

Bacterial strains and DNA manipulations. The strains and plasmids used in this study are listed in Table 1. For the study, we used *B. subtilis* 168 trp+ (BaSysBio) as the model organism (13). Competent *E. coli* cells were prepared as described previously (57); competent *B. subtilis* cells were prepared as described previously (58). PCR analysis was performed using the Expand High Fidelity PCR system (Roche). The list of the primers is shown in Table S1 in the supplemental material.

The Δ*sigI-rsgI*::spc knockout strain was prepared via double crossover. The upstream (primers 1478/sigI_rsgI_LA_F and 1479/sigI_rsgI_LA_R) and downstream (primers 1480/sigI_rsgI_RA_F and 1481/

sigI_rsgI_RA_R) regions of the *sigI-rsgI* operon were cloned into the pGEX-5X-3 plasmid vector bearing an inserted spectinomycin cassette (LK#475). The resulting plasmid (LK#1549) was transformed into BaSysBio competent cells. The final Δ*sigI-rsgI*::spc strain (LK#1550) was selected on spectinomycin plates. In the Δ*rsgI*::MLS strain (MGNA-A781; source, National BioResource Project [NBRP] *B. subtilis*, Japan), the *rsgI* gene is disrupted and not expressed. The Δ*rsgI*::MLS BaSysBio strain (LK#1456) was obtained by transformation of genomic DNA (gDNA) from the purchased MGNA-A781 strain into BaSysBio competent cells.

For overproduction of σ^I, the *sigI* gene was amplified with the primers 1164/sigI_For and 1166/sigI_Rev_His and cloned using NdeI and XhoI restriction enzymes into expression vector pET-22b (comprising the 6×His tag). The resulting plasmid, named pSigI-6×His (LK#1242), was transformed into BL21(DE3) competent cells. All promoter regions of σ^A- and σ^I-dependent genes were amplified from genomic DNA of *B. subtilis* BaSysBio with the primers 1067/PgsiB_For to 1897/PxlyA_R (Table S1) and cloned into the pRLG770 plasmid using EcoRI and HindIII restriction enzymes. Purified supercoiled plasmids for multiple-round *in vitro* transcription assays were obtained using the Wizard Plus Midipreps DNA purification system (Promega) with subsequent phenol-chloroform extraction and ethanol precipitation. The plasmids were dissolved in water. All constructs were verified by sequencing.

Media and growth conditions. For all experiments (with the exception of those testing iron requirement), precultures were inoculated from single colonies from LB agar plates and grown overnight in LB at 37°C. Overnight precultures were inoculated to fresh room temperature (RT) media to an optical density at 600 nm (OD_{600}) of 0.03 and grown at 37°C and 52°C, respectively. Precultures of Δ*sigI-rsgI*, Δ*rsgI*, and Δ*mreBH* strains were supplemented with spectinomycin (100 μg/ml), lincomycin (12.5 μg/ml) plus erythromycin (0.5 μg/ml), or kanamycin (10 μg/ml), respectively.

To monitor iron requirements, Δ*sigI-rsgI*, Δ*rsgI*, and wt strains were inoculated from a single colony on LB agar plates to MOPS medium containing or lacking iron and grown overnight at 37°C. Overnight precultures were inoculated to a fresh MOPS medium to an OD_{600} of 0.03; cultures were grown at 37°C for 24 h. Afterwards, cultures were inoculated into fresh MOPS medium at room temperature (RT) at an OD_{600} of 0.03 and grown at 37°C and 52°C. Growth was monitored at OD_{600}. MOPS medium containing iron consisted of 50 mM MOPS [3-(*N*-morpholino)propanesulfonic acid], 10 mM $(NH_4)_2SO_4$, 1 mM KH_2PO_4, 2 mM $MgCl_2$, 2 mM $CaCl_2$, 5 μM $MnCl_2$, 0.5 μM $FeCl_3$, 50 μg/ml of each amino acid, and 0.4% glucose. MOPS medium lacking iron consisted of 50 mM MOPS, 10 mM $(NH_4)_2SO_4$, 1 mM KH_2PO_4, 2 mM $MgCl_2$, 2 mM $CaCl_2$, 5 μM $MnCl_2$, 25 μM 2,2′-bipyridine, 50 μg/ml of each amino acid, and 0.4% glucose. To chelate iron, 2,2′-Bipyridine was added.

Spot assays. Δ*sigI-rsgI*, Δ*rsgI*, and wt strains were grown in LB broth at 37°C to mid-logarithmic phase (OD_{600} = 0.5). Serially diluted aliquots (1 μl; 10× dilutions between spots) were spotted on 1.5% LB agar plates lacking antibiotics and allowed to dry. Plates were incubated at 37°C and 52°C for 40 h. Bacterial colonies were visualized using an SZX10 stereomicroscope (Olympus) and photographed using an Olympus E-600 digital camera.

Electron microscopy. Cells were grown to exponential phase (OD_{600} = 0.5) at 37°C and 52°C and fixed in buffered 3% glutaraldehyde at 4°C. The extensively washed cells were then sedimented onto poly-L-lysine-coated glass coverslips at 4°C overnight. The coverslips were dehydrated through an alcohol series followed by absolute acetone and critical point dried in a K850 critical point dryer (Quorum Technologies Ltd., Ringmer, UK). The dried samples were sputter coated with 3 nm of platinum in a Q150T turbo-pumped sputter coater (Quorum Technologies Ltd., Ringmer, UK). The final samples were examined in an FEI Nova NanoSEM scanning electron microscope (FEI, Brno, Czech Republic) at 5 kV, using concentric backscatter (CBS) and through-the-lens (TLD) detectors. The cells were imaged according to a protocol described previously (59).

Bacterial growth for RNA sequencing. *Bacillus subtilis* Δ*sigI-rsgI* and wt strains (LK#1550 and LK#1432, respectively) were inoculated from a single colony to 10 ml of LB medium. Cultures were grown overnight at 37°C. The next day, the cultures were inoculated into 20 ml of LB medium (RT) to an OD_{600} of ~0.01 and grown at 37°C and 52°C, respectively. Cells were harvested in exponential phase (OD_{600}, ~0.5). Three ml of the culture were immediately treated with a double volume of RNAprotect bacteria reagent (Qiagen) for 5 min at RT to prevent degradation of RNA. Cells were pelleted and frozen immediately. In all steps of cultivation (with the exception of the last step of cultivation for total RNA isolation), the medium for the Δ*sigI-rsgI* strain was supplemented with spectinomycin (100 μg/ml). The experiment was repeated three times.

RNA extraction protocol. RNA was extracted using the RNeasy minikit 50 (Qiagen) according to the manufacturer's protocol. Finally, RNA was treated twice with DNase (Turbo DNA-free kit, Ambion).

RNA library construction. Two micrograms of total RNA were rRNA-depleted with RiboMinus transcriptome isolation kit, bacteria (Invitrogen). A strand-specific library was prepared for each sample with an Illumina-compatible NEXTflex rapid directional RNA-seq kit (Bioo Scientific) used according to the manufacturer's protocol.

Library sequencing. Transcriptome profiling with RNA-seq was performed at the Molecular Biology Laboratory (EMBL) Genomics Core Facility (Heidelberg, Germany). The pooled barcoded library (four samples in biological triplicates) was sequenced in a single lane using an Illumina HiSeq 2000 instrument (50 bp single end; ~8 to 16 million reads per sample regime). The quality of sequencing reads was checked with FastQC 0.11.2 (www.bioinformatics.babraham.ac.uk/projects/fastqc).

Alignment. Reads were aligned to the *Bacillus subtilis* subsp. *subtilis* strain 168 genome (NCBI nucleotide accession no. NC_000964) using Burrows-Wheeler Aligner (BWA) 0.7.9a-r786 (60) and samtools 0.1.19 (61). Alignment quality was checked using QualiMap 2.1.3 (62) and the Integrative

Genomics Viewer (IGV) 2.3 (63). *B. subtilis* genome annotation was obtained from the NCBI Assembly database (accession no. GCF_000009045.1). Analysis of differential gene expression was performed using R (www.r-project.org) and the Bioconductor package DESeq2 (64, 65) at a 5% false discovery rate (FDR). Data from RNA-seq can be found at https://www.ebi.ac.uk/arrayexpress/experiments/E-MTAB-6314.

Protein purification. *B. subtilis* RNAP with a 10×His-tagged β′ subunit was purified from the MH5636 strain, as described previously (66). σ^I protein purification was performed from the BL21/pSigI-6×His, BL21(DE3) strain (LK#1242) as described previously (66), with some modifications. Briefly, induction of σ^I was carried out at an OD_{600} of 0.6 with 0.05 mM IPTG (isopropyl-β-D-thiogalactopyranoside) for 3 h at RT. Cells were harvested by centrifugation, and the pellet was resuspended in P buffer (30 mM NaCl, 50 mM Na_2HPO_4, 3 mM 2-mercaptoethanol, and 1 mM PMSF [pH 7.3]) to avoid subsequent precipitation of the protein. The cells were then disrupted by sonication for 20 × 10 s on ice. Figure S9a in the supplemental material shows cell lysates before/after induction and soluble/insoluble fraction. The protein was purified from the soluble fraction by affinity chromatography using Ni-nitrilotriacetic acid (NTA)–agarose (Qiagen). After elution with 400 mM imidazole in P buffer, fractions containing σ^I were pooled and dialyzed against storage buffer (Fig. S9b in the supplemental material). The σ^A subunit of RNAP was overproduced from the pCD2 plasmid (67) (LK22) and purified as described previously (68). Proteins were dialyzed against storage buffer containing 50 mM Tris-HCl (pH 7.3 and 8.0 for σ^I and σ^A, respectively), 100 mM NaCl, 50% glycerol, and 3 mM 2-mercaptoethanol, and stored at −20°C. Proteins were visualized in NuPage 4 to 12% Bis-Tris gels (Invitrogen) with Novex Sharp prestained protein standard as a marker (Invitrogen).

***In vitro* transcription assays.** The *B. subtilis* RNA polymerase core was reconstituted with a saturating concentration of σ^A or σ^I (ratio 1:5) in storage buffer (50 mM Tris-HCl [pH 8.0], 0.1 M NaCl, and 50% glycerol) for 10 min at 37°C. Multiple-round transcription reactions were carried out in 10-μl reaction volumes with 30 nM RNAP holoenzyme and 100 ng of supercoiled plasmid DNA templates containing specific promoters (Fig. 5) or 100 ng of PCR-product templates containing promoter regions (Fig. 6). The transcription buffer contained 40 mM Tris-HCl (pH 8.0), 10 mM $MgCl_2$, 1 mM dithiothreitol (DTT), 0.1 mg/ml bovine serum albumin (BSA), and 60 mM NaCl. ATP, CTP, and GTP were at 200 μM, and UTP was at 10 μM plus 2 μM radiolabeled [α-^{32}P]UTP. All transcription experiments were done at 37°C. Transcription reaction was started with RNAP and allowed to proceed for 15 min. Transcription was stopped with equal volumes (10 μl) of formamide stop solution (95% formamide and 20 mM EDTA [pH 8.0]). Samples were loaded onto 7 M urea-7% polyacrylamide gels and electrophoresed. Dried gels were scanned with Molecular Imager FX (Bio-Rad) and visualized and analyzed using Quantity One software (Bio-Rad). The strong constitutive σ^A-dependent P*veg* promoter cloned into pRLG770 was used as a control.

Sequence logo creation. The promoter sequence logo (Fig. 5d) was created from eight promoter regions (Fig. 5a) using the WebLogo 3 tool available online (http://weblogo.threeplusone.com/create.cgi).

Phylogenetic tree creation. Selection of σ^I homologs was based on the BLAST search (https://blast.ncbi.nlm.nih.gov/). The selected sequences were aligned using MUSCLE 3.8.31 (69) with default parameters (70). The phylogenetic tree was inferred using the RAxML BlackBox Web server (71); settings for protein sequences and maximum likelihood search were chosen, and other settings were left as default (Jones-Taylor-Thornton [JTT] substitution matrix).

SUPPLEMENTAL MATERIAL

Supplemental material for this article may be found at https://doi.org/10.1128/JB.00251-18.

SUPPLEMENTAL FILE 1, PDF file, 1.8 MB.

SUPPLEMENTAL FILE 2, XLSX file, 0.1 MB.

ACKNOWLEDGMENTS

This work was funded by grants P305/12/G034 from the Czech Science Foundation (to L.K.), 17-29680A from the Czech Health Research Council (to L.K., bioinformatics), and 322815 from the Grant Agency of the Charles University (to O.R.). The work was also supported by the Czech research infrastructure for systems biology C4SYS (project LM2015055) and by the Charles University grants PRIMUS/MED/26 and UNCE 204013 (to M.P.). We also gratefully acknowledge the access to the electron microscopy facility supported by projects LO1509 of the Ministry of Education, Youth and Sports of the Czech Republic, and CZ.2.16/3.1.00/24023 of the Operational Program Prague-Competitiveness project, supported by the European Union.

We also thank Ivan Barvík for comments on the manuscript.

REFERENCES

1. Barvík I, Rejman D, Panova N, Šanderová H, Krásný L. 2017. Non-canonical transcription initiation: the expanding universe of transcription initiating substrates. FEMS Microbiol Rev 41:131–138. https://doi.org/10.1093/femsre/fuw041.

2. Minakhin L, Bhagat S, Brunning A, Campbell EA, Darst SA, Ebright RH, Severinov K. 2001. Bacterial RNA polymerase subunit ω and eukaryotic RNA polymerase subunit RPB6 are sequence, structural, and functional homologs and promote RNA polymerase assembly. Proc Natl Acad Sci U S A 98:892–897. https://doi.org/10.1073/pnas.98.3.892.
3. Weiss A, Moore BD, Tremblay MHJ, Chaput D, Kremer A, Shaw LN. 2017. The ω subunit governs RNA polymerase stability and transcriptional specificity in *Staphylococcus aureus*. J Bacteriol 199:e00459-16. https://doi.org/10.1128/JB.00459-16.
4. Lopez de Saro FJ, Woody AYM, Helmann JD. 1995. Structural analysis of the *Bacillus subtilis* δ factor: a protein polyanion which displaces RNA from RNA polymerase. J Mol Biol 252:189–202. https://doi.org/10.1006/jmbi.1995.0487.
5. Rabatinová A, Šanderová H, Matějčková JJ, Korelusová J, Sojka L, Barvík I, Veronika PapouŠková Sklenár V, Žídek L, Krásný L. 2013. The δ subunit of RNA polymerase is required for rapid changes in gene expression and competitive fitness of the cell. J Bacteriol 195:2603–2611. https://doi.org/10.1128/JB.00188-13.
6. Prajapati RK, Sengupta S, Rudra P, Mukhopadhyay J. 2016. *Bacillus subtilis* δ functions as a transcriptional regulator by facilitating the open complex formation. J Biol Chem 291:1064–1075. https://doi.org/10.1074/jbc.M115.686170.
7. Burgess RR. 1969. Separation and characterization of the subunits of ribonucleic acid polymerase. J Biol Chem 244:6168–6176.
8. Paget MS. 2015. Bacterial σ factors and anti-σ factors: structure, function and distribution. Biomolecules 5:1245–1265. https://doi.org/10.3390/biom5031245.
9. Dombroski AJ, Walter WA, Record MT, Slegele DA, Gross CA. 1992. Polypeptides containing highly conserved regions of transcription initiation factor σ^{70} exhibit specificity of binding to promoter DNA. Cell 70:501–512. https://doi.org/10.1016/0092-8674(92)90174-B.
10. Dombroski AJ, Walter WA, Gross CA. 1993. Amino-terminal amino acids modulate σ factor DNA-binding activity. Genes Dev 7:2446–2455. https://doi.org/10.1101/gad.7.12a.2446.
11. Gruber TM, Gross CA. 2003. Multiple σ subunits and the partitioning of bacterial transcription space. Annu Rev Microbiol 57:441–466. https://doi.org/10.1146/annurev.micro.57.030502.090913.
12. Helmann JD. 2016. *Bacillus subtilis* extracytoplasmic function (ECF) σ factors and defense of the cell envelope. Curr Opin Microbiol 30:122–132. https://doi.org/10.1016/j.mib.2016.02.002.
13. Nicolas P, Mäder U, Dervyn E, Rochat T, Leduc A, Pigeonneau N, Bidnenko E, Marchadier E, Hoebeke M, Aymerich S, Becher D, Bisicchia P, Botella E, Delumeau O, Doherty G, Denham EL, Fogg MJ, Fromion V, Goelzer A, Hansen A, Härtig E, Harwood CR, Homuth G, Jarmer H. 2012. Condition-dependent transcriptome reveals high-level regulatory architecture in *Bacillus subtilis*. Science 335:1103–1106. https://doi.org/10.1126/science.1206848.
14. McDonnell GE, Wood H, Devine KM, Mcconnell DJ. 1994. Genetic control of bacterial suicide: regulation of the induction of PBSX in *Bacillus subtilis*. J Bacteriol 176:5820–5830. https://doi.org/10.1128/jb.176.18.5820-5830.1994.
15. Zuber U, Drzewiecki K, Hecker M. 2001. Putative sigma factor SigI (YkoZ) of *Bacillus subtilis* is induced by heat shock. J Bacteriol 183:1472–1475. https://doi.org/10.1128/JB.183.4.1472-1475.2001.
16. Asai K, Ootsuji T, Obata K, Matsumoto T, Fujita Y, Sadaie Y. 2007. Regulatory role of RsgI in σ^I expression in *Bacillus subtilis*. Microbiology 153:92–101. https://doi.org/10.1099/mic.0.29239-0.
17. Salzberg LI, Powell L, Hokamp K, Botella E, Noone D, Devine KM. 2013. The WalRK (YycFG) and σ^I RsgI regulators cooperate to control CwlO and LytE expression in exponentially growing and stressed *Bacillus subtilis* cells. Mol Microbiol 87:180–195. https://doi.org/10.1111/mmi.12092.
18. Liu TY, Chu SH, Hu YN, Wang JJ, Shaw GC. 2017. Genetic evidence that multiple proteases are involved in modulation of heat-induced activation of the sigma factor SigI in *Bacillus subtilis*. FEMS Microbiol Lett 364:fnx054. https://doi.org/10.1093/femsle/fnx054.
19. Huang WZ, Wang JJ, Chen HJ, Chen JT, Shaw GC. 2013. The heat-inducible essential response regulator WalR positively regulates transcription of *sigI*, mreBH *and lytE* in *Bacillus subtilis* under heat stress. Res Microbiol 164:998–1008. https://doi.org/10.1016/j.resmic.2013.10.003.
20. Schirner K, Errington J. 2009. The cell wall regulator σ^I specifically suppresses the lethal phenotype of *mbl* mutants in *Bacillus subtilis*. J Bacteriol 191:1404–1413. https://doi.org/10.1128/JB.01497-08.
21. Tseng C-L, Shaw G-C. 2008. Genetic evidence for the actin homolog gene *mreBH* and the bacitracin resistance gene *bcrC* as targets of the alternative sigma factor SigI of *Bacillus subtilis*. J Bacteriol 190:1561–1567. https://doi.org/10.1128/JB.01497-07.
22. Tseng C-L, Chen J-T, Lin J-H, Huang W-Z, Shaw G-C. 2011. Genetic evidence for involvement of the alternative sigma factor SigI in controlling expression of the cell wall hydrolase gene *lytE* and contribution of LytE to heat survival of *Bacillus subtilis*. Arch Microbiol 193:677–685. https://doi.org/10.1007/s00203-011-0710-0.
23. Dubrac S, Bisicchia P, Devine KM, Msadek T. 2008. A matter of life and death: Cell wall homeostasis and the WalKR (YycGF) essential signal transduction pathway. Mol Microbiol 70:1307–1322. https://doi.org/10.1111/j.1365-2958.2008.06483.x.
24. Podlesek Z, Comino A, Herzog-Velikonja B, Zgur-Bertok D, Komel RGM. 1995. *Bacillus licheniformis* bacitracin-resistance ABC transporter: relationship to mammalian multidrug resistance. Mol Microbiol 16:969–976. https://doi.org/10.1111/j.1365-2958.1995.tb02322.x.
25. Cao M, Moore CM, Helmann JD. 2005. *Bacillus subtilis* paraquat resistance is directed by σ^M, an extracytoplasmic function σ factor, and is conferred by YqjL and BcrC. J Bacteriol 187:2948–2956. https://doi.org/10.1128/JB.187.9.2948-2956.2005.
26. Cao M, Helmann JD. 2002. Regulation of the *Bacillus subtilis bcrC* bacitracin resistance gene by two extracytoplasmic function σ factors. J Bacteriol 184:6123–6129. https://doi.org/10.1128/JB.184.22.6123-6129.2002.
27. Carballido-López R, Formstone A, Li Y, Ehrlich SD, Noirot P, Errington J. 2006. Actin homolog MreBH governs cell morphogenesis by localization of the cell wall hydrolase LytE. Dev Cell 11:399–409. https://doi.org/10.1016/j.devcel.2006.07.017.
28. Soufo HJD, Graumann PL. 2003. Actin-like proteins MreB and Mbl from *Bacillus subtilis* are required for bipolar positioning of replication origins. Curr Biol 13:1916–1920. https://doi.org/10.1016/j.cub.2003.10.024.
29. Kawai Y, Asai K, Errington J. 2009. Partial functional redundancy of MreB isoforms, MreB, Mbl and MreBH, in cell morphogenesis of *Bacillus subtilis*. Mol Microbiol 73:719–731. https://doi.org/10.1111/j.1365-2958.2009.06805.x.
30. Jones LJF, Carballido-López R, Errington J. 2001. Control of cell shape in bacteria: helical, actin-like filaments in *Bacillus subtilis*. Cell 104:913–922. https://doi.org/10.1016/S0092-8674(01)00287-2.
31. Margot P, Wahlen M, Gholamhuseinian A, Piggot P, Karamata D. 1998. The *lytE* gene of *Bacillus subtilis* 168 encodes a cell wall hydrolase. J Bacteriol 180:749–752.
32. Bisicchia P, Noone D, Lioliou E, Howell A, Quigley S, Jensen T, Jarmer H, Devine KM. 2007. The essential YycFG two-component system controls cell wall metabolism in *Bacillus subtilis*. Mol Microbiol 65:180–200. https://doi.org/10.1111/j.1365-2958.2007.05782.x.
33. Hashimoto M, Ooiwa S, Sekiguchi J. 2012. Synthetic lethality of the *lytE cwlO* genotype in *Bacillus subtilis* is caused by lack of D, L-endopeptidase activity at the lateral cell wall. J Bacteriol 194:796–803. https://doi.org/10.1128/JB.05569-11.
34. Völker U, Engelmann S, Maul B, Riethdorf S, Völker A, Schmid R, Mach H, Hecker M. 1994. Analysis of the induction of general stress proteins of *Bacillus subtilis*. Microbiology 140:741–752. https://doi.org/10.1099/00221287-140-4-741.
35. Mueller JP, Bukusoglu G, Sonenshein AL. 1992. Transcriptional regulation of *Bacillus subtilis* glucose starvation-inducible genes: control of *gsiA* by the ComP-ComA signal transduction system. J Bacteriol 174:4361–4373. https://doi.org/10.1128/jb.174.13.4361-4373.1992.
36. Muñoz-Gutiérrez I, Ortiz de Ora L, Rozman Grinberg I, Garty Y, Bayer EA, Shoham Y, Lamed R, Borovok I. 2016. Decoding biomass-sensing regulons of *Clostridium thermocellum* alternative sigma-I factors in a heterologous *Bacillus subtilis* host system. PLoS One 11:e0146316. https://doi.org/10.1371/journal.pone.0146316.
37. Jarmer H, Larsen TS, Krogh A, Saxild HH, Brunak S, Knudsen S. 2001. σ^A recognition sites in the *Bacillus subtilis* genome. Microbiology 147:2417–2424. https://doi.org/10.1099/00221287-147-9-2417.
38. Agarwala R, Barrett T, Beck J, Benson DA, Bollin C, Bolton E, Bourexis D, Brister JR, Bryant SH, Canese K, Charowhas C, Clark K, Dicuccio M, Dondoshansky I, Federhen S, Feolo M, Funk K, Geer LY, Gorelenkov V, Hoeppner M, Holmes B, Johnson M, Khotomlianski V, Kimchi A, Kimelman M, Kitts P, Klimke W, Krasnov S, Kuznetsov A, Landrum MJ, Landsman D, Lee JM, Lipman DJ, Lu Z, Madden TL, Madej T, Marchler-Bauer A, Karsch-Mizrachi I, Murphy T, Orris R, Ostell J, O'sullivan C, Panchenko A, Phan L, Preuss D, Pruitt KD, Rodarmer K, Rubinstein W, Sayers E, Schneider V, Schuler GD, Sherry ST, Sirotkin K, Siyan K, Slotta D, Soboleva A, Soussov V, Starchenko G, Tatusova TA, Todorov K, Trawick BW, Vakatov D, Wang Y, Ward M, Wilbur WJ, Yaschenko E, Zbicz K. 2016. Database

resources of the national center for biotechnology information. Nucleic Acids Res 44:D7–D19. https://doi.org/10.1093/nar/gkv1290.
39. May JJ, Wendrich TM, Marahiel MA. 2001. The *dhb* operon of *Bacillus subtilis* encodes the biosynthetic template for the catecholic siderophore 2,3-dihydroxybenzoate-glycine-threonine trimeric ester bacillibactin. J Biol Chem 276:7209–7217. https://doi.org/10.1074/jbc.M009140200.
40. Baichoo N, Wang T, Ye R, Helmann JD. 2002. Global analysis of the *Bacillus subtilis* Fur regulon and the iron starvation stimulon. Mol Microbiol 45:1613–1629. https://doi.org/10.1046/j.1365-2958.2002.03113.x.
41. Heath RJ, Su N, Murphy CK, Rock CO. 2000. The enoyl-[acyl-carrier-protein] reductases FabI and FabL from *Bacillus subtilis*. J Biol Chem 275:40128–40133. https://doi.org/10.1074/jbc.M005611200.
42. Hook-Barnard IG, Hinton DM. 2009. The promoter spacer influences transcription initiation via σ^{70} region 1.1 of *Escherichia coli* RNA polymerase. Proc Natl Acad Sci U S A 106:737–742. https://doi.org/10.1073/pnas.0808133106.
43. Gaballa A, Guariglia-Oropeza V, Dürr F, Butcher BG, Chen AY, Chandrangsu P, Helmann JD. 2018. Modulation of extracytoplasmic function (ECF) sigma factor promoter selectivity by spacer region sequence. Nucleic Acids Res 46:134–145. https://doi.org/10.1093/nar/gkx953.
44. Voskuil MI, Chambliss GH. 1998. The −16 region of *Bacillus subtilis* and other Gram-positive bacterial promoters. Nucleic Acids Res 26:3584–3590. https://doi.org/10.1093/nar/26.15.3584.
45. Ruff E, Record M, Artsimovitch I. 2015. Initial events in bacterial transcription initiation. Biomolecules 5:1035–1062. https://doi.org/10.3390/biom5021035.
46. Mitchell JE, Zheng D, Busby SJW, Minchin SD. 2003. Identification and analysis of "extended −10" promoters in *Escherichia coli*. Nucleic Acids Res 31:4689–4695. https://doi.org/10.1093/nar/gkg694.
47. Johnson S, Chen YJ, Phillips R. 2013. Poly(dA:dT)-rich DNAs are highly flexible in the context of DNA looping. PLoS One 8:e75799. https://doi.org/10.1371/journal.pone.0075799.
48. Okonogi TM, Alley SC, Reese AW, Hopkins PB, Robinson BH. 2002. Sequence-dependent dynamics of duplex DNA: the applicability of a dinucleotide model. Biophys J 83:3446–3459. https://doi.org/10.1016/S0006-3495(02)75344-7.
49. Helmann JD. 1995. Compilation and analysis of *Bacillus subtilis* σ^{A}-dependent promoter sequences: evidence for extended contact between RNA polymerase and upstream promoter DNA. Nucleic Acids Res 23:2351–2360. https://doi.org/10.1093/nar/23.13.2351.
50. Thompson J, Pikis A, Ruvinov SB, Henrissat B, Yamamoto H, Sekiguchi J. 1998. The gene *glvA* of *Bacillus subtilis* 168 encodes a metal-requiring, NAD(H)-dependent 6-phospho-α-glucosidase. J Biol Chem 273:27347–27356. https://doi.org/10.1074/jbc.273.42.27347.
51. Carlsson P, Hederstedt L. 1989. Genetic characterization of *Bacillus subtilis odhA* and *odhB*, encoding 2-oxoglutarate dehydrogenase and dihydrolipoamide transsuccinylase, respectively. J Bacteriol 171:3667–3672. https://doi.org/10.1128/jb.171.7.3667-3672.1989.
52. Domínguez-Cuevas P, Porcelli I, Daniel RA, Errington J. 2013. Differentiated roles for MreB-actin isologues and autolytic enzymes in *Bacillus subtilis* morphogenesis. Mol Microbiol 89:1084–1098. https://doi.org/10.1111/mmi.12335.
53. Rolfe MD, Rice CJ, Lucchini S, Pin C, Thompson A, Cameron ADS, Alston M, Stringer MF, Betts RP, Baranyi J, Peck MW, Hinton JCD. 2012. Lag phase is a distinct growth phase that prepares bacteria for exponential growth and involves transient metal accumulation. J Bacteriol 194:686–701. https://doi.org/10.1128/JB.06112-11.
54. O'Leary NA, Wright MW, Brister JR, Ciufo S, Haddad D, McVeigh R, Rajput B, Robbertse B, Smith-White B, Ako-Adjei D, Astashyn A, Badretdin A, Bao Y, Blinkova O, Brover V, Chetvernin V, Choi J, Cox E, Ermolaeva O, Farrell CM, Goldfarb T, Gupta T, Haft D, Hatcher E, Hlavina W, Joardar VS, Kodali VK, Li W, Maglott D, Masterson P, McGarvey KM, Murphy MR, O'Neill K, Pujar S, Rangwala SH, Rausch D, Riddick LD, Schoch C, Shkeda A, Storz SS, Sun H, Thibaud-Nissen F, Tolstoy I, Tully RE, Vatsan AR, Wallin C, Webb D, Wu W, Landrum MJ, Kimchi A, Tatusova T, DiCuccio M, Kitts P, Murphy TD, Pruitt KD. 2016. Reference sequence (RefSeq) database at NCBI: current status, taxonomic expansion, and functional annotation. Nucleic Acids Res 44:D733–D745. https://doi.org/10.1093/nar/gkv1189.
55. Kim JGY, Wilson AC. 2016. Loss of σ^{I} affects heat-shock response and virulence gene expression in *Bacillus anthracis*. Microbiology 162:564–574. https://doi.org/10.1099/mic.0.000236.
56. Mašek J, Machoň O, Kořínek V, Taketo MM, Kozmik Z. 2016. Tcf7l1 protects the anterior neural fold from adopting the neural crest fate. Development 143:2206–2216. https://doi.org/10.1242/dev.132357.
57. Hanahan D. 1983. Studies on transformation of *Escherichia coli* with plasmids. J Mol Biol 166:557–580. https://doi.org/10.1016/S0022-2836(83)80284-8.
58. Dubnau D, Davidoff-Abelson R. 1971. Fate of transforming DNA following uptake by competent *Bacillus subtilis*: I. Formation and properties of the donor-recipient complex. J Mol Biol 56:209–221.
59. Seydlová G, Pohl R, Zborníková E, Ehn M, Šimák O, Panova N, Kolář M, Bogdanová K, Večeřová R, Fišer R, Šanderová H, Vítovská D, Sudzinová P, Pospíšil J, Benada O, Křížek T, Sedlák D, Bartůněk P, Krásný L, Rejman D. 2017. Lipophosphonoxins II: design, synthesis, and properties of novel broad spectrum antibacterial agents. J Med Chem 60:6098–6118. https://doi.org/10.1021/acs.jmedchem.7b00355.
60. Li H, Durbin R. 2009. Fast and accurate short read alignment with Burrows-Wheeler transform. Bioinformatics 25:1754–1760. https://doi.org/10.1093/bioinformatics/btp324.
61. Li H, Handsaker B, Wysoker A, Fennell T, Ruan J, Homer N, Marth G, Abecasis G, Durbin R; 1000 Genome Project Data Processing Subgroup. 2009. The sequence alignment/map format and SAMtools. Bioinformatics 25:2078–2079. https://doi.org/10.1093/bioinformatics/btp352.
62. Okonechnikov K, Conesa A, García-Alcalde F. 2016. Qualimap 2: advanced multi-sample quality control for high-throughput sequencing data. Bioinformatics 32:292–294. https://doi.org/10.1093/bioinformatics/btv566.
63. Thorvaldsdóttir H, Robinson JT, Mesirov JP. 2013. Integrative Genomics Viewer (IGV): high-performance genomics data visualization and exploration. Brief Bioinform 14:178–192. https://doi.org/10.1093/bib/bbs017.
64. Love MI, Huber W, Anders S. 2014. Moderated estimation of fold change and dispersion for RNA-seq data with DESeq2. Genome Biol 15:550. https://doi.org/10.1186/s13059-014-0550-8.
65. Huber W, Carey VJ, Gentleman R, Anders S, Carlson M, Carvalho BS, Corrada Bravo H, Davis S, Gatto L, Girke T, Gottardo R, Hahne F, Hansen KD, Irizarry RA, Lawrence M, Love MI, MacDonald J, Obenchain V, Ole AK, Pages H, Reyes A, MM. 2015. Orchestrating high-throughput genomic analysis with Bioconductor. Nat Methods 12:115–121. https://doi.org/10.1038/nmeth.3252.
66. Qi Y, Hulett FM. 1998. Pho∼P and RNA polymerase σ^{A} holoenzyme are sufficient for transcription of Pho regulon promoters in *Bacillus subtilis*: PhoP∼P activator sites within the coding region stimulate transcription in vitro. Mol Microbiol 28:1187–1197. https://doi.org/10.1046/j.1365-2958.1998.00882.x.
67. Chang B, Doi R. 1990. Overproduction, purification, and characterization of *Bacillus subtilis* RNA polymerase σ^{A} factor. J Bacteriol 172:3257-3263. https://doi.org/10.1128/jb.172.6.3257-3263.1990.
68. Juang Y-L, Helmann JD. 1994. A promoter melting region in the primary σ factor of *Bacillus subtilis*. J Mol Biol 235:1470–1488. https://doi.org/10.1006/jmbi.1994.1102.
69. Edgar RC. 2004. MUSCLE: Multiple sequence alignment with high accuracy and high throughput. Nucleic Acids Res 32:1792–1797. https://doi.org/10.1093/nar/gkh340.
70. Waterhouse AM, Procter JB, Martin DMA, Clamp M, Barton GJ. 2009. Jalview Version 2—a multiple sequence alignment editor and analysis workbench. Bioinformatics 25:1189–1191. https://doi.org/10.1093/bioinformatics/btp033.
71. Stamatakis A, Hoover P, Rougemont J. 2008. A rapid bootstrap algorithm for the RAxML web servers. Syst Biol 57:758–771. https://doi.org/10.1080/10635150802429642.
72. Kobayashi K, Ehrlich SD, Albertini A, Amati G, Andersen KK, Arnaud M, Asai K, Ashikaga S, Aymerich S, Bessieres P, Boland F, Brignell SC, Bron S, Bunai K, Chapuis J, Christiansen LC, Danchin A, Debarbouille M, Dervyn E, Deuerling E, Devine K, Devine SK, Dreesen O, Errington J, Fillinger S, Foster SJ, Fujita Y, Galizzi A, Gardan R, Eschevins C, Fukushima T, Haga K, Harwood CR, Hecker M, Hosoya D, Hullo MF, Kakeshita H, Karamata D, Kasahara Y, Kawamura F, Koga K, Koski P, Kuwana R, Imamura D, Ishimaru M, Ishikawa S, Ishio I, Le Coq D, Masson A, Mauel C, Meima R, Mellado RP, Moir A, Moriya S, Nagakawa E, Nanamiya H, Nakai S, Nygaard P, Ogura M, Ohanan T, O'Reilly M, O'Rourke M, Pragai Z, Pooley HM, Rapoport G, Rawlins JP, Rivas LA, Rivolta C, Sadaie A, Sadaie Y, Sarvas M, Sato T, Saxild HH, Scanlan E, Schumann W, Seegers JFML, Sekiguchi J, Sekowska A, Seror SJ, Simon M, Stragier P, Studer R, Takamatsu H, Tanaka T, Takeuchi M, Thomaides HB, Vagner V, van Dijl JM, Watabe K, Wipat A, Yamamoto H, Yamamoto M, Yamamoto Y, Yamane K, Yata K, Yoshida K, Yoshikawa H, Zuber U, Ogasawara N. 2003. Essential *Bacillus subtilis* genes. Proc Natl Acad Sci U S A 100:4678–4683. https://doi.org/10.1073/pnas.0730515100.
73. Koo BM, Kritikos G, Farelli JD, Todor H, Tong K, Kimsey H, Wapinski I,

Galardini M, Cabal A, Peters JM, Hachmann AB, Rudner DZ, Allen KN, Typas A, Gross CA. 2017. Construction and analysis of two genome-scale deletion libraries for *Bacillus subtilis*. Cell Syst 4:291–305. https://doi.org/10.1016/j.cels.2016.12.013.

74. Ross W, Thompson JF, Newlands JT, Gourse RL. 1990. *E.coli* Fis protein activates ribosomal RNA transcription *in vitro* and *in vivo*. EMBO J 9:3733–3742.
75. Krásný L, Gourse RL. 2004. An alternative strategy for bacterial ribosome synthesis: *Bacillus subtilis* rRNA transcription regulation. EMBO J 23: 4473–4483. https://doi.org/10.1038/sj.emboj.7600423.
76. Kolasa IK, Łoziński T, Wierzchowski KL. 2003. Effects of distortions by A-tracts of promoter B-DNA spacer region on the kinetics of open complex formation by *Escherichia coli* RNA polymerase. Acta Biochim Pol 50:909–920.

Supplementary Materials

*Olga Ramaniuk[1,2], Martin Převorovský[3], Jiří Pospíšil[1], Dragana Vítovská[1], Olga Kofroňová[4], Oldřich Benada[4], Marek Schwarz[5], Hana Šanderová[1], Jarmila Hnilicová[1] and Libor Krásný[1]**

[1] Laboratory of Microbial Genetics and Gene Expression, Institute of Microbiology of the Czech Academy of Sciences, Vídeňská 1083, Prague 142 20, Czech Republic

[2] Department of Genetics and Microbiology, Faculty of Science, Charles University, Viničná 5, 128 43 Prague, Czech Republic

[3] Department of Cell Biology, Faculty of Science, Charles University, Viničná 7, Prague 128 43, Czech Republic

[4] Laboratory of Molecular Structure Characterization, Institute of Microbiology of the Czech Academy of Sciences, Vídeňská 1083, Prague 142 20, Czech Republic

[5] Laboratory of Bioinformatics, Institute of Microbiology of the Czech Academy of Sciences, Vídeňská 1083, Prague 142 20, Czech Republic

*Correspondence should be addressed to Libor Krásný: krasny@biomed.cas.cz

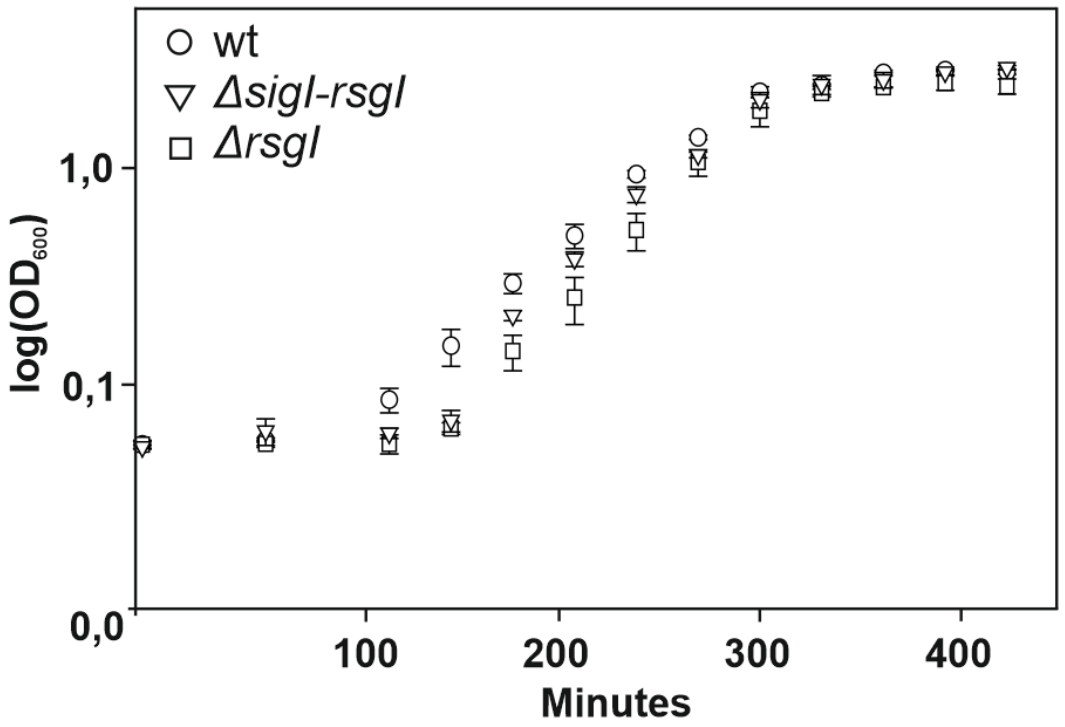

Supplementary Figure S1. Growth curves (log scale) of the Δ*sigI-rsgI* (triangles), Δ*rsgI* (squares) and wt (circles) strains / #1550, #1456 and #1432 strains, respectively /, grown in LB at 37°C.

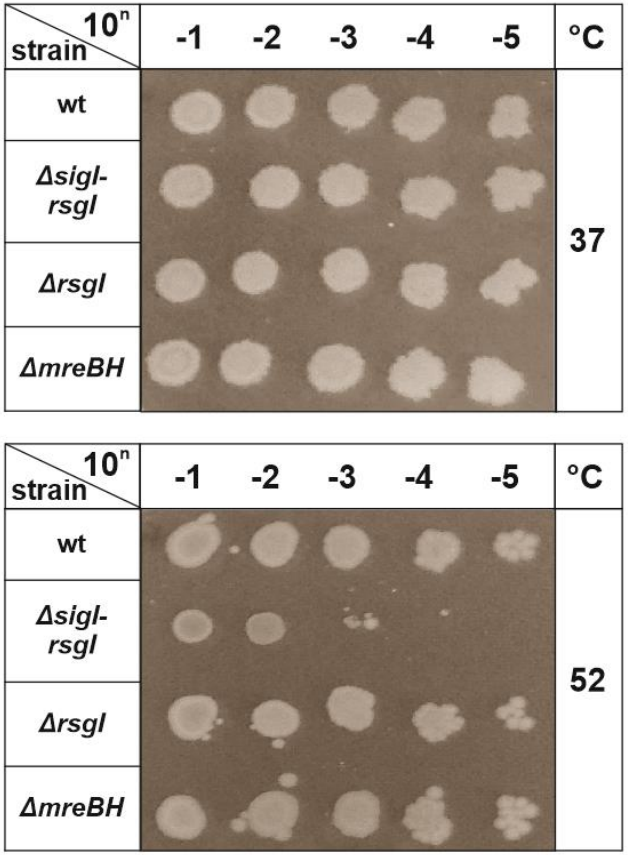

Supplementary Figure S2. Spot assays of *B. subtilis* wt, Δ*sigI-rsgI*, Δ*rsgI* and Δ*mreBH* strains on agar plates at 37°C and 52°C. Serial dilutions of mid-logarithmic phase cultures (OD_{600}~0.45) of wt, Δ*sigI-rsgI*, Δ*rsgI* and Δ*mreBH* strains were spotted on LB agar plates, and incubated at 37°C and 52°C for 40 hours. The experiment was repeated three times with the same result.

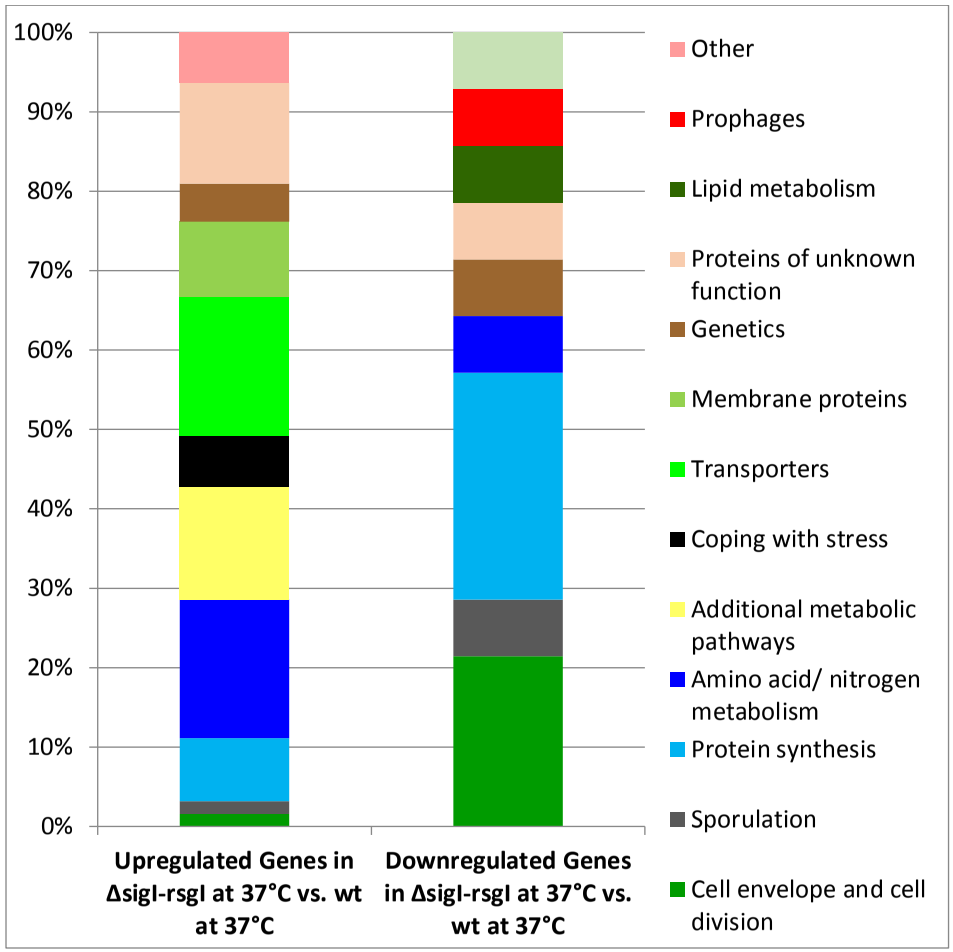

Supplementary Figure S3. Gene ontology of the Differentially Expressed Genes (DEGs) in the Δ*sigI-rsgI* strain at 37°C versus wt strain at 37°C. Data corresponds to Supplementary Tables S2 and S3. In this and the following Figures the ontology was based on SubtiWiki datasets[1].

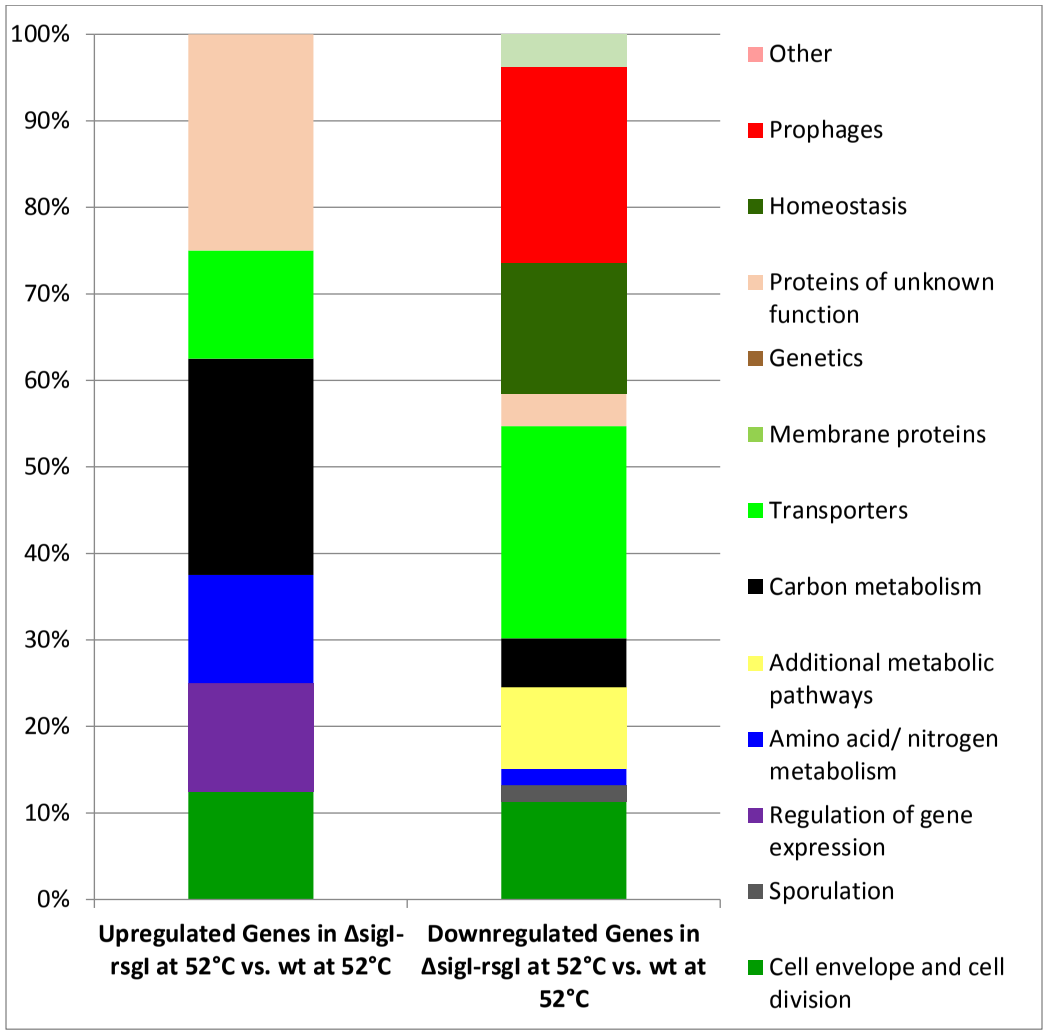

Supplementary Figure S4. Gene ontology of the DEGs in the Δ*sigI-rsgI* strain at 52°C versus wt strain at 52°C. Data corresponds to Supplementary Tables S4 and S5.

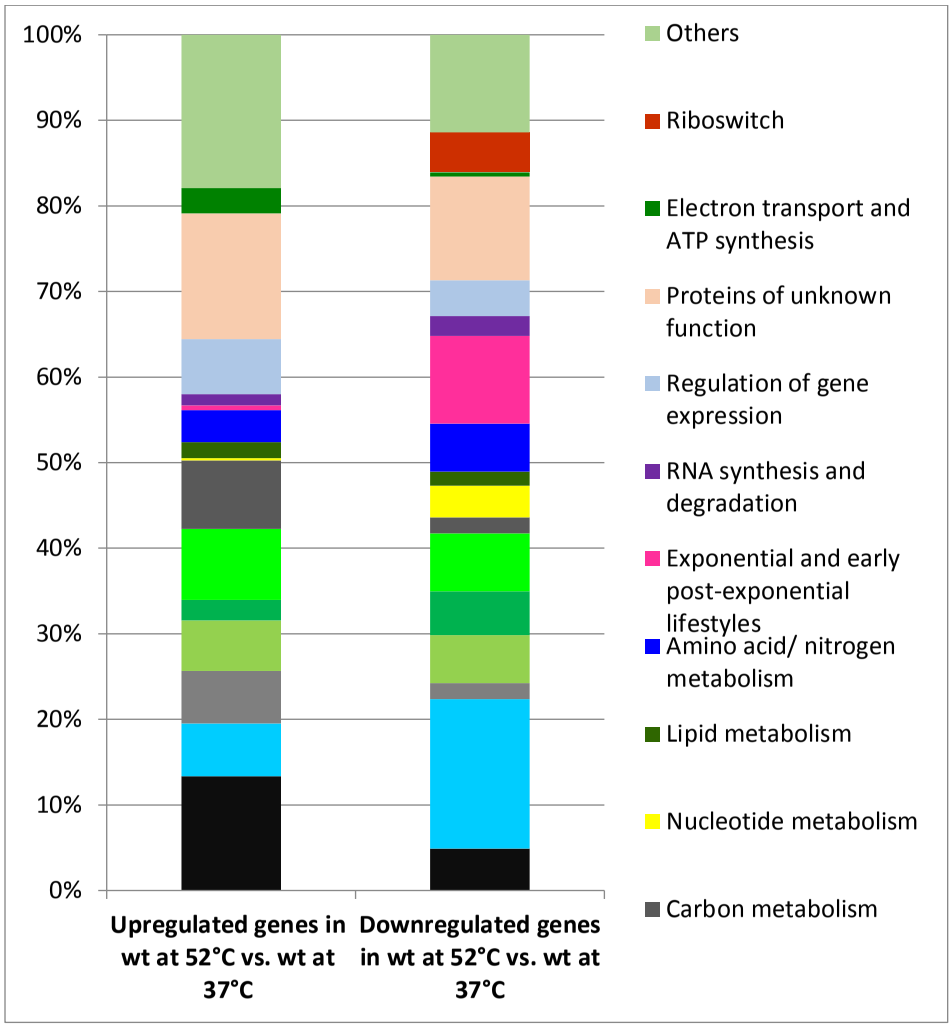

Supplementary Figure S5. Gene ontology of the DEGs in the wt strain at 52°C versus wt strain at 37°C. Data corresponds to Supplementary Tables S6 and S7 (Additional Excel files).

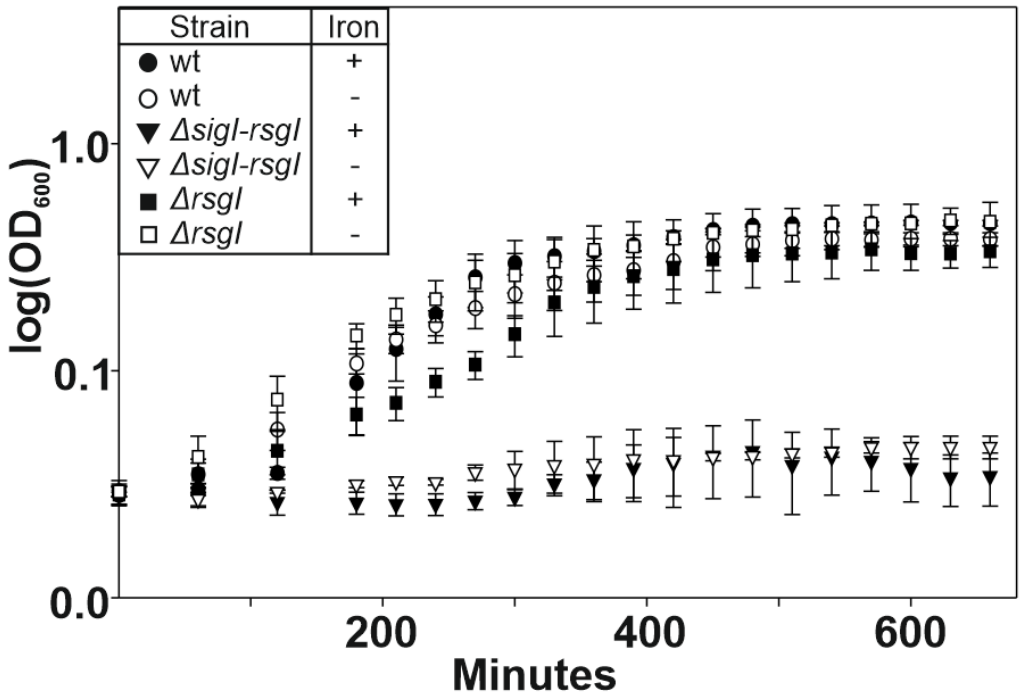

Supplementary Figure S6. Growth of Δ*sigI-rsgI* mutant is heat-sensitive in MOPS medium at 52°C regardless of the presence or absence of iron. Growth curves of the Δ*sigI-rsgI* (triangles), Δ*rsgI* (squares) and wt (circles) strains grown in defined MOPS medium at 52°C in the presence (filled shapes) / absence (empty shapes) of $FeCl_3$. The experiment was repeated three times. The error bars show ±SD.

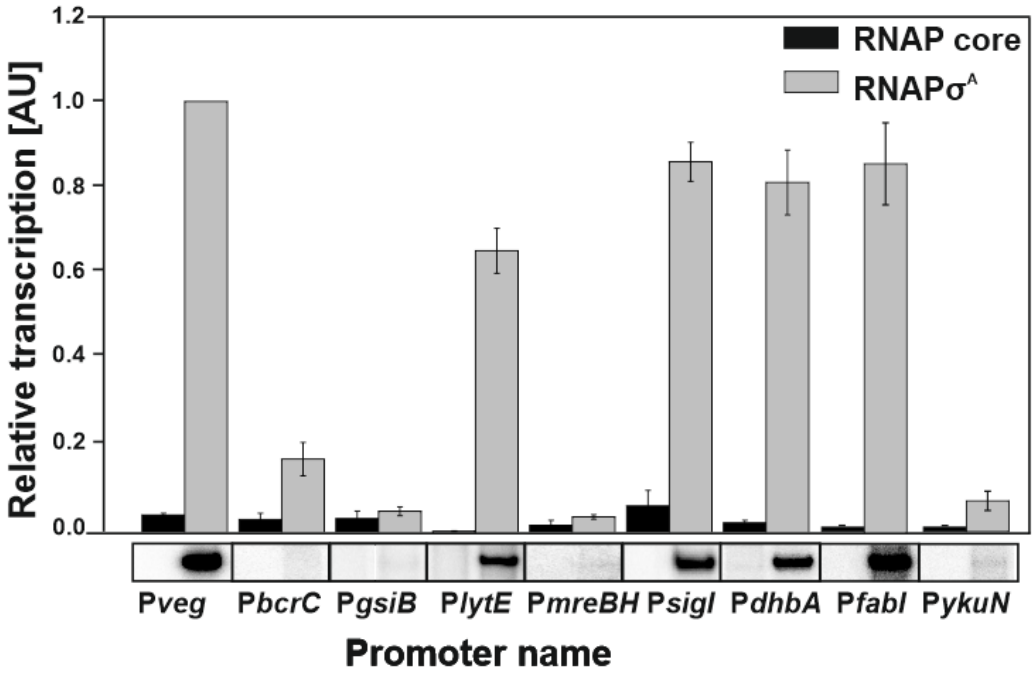

Supplementary Figure S7. Multiple-round *in vitro* transcription assays with promoter regions of σ^I-regulated genes and RNAPσ^A. The strong constitutive σ^A-dependent promoter P*veg* was used as a control and its transcription was set as 1. Transcription was performed with RNAPσ^A holoenzyme and the RNAP core. Transcription with the RNAP core was used to assess potential contamination of the RNAP core with σ factors. Primary data (radioactively labeled transcripts resolved on PAA gels) are shown below the graph. The error bars show averages from three independent experiments ±SD.

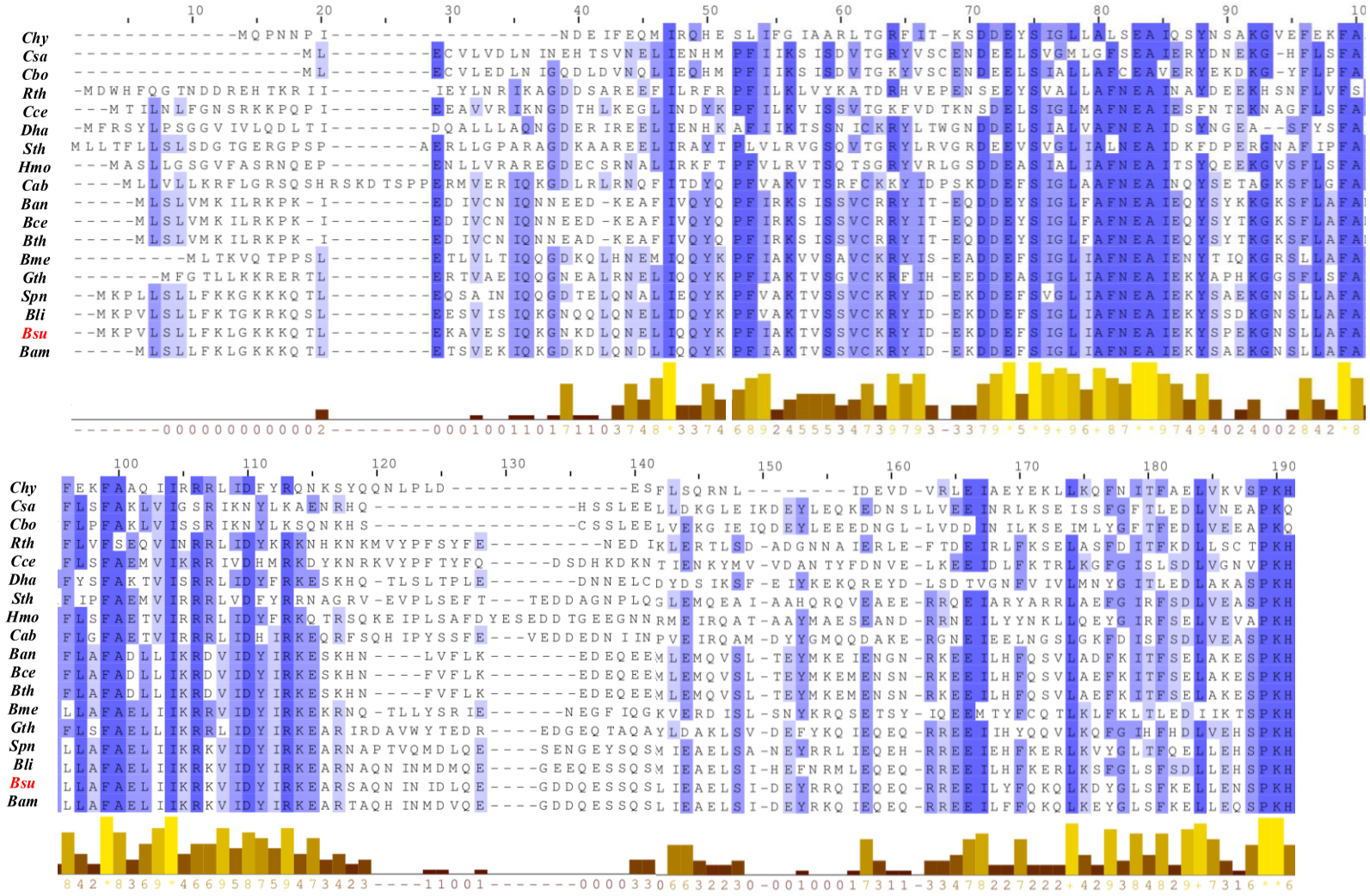
Chy
Csa
Cbo
Rth
Cce
Dha
Sth
Hmo
Cab
Ban
Bce
Bth
Bme
Gth
Spn
Bli
Bsu
Bam

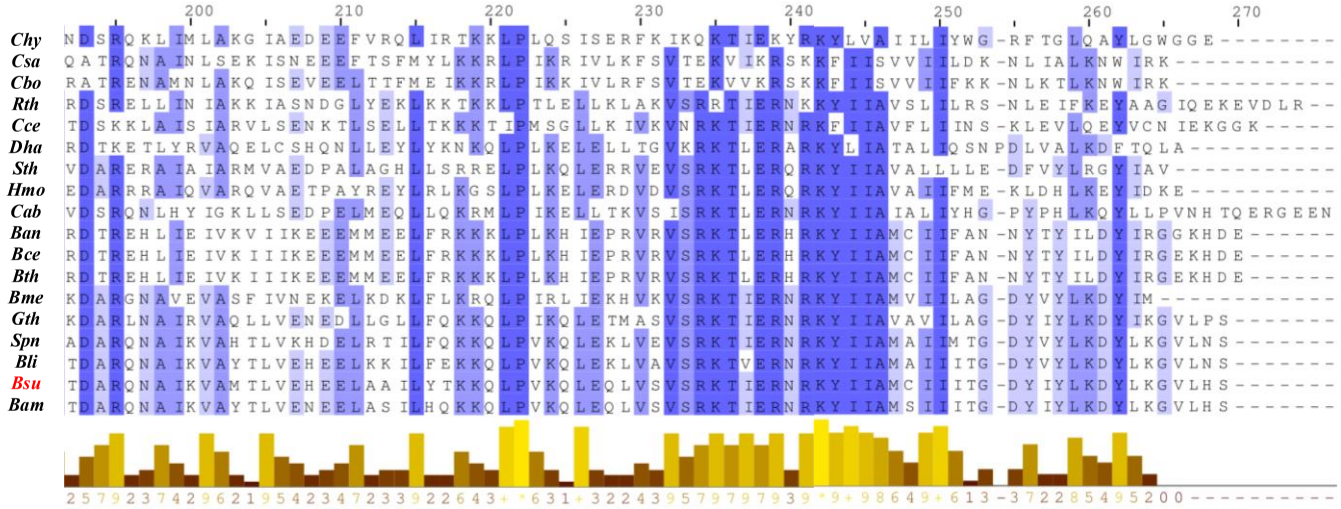

Supplementary Figure S8. Alignment of σ^I homologs from different bacterial species. Alignment of selected sequences was performed with MUSCLE[2]. Picture, conservation score and percentage identity were computed with Jalview[3]. The coloring denotes percentage identity in each column, only residues which match consensus sequence are colorored, ranging from lightest blue to deep blue respective to increasing percentage identity. Consensus sequence is not shown. Conservation annotation score ranges from 0 to 11, where 10 and 11 are denoted by ("+" and "*" respectively), "-" means no score was computed. *Cbo – Clostridium botulinum* (YP_001886509.1), *Csa – Clostridium sacharobutylicum* (AGX42763.1), *Chy – Carboxydothermus hydrogenoformans* (YP_360351.1), *Rth – Rumuniclostridium thermocellum* (EEU02047.1), *Cce – Clostridium cellulolyticum* (YP_002506070.1), *Dha – Desulfitobacterium hafniense* (YP_002461192.1), *Ban – Bacillus anthracis (*NP_845764), *Bth – Bacillus thuringiensis* (YP_037527.1), *Bce – Bacillus cereus (*YP_002368137.1), *Gth – Geobacillus thermodenitrificans* (YP_001124942), *Bsu – Bacillus subtilis* (NP_389228.1), *Bam – Bacillus amyloliquefaciens* (YP_001420916.1), *Spn – Streptococcus pneumoniae* (CVM72501.1), *Bli – Bacillus licheniformis* (YP_091093.1), *Bme – Bacillus megaterium* (YP_003561691.1), *Cab – Chlamydia abortus* (SHE13887.1), *Sth – Symbiobacterium thermophilum* (YP_074991.1), *Hmo – Heliobacterium modesticaldum* (WP_012282894.1)

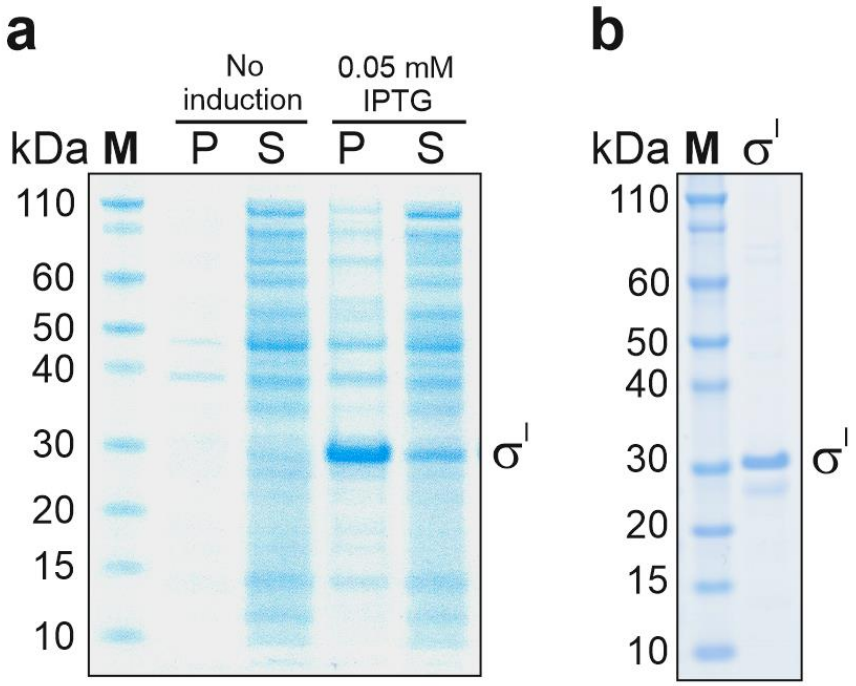

Supplementary Figure S9. σ^I overexpression. a) SDS-PAGE of cell lysates from the #1242 strain (BL21/pSigI-6×His) after 3 hrs (time zero was at OD_{600}=0.6) of growth in the presence/absence of an inducer (0.05 mM IPTG; indicated). P, pellet; S, supernatant. **b)** SDS-PAGE of the σ^I protein (1 μg) in storage buffer. In a) and b) M represents protein marker (Novex™ Sharp Pre-stained Protein Standard).

Supplementary Table S1. List of primers

Primer number/name	Sequence 5'→3'
1164/sigI_For	GGAATTCCATATGGTGAAACCAGTGCTTAGCC
1166/sigI_Rev_His	CCGCTCGAGTGAGTGCAGCACCCCTTTAAG
1478/sigI_rsgI_LA_F	CGCGGATCCGCTTGCTTTATATACGCTTGC
1479/sigI_rsgI_LA_R	CCCAAGCTTCTCAGTTCCTCCCTATAACTA
1480/sigI_rsgI_RA_F	CGGTCGACAGACCTGAATTTATTTAGTTGTG
1481/sigI_rsgI_RA_R	AAATATGCGGCCGCCTGATGATGTCATCAGCCCG
1702/Pveg-50+10_6-FAM	CTTCAAGAATTCTATTTGACAAAAATGGGCTCGTGTTGTACAATAAATGTGTCTAAGCTT
1703/RC Pveg-50+10	AAGCTTAGACACATTTATTGTACAACACGAGCCCATTTTTGTCAAATAGAATTCTTGAAG
1758/PsigI-50+10_6-FAM	ACACGCATAAAACCCCCTTAATTCTTTAGAAAGGCACGAAATCATGTATAGAACGTCAGA
1759/PsigI-50+10_RC1758	TCTGACGTTCTATACATGATTTCGTGCCTTTCTAAAGAATTAAGGGGGTTTTATGCGTGT
1067/PgsiB_For	CCGGAATTCCAGATAGTGCCGGTTGCCG
1068/PgsiB_Rev	CCCAAGCTTAATTGGTGTTGGTTGTTGTATTC
1081/PlytE_For	CCGGAATTCAAAGTTTTTCATTTATTTCCTTTATG
1082/PlytE_Rev	CCCAAGCTTATTTTCCTCCCCAAATGTTAAC
1083/PbcrC_For	TTCGAATTCTTCAAGCGCCGTTATTTC
1084/PbcrC_Rev	CCCAAGCTTTACATTTTTATATTTAGTAGAC
1372/PmreBH_For	CCGGAATTCCCCTTCTTCCTTTAAATGTTTC
1373/PmreBH_Rev	CCCAAGCTTCTATCCTAATTTAATATGATTCTAC
1390/PsigI_For_2	CCGGAATTCTGGGGTGTCTTAGCAG
1391/PsigI_Rev_2	CCCAAGCTTACTGGTTTCACCTCAGTTC
1882/PybbA_F	CCGGAATTCCAAATAAAGAAAAAACCATCCTTC
1883/PybbA_R	CCCAAGCTTGCATTCTCCCCCTTTTTTTGC
1884/PfeuA_F	CCGGAATTCCTGACTGTATGATGCTTTTTC
1885/PfeuA_R	CCCAAGCTTCTATAGAGCCTCCTGTTCAATTG
1886/PycdA_F	CCGGAATTCCAAAAAGTAATAGTCTAAAATAC
1887/PycdA_R	CCCAAGCTTTCATTTTTCCTCCTCAAATGG
1888/PmalA_F	CCGGAATTCCGCACAATTGGATGTTTTATATA

1889/PmalA_R	CCCAAGCTTATGACGACCTCCTTGATAACG
1890/PdhbA_F	CCGGAATTCGAATTTTGCGAGTTTTCAGGAG
1891/PdhbA_R	CCCAAGCTTATCATCAATTCCTTTCTTCGCTC
1892/PbesA_F	CCGGAATTCCGAAAGAAAATCACCCTGGC
1893/PbesA_R	CCCAAGCTTGCAGTACGACATTCCTCTCC
1894/PsrfAA_F	CCGGAATTCCATTTAAACTGAACGGTAGAAAG
1895/PsrfAA_R	CCCAAGCTTATTGTCATACCTCCCCTAATC
1896/PxlyA_F	CCGGAATTCCTGCAGCATTAAAGGGGG
1897/PxlyA_R	CCCAAGCTTTTTCATCTCTCCTTATTTCGTC
2525/PykuN_F	CGGTTATGCCATTTTGCCG
2526/PykuN_R	CAATCGATATCCAACTCATATTC
2527/PodhA_F	GTATATTTGTCCCGGATGTTG
2528/PodhA_R	GTTCGGATCCTGGGTATACTG
2529/PyxeB_F	CTATTTCTAACCTTGATGCC
2530/PyxeB_R	GAAGCAGAATCGCTTGAGCTC
2531/PfabI_F	CTTTAACGGCCCAAACGGC
2532/PfabI_R	GTGCACCCGCTTCATGTAAAG
2533/PqueC_F	GCAAAAAAGCTCCTCGGCGG
2534/PqueC_R	GTCACCGTTTCGACTTCTTC
2537/PyxkC_F	CTATGTGTTTTCTCTCGGTC
2538/PyxkC_R	GCATAAAAAAGTTACGTTGATC
2539/PyfmB_F	CCTCTACATCTTTCATGAGC
2540/PyfmB_R	CGTGAATTCCTGGTGAACATC
2541/PxtmA_F	CAGAGATAGAATTCGAGAAGC
2542/PxtmA_R	GTTTTCGCGGAAACACCGATTG
2543/PcysH_F	GAATTGTGCTAAAATTTACTAC
2544/PcysH_R	CGTAATGGCCGTATGCCC
2557/PspoVD_F	CGGCAAAATCAAAATGCCTG
2558/PspoVD_R	GATCAGAAACACGATCACGC
2628/PfhuB_F	GTAATAGCCGTCTGCCATGAC
2629/PfhuB_R	CAATTGCTGTTTCAGTATATCAC

2630/PfhuD_F	CATAGACCTGCGATAAGGAC
2631/PfhuD_R	CGCAGGCTGCCAGCGCTG
2636/PyfiY_F	CTTGATGATGACATGCTCATTTG
2637/PyfiY_R	CTGAACTATTACAGGCAGAAAG
2638/PyhfQ_F	GAAGTATCATTGGAAGAAACGC
2639/PyhfQ_R	GCTTGAAGACGAGCAAGCAG
2507/PsigI_Native_F	CAAAAAACACGCATAAAACCCCCTTAATTCTTTAGAAAGGCACGAAATCATG
2508/PsigI_M-35_F	CAAAAAACACGCATAAAACttCCTTAATTCTTTAGAAAGGCACGAAATCATG
2509/PsigI_M_Ex-35_F	CAAAAAACACGCATAAAACCCCCTTggTTCTTTAGAAAGGCACGAAATCATG
2510/PsigI_2M-35_F	CAAAAAACACGCATAAAACttCCTTggTTCTTTAGAAAGGCACGAAATCATG
2511/PsigI_M-10_F	CAAAAAACACGCATAAAACCCCCTTAATTCTTTAGAAAGGCACGggATCATG
2512/PsigI_M_Ex-10_F	CAAAAAACACGCATAAAACCCCCTTAATTCTTTAGggAGGCACGAAATCATG
2513/PsigI_2M-10_F	CAAAAAACACGCATAAAACCCCCTTAATTCTTTAGggAGGCACGggATCATG
2524/PsigI_M-35/-10_F	CAAAAAACACGCATAAAACttCCTTAATTCTTTAGAAAGGCACGggATCATG
2688/PsigI2M_Ex-35/-10F	CAAAAAACACGCATAAAACCCCCTTggTTCTTTAGggAGGCACGAAATCATG
2705/PsigI_K-_UP-35	CAAAAAACACGCAggAAACCCCCTTAATTCTTTAGAAAGGCACGAAATCATG
2708/PsigI_K-DOWN-10B	CAAAAAACACGCATAAAACCCCCTTAATTCTTTAGAAAGGCACGAAATCATGTggAG
2514/PsigI_PCRpr_R	GGCTAAGCACTGGTTTCACC

Supplementary Table S2. DEGs – Genes DOWN-regulated in the Δ*sigI-rsgI* strain at 37°C vs. wt strain at 37°C.

Locus	Gene Name	Gene Product/Function	log2 FoldChange (Δ vs wt)	FDR corrected p-value	Operon
BSU13460	*rsgI*	Regulation of gene expression	-3.54	6.76E-39	*sigI-rsgI*
BSU13450	*sigI*	RNA polymerase sigma factor SigI/Control of a class of heat shock genes, RNA synthesis and degradation	-3.43	1.68E-35	*sigI-rsgI*
BSU09420	*lytE*	Cell wall hydrolase (major autolysin),endopeptidase-type autolysin/cell elongation and separation	-1.71	5.33E-19	*lytE*
BSU14470	*mreBH*	Cell shape-determining protein/Cell envelope and cell division; restrict the mobility of the cell wall elongation enzyme complex, required for LytE activity	-1.61	1.30E-07	*mreBH-ykpC*
BSU15170	*spoVD*	Mother-cell specific penicillin-binding protein (spore cortex)/pore morphogenesis; Cell envelope and cell division	-1.25	2.93E-04	*spoVD*
BSU14460	*ykpC*	Unknown/Unknown	-1.17	1.16E-03	*mreBH-ykpC*
BSU21540	*yolA*	Unknown/Unknown	-0.78	1.73E-02	*yolA-yolB*
BSU11720	*fabI*	Enoyl-acyl carrier protein reductase	-0.66	4.34E-03	*fabI*
BSU13740	*queE*	7-carboxy-7-deazaguanine (CDG) synthase, required for the synthesis of the modified ribonucleotide queuosine / Protein synthesis	-0.75	1.09E-02	*queC-queD-queE-queF*
BSU38850	*yxkC*	Unknown/Unknown	-0.68	4.60E-03	*yxkC*
BSU_misc_RNA_5	*glmS riboswitch*		-0.67	4.33E-02	
BSU13750	*queF*	Nitrile reductase/synthesis of the modified ribonucleotide queuosine	-0.67	3.99E-02	*queC-queD-queE-queF*
BSU37070	*rpmE*	Ribosomal protein L31/translation	-0.62	9.61E-03	*rho-rpmE*
BSU41060	*rpmH*	Ribosomal protein L34/translation	-0.59	3.70E-02	*rpmH*

Supplementary Table S3. DEGs – Genes UP-regulated in the Δ*sigI-rsgI* strain at 37°C versus wt strain at 37°C.

Locus	Gene Name	Gene Product/Function	log2 FoldChange (Δ vs wt)	FDR corrected p-value	Operon
BSU26510	*yrkH*	Unknown/Unknown	2.47	3.98E-27	
BSU22670	*trpD*	Anthranilate phosphoribosyltransferase/biosynthesis of tryptophan	2.11	3.82E-14	*trpE-trpD-trpC-trpF-trpB-trpA*
BSU26500	*yrkI*	Unknown/Unknown	2.10	4.57E-16	
BSU22640	*trpB*	Tryptophan synthase (beta subunit)/biosynthesis of tryptophan	1.96	2.75E-13	*trpE-trpD-trpC-trpF-trpB-trpA*
BSU26530	*yrkF*	Unknown/Unknown	1.77	5.11E-09	
BSU26540	*yrkE*	Unknown/Unknown	1.75	8.32E-09	
BSU13700	*clpE*	AAA unfoldase, ATPase subunit of the ClpE-ClpP protease (class III stress gene)/ protein degradation	1.75	7.83E-12	*clpE*
BSU17260	*aprX*	Intracellular alkaline serine proteas/ protein degradation	1.65	2.15E-07	*aprX*
BSU22650	*trpF*	Pphosphoribosylanthranilate isomerase/ biosynthesis of tryptophan	1.65	5.80E-08	*trpE-trpD-trpC-trpF-trpB-trpA*
BSU22680	*trpE*	Anthranilate synthase (subunit I)/biosynthesis of tryptophan	1.64	4.34E-09	*trpE-trpD-trpC-trpF-trpB-trpA*
BSU31060	*gbsA*	Glycine betaine-aldehyde dehydrogenase/glycine betaine synthesis, osmoprotection	1.63	8.14E-09	*gbsA-gbsB*
BSU22660	*trpC*	Indole-3-glycerol-phosphate synthase/biosynthesis of tryptophan	1.62	8.83E-08	*trpE-trpD-trpC-trpF-trpB-trpA*
BSU26490	*yrkJ*	Unknown/Unknown	1.54	4.74E-07	
BSU32990	*mrgA*	Mini-ferritin/DNA-binding stress protein; iron storage protein, DNA-binding stress protein	1.49	9.91E-09	*mrgA*
BSU06660	*opuE*	Proline transporter/compatible solute transport	1.37	1.23E-08	*opuE*
BSU08910	*queG*	Epoxyqueuosine reductase/synthesis of queuosine, tRNA modification	1.37	2.15E-07	

BSU17180	*pksJ*	Polyketide synthase/polyketide synthesis	1.36	2.47E-06	*pksC-pksD-pksE-acpK-pksF-pksG-pksH-pksI-pksJ-pksL-pksM-pksN-pksR*
BSU33730	*opuBA*	choline ABC transporter (binding protein)/compatible solute transport	1.35	2.28E-05	*opuBA-opuBB-opuBC-opuBD*
BSU20490	*yoqW*	Unknown/similar to general secretion pathway protein	1.31	2.41E-05	
BSU18330	*ppsB*	Plipastatin synthetase/production of the antibacterial compound plipastatin	1.29	2.76E-05	*ppsA-ppsB-ppsC-ppsD-ppsE*
BSU33700	*opuBD*	Choline ABC transporter (membrane protein)/ compatible solute transport	1.29	2.32E-04	*opuBA-opuBB-opuBC-opuBD*
BSU08920	*yhbB*	Amidase/spore coat protein	1.28	2.32E-04	*yhbB-cspR*
BSU31050	*gbsB*	Choline dehydrogenase (FAD-dependent)/glycine betaine synthesis, osmoprotection	1.26	6.72E-05	*gbsA-gbsB*
BSU33500	*copA*	Copper transporting ATPase/copper export, detoxification	1.24	3.85E-07	*copZ-copA*
BSU20500	*ligB*	DNA ligase (ATP-dependent)/phage SP-beta replication	1.19	1.03E-03	
BSU08820	*katA*	Vegetative catalase/detoxification (degradation) of hydrogen peroxide (main vegetative catalase 1)	1.18	8.28E-06	*katA*
BSU33490	*cadA*	Cadmium exporting ATPase/resistance to cadmium	1.18	5.18E-07	*cadA*
BSU06820	*yeeG*	Unknown/Unknown	1.17	1.42E-03	
BSU21780	*yplP*	Transcriptional activator (for SigL-dependent promoter)/required for survival at low temperatures	1.16	2.01E-04	
BSU20370	*yorI*	Unknown/similar to putative replicative DNA helicase	1.09	4.27E-03	
BSU18340	*ppsA*	Plipastatin synthetase/production of the antibacterial compound plipastatin	1.06	3.17E-03	*ppsA-ppsB-ppsC-ppsD-ppsE*
BSU13520	*ykrP*	Unknown/Unknown	1.04	8.71E-03	
BSU21790	*yplQ*	Unknown/similar to hemolysin III	1.03	6.95E-03	*yplQ*
BSU17190	*pksL*	Polyketide synthase of type I/polyketide synthesis	1.03	4.47E-04	*pksC-pksD-pksE-acpK-pksF-pksG-pksH-pksI-pksJ-pksL-pksM-pksN-pksR*
BSU11400	*appC*	Oligopeptide ABC transporter (permease))/uptake of oligopeptides	1.03	9.26E-03	*appD-appF-appA/1-appA/2-appB-appC*
BSU17860	*yneA*	Cell division control protein/inhibits cell division during SOS response	1.03	9.74E-03	*yneA-yneB-ynzC*
BSU27870	*nadB*	L-aspartate oxidase/NAD biosynthesis	1.02	1.02E-02	*nadB-nadC-nadA*
BSU02170	*ybfB*	Unknown/Unknown	1.00	1.14E-02	

BSU17870	*yneB*	Unknown/similar to resolvase	0.99	2.80E-03	*yneA-yneB-ynzC*
BSU13850	*pfeT*	Fe(II) efflux pump (P1B4 -type ATPase)/protects the cell against iron intoxication	0.99	2.38E-03	*pfeT*
BSU11900	*yjcL*	Unknown/Unknown	0.97	1.14E-02	*yjcL-yjcK*
BSU31130	*yubD*	Unknown/similar to multidrug resistance protein	0.96	4.07E-03	
BSU37990	*ywdE*	Unknown/Unknown	0.96	2.21E-02	
BSU02140	*glpT*	Glycerol-3-phosphate permease/glycerol-3-phosphate uptake	0.93	6.91E-04	*glpT-glpQ*
BSU39890	*yxbB*	Unknown/Unknown	0.93	1.73E-02	*yxbB-yxbA-yxnB*
BSU33710	*opuBC*	Choline ABC transporter (membrane protein)/compatible solute transport	0.92	3.12E-02	*opuBA-opuBB-opuBC-opuBD*
BSU13580	*mtnE*	Glutamine transaminase/methionine salvage	0.92	1.27E-02	*mtnE*
BSU18880	*yobE*	Unknown/similar to general secretion pathway	0.91	1.73E-02	
BSU18470	*proJ*	Glutamate 5-kinase/osmoadaptive de novo production of proline	0.91	4.84E-03	*proH-proJ*
BSU02130	*glpQ*	Glycerolphosphate diester phosphodiesterase/degrades wall teichoic acid during phosphate starvation	0.90	2.78E-03	*glpT-glpQ*
BSU28680	*ysfC*	Unknown/Unknown	0.90	2.41E-02	
BSU11370	*appF*	Oligopeptide ABC transporter (ATP-binding protein))/uptake of oligopeptides	0.89	3.39E-02	*appD-appF-appA/1-appA/2-appB-appC*
BSU18480	*proH*	Pyrroline-5-carboxylate reductase/osmoadaptive de novo production of proline	0.87	2.47E-02	*proH-proJ*
BSU21870	*ilvD*	Dihydroxy-acid dehydratase/biosynthesis of branched-chain amino acids	0.85	4.34E-02	*ilvD*
BSU18320	*ppsC*	Plipastatin synthetase/production of the antibacterial compound plipastatin	0.85	3.99E-02	*ppsA-ppsB-ppsC-ppsD-ppsE*
BSU35970	*ywsB*	Product unknown/general stress protein, survival of ethanol and salt stresses	0.81	1.63E-02	*ywsB*
BSU31580	*maeN*	Na+/malate symporter/malate uptake	0.80	4.33E-02	*maeN*
BSU18310	*ppsD*	Plipastatin synthetase/production of the antibacterial compound plipastatin	0.79	3.99E-02	*ppsA-ppsB-ppsC-ppsD-ppsE*
BSU38018	*ywzG*	Unknown/Unknown	0.77	4.71E-02	
BSU01580	*ybaR*	Fumarate:proton symporter/fumarate transporter	0.72	8.59E-03	*ybaR*
BSU22630	*trpA*	Tryptophan synthase (alpha subunit)/biosynthesis of tryptophan	0.72	1.14E-02	*trpE-trpD-trpC-trpF-trpB-trpA*

BSU00640	*spoIIE*	Protein serine phosphatase, septum-associated PP2C/control of SigF activity, required for normal formation of the asymmetric septum	0.68	4.95E-02	*spoIIE*
BSU10160	*yhgE*	Unknown/Unknown	0.62	4.65E-02	

Supplementary Table S4. DEGs – Genes DOWN-regulated in the Δ*sigI-rsgI* strain at 52°C versus wt strain at 52°C.

Locus	Gene Name	Gene Product/Function	log2 FoldChange (Δ vs wt)	FDR corrected p-value	Operon
BSU13460	*rsgI*	Anti-sigma factor/Control of SigI activity	-4.57	8.82E-73	*sigI-rsgI*
BSU13450	*sigI*	RNA polymerase sigma factor SigI/Control of a class of heat shock genes	-4.48	3.65E-67	*sigI-rsgI*
BSU14470	*mreBH*	Cell shape-determining protein/Cell envelope and cell division; restrict the mobility of the cell wall elongation enzyme complex, required for LytE activity	-4.05	2.88E-70	*mreBH-ykpC*
BSU14460	*ykpC*	Unknown/ Unknown	-3.06	3.83E-29	*mreBH-ykpC*
BSU09420	*lytE*	Cell wall hydrolase (major autolysin),endopeptidase-type autolysin, cell elongation and separation	-2.63	1.97E-41	*lytE*
BSU31960	*dhbF*	Product unknown, biosynthesis of the siderophore bacillibactin	-2.31	1.37E-28	*dhbA-dhbC-dhbE-dhbB-dhbF*
BSU31980	*dhbE*	2,3-dihydroxybenzoate-AMP ligase (enterobactin synthetase component E), biosynthesis of the siderophore bacillibactin	-2.23	2.36E-19	*dhbA-dhbC-dhbE-dhbB-dhbF*
BSU31970	*dhbB*	Isochorismatase, Biosynthesis of the siderophore bacillibactin	-2.15	2.91E-17	*dhbA-dhbC-dhbE-dhbB-dhbF*
BSU32000	*dhbA*	2,3-dihydro-2,3-dihydroxybenzoate dehydrogenase, biosynthesis of the siderophore bacillibactin	-2.00	4.82E-13	*dhbA-dhbC-dhbE-dhbB-dhbF*
BSU31990	*dhbC*	Isochorismate synthase, biosynthesis of the siderophore bacillibactin	-1.75	4.69E-10	*dhbA-dhbC-dhbE-dhbB-dhbF*
BSU14160	*ykuO*	Unknown/ Unknown	-1.68	3.58E-10	*ykuN-ykuO-ykuP*

BSU01630	*feuA*	ABC transporter for the siderophores Fe-enterobactin and Fe-bacillibactin (binding protein)	-1.61	3.68E-12	*feuA-feuB-feuC-ybbA*
BSU32010	*besA*	Trilactone hydrolase, catalyses ferri-bacillibactin hydrolysis leading to cytosolic iron release	-1.47	8.79E-09	*besA*
BSU01620	*feuB*	ABC transporter for the siderophores Fe-enterobactin and Fe-bacillibactin (integral membrane protein)	-1.39	7.05E-07	*feuA-feuB-feuC-ybbA*
BSU01600	*ybbA*	Putative bacillibactin esterase/ Iron acquisition from bacillibactin	-1.36	1.63E-05	*feuA-feuB-feuC-ybbA*
BSU03480	*srfAA*	Surfactin synthetase, antibiotic synthesis	-1.34	3.45E-07	*srfAA-srfAB-comS-srfAC-srfAD*
BSU01610	*feuC*	ABC transporter for the siderophores Fe-enterobactin and Fe-bacillibactin (integral membrane protein); acquisition of iron	-1.31	1.37E-05	*feuA-feuB-feuC-ybbA*
BSU39610	*yxeB*	Hydroxamate siderophore ABC transporter, siderophore uptake	-1.28	3.31E-07	*yxeB*
BSU12810	*xlyA*	N-acetylmuramoyl-L-alanine amidase, PBSX prophage-mediated lysis Cell envelope and cell division	-1.24	1.18E-06	*xhlA-xhlB-xlyA*
BSU03490	*srfAB*	Surfactin synthetase, antibiotic synthesis	-1.22	1.07E-05	*srfAA-srfAB-comS-srfAC-srfAD*
BSU14170	*ykuP*	Flavodoxin, binds FMN, replaces ferredoxin under conditions of iron limitation	-1.13	1.71E-03	*ykuN-ykuO-ykuP*
BSU36269	*ywzD*	Unknown/ Unknown	-1.06	2.23E-03	
BSU12800	*xhlB*	putative holin	-1.05	5.71E-03	*xhlA-xhlB-xlyA*
BSU15600	*cysC*	adenylyl-sulfate kinase, sulfate reduction and activation	-1.04	9.33E-03	*cysH-cysP-sat-cysC-ylnD-ylnE-ylnF*
BSU33320	*fhuD*	hydroxamate siderophore ABC transporter (only ferrichrome) (binding protein), siderophore uptake	-1.02	1.46E-04	*fhuD*
BSU12610	*xkdG*	PBSX prophage capsid protein	-1.00	9.66E-04	*xtmA-xtmB-xkdE-xkdF-xkdG-xkdH-xkdI-xkdJ-xkdK-xkdM*
BSU15170	*spoVD*	mother-cell specific penicillin-binding protein (spore cortex), spore morphogenesis	-0.99	1.20E-02	*spoVD*
BSU08200	*malP*	Maltose-specific phosphotransferase system, EIICB of the PTS, maltose uptake and phosphorylation	-0.98	6.81E-03	*malA-glvR-malP*
BSU03520	*srfAD*	Surfactin synthetase, antibiotic synthesis	-0.97	2.37E-03	*srfAA-srfAB-comS-srfAC-srfAD*
BSU12650	*xkdK*	PBSX prophage capsid protein	-0.96	9.25E-04	*xtmA-xtmB-xkdE-xkdF-xkdG-xkdH-xkdI-xkdJ-xkdK-xkdM*

BSU12640	*xkdJ*	PBSX prophage	-0.95	1.59E-02	*xtmA-xtmB-xkdE-xkdF-xkdG-xkdH-xkdI-xkdJ-xkdK-xkdM*
BSU15610	*ylnD*	probable uroporphyrin-III C-methyltransferase, siroheme biosynthesis , sulfite reduction	-0.92	2.85E-02	*cysH-cysP-sat-cysC-ylnD-ylnE-ylnF*
BSU12790	*xhlA*	Product unknown, function - host cell lysis (involved in cell lysis upon induction of PBSX)	-0.91	2.86E-02	*xhlA-xhlB-xlyA*
BSU12740	*xkdU*	unknown PBSX prophage protein	-0.89	3.39E-02	
BSU37780	*rocA*	3-hydroxy-1-pyrroline-5-carboxylate dehydrogenase/arginine, ornithine and citrulline utilization	-0.89	4.00E-02	*rocA-rocB-rocC*
BSU12660	*xkdM*	PBSX prophage capsid protein	-0.88	6.37E-03	*xtmA-xtmB-xkdE-xkdF-xkdG-xkdH-xkdI-xkdJ-xkdK-xkdM*
BSU12780	*xepA*	PBSX prophage lytic exoenzyme	-0.88	3.39E-02	
BSU12100	*yjeA*	Polysaccharide deacetylase C/cell wall modification	-0.88	5.77E-03	*yjeA*
BSU02780	*ycdA*	Lipoprotein, required for swarming motility	-0.87	2.71E-03	*ycdA*
BSU08180	*malA*	6-phospho-alpha-glucosidase, maltose utilization	-0.84	5.56E-03	*malA-glvR-malP*
BSU12600	*xkdF*	PBSX prophage	-0.83	1.44E-02	*xtmA-xtmB-xkdE-xkdF-xkdG-xkdH-xkdI-xkdJ-xkdK-xkdM*
BSU12590	*xkdE*	PBSX prophage	-0.80	2.59E-02	*xtmA-xtmB-xkdE-xkdF-xkdG-xkdH-xkdI-xkdJ-xkdK-xkdM*
BSU12671	*xkdN*	Unknown PBSX prophage protein	-0.79	4.32E-02	
BSU04530	*fbpB*	Fur-regulated basic protein, acts as RNA chaperone for fsrA, response to iron limitation, RNA chaperone	-0.79	4.32E-02	*fbpA-fbpB*
BSU19370	*odhA*	2-oxoglutarate dehydrogenase (E1 subunit), TCA cycle	-0.79	1.85E-02	*odhA-odhB*
BSU03830	*yclQ*	Petrobactin (3.4-catecholate siderophore) ABC transporter (binding protein), major component of the secretome, acquisition of iron	-0.78	4.57E-03	*yclN-yclO-yclP-yclQ*
BSU12750	*xkdV*	Unknown PBSX prophage protein	-0.78	1.74E-02	
BSU10330	*yhfQ*	Iron/ citrate ABC transporter (solute-binding protein), iron uptake	-0.77	6.98E-03	*yhfQ*
BSU33310	*fhuB*	Hydroxamate siderophore ABC transporter (ferrichrome und ferrioxamine) (permease)/siderophore uptake	-0.77	2.76E-02	*fhuB-fhuG-fhuC*
BSU08440	*yfiY*	ABC transporter for the siderophore schizokinen and arthrobactin (binding protein), acquisition of iron	-0.74	3.32E-02	*yfiY*

BSU03820	*yclP*	Petrobactin (3.4-catecholate siderophore) ABC transporter (ATP-binding protein)/acquisition of iron	-0.72	1.05E-02	*yclN-yclO-yclP-yclQ*
BSU19360	*odhB*	2-oxoglutarate dehydrogenase complex/TCA cycle	-0.72	2.24E-02	*odhA-odhB*
BSU07520	*yfmC*	Iron/ citrate ABC transporter (binding protein)/iron uptake	-0.69	2.03E-02	*yfmB-yfmC*
BSU12680	*xkdO*	Unknown PBSX prophage protein	-0.66	4.65E-02	
BSU04470	*dctP*	C4-dicarboxylate transport protein, uptake of succinate, fumurate, malate and oxaloacetate via proton symport	-0.65	2.76E-02	*dctPdctS-dctR-dctP*

Supplementary Table S5. DEGs – Genes UP-regulated in the Δ*sigI-rsgI* strain at 52°C versus wt strain at 52°C.

Locus	Gene Name	Gene Product/Function	log2 FoldChange (Δ vs wt)	FDR corrected p-value	Operon
BSU03990	*mtlD*	Mannitol-1-phosphate 5-dehydrogenase/mannitol utilization	1.12	6.39E-04	*mtlA-mtlF-mtlD*
BSU03981	*mtlA*	Trigger enzyme: mannitol-specific phosphotransferase system, EIICB/mannitol uptake and phosphorylation, control of MtlR activity	1.09	1.07E-03	*mtlA-mtlF-mtlD*
BSU09300	*glpD*	Glycerol-3-phosphate dehydrogenase (menaquinone 7)/ glycerol utilization	0.98	8.78E-05	*glpD*
BSU19210	*yocH*	Peptidoglycan hydrolase (amidase)/cell wall turnover	0.90	1.51E-03	*yocH*
BSU13520	*ykrP*	Unknown/ Unknown	0.90	2.67E-02	
BSU26510	*yrkH*	Unknown/ Unknown	0.88	3.39E-02	
BSU13480	*ykrK*	Transcription repressor of htpX expression/regulation of membrane protein quality control	0.82	6.27E-03	*ykrK*
BSU23580	*ansA*	L-asparaginase/asparagine degradation	0.82	2.59E-02	*ansA-ansB*

Supplementary Tables S6 and S7. DEGs – Genes DOWNregulated and UPregulated in the wt strain at 52°C versus wt at 37°C – see additional data sets – Excel Tables S6 and S7, respectively.

References:

1. Michna RH, Zhu B, Mäder U, Stülke J. *Subti* Wiki 2.0—an integrated database for the model organism *Bacillus subtilis*. *Nucleic Acids Res*. 2016;44(D1):D654-D662. doi:10.1093/nar/gkv1006.

2. Edgar RC. MUSCLE: Multiple sequence alignment with high accuracy and high throughput. *Nucleic Acids Res*. 2004;32(5):1792-1797. doi:10.1093/nar/gkh340.

3. Waterhouse AM, Procter JB, Martin DMA, Clamp M, Barton GJ. Jalview Version 2-A multiple sequence alignment editor and analysis workbench. *Bioinformatics*. 2009;25(9):1189-1191. doi:10.1093/bioinformatics/btp033.

Molecular Microbiology (2019) 111(2), 354–372

doi:10.1111/mmi.14159
First published online 11 December 2018

Ms1 RNA increases the amount of RNA polymerase in *Mycobacterium smegmatis*

Michaela Šiková,[1] Martina Janoušková,[1,2] Olga Ramaniuk,[1] Petra Páleníková,[1] Jiří Pospíšil,[1] Pavel Bartl,[3] Agnieszka Suder,[1] Petr Pajer,[4] Pavla Kubičková,[4] Ota Pavliš,[4] Miluše Hradilová,[5] Dragana Vítovská,[1] Hana Šanderová,[1] Martin Převorovský,[6] Jarmila Hnilicová[1]* and Libor Krásný [1]*

[1] *Laboratory of Microbial Genetics and Gene Expression, Institute of Microbiology, Czech Academy of Sciences, Prague, Czech Republic.*
[2] *Faculty of Science, Department of Genetics and Microbiology, Charles University, Prague, Czech Republic.*
[3] *Faculty of Nuclear Science and Physical Engineering, Department of Nuclear Chemistry, Czech Technical University in Prague, Prague, Czech Republic.*
[4] *Military Health Institute, Military Medical Agency, Prague, Czech Republic.*
[5] *Department of Genomics and Bioinformatics, Institute of Molecular Genetics, Czech Academy of Sciences, Prague, Czech Republic.*
[6] *Faculty of Science, Department of Cell Biology, Charles University, Prague, Czech Republic.*

Summary

Ms1 is a sRNA recently found in mycobacteria and several other actinobacterial species. Ms1 interacts with the RNA polymerase (RNAP) core devoid of sigma factors, which differs from 6S RNA that binds to RNAP holoenzymes containing the primary sigma factor. Here we show that Ms1 is the most abundant non-rRNA transcript in stationary phase in *Mycobacterium smegmatis*. The accumulation of Ms1 stems from its high-level synthesis combined with decreased degradation. We identify the Ms1 promoter, P_{Ms1}, and cis-acting elements important for its activity. Furthermore, we demonstrate that PNPase (an RNase) contributes to the differential accumulation of Ms1 during growth. Then, by comparing the transcriptomes of *wt* and Δ*Ms1* strains from stationary phase, we reveal that Ms1 affects the intracellular level of RNAP. The absence of Ms1 results in decreased levels of the mRNAs encoding β and β′ subunits of RNAP, which is also reflected at the protein level. Thus, the Δ*Ms1* strain has a smaller pool of RNAPs available when the transcriptional demand increases. This contributes to the inability of the Δ*Ms1* strain to rapidly react to environmental changes during outgrowth from stationary phase.

Accepted 1 November, 2018. *For correspondence. E-mails: krasny@biomed.cz (LK) and hnilicova@biomed.cas.cz (JH); Tel. +420 241 063 208.
Michaela Šiková and Martina Janoušková are joint first authors.
Jarmila Hnilicová and Libor Krásný are joint senior authors.

Introduction

Bacterial growth, adaptation, and survival depend on accurate responses to environmental changes. These responses result from changes in gene expression. A key enzyme responsible for this process is RNA polymerase (RNAP), which transcribes the genetic information from DNA into RNA.

The bacterial RNAP core (E) consists of two α subunits, two large catalytic subunits, β and β′, and the small ω subunit. The RNAP core is capable of transcription elongation but cannot initiate transcription. The RNAP core binds a σ factor (this complex is called RNAP holoenzyme, Eσ). The σ factor, then, helps RNAP recognize the specific promoter sequence, open the transcription bubble, and synthesize the first few nucleotides of the transcript (Browning and Busby, 2016). The promoter specificity of RNAP thus depends on the associated σ factor. Bacteria contain one primary σ factor (such as σ^{70} in *Escherichia coli* or σ^{A} in *Mycobacterium smegmatis*), which is responsible for the majority of transcription during vegetative growth, and various numbers of alternative σ factors that recognize specific promoters necessary to cope with stress (Feklístov *et al.*, 2014). In mycobacteria, two essential regulators of transcription initiation, RbpA and CarD, interact with Eσ and stabilize its association with DNA (Srivastava *et al.*, 2013; Hu *et al.*, 2014; Verma and Chatterji, 2014; Davis *et al.*, 2015; Hubin *et al.*, 2015; Rammohan *et al.*, 2015; Rammohan *et al.*, 2016).

Previously we identified a ~300 nt long small RNA (sRNA) in *M. smegmatis* termed Ms1 (Pánek *et al.*, 2011) that interacts with the RNAP core devoid of σ factors (Hnilicová *et al.*, 2014). An Ms1 homolog was also found in *M. tuberculosis* (a sRNA named MTS2823) (Arnvig *et al.*, 2011) and predicted in other mycobacterial and actinobacterial species such as *Nocardia* or *Rhodococcus* (Hnilicová *et al.*, 2014). Both Ms1 and MTS2823 accumulate during stationary phase of growth (Arnvig *et al.*, 2011; Hnilicová *et al.*, 2014).

Ms1 shares a similar predicted secondary structure with 6S RNA – the double stranded hairpin interrupted with the central bubble. In addition, Ms1 has two short hairpins at the 5' and 3' ends (Hnilicova *et al.*, 2014). The main difference between Ms1 and 6S RNA is that 6S RNA associates with RNAP holoenzyme – the complex of RNAP with the primary σ factor (Eσ) (Wassarman and Storz, 2000; Trotochaud and Wassarman, 2005; Cavanagh and Wassarman, 2014), whereas Ms1 binds the RNAP core devoid of σ factors (Hnilicová *et al.*, 2014). 6S RNA regulates expression of several hundred genes in *E. coli* (Cavanagh *et al.*, 2008; Neusser *et al.*, 2010) by binding to $E\sigma^{70}$. Previously, artificial MTS2823 overexpression in exponential phase in *M. tuberculosis* downregulated expression of 301 genes and upregulated two genes (Arnvig *et al.*, 2011). However, it is unclear how expression of Ms1 is regulated from its natural locus, and importantly, what the role(s) of Ms1 are in stationary phase when it is most abundant and physiologically relevant.

Here we identify the Ms1 promoter in *M. smegmatis* and *M. tuberculosis* and characterize Ms1 expression and degradation in different growth phases. Furthermore, with a Δ*Ms1* strain we demonstrate the effect of Ms1 on bacterial survival and growth. Then, we compare the transcriptomes of the Δ*Ms1* strain versus wild type (*wt*) both in exponential and stationary phase and we identify genes regulated in Ms1-dependent manner. We show that Ms1 affects gene expression of RNAP subunits β and β′. Based on Ms1's effect on mycobacterial transcription we discuss hypotheses of how Ms1 functions mechanistically.

Results

Ms1 is the most expressed non-rRNA gene in stationary phase

To start characterizing Ms1, we performed RNA-seq experiments. We compared transcriptomes of *wt M. smegmatis* in exponential and stationary phases to quantify Ms1 expression during mycobacterial growth.

We isolated RNA from mid-log exponential phase (OD_{600} 0.5) and from stationary phase after 24 h of cultivation (OD_{600} 2.5, approximately 12 h after the entry into stationary phase). In *wt M. smegmatis*, the most upregulated genes after the entry into the stationary phase were Ms1 and genes from the *MSMEG_1971-MSMEG_1979* cluster. Importantly, over 30% of non-rRNA transcripts in stationary phase belonged to Ms1. Thus, Ms1 is the most abundant transcript (disregarding the ribosomal rRNAs) in stationary phase (Supporting Table 1). In exponential phase, the Ms1 amount decreased to ~0.1% of non-rRNA transcripts. Nevertheless, Ms1 was still in the Top-20 most expressed exponential phase genes (Supporting Table 1).

Based on RNA-seq experiment (where we used the same amount of RNA per sample), Ms1 expression increased > 350-fold in stationary phase RNA sample compared to exponential phase RNA. However, to conclude that Ms1 expression increased > 350-fold per cell, we have to assume that the overall yields of the RNA sample is identical per cell under different experimental conditions (Chen *et al.*, 2015). Therefore, we verified the Ms1 increase in stationary phase by quantitative PCR (qPCR) (Fig. 1A). Immediately at the beginning of RNA

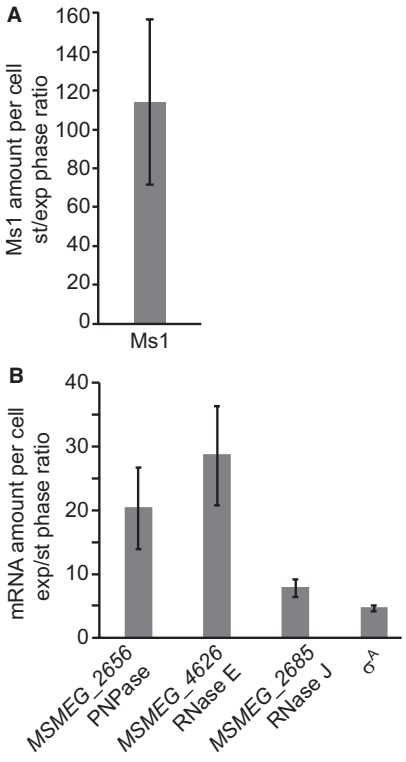

Fig. 1. Expression of Ms1 and RNases in exponential and stationary phase.
A. Expression of Ms1 measured by qPCR was normalized per cell. Ms1 level increases ~115-fold in stationary versus exponential phase. The average represents three independent biological experiments and error bars show ±SEM.
B. Expression of several RNases and the primary σ factor, σ^A, was measured by qPCR and normalized per cell. The average from three independent biological experiments is shown with ±SEM.

isolation from a known number of cells, we added *in vitro* transcribed *B. subtilis* 6S RNA as the RNA recovery marker as control for the efficiency of RNA isolation or potential RNA degradation. Then, the amount of Ms1 was normalized to the cell number and RNA recovery marker. This approach yielded a ~115-fold increase in the Ms1 level in stationary phase. This suggests that to obtain the same amount of RNA from stationary phase and exponential phase, it is necessary to use three-times as many stationary phase cells. In other words, approximately three-fold less RNA is isolated from the same number of stationary phase *M. smegmatis* cells compared to exponential phase. Contrary to Ms1, the amount of the primary σ factor (σ^A) mRNA per cell increased in exponential phase ~4.5-fold compared to stationary phase (Fig. 1B). Also, the expression of the three main RNases, PNPase (*MSMEG_2656*), RNase J (*MSMEG_4626*) and RNase E (*MSMEG_2685*), per cell was higher in exponential phase compared to stationary phase (Fig. 1B).

Ms1 is transcribed from a single promoter

Next, we wished to determine the mechanisms of the high intracellular accumulation of Ms1. As the accumulation is a combined effect of synthesis and degradation, we investigated these two processes, focusing first on synthesis. Previously we identified the first nucleotide of Ms1 and the putative Ms1 promoter (P_{Ms1}) in *M. smegmatis* (Hnilicová *et al.*, 2014). In *M. tuberculosis*, the 5' end of MTS2823 (Ms1 homolog) was mapped 15 nucleotides upstream compared to *M. smegmatis* (Arnvig *et al.*, 2011). The region upstream of the reported MTS2823 transcription start site contains no obvious match for a promoter consensus sequence; correspondingly, no promoter sequence for the Ms1 homolog in *M. tuberculosis* was reported (Arnvig *et al.*, 2011). Nevertheless, a sequence identical with the *M. smegmatis* putative Ms1 promoter is present in the same location also in *M. tuberculosis*.

Therefore we first tested in *M. smegmatis* (i) whether the predicted Ms1 core promoter (Hnilicová *et al.*, 2014) is functional; (ii) whether Ms1 has one or several promoters; (iii) whether any repressor/activator binds to the sequence upstream of the Ms1 promoter(s), and (iv) whether *M. smegmatis* and *M. tuberculosis* Ms1 transcripts have the same 5' ends, and therefore might be similarly regulated by their upstream sequences.

We cloned several *M. smegmatis* promoter region fragments (–38/+9 – the putative core promoter; –131/+9; –231/+9; –331/+9; and –491/+9, see Fig. 2A) into the integrative pSM128 vector (Dussurget *et al.*, 1999) encoding the *lacZ* reporter gene and measured β-galactosidase activity in *M. smegmatis* in different growth phases (Fig. 2B). The –38/+9 region supported significantly above-background β-galactosidase activities (Fig. 2B), confirming that this region contained a core promoter sequence. The relative activities of other promoter fragments were then normalized to the activity of the –38/+9 core promoter in exponential phase, which was set as 100 (Fig. 2B). By the β-galactosidase measurements, the activity of the P_{Ms1} core promoter was highest in late stationary phase (after 48 hours of growth). When we added 100 bp (of the native sequence) upstream to the core promoter (region –131/+9), promoter activity increased both in exponential and stationary phases ~10-fold. A further 100 bp extension of the promoter fragment (–231/+9) led to an additional ~8-fold increase promoter activity in both growth phases, indicating the presence of either general transcriptional activator(s) or promoter(s) similarly active in exponential and stationary phases. Yet another two sequential extensions by 100 bp (–331/+9 and –491/+9) had only a minor effect (max. ~1.5-fold transcription increase) that was not growth phase specific.

To distinguish whether the upstream region of the core promoter contained any other promoter(s) or whether it contained binding site(s) for transcription factors, we deleted a part of the core promoter sequence (fragment –491/–22) or mutated the –10 region of the core promoter (–491/+9mut) (Fig. 2A and C). Both fragments (–491/–22, –491/+9mut) were unable to initiate transcription of *lacZ* (Fig. 2B). Thus, no other promoter is located within the –491/–22 region. From this result, we can conclude that Ms1 is transcribed from the single core promoter and this promoter is regulated by additional transcription factors. In addition, the Ms1 promoter (P_{Ms1}) is very strong and its activity in stationary phase is comparable to the ribosomal *rrnB* promoter (–72/+20 fragment) (China *et al.*, 2010; Tare *et al.*, 2012) when it is most active in exponential phase (Fig. 2B). We note that the background activity of the promoter-less pSM128 vector was relatively high (but significantly lower than the activity of the core promoter). In the Ms1 core promoter mutants, the cloning of DNA fragments completely devoid of promoter sequences likely disrupted the background-generating sequence around the cloning site.

Nevertheless, the β-galactosidase activity of the control *rrnB* promoter (–72/+20 fragment) remained high both in early and late stationary phases (Fig. 2B) which contradicts the well established knowledge from other bacterial species that expression of ribosomal RNAs decreases upon starvation and on entry into stationary phase (Aviv *et al.*, 1996; Murray *et al.*, 2003; Krásný and Gourse, 2004; Paul *et al.*, 2004). The high activity of the *rrnB* promoter in stationary phase measured by the β-galactosidase assay could have been caused by the increased stability of the β-galactosidase (LacZ) enzyme during mycobacterial growth. Therefore, we measured by qPCR directly the amount of the relatively unstable *lacZ* mRNA that better

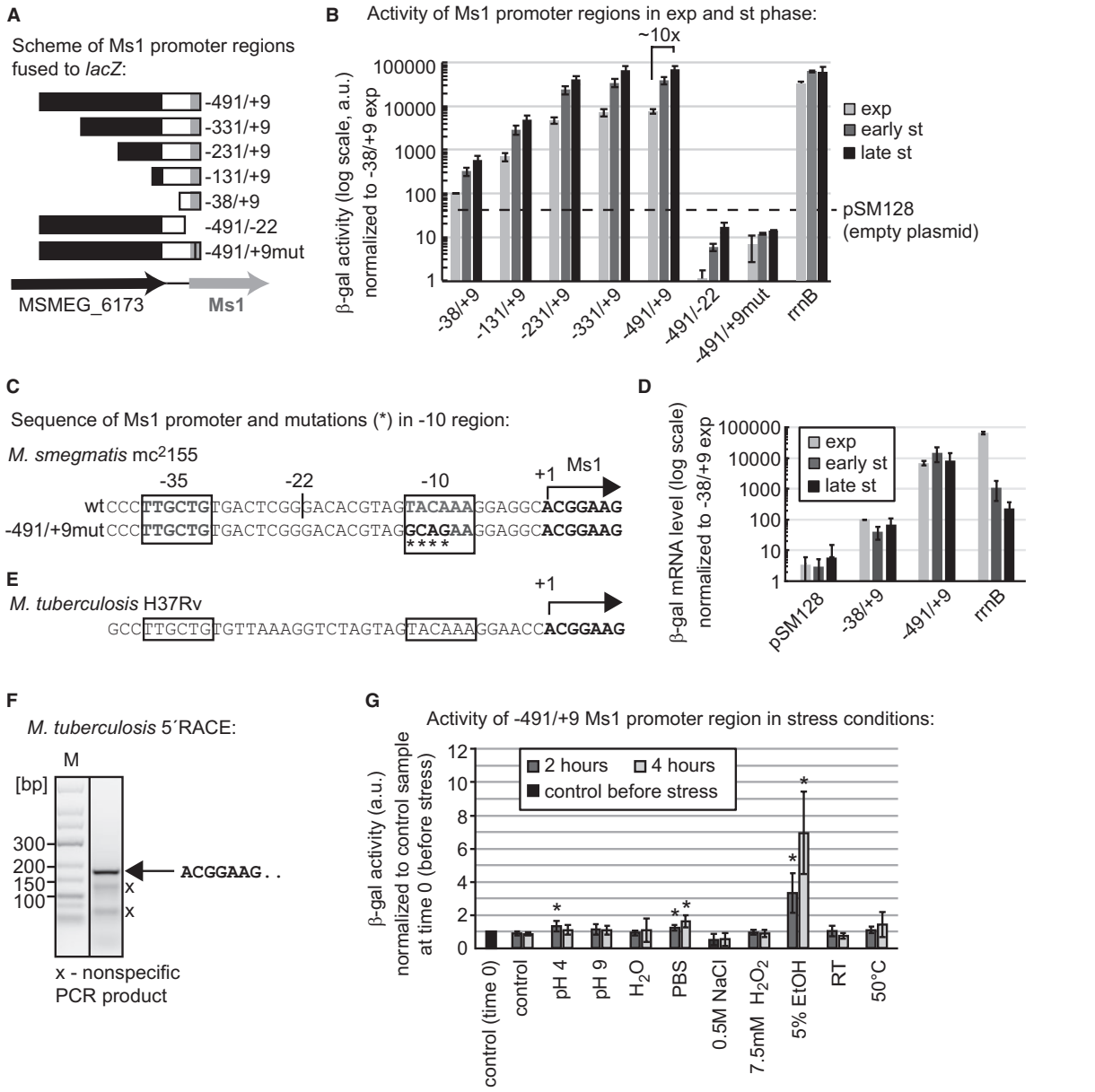

Fig. 2. Identification of the Ms1 promoter.

A. Ms1 promoter region fragments differing in length of the upstream region were fused to *lacZ*. Shortened and mutated Ms1 promoter variants (−491/−22; −491/+9mut) were used to show that Ms1 was transcribed from a single promoter, P_{Ms1}.

B. The graph shows results of β-galactosidase assays for constructs shown in A. β-galactosidase activity was measured in exponential (exp, OD_{600} 0.5, ~6 h of growth), early stationary (OD_{600} 2–3, ~24 h of growth) and late stationary (OD_{600} 2, ~48 h of growth) phases. Data were normalized to the value for the core promoter (−38/+9 construct) in exponential phase which was set to 100. The averages from at least three independent biological experiments performed in duplicates are shown with ±SEM. The dotted horizontal line represents β-galactosidase activity measured in control cells with an empty pSM128 plasmid. rrnB – ribosomal promoter (−72/+20), a.u. – arbitrary units.

C. Sequences of the unmodified and mutated (mutations in −491/+9mut indicated with asterisks) Ms1 core promoter. −22 indicates the endpoint of the −491/−22 fragment.

D. The bar graph shows relative *lacZ* mRNA levels of β-galactosidase (LacZ) per cell for empty pSM128 plasmid, −38/+9 core promoter, −491/+9 largest Ms1 promoter fragment and ribosomal promoter (rrnB, −72/+20). Data were normalized to the value of the −38/+9 construct in exponential phase which was set to 100. The averages from three independent biological experiments performed in duplicates are shown with ±SEM.

E. Putative promoter elements of the Ms1 homolog in *M. tuberculosis* H37Rv are shown in boxes, the transcription start site (+1) identified by 5′RACE is indicated with the horizontal arrow.

F. The transcription start site of the Ms1 homolog (MTS2823) was identified by 5′RACE in *M. tuberculosis*. PCR products of 5′RACE were resolved on agarose gel and sequenced. The arrow indicates the specific band and its sequence from the 5′end.

G. The graph shows β-galactosidase activity of the −491/+9 Ms1 promoter fragment 2 and 4 h after the induction of various types of stress. β-galactosidase activity was normalized to the activity of a control sample at the time 0 (before stress). The graph shows at least three independent biological experiments performed in duplicates. Error bars represent standard deviation; a.u. – arbitrary units, statistically significant difference (*P*-value < 0.05, *T*-test) is marked by asterisk.

reflects promoter activity changes (Krásný *et al.*, 2008). To do so, we isolated RNA from the known number of cells and we added *in vitro* transcribed *B. subtilis* 6S RNA as RNA recovery marker as control for the efficiency of RNA isolation or potential RNA degradation. Then, the amount of the *lacZ* mRNA was normalized to the cell number and RNA recovery marker. The activity of the *rrnB* promoter decreased ~60-fold in early stationary and ~300-fold in late stationary phase compared to exponential phase (Fig. 2D), consistent with the situation in other species mentioned above. This approach revealed that the activity of the P_{Ms1} largest promoter fragment (–491/+9) did not vary much throughout the growth cycle: it increased ~two-fold in early stationary phase and in late stationary phase returned to the exponential phase level (Fig. 2D), indicating almost constitutive expression. A comparison of P_{Ms1} with the *rrnB* promoter then revealed that P_{Ms1} is a strong promoter albeit somewhat less active than P_{rrnB} in exponential phase.

Further comparisons of the lacZ mRNA-based and β-galactosidase data revealed that the addition of upstream promoter elements (–491/+9) increased the activity of the Ms1 –38/+9 core promoter about 70-fold based on the *lacZ* mRNA level compared to the ~77-fold increase based on the LacZ protein level (Fig. 2B and D, exponential phase), indicating that both measurements were comparable, except for the LacZ protein accumulation during the mycobacterial growth.

Finally, to resolve the discrepancy between the transcription start sites (TSS) of Ms1 and its *M. tuberculosis* homolog MTS2823, we mapped the *M. tuberculosis* TSS. We treated total RNA with Terminator 5'-Phosphate-Dependent Exonuclease (TEX) to degrade monophosphorylated 5' ends and followed this by 5' RACE. We obtained one dominant MTS2823-specific PCR product (Fig. 2F) that corresponded to the same transcription start site as Ms1 in *M. smegmatis* (Fig. 2C). Thus, both Ms1 and MTS2823 have the same transcription start site and the promoter sequences we found in *M. smegmatis* are conserved also in *M. tuberculosis* (Fig. 2E).

Ms1 transcription increases during ethanol stress and starvation

To determine what types of stress induce transcription of Ms1 in addition to the harsh nutritional conditions in stationary phase, we quantified the activity of the –491/+9-*lacZ* promoter fragment under various stress conditions: heat-stress (50°C), cold-stress (RT – room temperature), ethanol (5% v/v), oxidative stress (7.5 mM H_2O_2), hyperosmotic stress (0.5 M NaCl), hypoosmotic stress (H_2O), acidic stress (pH 4), alkaline stress (pH 9), and starvation (PBS). The cells were cultivated to exponential phase (OD_{600} 0.5, ~6 h of growth), stressed for 2 and 4 h, and then β-galactosidase activity was measured (Fig. 2G). The β-galactosidase activities of the –491/+9-*lacZ* construct under stress conditions were normalized to the control sample at time 0 (before stresses, Fig. 2G) which was set as 1.

Ethanol stress induced *lacZ* transcription almost ~7-fold. The Ms1 promoter was also activated during growth in PBS (~1.6-fold), which simulates starvation. Thus, Ms1 transcription is enhanced especially under specific stress conditions (ethanol, starvation) and not generally by stress. Except for ethanol, no other stress induced Ms1 in a similar manner as the entry into stationary phase of growth (Fig. 2B and G) and under no stress condition the P_{Ms1} activity was as high as in stationary phase (Fig. 2G).

Ms1 is more stable in stationary phase

The Ms1 level increases ~115-fold upon entry into stationary phase (Fig. 1A). However, the longest Ms1 promoter fragment (–491/+9) increased its activity only ~2-fold under the same conditions when we measured the mRNA level of *lacZ* gene (Fig. 2D). Thus, the number of Ms1 molecules must be regulated also by another mechanism besides transcription. Therefore, we compared the stability of Ms1 in exponential and stationary phases. To efficiently detect Ms1 in exponential phase, we used a strain bearing a replicative plasmid, pJAM2-*rrnB-Ms1*, where Ms1 was highly expressed from the strong *rrnB* promoter in exponential phase (Hnilicová *et al.*, 2014). We added rifampicin to stop *de novo* transcription and isolated total RNA from several time points after the addition of rifampicin. RNA was then isolated from each time point and RNA recovery marker was added (in this case we used Ms1notail – a shortened version of Ms1, see Experimental Procedures section) and the amount of Ms1 was determined by northern blotting (Fig. 3A and B) and normalized to the RNA recovery marker (Fig. 3C). The Ms1 half-life was 8 min in exponential phase and ~8 h in stationary phase (Fig. 3C), revealing that the increased stability in stationary phase contributes to Ms1 accumulation.

To test whether rifampicin affects the cell numbers and/or viability which could have potentially influenced RNA stability, we calculated CFU in rifampicin-treated cells and in control cells that were cultivated without the addition of rifampicin. In exponential phase, rifampicin treatment for 30 min had no effect on CFU: cells treated with rifampicin had CFU $[1.7 \pm 1.4]*10^7$, control cells $[3.3 \pm 2.5]*10^7$. This confirms that rapid degradation of Ms1 in exponential phase is not a secondary effect caused by bacterial death after rifampicin treatment. The 6 h-long treatment with rifampicin in stationary phase decreased CFU ~three-fold: control cells without rifampicin had $[1.7 \pm 1]*10^8$ and rifampicin-treated

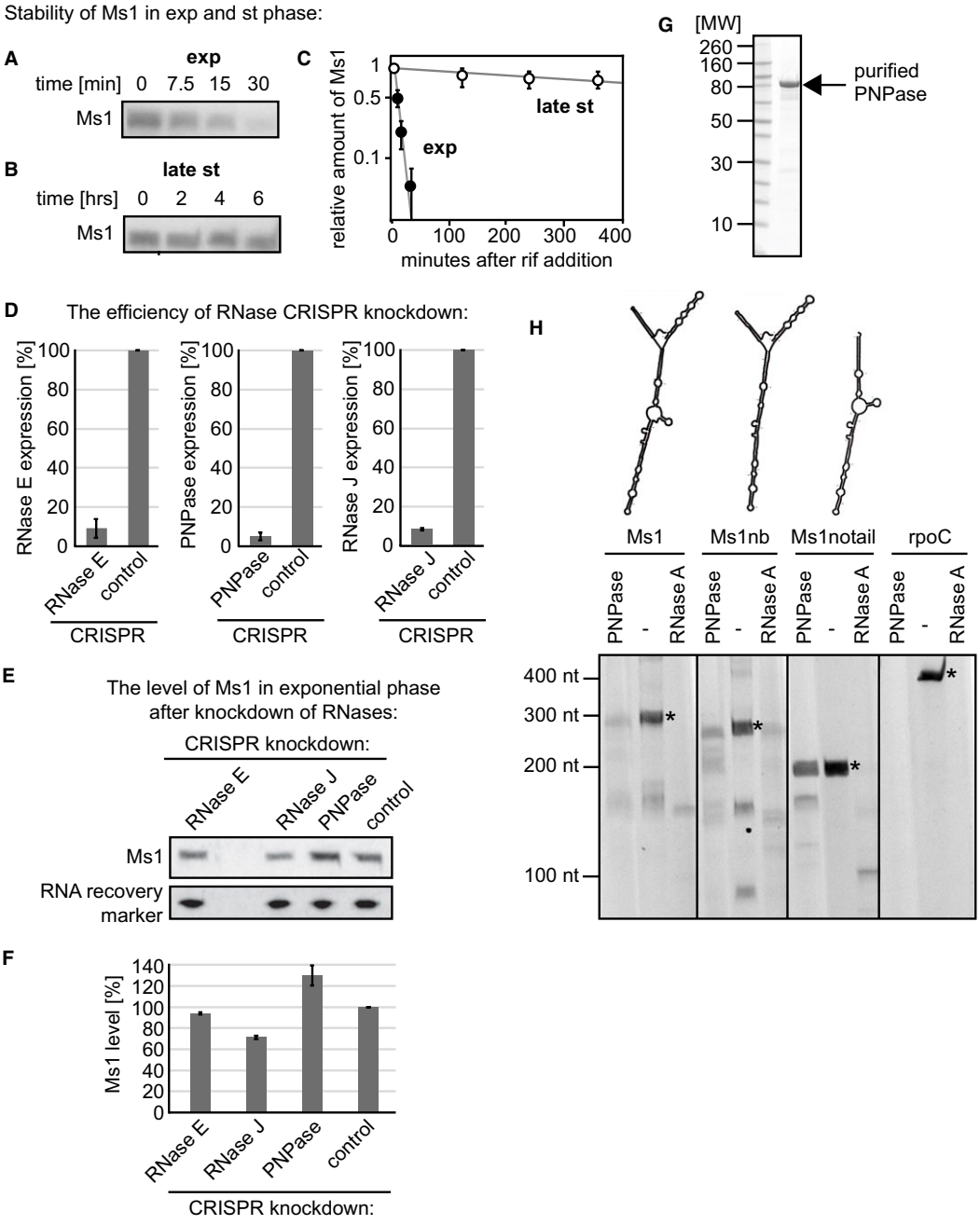
Stability of Ms1 in exp and st phase:
A
exp
time [min] 0 7.5 15 30
Ms1
B
late st
time [hrs] 0 2 4 6
Ms1
C
relative amount of Ms1
1
0.5
0.1
late st
exp
0 100 200 300 400
minutes after rif addition
G
[MW]
260
160
80
50
30
10
purified PNPase
D
The efficiency of RNase CRISPR knockdown:
RNase E expression [%]
PNPase expression [%]
RNase J expression [%]
100
80
60
40
20
0
RNase E
control
PNPase
control
RNase J
control
CRISPR
CRISPR
CRISPR
H
Ms1
Ms1nb
Ms1notail
rpoC
PNPase
-
RNase A
400 nt
300 nt
200 nt
100 nt
E
The level of Ms1 in exponential phase after knockdown of RNases:
CRISPR knockdown:
RNase E
RNase J
PNPase
control
Ms1
RNA recovery marker
F
Ms1 level [%]
140
120
100
80
60
40
20
0
RNase E
RNase J
PNPase
control
CRISPR knockdown:

Fig. 3. Stability of Ms1 in exponential and stationary phase.
A. Northern blots of total RNA isolated from *pJAM2-rrnB-Ms1* (a strain overexpressing Ms1) in exponential phase probed with an oligonucleotide complementary to Ms1. Time shows minutes after rifampicin addition.
B. Northern blots of total RNA isolated from *pJAM2-rrnB-Ms1* (a strain overexpressing Ms1) in stationary phase probed with an oligonucleotide complementary to Ms1. Time shows hours after rifampicin addition.
C. The graph shows averaged data ±SD (standard deviation) for Ms1 stability from three biological replicates. The graph was used to calculate the half-lives of Ms1: 8 min in exponential and ~8 h in stationary phase.
D. The knockdown of RNase E (*LK2197* strain), RNase J (*LK2198*), PNPase (*LK2219*) was induced for 3 h with anhydrotetracycline. A control strain (*LK2261*, that contains non-targeting control sgRNA) was used as a negative control and also treated for 3 h with anhydrotetracycline. The cells were harvested at mid-exponential phase and total RNA isolated from the same amount of cells. *B. subtilis* 6S RNA was added directly at the beginning of RNA isolation as the RNA recovery marker that controls for efficient RNA isolation. The efficiency of RNase knockdown was determined by qPCR in individual strains. The amounts of RNase E mRNA in *LK2197*, RNase J mRNA in *LK2198*, PNPase mRNA in *LK2219* and all RNases in the control strain (*LK2261*) were normalized to the RNA recovery marker (*B. subtilis* 6S RNA). The graphs show relative decreases of mRNA levels in individual knockdown strains compared to the *LK2261* control strain. The averages represent two independent biological experiment, the error bars indicates ±SD.
E. RNA isolated from RNase E (*LK2197* strain), RNase J (*LK2198*), PNPase (*LK2219*) and control strain *LK2261* strain was resolved by northern blotting and probed with oligonucleotides complementary to Ms1 and *B. subtilis* 6S RNA. *B. subtilis* 6S RNA serves as a loading control. The experiment was repeated two times with the same result.
F. Quantification of Ms1 level from Fig. 3E. Ms1 levels in RNase depleted strains (*LK2197*, *LK2198* and *LK2219*) were normalized to the Ms1 level in control (*LK2261*) strain. The bar graph shows averages from two independent experiments with ±SD.
H. *In vitro* digestion assays were performed with three variants of Ms1: 'Ms1nb' is a mutant variant lacking the central bubble; 'Ms1notail' is a mutant variant lacking the tails at 5' and 3' ends. Ms1, Ms1nb and Ms1notail predicted secondary structures are shown above the gel. A 371 nt fragment of the *rpoC* mRNA was used as a control. RNAs were incubated with PNPase, RNase A or no enzyme (negative control, '–'), resolved on a polyacrylamide gel and stained with GelRed. Full length RNAs are marked with asterisks.

cells had $[6.3 \pm 3.8]*10^7$ CFU. Thus, the observed Ms1 decay in stationary phase was probably partly affected by the decreased viability of cells during rifampicin treatment and the Ms1 half-life in stationary phase might be even somewhat longer than 8 h (Fig. 3C).

PNPase contributes to degradation of Ms1

Next, we investigated which RNase might play a role in Ms1 degradation. Previously, we identified PNPase (*MSMEG_2656*, 3′ – 5′phosphorolytic activity) as a binding partner of Ms1 (Hnilicová *et al.*, 2014). PNPase expression increased ~20-fold in stationary phase compared to exponential phase (Fig. 1B) indicating that this RNase might specifically degrade Ms1 in exponential phase. However, the expression of RNase E and RNase J is also elevated in exponential phase (~28-fold and ~8-fold, respectively, Fig. 1B). To test the direct role of PNPase, RNase J and RNase E in Ms1 degradation *in vivo*, we prepared strains in which RNase expression can be reduced by CRISPR (Rock *et al.*, 2017) (strains *LK2197, LK2198, LK2219* and control strain *LK2261*, the control strain contains non-targeting sgRNA). The depletion of particular RNase was induced at the onset of exponential phase (OD_{600} ~ 0.2) and, after 3 h of growth, cells were harvested at mid-log exponential phase (OD_{600} ~ 0.5). We isolated total RNA from each strain from the same amount of cells and immediately at the beginning of isolation we added RNA recovery marker (6S RNA from *B. subtilis*) to control for the efficiency of RNA isolation. We quantified the efficiency of CRISPR knockdowns by qPCR, the mRNA levels of individual RNases were normalized to the RNA recovery marker. CRISPR efficiently depleted each RNase (the expression decreased > 90% in individual strains, Fig. 3D). Then, we determined Ms1 amount by northern blotting (Fig. 3E and F). RNase E and RNase J depletion did not elevate Ms1 level (Fig. 3E). The depletion of PNPase in exponential phase increased the level of Ms1, confirming that PNPase contributes to the Ms1 degradation *in vivo*. However, the Ms1 increase was moderate, about 30% (Fig. 3F) – PNPase depletion did not completely stop Ms1 degradation (the Ms1 increase in stationary phase is ~115-fold, therefore we expected a higher increase in the Ms1 level in exponential phase after almost complete inhibition of Ms1 degradation). A possibility is that another exponential phase-dependent cofactor (e.g. RNA helicase) contributes to the degradation of the highly structured Ms1 RNA in exponential phase.

Therefore, we tested whether (i) PNPase alone is able to degrade Ms1 RNA *in vitro* and (ii) if Ms1 has any structural features that would block its degradation by PNPase. We overexpressed and purified His-tagged *M. smegmatis* PNPase (Fig. 3G). We performed digestion assays *in vitro* with Ms1 and two Ms1 mutant variants: (i) 'Ms1nb', lacking the central bubble (Hnilicová *et al.*, 2014), and (ii) 'Ms1notail', lacking the tails at 5' and 3' ends (Fig. 3H), and part of the RpoC mRNA as a control. PNPase significantly (but not completely) degraded both the unmodified Ms1 and Ms1nb (Fig. 3H), indicating that this Ms1-interacting RNase might be responsible, at least in part, for Ms1 degradation and that the central bubble is not required for the degradation. To the contrary, the Ms1notail mutant was degraded only modestly by PNPase, indicating that the tail motif enhances Ms1 degradation. Control RNase A did not show any substrate specificity with respect to Ms1 variants.

Thus, PNPase degrades Ms1 both *in vivo* and *in vitro* and the degradation efficiency depends on the Ms1

sequence/secondary structure. However, another RNase or RNA helicase releasing Ms1 secondary structure is probably necessary for complete Ms1 degradation inside the cell.

Δ*Ms1 cells are viable*

To determine whether Ms1 is essential for the cell, we deleted 255 nucleotides from the 304 nt-long *Ms1* gene (the +3 to +257 region was replaced with a hygromycin resistance cassette, see Fig. 4A). Surprisingly, Δ*Ms1* cells reproducibly reached slightly higher OD_{600} at the end of exponential phase (Fig. 4B). We did not detect any morphological changes in Δ*Ms1* cells by electron microscopy neither in exponential nor in stationary phase (data not shown).

Next, we examined the Δ*Ms1* growth in several stress conditions: ethanol stress (5% EtOH), high salt conditions (0.5 M NaCl), oxidative stress (diamide) or acidic pH (pH 5). Mostly, no significant phenotypic effects (compared to *wt*) were detected (data not shown). However, cell survival after γ irradiation was significantly affected by the presence of Ms1. Δ*Ms1* stationary phase cells chronically irradiated with the dose of 150 Gy formed about 50% less

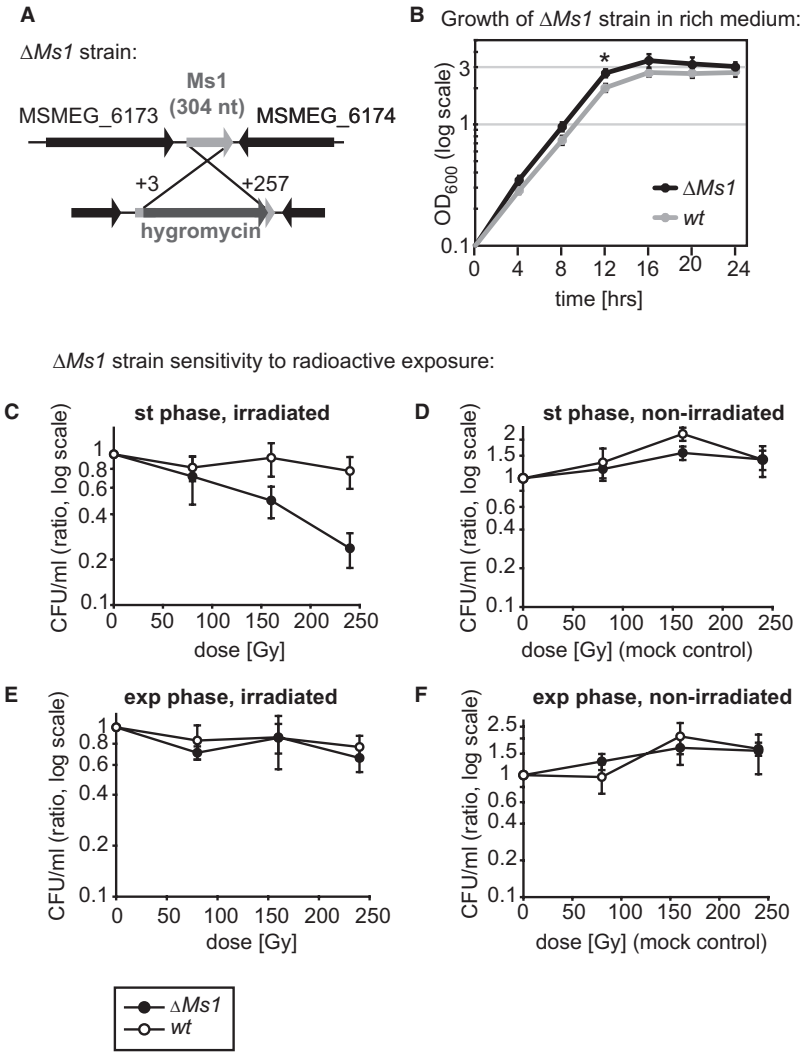

Fig. 4. Characterization of the Δ*Ms1* strain.
A. The Ms1 gene was replaced with a hygromycin resistance gene in *M. smegmatis wt* cells.
B. Δ*Ms1* and *wt* growth was monitored for 24 h; statistically significant difference ($P < 0.05$, *T*-test) in OD_{600} was observed after 12 h cultivation in 7H9 medium supplemented with glycerol. The data are averages from six independent experiments. The error bars show ±SEM.
C. Survival (colony forming units; CFU) of stationary phase chronically γ irradiated Δ*Ms1* and *wt* cells.
D. Survival (CFU) of stationary phase non-irradiated control Δ*Ms1* and *wt* cells.
E. Survival (CFU) of exponential phase chronically γ irradiated Δ*Ms1* and *wt* cells.
F. Survival (CFU) of exponential phase non-irradiated control Δ*Ms1* and *wt* cells. The mock controls represent non-irradiated samples that were otherwise treated as irradiated samples. The data points are averages from four independent experiments, error bars represent ±SD.

colony forming units (CFU) than *wt*, while irradiation with 250 Gy was lethal for almost ~80% of Δ*Ms1* cells compared to *wt* (Fig. 4C). Half of samples were chronically irradiated at room temperature (Fig. 4C and E) and the second half was kept at room temperature without irradiation as a control of cell viability (Fig. 4D and F, labelled as 'mock controls'). No difference was observed between Δ*Ms1* and *wt* cells in exponential phase (Fig. 4E) when Ms1 is present in low amounts or in non-irradiated controls (Fig. 4D and F). Ms1 thus helped protect stationary phase cells from radioactive exposure.

Ms1 regulates the amount of RNA polymerase

Next, we compared transcriptomes of *wt* and Δ*Ms1* strains in exponential and stationary phases. Despite the fact that Ms1 is so abundant in *M. smegmatis*, RNA-seq revealed only minor changes in gene expression upon deletion of Ms1. In exponential phase of growth, we detected five statistically significant differentially expressed genes in Δ*Ms1* cells (FDR corrected *P*-value 0.05, see Supporting Table 2). In stationary phase of growth, fourteen genes altered their expression in the Δ*Ms1* strain (FDR corrected *P*-value 0.05, see Supporting Table 2) including *MSMEG_1367* and *MSMEG_1368* (*rpoB* and *rpoC*, respectively) genes that encode two main RNAP subunits β and β'. In the RNA-seq data, the expression of β and β' decreased by half in Δ*Ms1* compared to *wt*.

We decided to confirm the effect of Ms1 on the expression of genes identified by RNA-seq in stationary phase. We selected the following genes: *MSMEG_1205*, a cyclopropane-fatty-acyl-phospholipid synthase, playing a role in fatty acid metabolism (2x↑ in ΔMs1); *MSMEG_5540*, encoding an unknown protein (2x↓ in ΔMs1); *MSMEG_5556* encoding MFS permease (2x↓ in ΔMs1); and *rpoB* and *rpoC* genes encoding RNAP subunits β and β' (both 2x↓ in ΔMs1).

For the validation experiments, we also created a complemented Δ*Ms1* + *Ms1* strain and compared it with *wt* and Δ*Ms1* strains. Δ*Ms1* + *Ms1* contained a plasmid (stably integrated into the genome) carrying Ms1 under its native promoter. The amount of Ms1 in stationary phase in the Δ*Ms1* + *Ms1* strain was comparable to the amount of Ms1 in *wt* (Fig. 5A, the gel shows total RNA stained with GelRed). In Δ*Ms1*, no band corresponding to the size of Ms1 was visible and the Ms1 level decreased to ~ zero in RNA-seq data. Subsequently, we extracted RNA from *wt,* Δ*Ms1* and Δ*Ms1* + *Ms1* stationary phase cells and quantified the mRNA levels of selected genes by qPCR to validate the RNA-seq data. As a reference gene, we used the gene encoding σ^A that did not alter expression in stationary phase in the Δ*Ms1* transcriptome compared to *wt* according to the RNA-seq experiment. The qPCR results correlated with the RNA-seq data, and importantly,

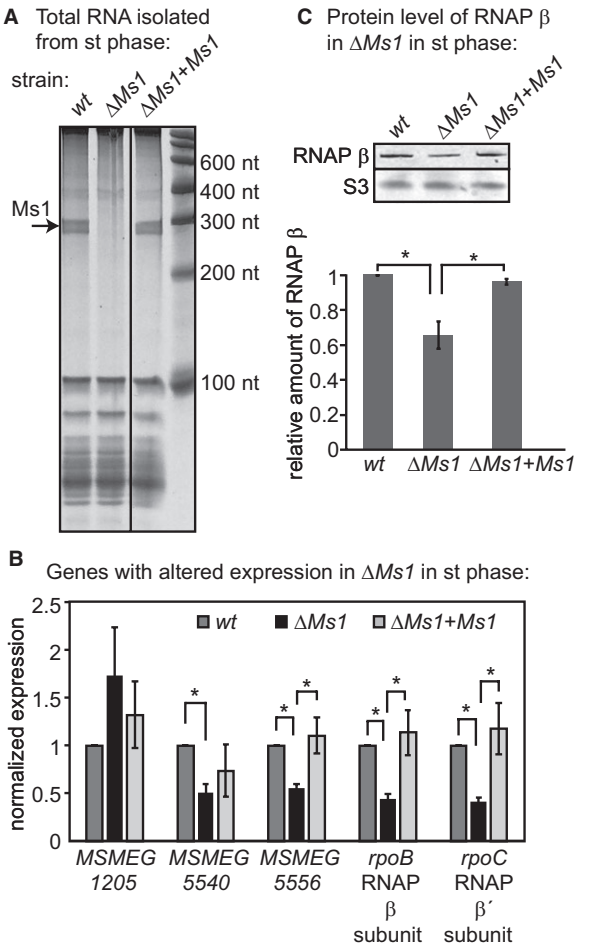

Fig. 5. Ms1-regulated genes.
A. Total RNA from Δ*Ms1* and *wt* stationary phase cells was isolated, resolved on a polyacrylamide gel and stained with GelRed; in Δ*Ms1* strain, Ms1 is absent. In Δ*Ms1+Ms1* strain, *Ms1* under its native promoter is integrated into the genome and Ms1 expression is restored to the level of *wt*.
B. Expression of five selected genes was measured by qPCR in Δ*Ms1, wt* and Δ*Ms1+Ms1* strains. *MSMEG_1205, MSMEG_5540, MSMEG_5556* and *rpoB*, *rpoC* genes encoding β and β' RNAP subunits altered their expression in Δ*Ms1* and these changes were reverted by the addition of the *Ms1* wt copy (Δ*Ms1+Ms1* strain). Expression levels were normalized in each sample to the reference gene encoding σ^A and then compared to *wt* (set as 1). The average value represents four biological replicates, error bars ±SEM. Statistically significant differences (*P*-value < 0.05, *T*-test) are marked with asterisks.
C. The total protein level of the RNAP β subunit in stationary phase is significantly lower in Δ*Ms1* versus *wt* (*P*-value < 0.05, *T*-test, marked by asterisk) and restored in the Δ*Ms1+Ms1* strain. Five milligrams of protein lysate was loaded and the amount of RNAP was quantified by western blotting with an anti- β subunit RNAP antibody. The S3 ribosomal protein represents loading control. Three independent experiments were performed; averages are shown, error bars represent ±SEM

the complemented strain displayed a reversal of the levels of the tested genes to near *wt* values (Fig. 5B). Therefore, the expression of these genes (including RNAP β and β' subunits) was indeed dependent on the presence of Ms1.

In other words, the changes in the expression were not caused by any kind of mutations in the gene promoters that could be randomly created during Δ*Ms1* strain preparation and selection.

To define if the lowered amount of RNAP is associated with a decreased protein level of the RNAP β subunit, we used quantitative western blotting (Fig. 5C). The level of the RNAP β subunit in the Δ*Ms1* strain was at ~70% of its level in the *wt* strain. The addition of the Ms1 copy into the Δ*Ms1* strain restored the level of the RNAP β subunit and we observed no difference between *wt* and Δ*Ms1* + *Ms1* strains (Fig. 5C).

Ms1 accelerates outgrowth from stationary phase

As Ms1 increases the total amount of RNAP in stationary phase it suggests that Ms1 (and the higher amount of RNAP) could be beneficial during outgrowth. To test this hypothesis, we cultured Δ*Ms1* and *wt* strains to stationary phase (OD_{600} 2.5, approximately 12 h after the end of exponential phase) and then diluted both strains into fresh medium and measured OD_{600}. Both strains were diluted to the same OD_{600} (0.1) and their growth was monitored for 6 h. Immediately before the dilution, we measured CFU of Δ*Ms1* and *wt*. There was no difference in viability and cell number of both strains: *wt* had $[2.31 \pm 1]*10^8$ and Δ*Ms1* $[2.37 \pm 0.9]*10^8$. The *wt* strain grew faster immediately after the dilution and the difference in OD_{600} between *wt* and Δ*Ms1* lasted for ~3 h after the dilution (Fig. 6A). The average doubling time in the first 2 h after the dilution was 133 ± 5 min for the *wt* strain and 146 ± 3 min for the Δ*Ms1* and the difference was significant (*P*-value 0.006, *T*-test). There was no statistically significant difference in doubling times 2–6 h after the dilution. No difference in growth was observed between *wt* and Δ*Ms1+Ms1* complemented strain (Fig. 6B). In addition, we prepared the *LK2200* strain, where we could efficiently knockdown Ms1 by CRISPR (Fig. 6E). The Ms1 knockdown was induced by anhydrotetrycycline (Rock *et al.*, 2017). We depleted Ms1 in stationary phase (Fig. 6E) in *LK2200*, diluted the strain into a fresh medium and measured OD_{600} during the outgrowth (Fig. 6C). *LK2200* with depleted Ms1 (with added anhydrotetracycline) grew more slowly than *LK2200* without anhydrotetracycline (no Ms1 knockdown was induced) and the difference in OD_{600} remained for ~4 h after the dilution (Fig. 6C). The average doubling time in the first two hours after the dilution was 162 ± 8 min for the *LK2200* strain with anhydrotetracycline and 190 ± 8 min for the *LK2200* strain without anhydrotetracycline; the difference was statistically significant (*P*-value 0.008, *T*-test). The doubling times did not significantly differ in the next four hours (hour 2–6 after the dilution). No difference during outgrowth was observed when we added anhydrotetracycline to *LK2261* control strain with non-targeting sgRNA oligo (Fig. 6D). Thus, by an independent method (CRISPR induced Ms1 knockdown) we confirmed that Ms1 is important during the outgrowth.

Next, we monitored the correlation between the RNAP and Ms1 levels between Δ*Ms1* and *wt* strains during outgrowth. The Δ*Ms1* strain had a decreased level of the RNAP β protein subunit compared to *wt* at the time of dilution and the difference was still detectable 15 min after the dilution (Fig. 6F and G). Thirty minutes after the dilution however, the amount of RNAP in both strains was comparable. It is possible that at this time Ms1 was already degraded because Ms1 is highly unstable in exponential phase of growth (Fig. 3A). Therefore, we quantified the degradation of endogenous Ms1 after dilution of *wt* cells from stationary phase into fresh medium. Ms1 was reduced to 50% within ~18 min after the dilution (Fig. 6H), indicating that the degradation rate of endogenous Ms1 was comparable with the effect of Ms1 on the level of RNAP.

Previously, it was shown that the addition of rifampicin during the outgrowth stabilizes 6S RNA (Wurm *et al.*, 2010; Beckmann *et al.*, 2012). 6S RNA serves as a template for transcription of small 'product' RNAs (pRNAs), and active transcription is necessary for the release of 6S RNA from the primary RNAP holoenzyme and subsequent 6S RNA degradation (Wassarman and Saecker, 2006; Gildehaus *et al.*, 2007; Beckmann *et al.*, 2011; Beckmann *et al.*, 2012; Cavanagh *et al.*, 2012). Therefore we tested if inhibition of transcription by rifampicin could stabilize Ms1 during the outgrowth. We cultured *wt* cells to stationary phase (24 h), diluted them to OD_{600} 0.1 into a fresh medium with or without rifampicin and measured the level of Ms1 by qPCR (Fig. 6I). Contrary to 6S RNA, rifampicin had no effect on Ms1 degradation (Fig. 6I). This further suggests that Ms1 and 6S RNA differ not only in binding RNAP core and holoenzyme, but both molecules have distinct mechanisms of operation in the bacterial cells.

Taken together, we show (i) that the number of RNAP molecules is positively correlated with the Ms1 presence both in stationary phase and shortly after the dilution into a fresh medium; and (ii) that the presence of Ms1 is advantageous for the mycobacterial cell during outgrowth.

Discussion

In this study, we characterize synthesis and degradation of Ms1 and the effects of Ms1 on gene expression and cell fitness. Ms1 is the most abundant non-rRNA transcript in stationary phase in *M. smegmatis* and its accumulation depends on its strong and almost constitutive promoter and differential RNA degradation. Our data further reveals that deletion of Ms1 affects

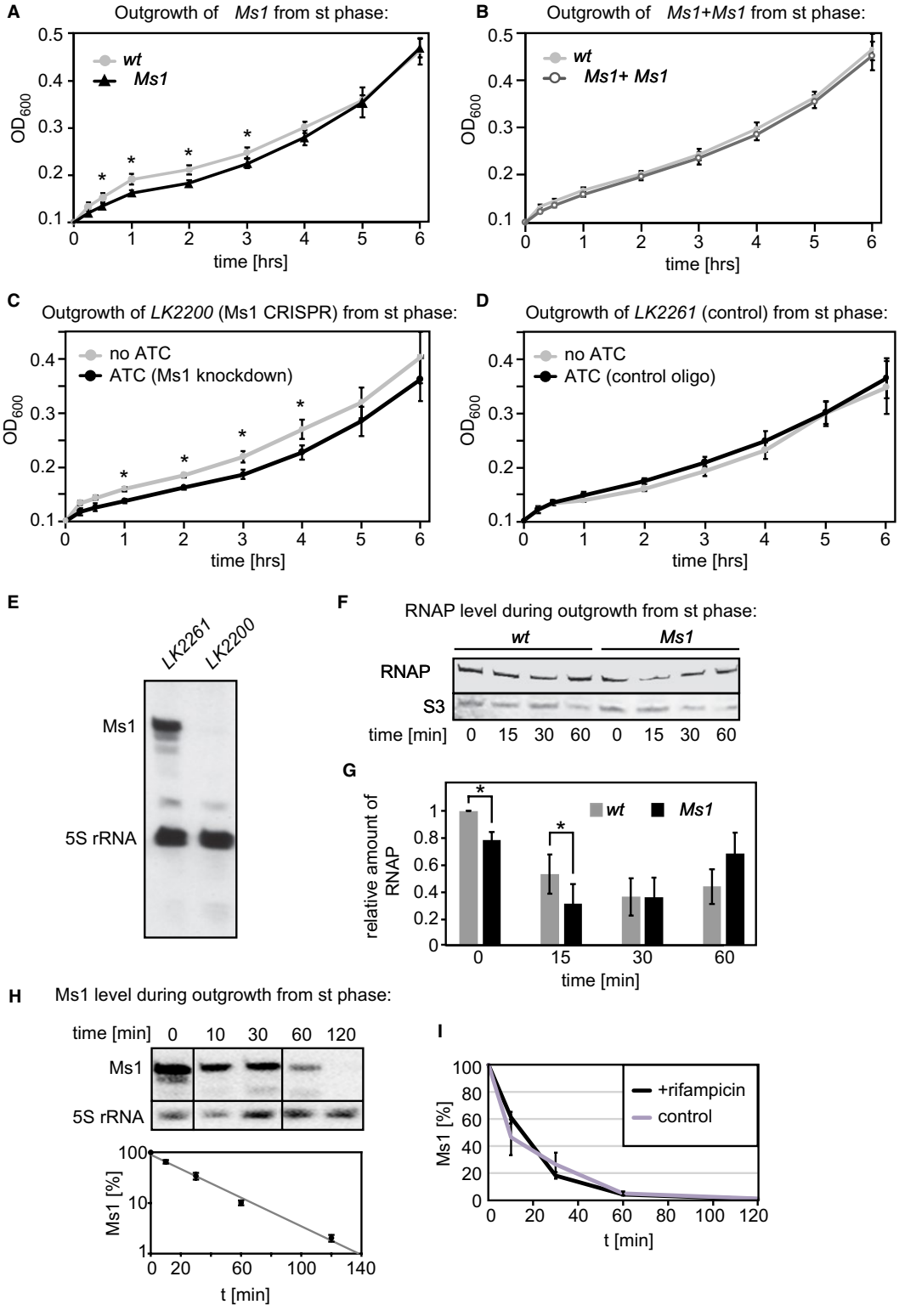
A
Outgrowth of Ms1 from st phase:
wt
Ms1
OD600
time [hrs]
B
Outgrowth of Ms1+Ms1 from st phase:
wt
Ms1+ Ms1
OD600
time [hrs]
C
Outgrowth of LK2200 (Ms1 CRISPR) from st phase:
no ATC
ATC (Ms1 knockdown)
OD600
time [hrs]
D
Outgrowth of LK2261 (control) from st phase:
no ATC
ATC (control oligo)
OD600
time [hrs]
E
LK2261
LK2200
Ms1
5S rRNA
F
RNAP level during outgrowth from st phase:
wt
Ms1
RNAP
S3
time [min] 0 15 30 60 0 15 30 60
G
wt
Ms1
relative amount of RNAP
time [min]
H
Ms1 level during outgrowth from st phase:
time [min] 0 10 30 60 120
Ms1
5S rRNA
Ms1 [%]
t [min]
I
+rifampicin
control
Ms1 [%]
t [min]

Fig. 6. Outgrowth of Δ*Ms1* from stationary phase.
A. Δ*Ms1* and *wt* stationary phase cells (after 24 h cultivation) were diluted into a fresh medium to OD_{600} 0.1 and their growth was monitored for 6 h. During the first 3 h, we detected a statistically significant delay in Δ*Ms1* growth (*P*-value < 0.05, *T*-test, marked with asterisks). The data represent averages from seven independent experiments ±SEM.
B. Δ*Ms1+Ms1* and *wt* stationary phase cells (after 24 h cultivation) were diluted into a fresh medium to OD_{600} 0.1 and their growth was measured for 6 h. The data represent averages from three independent experiments ±SEM.
C. In the *LK2200* strain, Ms1 CRISPR knockdown can be induced by anhydrotetracycline. The *LK2200* strain was inoculated to OD_{600} 0.1; after 8 h of cultivation, the Ms1 knockdown was induced by anhydrotetracycline (ATC) or not (control) and the strain was cultivated for another 16 h to reach stationary phase. Then, cells were diluted into a fresh medium to OD_{600} 0.1 without anhydrotetracycline and their growth was measured for 6 h similarly as in experiment in Fig. 6A. The cells, where Ms1 was depleted in stationary phase by anhydrotetracycline, displayed slower outgrowth than control cells without anhydrotetracycline. Three independent experiments were performed. Statistically significant delay in outgrowth between *LK2200* with anhydrotetracycline compared to *LK2200* without anhydrotetracycline (*P*-value < 0.05, *T*-test) is marked with asterisks.
D. The *LK2261* strain (negative control that contains non-targeting control sgRNA) was cultivated as the *LK2200* strain in Fig. 6C. Addition of anhydrotetracycline (ATC) had no effect on the outgrowth.
E. CRISPR knockdown in *LK2200* strain was verified by northern blotting. *LK2200* and *LK2261* control strains were inoculated to OD_{600} 0.1; after 8 h of cultivation anhydrotetracycline (ATC) was added and the strains were cultivated for another 16 h to reach stationary phase. Total RNA was isolated from stationary phase, resolved on polyacrylamide gels and analyzed by northern blotting with oligonucleotide probes complementary to Ms1 or 5S rRNA (loading control). In *LK2200*, Ms1 was depleted below the detection liming.
F. The RNAP level during outgrowth was determined by quantitative western blotting with an anti-β subunit RNAP antibody. The antibody against the S3 protein was used as a control. Time 0 was before dilution into fresh media. Five milligrams of protein lysate were loaded from indicated time points.
G. Quantification of RNAP amount from Fig. 6F. The bar graph shows averages from four independent experiments with ±SEM; statistically significant differences (*P*-value < 0.05, *T*-test) are marked with asterisks.
H. The level of endogenous Ms1 after dilution of stationary phase cells into a fresh medium was determined by northern blotting and normalized to 5S rRNA. The experiment was performed in three biological replicates. The graph (averages ± SD) shows the decay of Ms1: a 50% reduction after ~18 min in exponential phase.
I. The level of endogenous Ms1 after dilution of stationary phase cells into a fresh medium was determined by qPCR and normalized to 16S rRNA in the presence or absence of rifampicin. The experiment was performed in two biological replicates, error bars represent ±SD.

expression of only several genes during steady state. However, Ms1 influences the RNAP level and likely sequesters RNAP cores in a cache of inactive enzymes that can be reactivated when needed. This appears to be crucial when the demand for RNAP increases during environmental changes such as outgrowth from stationary phase.

Regulation of Ms1 accumulation: promoter activity and Ms1 stability

Ms1 is transcribed from a single promoter in *M. smegmatis* (Fig. 2B). The same promoter-like sequence is present also upstream of the Ms1 homolog MTS2823 in *M. tuberculosis* as we mapped the 5' end of MTS2823 to the same position of the 5' end of *M. smegmatis* Ms1 (Fig. 2F). The 3' end of Ms1 is then the result of intrinsic termination due to the presence of a stem-loop structure followed by a run of Us (Hnilicova *et al.*, 2014). This contrasts with 6S RNA in *E. coli* where the termination is Rho-dependent (Chae *et al.*, 2011).

The sequences of the –35 and –10 hexamers indicate that P_{Ms1} could be dependent on σ^A, similarly to 6S RNA in *E. coli* where there are two promoters, P1 and P2, recognized by the primary σ factor, σ^{70} (Kim and Lee, 2004). Nevertheless, transcription from the P2 promoter is both σ^{70}- and σ^S-dependent (Kim and Lee, 2004). The activity of P_{Ms1} is stimulated by upstream sequences that must contain binding sites for transcription factors, because no other promoter is located within the ~500 bp upstream of the Ms1 TSS (Fig. 2B). *MSMEG_6173* (morphological differentiation associated protein, similar to HAD family hydrolase), a gene preceding Ms1 in the *M. smegmatis* genome, ends 114 bp upstream of the Ms1 transcription start site and it is in the same orientation as Ms1. Ms1 could be theoretically transcribed in one operon with *MSMEG_6173*; however, based on the RNA-seq data, *MSMEG_6173* is much less expressed than Ms1 (normalized expression of *MSMEG_6173* is ~12 versus ~66,000 for Ms1 in stationary phase, Supporting Table 1).

The P_{Ms1} activity is roughly comparable to the activity of the *rrnB* promoter (–72/+20 promoter fragment) in exponential phase of growth. Similarly to P_{Ms1}, the P_{rrnB} core promoter is rather weak and is activated by the upstream elements more than 300-fold (Arnvig *et al.*, 2005). Thus, transcriptional activators are probably responsible for activation of both P_{rrnB} (~300-fold increase) and P_{Ms1} (~70-fold increase in exponential, ~360-fold increase in early stationary phase by addition of upstream elements to the core promoter, based on *lacZ* mRNA expression data, Fig. 2D). This suggests that transciption factors strongly affect expression of the most abundant mycobacterial RNAs and are important gene expression activators in mycobacteria.

The activity of P_{Ms1} including upstream regulatory elements (–491/+9 region) increased ~two-fold in exponential versus stationary phase (Fig. 2D). Even more notably, the Ms1 stability increased ~60-70-fold in stationary compared to exponential phase, which together with the elevated transcription initiation results in a predicted

~130-fold increase in the Ms1 level in stationary phase. This then corresponds to the actual ~115-fold increase in the Ms1 level as quantified by qPCR (Fig. 1A). A similar mechanism – regulated sRNA degradation – could also influence the accumulation of other sRNAs such as 6S RNAs that has not been fully elucidated yet (Cavanagh and Wassarman, 2014).

Here, as illustrated by our promoter activity results obtained by two different approaches (β-galactosidase assays and direct measurements of the *lacZ* mRNA), we insert a cautionary note that β-galactosidase assay-derived promoter activities may be in some cases inacurate, especially when determining promoter activity decreases.

The promoter activity could not explain the Ms1 accumulation. The increased stability of Ms1 in stationary phase suggested that Ms1 accumulation might be regulated by an RNase. Therefore, we investigated the role of PNPase in Ms1 degradation because previously we had pulled down PNPase with Ms1 (Hnilicová *et al.*, 2014). First, we confirmed that PNPase degrades Ms1 in exponential phase *in vivo* (Fig. 3E). PNPase is an exoribonuclease that catalyzes phosphorolytic degradation of RNA from the 3' end and also the reverse reaction – polymerization of nucleoside diphosphates (Briani *et al.*, 2016). PNPase participates in maturation and quality control of stable RNA: tRNAs (Li *et al.*, 2002) and rRNAs (Cheng and Deutscher, 2003), sRNAs (Andrade and Arraiano, 2008; De Lay and Gottesman, 2011; Andrade *et al.*, 2012; Saramago *et al.*, 2014) and affects stability of numerous mRNAs (Mohanty and Kushner, 2003). In *E. coli*, PNPase is present either as homotrimer or in the complex with RNA helicase RhlB (Portier, 1975; Lin and Lin-Chao, 2005) or as a part of the degradosome, assembled from RNase E, PNPase, RhlB and enolase (Bandyra *et al.*, 2013). RhlB helps PNPase to overcome secondary structures in substrate RNA that would otherwise inhibit PNPase degradation activity.

In this study we isolated a recombinant PNPase without any accessory protein (Fig. 3G) and showed that PNPase was able to degrade Ms1 *in vitro* (Fig. 3H). Interestingly, the Ms1 'tails' (regions at 5' and 3' ends) were necessary for Ms1 degradation by PNPase. This indicated that the putative Ms1 terminator likely plays a role in modulation of Ms1 stability and degradation. Based on RNA-seq data, PNPase (*MSMEG_2656*) is the most expressed RNase in exponential phase in *M. smegmatis.* PNPase is even more abundant than RNase E (*MSMEG_4626*) or RNase J (*MSMEG_2685*) (Supporting Table 1) that are involved in maturation of ribosomal RNA in *M. smegmatis* (Taverniti *et al.*, 2011). Importantly, PNPase expression increases ~20-fold in exponential compared to stationary phase (Fig. 1B), and this is consistent with the short biological half-life of Ms1 in this phase.

To conclude, Ms1 is transcribed from the strong P_{Ms1}promoter and its accumulation is achieved, at least in part, by differential degradation by PNPase.

Dissociation of Ms1 from RNAP

The mechanism of Ms1-RNAP complex disruption and its role in Ms1 protection is unknown. 6S RNA, which binds the RNAP-primary σ factor holoenzyme, serves as a template for transcription of pRNAs, which results in the dissociation of the 6S RNA:RNAP complex during outgrowth from stationary phase (Wassarman and Saecker, 2006; Gildehaus *et al.*, 2007; Beckmann *et al.*, 2011; Beckmann *et al.*, 2012; Cavanagh *et al.*, 2012). Inhibition of transcription by rifampicin stabilizes 6S RNA:RNAP complex and protects 6S RNA from degradation during the outgrowth (Wurm *et al.*, 2010; Beckmann *et al.*, 2012). However, rifampicin did not protect Ms1 from degradation during the outgrowth (Fig. 6I) indicating a different mechanism of Ms1 release from RNAP than active transcription. Previously, we showed that Ms1 could bind RNAP in exponential phase to a similar extent as in stationary phase (Hnilicova *et al.*, 2014). When we measured the stability of Ms1 in mid-exponential phase, we used rifampicin to block *de novo* transcription and Ms1 was again rapidly degraded (Fig. 3A). During the outgrowth and in exponential phase rifampicin did not affect Ms1 level. This suggests that either rifampicin does not stabilize Ms1-RNAP complex or the interaction with RNAP does not protect Ms1 from degradation.

Ms1 is highly unstable in exponential phase; therefore, the Ms1-RNAP interaction in exponential phase must be also unstable. Previously we showed that the overexpression of the primary σ factor, σ^A, in stationary phase decreased the amount of Ms1-RNAP (Hnilicova *et al.*, 2014). A hypothesis that needs to be examined in the future is whether the primary or alternative σ factors participate in dissociation of Ms1-RNAP complex during the outgrowth and in exponential phase of growth.

Ms1 affects the RNAP level

The low overall effect of Ms1 on transcription was surprising as we had expected that due to the sequestration of RNAP by Ms1, Δ*Ms1* would contain more free RNAPs that would widely influence gene expression. However, the total RNAP level decreases in Δ*Ms1* compared to *wt* (Fig. 5C) and Δ*Ms1* thus lacks the extra reservoir of RNAP that is sequestered in complex with Ms1 in *wt.* It is then possible, that the relative amount of RNA polymerase available for transcription remains the same in Δ*Ms1* and *wt* (Fig. 7). It is not clear, how the level of the mRNA encoding β and β' subunits is regulated.

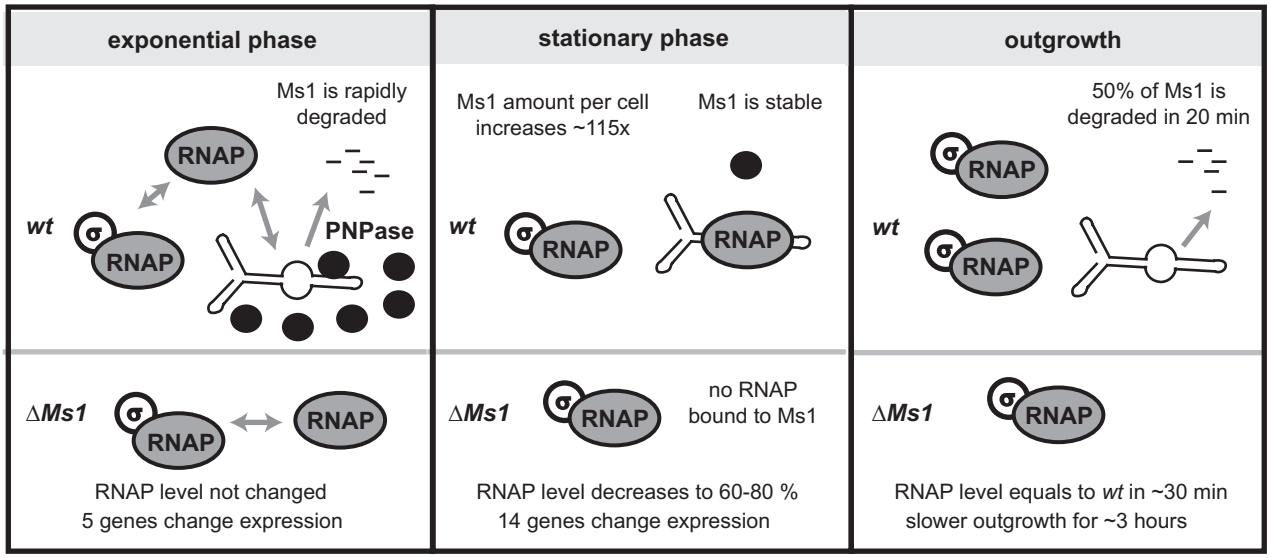

Fig. 7. RNAP level in *wt* and Δ*Ms1* strains. In exponential phase, Ms1 is unstable and rapidly degraded, PNPase contributed to the degradation. The level of RNAP is unchanged in Δ*Ms1* compared to *wt* strain. In the stationary phase, Ms1 interacts with RNAP in the *wt* strain and a fraction of RNAP is sequestered by Ms1. In Δ*Ms1*, no Ms1 is present. When Ms1 is missing, a corresponding fraction of the cellular RNAP is absent. This suggests that the Ms1 absence is compensated for by a decreased amount of RNAP molecules and the pool of RNAPs dedicated to transcription remains similar both in *wt* and Δ*Ms1* strains. During the outgrowth, the difference in RNAP level between Δ*Ms1* and *wt* remains similar for ~30 min and the growth Δ*Ms1* is slowed down for ~3 h.

What is the advantage to synthetize Ms1?

In exponential phase, Ms1 represents about 0.1% of all non-rRNA. The expense of its synthesis and degradation in *wt* may account for the slightly improved growth of Δ*Ms1* at the end of exponential phase in the defined rich medium (Fig. 4B). In stationary phase the Ms1 amount increases ~115-fold (Fig. 1A) which constitutes more than 30% of non-rRNA. What is the purpose of synthetizing such an enormous amount of this sRNA in the cell?

The presence of Ms1 increases the cell fitness in stationary phase where the Δ*Ms1* strain is less resistant to gamma irradiation. A contributing factor to this phenotype could be the lowered expression of *MSMEG_5556*, a major facilitator superfamily transporter (Li *et al.*, 2017). It may be involved in transport of detrimental metabolites out of the cell (Ramón-García *et al.*, 2009). Alternatively, higher amounts of RNAP in stationary phase *wt* cells might help *M. smegmatis* overcome consequences of radioactive exposure by an unknown mechanism. If γ irradiation destroyed a fraction of RNAP in the bacterial cell, a higher number of functional RNAP would remain in *wt* cells as these cells had a higher amount of RNAP before γ irradiation. Chronic γ irradiation produces complex oxidative stress for cells. In these conditions, cells have to respond to the resulting reactive oxygen species (ROS) that damage DNA and proteins. This can partially mimic growth in macrophages, which produce reactive oxygen and nitrogen intermediates (Burney *et al.*, 1999; Nathan and Shiloh, 2000). In *M. tuberculosis*, the Ms1 homolog MTS2823 is present at a high level during chronic stages of infection in lungs where it may contribute to the ability of the pathogen to survive in the hostile environment (Arnvig *et al.*, 2011; Arnvig and Young, 2012). The activity of Ms1 promoter also increased during ethanol stress (Fig. 2G). In bacteria, ethanol damages cell wall and membrane integrity and causes increased level of reactive oxygen species (Cao *et al.*, 2017) that is similar to chronic γ irradiation stress. Ms1 could be therefore specifically connected with this type of stress.

Finally, it appears that Ms1 increases the pool of RNAP molecules that can become important during rapid changes in the environment such as outgrowth from stationary phase. This is consistent with the fact that the intracellular level of RNAP generally positively correlates with the growth rate (Klumpp and Hwa, 2008). Thus, it is likely advantageous for mycobacterial cells to have stored RNAP enzymes that can rapidly start transcription of appropriate genes when surrounding conditions become favorable. This 'jump start' is probably beneficial for the cell especially when it faces competition from other species or for pathogens that must deal with its host's immune system.

Experimental procedures

Bacterial strains, growth conditions, plasmids

For detailed description of individual strains, see List of strains and plasmids in Supporting Data. *M. smegmatis*

mc^2 155 (*wt*, *LK865*) were grown at 37°C in Middlebrook 7H9 medium with 0.2% glycerol and 0.05% Tween 80, and harvested in exponential (OD_{600} ~0.5; 6 h of cultivation), early stationary (OD_{600} ~2.5–3, 24 h of cultivation) or late stationary (OD_{600} ~2, 48 h of cultivation) phase unless stated otherwise. When required, media were supplemented with hygromycin (50 μg ml^{-1}), kanamycin (20 μg ml^{-1}), spectinomycin (20 μg ml^{-1} for *M. smegmatis*, 100 μg ml^{-1} for *E. coli*), rifampicin (250 μg ml^{-1}) or anhydrotetracycline (100 ng ml^{-1}). Transformations of *M. smegmatis* mc^2 155 cells were performed by electroporation. To test the stress response, NaCl (final concentration 0.5 M), diamide (final concentration: 0–10 mM dilution series) and EtOH (5% final concentration) were pipetted directly into 7H9 medium; or 25 ml of culture was filtered using MF^{TM} – Membrane Filters 0.45 μm HA (Millipore) and cells were resuspended either in 25 ml of preheated 7H9 medium with adjusted pH, PBS or distilled water. For γ irradiation, *wt* (*LK865*) and Δ*Ms1 (LK1611)* strains were aliquoted, and transported at 4°C in sterilized cuvettes. Half of samples were chronically irradiated by gammacell 220 (Dose 40 Gy h^{-1}) at room temperature (RT). The second half was kept at RT without irradiation as a control of cell viability. Every 2 h, samples were collected (irradiated and non-irradiated), diluted and plated in triplicates. CFU per millilitres values were counted after 2 days of incubation at 37°C. The CFU per millilitres values for *wt* (*LK865*) and Δ*Ms1 (LK1611)* in stationary phase and after rifampicin treatment and were calculated in duplicates and are shown as an average from three independent experiments ± SEM (standard error of the mean). The doubling times were calculated with ±SEM.

Δ*Ms1 and* Δ*Ms1+Ms1 strains*

ΔMs1 *(LK1611)* strain was prepared by recombineering (van Kessel and Hatfull, 2007). Briefly, 100 ng of linear allelic exchange substrate (AES) was electroporated into *M. smegmatis* mc^2 pJV53 cells *(LK1321)*. To prepare AES, first the *hyg* resistance gene was amplified by PCR with Phusion High-Fidelity DNA Polymerase (NEB) from the pML1342 plasmid (Huff *et al.*, 2010) and cloned into pUC18 into PstI/XbaI (for primers see List of primers in Supporting Data). Then LA (left arm – upstream of the 5' end of Ms1) was PCR amplified from genomic DNA and cloned into HindIII/PstI; a short DNA linker was then cloned into XbaI to separate the close XbaI/BamHI restriction sites that were preventing the cloning. Subsequently, RA (right arm) was cloned into XbaI/BamHI. RA was commercially synthetized by GeneArt Gene Synthesis service (Invitrogen, for the sequence see Supporting Data). The construct was verified by sequencing. After transformation into *M. smegmatis* mc^2 pJV53 *kan* cells *(LK1321)*, colonies were selected at hygromycin/kanamycin plates; deletion of Ms1 was verified by PCR, and the absence of the Ms1 band in total RNA. Then, the Δ*Ms1* strain was cured from pJV53 by passaging without the kanamycin *(LK1611)*. For Δ*Ms1* strain complementation *(LK2223)*, *Ms1* gene plus 483 bp upstream and 50 bp downstream were cloned into NotI/PacI restriction sites of pTC-mcs vector (Klotzsche *et al.*, 2009) and transformed into Δ*Ms1 (LK1611)* strain.

RNA isolation and RT-qPCR

Twenty-five milliliters cells from the indicated growth phases were quickly cooled on ice, pelleted and immediately frozen. The pellet was then suspended in 240 μl TE (pH 8.0) plus 60 μl lysis buffer (50 mM Tris-HCl pH 8.0, 500 mM LiCl, 50 mM EDTA pH 8.0, 5% SDS) and 600 μl acidic phenol (pH~3):chloroform (1:1). Lysates were sonicated in a fume hood, centrifuged, the aqueous phase extracted three times with acidic phenol (pH~3):chloroform and precipitated with ethanol. RNA was dissolved in water, treated with DNase (TURBO DNA-free Kit, Ambion) and visualized on a 7 M urea 7% polyacrylamide gel by staining with GelRed (LabMark). RNA was reverse transcribed into cDNA (SuperScriptIII, Invitrogen) using random hexamers and amplified by quantitative reverse transcription PCR (RT-qPCR) in a LightCycler 480 System (Roche Applied Science) in duplicate reactions containing LightCycler 480 SYBR Green I Master and 0.5 μM primers (each). Primers were designed with Primer3 software and their sequences are in the Supporting Data. Negative controls (no template reactions and reactions with RNA as a template to control for contamination with genomic DNA) were run in each experiment, the quality of the PCR products was determined by dissociation curve analysis and the efficiency of the primers determined by standard curves. The mRNA level was quantified on the basis of the threshold cycle (Ct) for each PCR product that was normalized to reference gene value according to the formula $2\text{^}(Ct^{(ref)} - Ct^{(mRNA)})$ and expression (E) normalized to *wt* strain ($E = E_{\Delta Ms1}/E_{wt}$).

β-*galactosidase assay and promoter constructs*

Annealed oligonucleotides (for the −38 +9 construct, −72/+20 *rrnB* promoter) or PCR amplified promoter fragments with Phusion High-Fidelity DNA Polymerase (NEB) (see List of primers in Supporting Data) were cloned via the ScaI site preceding the *lacZ* reporter gene in the pSM128 integrative vector (Dussurget *et al.*, 1999). Sequence verified constructs were transformed into *M. smegmatis* mc^2 155 (*wt*, *LK865*). One milliliter of bacterial culture (see growth conditions) was centrifuged (13200 × *g*, 10 min, 4°C) and pellets washed with 500 μl of Z buffer 2 (Z buffer with 2.7 μl of 2-mercaptoethanol/ml; Z buffer: 60 mM Na_2HPO_4, 40 mM NaH_2PO_4, 10 mM KCl, 1 mM $MgSO_4$, pH 7.0), centrifuged again and resuspended in 500 μl of Z buffer 2. Cells were sonicated 3× 20 s (amplitude 50%) on ice with 1 min pauses between sonications and centrifuged (17900 × *g*, 10 min, 4°C). 100 μl of sonicate and 900 μl of Z buffer were incubated for 5 min at 30°C and 200 μl of orthonitrophenyl-β-D-galactopyranoside (ONPG) solution was added (4 mg ml^{-1} ONPG in Z-buffer). After 20 min, the reaction was stopped with 500 μl of 1 M Na_2CO_3, OD_{420} and OD_{550} were measured, and β-galactosidase activity (in arbitrary units) calculated: activity = $1000*(OD_{420} - 1.75*OD_{550})/(v*t*c)$, where v is sample volume [ml], *t* time of reaction, c protein concentration [mg ml^{-1}] measured by Bradford protein assay. To determine *lacZ* mRNA amount, 20 ml of exponential phase and 10 ml of stationary phase cells were quickly cooled on ice, pelleted and immediately frozen. Paralelly, OD_{600} of

cell cultures was measured. 40 ng of *in vitro* transcribed 6S RNA from *B. subtilis* was added to each RNA isolation as an RNA recovery marker. RNA was isolated, treated with DNase, reverse transcribed into cDNA amplified by qPCR. The mRNA level was quantified on the basis of the threshold cycle (Ct) for each PCR product that was normalized to 6S RNA recovery marker value according to the formula $2^{\wedge}(Ct^{(6S\ RNA)} - Ct^{(mRNA)})$ and *lacZ* expression normalized to OD_{600} of individual cell cultures.

RNA-seq

Isolated RNA was dissolved in water and two times treated with DNase (TURBO DNA-free Kit, Ambion). Five µg of total RNA were rRNA depleted with a Ribo-Zero rRNA Removal Kit (Gram-Positive Bacteria) (Illumina), and strand specific libraries were prepared with Illumina compatible NEXTflex Rapid Directional RNA-Seq Kit (Bioo Scientific) according to manufacturer's instructions. Pooled barcoded libraries (four samples in biological triplicates) were sequenced in a single lane at Illumina HiSeq 2000 in 50 bp single end regime at EMBL Genomics Core Facility, Heidelberg, Germany. Reads were aligned to *M. smegmatis* str. mc^2 155 (NCBI Reference Sequence: NC_008596.1) using HISAT2 (Kim *et al*., 2015) version 2.1.0 (with parameters '--rna-strandness R' and '--no-spliced-alignment') and samtools (Li *et al*., 2009) version 1.3.1. and inspected using IGV browser 2.0.23 and the igvtools package (Thorvaldsdóttir *et al*., 2013). Differentially expressed genes were detected by DESeq2 (Love *et al*., 2014), Benjamini-Hochberg FDR corrected *P*-value 0.05 was used as a cutoff. RNA-seq data are available in the ArrayExpress database (www.ebi.ac.uk/arrayexpress) under accession number E-MTAB-7004. Normalized gene expression was calculated as a number of mapped reads per gene divided by gene length and the size of non-rRNA library (sum of all mapped reads except for reads mapping to 3,819,833-3,825,494 and 5,024,129-5,031,105 that represents rRNA operons *MSMEG_3755-MSMEG_3757* and *MSMEG_4929-MSMEG_4931* plus surrounding intergenic regions). Normalized expression was averaged from three biological replicates and multiplied by 10^8.

Northern blotting, western blotting

RNAs were resolved on a 7% polyacrylamide gel and transferred onto an Amersham Hybond-N membrane according to the protocol described in (Pánek *et al*., 2011). Probes were 5′ ^{32}P-labeled oligonucleotides (anti-Ms1: 5′-TCGTGGCCGTCCGCTTTTCGAAACTACGC-3′; anti-5S: 5′-CTGGCAGGCTTAGCTTCCGGGTTCGGGATG-3′), and signals were captured in Fuji MS phosphor storage screens, scanned with a Molecular Imager_FX (Bio-Rad) and quantified with QuantityOne software (Bio-Rad). Alternatively, 5′end biotinylated oligonucleotides (with the same sequence) were hybridized to the membrane and detected with BrightStar BioDetect Kit (Ambion) according to manufacturer's instructions. Northern blot signals were normalized either to 5S rRNA or to recovery marker RNA. Recovery markers RNA (Ms1notail; the recovery marker was a shorter version of the Ms1 allowing to distinguish these two according to molecular mass in gels or *B. subtilis* 6S RNA) were added at the beginning of RNA extraction as a control for RNA degradation or pipetting errors (Rabatinová *et al*., 2013). Proteins were analyzed by SDS-PAGE and detected by western blotting using mouse monoclonal antibody against the β subunit of RNAP [clone name 8RB13] and secondary antibody conjugated with a fluorophore dye and quantified with an Odyssey reader (LI-COR Biosciences) or goat anti-S3 ribosomal protein conjugated with HRP (kindly provided by Dr. Isabella Moll, Max F. Perutz Laboratories Vienna, Austria). After the last wash in PBS/0.05% Tween 20, the membrane was washed three times in 100 mM Tris-HCl pH 9, 150 mM NaCl, 1 mM $MgCl_2$, then 66 µl NBT and 33 µl BCIP (both from Promega) were added into 10 ml of the same buffer and the colorimetric reaction was stopped by water. The signal was quantified using the QuantityOne (Bio-Rad) software.

CRISPR knockdown

sgRNA oligos (see Supporting data) were designed and cloned into PLJR962 according to the published protocol (Rock *et al*., 2017). Sequence-verified constructs were electroporated into *wt* (*LK865*) *M. smegmatis* resulting in strains *LK2197* (*MSMEG_2685,* RNase E knockdown), *LK2198* (*MSMEG_4626,* RNase J knockdown), *LK2219* (*MSMEG_2656,* PNPase knockdown), *LK2200* (Ms1 knockdown) and *LK2261* – negative control, non-targeting control sgRNA (Rock *et al*., 2017). The knockdowns of RNases were induced in exponential phase with anhydrotetracycline for 3 h, OD_{600} of cell cultures was measured and the same amout of cells harvested. 200 ng of *in vitro* transcribed 6S RNA from *B. subtilis* was added to each RNA isolation as an RNA recovery marker. RNA was isolated and analysed by northern blotting or treated with DNase, reverse transcribed into cDNA amplified by qPCR. The RNase J, RNase E and PNPase mRNA level was quantified on the basis of the threshold cycle (Ct) for each PCR product that was normalized to 6S RNA recovery marker value according to the formula $2^{\wedge}(Ct^{(6S\ RNA)} - Ct^{(mRNA)})$.

5′RACE from M. tuberculosis *H37Rv*

M. tuberculosis H37Rv ATCC 27294 strain was cultivated for 3 weeks on Lowenstein-Jensen agar plates at 35.5°C in aerobic conditions. The cells were harvested and directly lysed in TRI Reagent (Sigma Aldrich) and RNA isolated according to manufacturer's instructions. Five milligrams of total RNA was treated with 5U TEX (Terminator 5'-Phosphate-Dependent Exonuclease; Epicentre) for 1 h at 37°C. After the reaction, RNA was extracted with TRIzol and precipitated with ethanol. Purified RNA was treated with 1U of Tobacco Acid Pyrophosphatase (TAP; Epicentre) for 1 h at 37°C, extracted with TRIzol again, precipitated with ethanol, and a 5′-adaptor DNA/RNA oligonucleotide (5′-ATCGTaggcaccugaaa-3′, DNA in upper case letters) was ligated to the 5' ends (1 h at 37°C). RNA was then extracted and reversely transcribed into cDNA (SuperScriptIII, Invitrogen) with an MTS2823 (Ms1 homolog) specific reverse primer (5′-CATCTGCTGTTCGCAATTAC-3′). The same reverse primer and the 5′-ATCGTAGGCACCTGAAA-3′ forward primer were used for polymerase chain reaction (PCR)

with Taq DNA polymerase (Biotools). The PCR products were sequenced and mapped to the *M. tuberculosis* H37Rv (GenBank #AL123456.2).

Purification of PNPase-His6, in vitro *digestion assay*

Gene *MSMEG_2656* (*gpsI*) encoding PNPase was amplified by PCR with Phusion High-Fidelity DNA Polymerase (NEB) (for primers see Supporting Data) from *M. smegmatis* mc^2 155 genomic DNA, inserted into NdeI–NotI sites of pET-22b(+) and transformed into *E. coli* BL21 (DE3). Induction of PNPase-His6 was carried out at OD_{600} = 0.5 with 1 mM IPTG for 2 h at room temperature. Rifampicin (f.c. 100 μg ml^{-1}) was added together with IPTG. Cells were harvested by centrifugation, washed, resuspended in buffer P (300 mM NaCl, 50 mM Na_2HPO_4, 5% glycerol, 3 mM 2-mercaptoethanol, 0.1 mM phenylmethylsulfonylfluoride) and disrupted by sonication. Cell debris was removed by centrifugation, the supernatant was mixed with 1 ml Ni-NTA Agarose (Qiagen) and incubated for 1 h at 4°C with gentle shaking. Ni-NTA was washed with buffer P, then with buffer P supplemented with 30 mM (P + 30) imidazole and PNPase eluted with buffer P + 400 mM imidazole and dialysed against storage buffer (10 mM Tris-HCl, pH 8.0, 25 mM NH_4Cl, 100 μM EDTA, 10 mM $MgCl_2$, 30 μM DTT, 50% glycerol). $MgCl_2$ (f.c. 5 mM) was added and PNPase stored at –20°C. Proteins were separated on NuPAGE 4-12% Bis-Tris gels (Invitrogen) and visualized by Coomassie blue staining (SimplyBlue, Invitrogen). The identity of PNPase was verified by excising the corresponding band followed by mass spectrometry. Ms1, Ms1nb, Ms1notail DNA templates were designed based on secondary structure *in silico* modeling (Pánek *et al.*, 2011; Hnilicová *et al.*, 2014) and purchased from Invitrogen DNA (GeneArt Strings DNA Fragments) with T7 promoters at their 5' ends; they were amplified by PCR with Phusion High-Fidelity DNA Polymerase (NEB) (Hnilicová *et al.*, 2014). The 371 nt-long *rpoC* template was amplified from genomic DNA with primers carrying a T7 promoter at the 5′ end (see Supporting Data) and all RNAs were prepared with T7 RiboMAX Express Large Scale RNA Production System (Promega). RNA degradation assay (10 μl total volume) contained 400 ng RNA, 10 mM $MgCl_2$, 10 mM Na_2HPO_4, 20 mM Tris-HCl pH 7.6, 6.9 μM PNPase (or RNase A, Sigma Aldrich). The mixture was incubated for 30 min at 37°C (Nurmohamed *et al.*, 2011). Reaction was stopped with 10 μl of 200 mM EDTA; In control reactions, no enzyme was added and samples were incubated as described above. Samples were mixed 2:1 with sample buffer (95% formamide, 20 mM EDTA pH 8.0), heated for 1 min at 90°C and electrophoresed in 7 M urea 7% polyacrylamide gels. The gels were stained for 20 min with GelRed (LabMark) and visualized using a UV transilluminator and quantified with QuantityOne software (Bio-Rad).

Acknowledgements

We thank Dr. Isabella Moll (Max F. Perutz Laboratories, Austria) for provision of antibody. We thank Brian Grogan for English language editing. This work used instruments provided by C4Sys infrastructure. This work was supported by grants from the Czech Science Foundation [13-27150P to J.H., P305/12/G034 to L.K.], Charles University [PRIMUS/MED/26 and UNCE 204013 to M.P.], the Grant Agency of Charles University [946216 to M.J.], Ministry of the Interior of the Czech Republic [VI20152020044], and Ministry of Education, Youth and Sports of the Czech Republic within project the Center for advanced applied science, project number CZ.02.1.01/0.0/0.0/16_019/0000778. The authors have no conflict of interest to declare.

Author contributions

JH, MS, LK designed the study, MS, MJ, JH, OR, PP, DV, JP, PB, AS, OP, PK, PP, HS and MH performed the experiments, JH, MP, MS, MJ and LK analyzed the data and JH, LK wrote the manuscript.

References

Andrade, J.M. and Arraiano, C.M. (2008) PNPase is a key player in the regulation of small RNAs that control the expression of outer membrane proteins. *RNA*, **14**, 543–551.

Andrade, J.M., Pobre, V., Matos, A.M. and Arraiano, C.M. (2012) The crucial role of PNPase in the degradation of small RNAs that are not associated with Hfq. *RNA*, **18**, 844–855.

Arnvig, K. and Young, D. (2012) Non-coding RNA and its potential role in *Mycobacterium tuberculosis* pathogenesis. *RNA Biology*, **9**, 427–436.

Arnvig, K.B., Comas, I., Thomson, N.R., Houghton, J., Boshoff, H.I., Croucher, N.J. et al. (2011) Sequence-based analysis uncovers an abundance of non-coding RNA in the total transcriptome of *Mycobacterium tuberculosis*. *PLoS Pathogens*, **7**, e1002342.

Arnvig, K.B., Gopal, B., Papavinasasundaram, K.G., Cox, R.A. and Colston, M.J. (2005) The mechanism of upstream activation in the rrnB operon of *Mycobacterium smegmatis* is different from the *Escherichia coli* paradigm. *Microbiology*, **151**, 467–473.

Aviv, M., Giladi, H., Oppenheim, A.B. and Glaser, G. (1996) Analysis of the shut-off of ribosomal RNA promoters in *Escherichia coli* upon entering the stationary phase of growth. *FEMS Microbiology Letters*, **140**, 71–76.

Bandyra, K.J., Bouvier, M., Carpousis, A.J. and Luisi, B.F. (2013) The social fabric of the RNA degradosome. *Biochimica et Biophysica Acta (BBA)*, **1829**, 514–522.

Beckmann, B.M., Burenina, O.Y., Hoch, P.G., Kubareva, E.A., Sharma, C.M. and Hartmann, R.K. (2011) In vivo and in vitro analysis of 6S RNA-templated short transcripts in *Bacillus subtilis*. *RNA Biology*, **8**, 839–849.

Beckmann, B.M., Hoch, P.G., Marz, M., Willkomm, D.K., Salas, M. and Hartmann, R.K. (2012) A pRNA-induced structural rearrangement triggers 6S–1 RNA release from RNA polymerase in *Bacillus subtilis*. *The EMBO Journal*, **31**, 1727–1738.

Briani, F., Carzaniga, T. and Dehò, G. (2016) Regulation and functions of bacterial PNPase. *Wiley Interdisciplinary Reviews: RNA*, **7**, 241–258.

Browning, D.F. and Busby, S.J. (2016) Local and global regulation of transcription initiation in bacteria. *Nature Reviews Microbiology*, **14**, 638–650.

Burney, S., Caulfield, J.L., Niles, J.C., Wishnok, J.S. and Tannenbaum, S.R. (1999) The chemistry of DNA damage from nitric oxide and peroxynitrite. *Mutation Research/Fundamental and Molecular Mechanisms of Mutagenesis*, **424**, 37–49.

Cao, H., Wei, D., Yang, Y., Shang, Y., Li, G., Zhou, Y. et al. (2017) Systems-level understanding of ethanol-induced stresses and adaptation in *E. coli*. *Scientific Reports*, **7**, 44150.

Cavanagh, A.T., Klocko, A.D., Liu, X. and Wassarman, K.M. (2008) Promoter specificity for 6S RNA regulation of transcription is determined by core promoter sequences and competition for region 4.2 of sigma70. *Molecular Microbiology*, **67**, 1242–1256.

Cavanagh, A.T., Sperger, J.M. and Wassarman, K.M. (2012) Regulation of 6S RNA by pRNA synthesis is required for efficient recovery from stationary phase in *E. coli* and *B. subtilis*. *Nucleic Acids Research*, **40**, 2234–2246.

Cavanagh, A.T. and Wassarman, K.M. (2014) 6S RNA, a global regulator of transcription in *Escherichia coli*, *Bacillus subtilis*, and beyond. *Annual Review Microbiology*, **68**, 45–60.

Chae, H., Han, K., Kim, K.S., Park, H., Lee, J. and Lee, Y. (2011) Rho-dependent termination of ssrS (6S RNA) transcription in *Escherichia coli*: implication for 3' processing of 6S RNA and expression of downstream ygfA (putative 5-formyl-tetrahydrofolate cyclo-ligase). *Journal of Biological Chemistry*, **286**, 114–122.

Chen, K., Hu, Z., Xia, Z., Zhao, D., Li, W. and Tyler, J.K. (2015) The overlooked fact: fundamental need for spike-in control for virtually all genome-wide analyses. *Molecular and Cellular Biology*, **36**, 662–667.

Cheng, Z.F. and Deutscher, M.P. (2003) Quality control of ribosomal RNA mediated by polynucleotide phosphorylase and RNase R. *Proceedings of the National Academy of Sciences*, **100**, 6388–6393.

China, A., Tare, P. and Nagaraja, V. (2010) Comparison of promoter-specific events during transcription initiation in mycobacteria. *Microbiology*, **156**, 1942–1952.

Davis, E., Chen, J., Leon, K., Darst, S.A. and Campbell, E.A. (2015) Mycobacterial RNA polymerase forms unstable open promoter complexes that are stabilized by CarD. *Nucleic Acids Research*, **43**, 433–445.

De Lay, N. and Gottesman, S. (2011) Role of polynucleotide phosphorylase in sRNA function in *Escherichia coli*. *RNA*, **17**, 1172–1189.

Dussurget, O., Timm, J., Gomez, M., Gold, B., Yu, S., Sabol, S.Z., Holmes, R.K. et al. (1999) Transcriptional control of the iron-responsive fxbA gene by the mycobacterial regulator IdeR. *Journal of Bacteriology*, **181**, 3402–3408.

Feklístov, A., Sharon, B.D., Darst, S.A. and Gross, C.A. (2014) Bacterial sigma factors: a historical, structural, and genomic perspective. *Annual Review of Microbiology*, **68**, 357–376.

Gildehaus, N., Neusser, T., Wurm, R. and Wagner, R. (2007) Studies on the function of the riboregulator 6S RNA from *E. coli*: RNA polymerase binding, inhibition of in vitro transcription and synthesis of RNA-directed de novo transcripts. *Nucleic Acids Research*, **35**, 1885–1896.

Hnilicova, J., Matejckova, J.J., Sikova, M., Pospisil, J., Halada, P., Panek, J. et al. (2014) Ms1, a novel sRNA interacting with the RNA polymerase core in mycobacteria. *Nucleic Acids Research*, **42**, 11763–11776.

Hnilicová, J., Jirát Matějčková, J., Šiková, M., Pospíšil, J., Halada, P., Pánek, J. et al. (2014) Ms1, a novel sRNA interacting with the RNA polymerase core in mycobacteria. *Nucleic Acids Research*, **42**, 11763–11776.

Hu, Y., Morichaud, Z., Perumal, A.S., Roquet-Baneres, F. and Brodolin, K. (2014) Mycobacterium RbpA cooperates with the stress-response σB subunit of RNA polymerase in promoter DNA unwinding. *Nucleic Acids Research*, **42**, 10399–10408.

Hubin, E.A., Tabib-Salazar, A., Humphrey, L.J., Flack, J.E., Olinares, P.D., Darst, S.A. et al. (2015) Structural, functional, and genetic analyses of the actinobacterial transcription factor RbpA. *Proceedings of the National Academy of Sciences*, **112**, 7171–7176.

Huff, J., Czyz, A., Landick, R. and Niederweis, M. (2010) Taking phage integration to the next level as a genetic tool for mycobacteria. *Gene*, **468**, 8–19.

Kim, D., Langmead, B. and Salzberg, S.L. (2015) HISAT: a fast spliced aligner with low memory requirements. *Nature Methods*, **12**, 357–360.

Kim, K.S. and Lee, Y. (2004) Regulation of 6S RNA biogenesis by switching utilization of both sigma factors and endoribonucleases. *Nucleic Acids Research*, **32**, 6057–6068.

Klotzsche, M., Ehrt, S. and Schnappinger, D. (2009) Improved tetracycline repressors for gene silencing in mycobacteria. *Nucleic Acids Research*, **37**, 1778–1788.

Klumpp, S. and Hwa, T. (2008) Growth-rate-dependent partitioning of RNA polymerases in bacteria. *Proceedings of the National Academy of Sciences*, **105**, 20245–20250.

Krásný, L. and Gourse, R.L. (2004) An alternative strategy for bacterial ribosome synthesis: *Bacillus subtilis* rRNA transcription regulation. *The EMBO Journal*, **23**, 4473–4483.

Krásný, L., Tiserová, H., Jonák, J., Rejman, D. and Sanderová, H. (2008) The identity of the transcription +1 position is crucial for changes in gene expression in response to amino acid starvation in *Bacillus subtilis*. *Molecular Microbiology*, **69**, 42–54.

Li, H., Handsaker, B., Wysoker, A., Fennell, T., Ruan, J., Homer, N. et al. (2009) The sequence alignment/map format and SAMtools. *Bioinformatics*, **25**, 2078–2079.

Li, P., Gu, Y., Li, J., Xie, L., Li, X. and Xie, J. (2017) *Mycobacterium tuberculosis* major facilitator superfamily transporters. *The Journal of Membrane Biology*, **250**, 573–585.

Li, Z., Reimers, S., Pandit, S. and Deutscher, M.P. (2002) RNA quality control: degradation of defective transfer RNA. *The EMBO Journal*, **21**, 1132–1138.

Lin, P.H. and Lin-Chao, S. (2005) RhlB helicase rather than enolase is the beta-subunit of the *Escherichia coli* polynucleotide phosphorylase (PNPase)-exoribonucleolytic complex. *Proceedings of the National Academy of Sciences*, **102**, 16590–16595.

Love, M.I., Huber, W. and Anders, S. (2014) Moderated estimation of fold change and dispersion for RNA-seq data with DESeq2. *Genome Biol*, **15**, 550.
Mohanty, B.K. and Kushner, S.R. (2003) Genomic analysis in *Escherichia coli* demonstrates differential roles for polynucleotide phosphorylase and RNase II in mRNA abundance and decay. *Molecular Microbiology*, **50**, 645–658.
Murray, H.D., Schneider, D.A. and Gourse, R.L. (2003) Control of rRNA expression by small molecules is dynamic and nonredundant. *Molecular Cell*, **12**, 125–134.
Nathan, C. and Shiloh, M.U. (2000) Reactive oxygen and nitrogen intermediates in the relationship between mammalian hosts and microbial pathogens. *Proceedings of the National Academy of Sciences*, **97**, 8841–8848.
Neusser, T., Polen, T., Geissen, R. and Wagner, R. (2010) Depletion of the non-coding regulatory 6S RNA in *E. coli* causes a surprising reduction in the expression of the translation machinery. *BMC Genomics*, **11**, 165.
Nurmohamed, S., Vincent, H.A., Titman, C.M., Chandran, V., Pears, M.R., Du, D. et al. (2011) Polynucleotide phosphorylase activity may be modulated by metabolites in *Escherichia coli*. *Journal of Biological Chemistry*, **286**, 14315–14323.
Paul, B.J., Ross, W., Gaal, T. and Gourse, R.L. (2004) rRNA transcription in *Escherichia coli*. *Annual Review of Genetics*, **38**, 749–770.
Portier, C. (1975) Quaternary structure of polynucleotide phosphorylase from *Escherichia coli*: evidence of a complex between two types of polypeptide chains. *European Journal of Biochemistry*, **55**, 573–582.
Pánek, J., Krásny, L., Bobek, J., Jezková, E., Korelusová, J. and Vohradsky, J. (2011) The suboptimal structures find the optimal RNAs: homology search for bacterial non-coding RNAs using suboptimal RNA structures. *Nucleic Acids Research*, **39**, 3418–3426.
Rabatinová, A., Šanderová, H., Jirát Matějčková, J., Korelusová, J., Sojka, L., Barvík, I. et al. (2013) The δ subunit of RNA polymerase is required for rapid changes in gene expression and competitive fitness of the cell. *Journal of Bacteriology*, **195**, 2603–2611.
Rammohan, J., Ruiz Manzano, A., Garner, A.L., Prusa, J., Stallings, C.L. and Galburt, E.A. (2016) Cooperative stabilization of *Mycobacterium tuberculosis* rrnAP3 promoter open complexes by RbpA and CarD. *Nucleic Acids Research*, **44**, 7304–7313.
Rammohan, J., Ruiz Manzano, A., Garner, A.L., Stallings, C.L. and Galburt, E.A. (2015) CarD stabilizes mycobacterial open complexes via a two-tiered kinetic mechanism. *Nucleic Acids Research*, **43**, 3272–3285.
Ramón-García, S., Martín, C., Thompson, C.J. and Aínsa, J.A. (2009) Role of the *Mycobacterium tuberculosis* P55 efflux pump in intrinsic drug resistance, oxidative stress responses, and growth. *Antimicrobial Agents and Chemotherapy*, **53**, 3675–3682.
Rock, J.M., Hopkins, F.F., Chavez, A., Diallo, M., Chase, M.R., Gerrick, E.R. et al. (2017) Programmable transcriptional repression in mycobacteria using an orthogonal CRISPR interference platform. *Nature Microbiology*, **2**, 16274.
Saramago, M., Bárria, C., Dos Santos, R.F., Silva, I.J., Pobre, V., Domingues, S. et al. (2014) The role of RNases in the regulation of small RNAs. *Current Opinion in Microbiology*, **18**, 105–115.
Srivastava, D.B., Leon, K., Osmundson, J., Garner, A.L., Weiss, L.A., Westblade, L.F. et al. (2013) Structure and function of CarD, an essential mycobacterial transcription factor. *Proceedings of the National Academy of Sciences*, **110**, 12619–12624.
Tare, P., China, A. and Nagaraja, V. (2012) Distinct and contrasting transcription initiation patterns at *Mycobacterium tuberculosis* promoters. *PLoS One*, **7**, e43900.
Taverniti, V., Forti, F., Ghisotti, D. and Putzer, H. (2011) *Mycobacterium smegmatis* RNase J is a 5′-3′ exo-/endoribonuclease and both RNase J and RNase E are involved in ribosomal RNA maturation. *Molecular Microbiology*, **82**, 1260–1276.
Thorvaldsdóttir, H., Robinson, J.T. and Mesirov, J.P. (2013) Integrative Genomics Viewer (IGV): high-performance genomics data visualization and exploration. *Briefings in Bioinformatics*, **14**, 178–192.
Trotochaud, A.E. and Wassarman, K.M. (2005) A highly conserved 6S RNA structure is required for regulation of transcription. *Nature Structural & Molecular Biology*, **12**, 313–319.
van Kessel, J.C. and Hatfull, G.F. (2007) Recombineering in *Mycobacterium tuberculosis*. *Nature Methods*, **4**, 147–152.
Verma, A.K. and Chatterji, D. (2014) Dual role of MsRbpA: transcription activation and rescue of transcription from the inhibitory effect of rifampicin. *Microbiology*, **160**, 2018–2029.
Wassarman, K.M. and Saecker, R.M. (2006) Synthesis-mediated release of a small RNA inhibitor of RNA polymerase. *Science*, **314**, 1601–1603.
Wassarman, K.M. and Storz, G. (2000) 6S RNA regulates *E. coli* RNA polymerase activity. *Cell*, **101**, 613–623.
Wurm, R., Neusser, T. and Wagner, R. (2010) 6S RNA-dependent inhibition of RNA polymerase is released by RNA-dependent synthesis of small de novo products. *Biological Chemistry*, **391**, 187–196.

Supporting information

Additional supporting information may be found online in the Supporting Information section at the end of the article.

Supplementary data

Title: Ms1 RNA increases the amount of RNA polymerase in *Mycobacterium smegmatis*

Running Title: Function of Ms1 RNA in mycobacteria

Michaela Šiková[1], Martina Janoušková[1,2], Olga Ramaniuk[1], Petra Páleníková[1], Jiří Pospíšil[1], Pavel Bartl[3], Agnieszka Suder[1], Petr Pajer[4], Pavla Kubičková[4], Ota Pavliš[4], Miluše Hradilová[5], Dragana Vítovská[1], Hana Šanderová[1], Martin Převorovský[6], Jarmila Hnilicová[1] and Libor Krásný[1]

[1] Department of Microbial Genetics and Gene Expression, Institute of Microbiology, Czech Academy of Sciences, Prague, Czech Republic

[2] Department of Genetics and Microbiology, Faculty of Science, Charles University, Prague, Czech Republic

[3] Department of Nuclear Chemistry, Faculty of Nuclear Science and Physical Engineering, Czech Technical University in Prague, Prague, Czech Republic

[4] Military Health Institute, Military Medical Agency, Prague, Czech Republic.

[5] Department of Genomics and Bioinformatics, Institute of Molecular Genetics, The Czech Academy of Sciences, Prague, Czech Republic

[6] Department of Cell Biology, Faculty of Science, Charles University, Prague, Czech Republic

Michaela Šiková and Martina Janoušková should be considered joint first author

Jarmila Hnilicová and Libor Krásný should be considered joint senior author and corresponding author

Contact Information: E-mail: krasny@biomed.cz (LK) and hnilicova@biomed.cas.cz (JH), Tel. +420 241 063 208

List of strains and plasmids

Strain/plasmid	Relevant characteristics	Source
Escherichia coli		
LK1249	DH5α/pSM128 *spc*	(Dussurget *et al.*, 1999)
LK1439	DH5α/pSM128, PMs1(-38 +9) *spc*	This work
LK1420	DH5α/pSM128, PMs1(-131 +9) *spc*	This work
LK1409	DH5α/pSM128, PMs1(-231+9) *spc*	This work
LK1411	DH5α/pSM128, PMs1(-331 +9) *spc*	This work
LK1421	DH5α/pSM128, PMs1(-491 +9) *spc*	This work
LK1547	DH5α/pSM128, PMs1(-491 +9) *spc* mutations: T-12G, A-11C,C-10A, A-9G	This work
LK1551	DH5α/pSM128, PMs1(-491 -22) *spc*	This work
LK2146	DH5α/pSM128 PrrnB *spc*	This work
LK1270	DH5α/pJAM2 *kan*	(Hnilicová *et al.*, 2014)
LK1363	DH5α/pML1342 *hyg*	(Huff *et al.*, 2010)
LK1463	DH5α/pUC18 *hyg amp*	This work
LK1485	DH5α/pUC18-LA *hyg amp*	This work
LK1518	DH5α/pUC18-LA-linker *hyg amp*	This work
LK1526	DH5α/pUC18-LA-linker-RA *hyg amp*	This work
LK1528	DE3/pET22b- *MSMEG_2656 (PNPase) amp*	This work
Lk1396	DH5α/pTC-mcs *kan*	(Klotzsche *et al.*, 2009)
LK2178	DH5α/pTC-mcs *Ms1 kan*	This work
LK2070	DH5α/ pLJR962 *kan*	(Rock *et al.*, 2017)
LK2170	DH5α/ pLJR962 sgRNA_RNase E *kan*	This work
LK2171	DH5α/ pLJR962 sgRNA_RNase J *kan*	This work
LK2211	DH5α/ pLJR962 sgRNA_PNPase *kan*	This work
LK2173	DH5α/ pLJR962 sgRNA_Ms1 *kan*	This work
LK2255	DH5α/ pLJR962 sgRNA_control *kan*	(Rock *et al.*, 2017)

Mycobacterium smegmatis		
LK865	wt mc^2 155	Laboratory strain
LK1442	mc^2 155/pSM128 *str*	This work
LK1443	mc^2 155/pSM128, PMs1(-38 +9) *str*	This work
LK1444	mc^2 155/pSM128, PMs1(-131 +9) *str*	This work
LK1445	mc^2 155/pSM128, PMs1(-231 +9) *str*	This work
LK1446	mc^2 155/pSM128, PMs1(-331 +9) *str*	This work
LK1447	mc^2 155/pSM128, PMs1(-491 +9) *str*	This work
LK1578	mc^2 155/pSM128, PMs1(-491 +9) *str* mutations: T-12G, A-11C, C-10A, A-9G	This work
LK1590	mc2 155 pSM128 PMs1(-491 -22) *str*	This work
LK2206	mc2 155 pSM128 PrrnB *str*	This work
LK1302	mc^2 155 pJAM2 *kan*	(Triccas *et al.*, 1998)
LK1323	mc^2 155/pJAM2-*rrnB*-Ms1 *kan*	(Hnilicová *et al.*, 2014)
LK1321	mc^2 155 pJV53 *kan*	(van Kessel & Hatfull, 2007)
LK1611	mc^2 155 ΔMs1 *hyg*	This work
LK2223	mc^2 155 ΔMs1 pTC-mcs *Ms1 hyg kan*	This work
LK2197	mc^2 155/pLJR962 sgRNA_RNase E *kan*	This work
LK2198	mc^2 155/pLJR962 sgRNA_RNase J *kan*	This work
LK2219	mc^2 155/pLJR962 sgRNA_PNPase *kan*	This work
LK2200	mc^2 155/pLJR962 sgRNA_Ms1 *kan*	This work
LK2261	mc^2 155/pLJR962 sgRNA_control *kan*	This work
Mycobacterium tuberculosis		
-	H37Rv ATCC 27294	ATCC; Derived from E.R. Baldwin's 1905 human-lung isolate H37 by W. Steenken in 1934

LA – left arm, RA – right arm for Ms1 linear allelic exchange substrate (AES)

DNA fragment for Ms1-null strain AES

Right Arm GeneArt Strings DNA Fragments (Invitrogen)

tctagaGCGGGCGGCGAACCGGACATTGTCCGGGACGCCGCCCGATTTCTTTTGCTGGACCCGGT
CAAGTTCGTCACTGCGCCTGGGCTTCCCGGTACCCCATCGCCGACGAGATGCGCGCCGCGCTG
CGCCGCACCACGGGCACCAGGCCGCGCATCCGCGCGGCGGGCATGTAGGGCCGCGTCGCCGA
CACACTGATCGCCCCGACGATGGCCTTCGAGGCGTCGCGCACCGGGGCCGCCACGCACCGGAT
ACCGGGCTCGTTGTCCTCCAGGTCCATCGCAGAACCGCTCTTGGCGTAGGTCTGCATGCGCGTG
CAGAACTCGGCGCACCGCTCGGCGAGCTCGCCGCGTCGCACCACCGTCGGGACCGTCACGCG
GTCCTCGTCGGCGATGTACAGCTCTTCCCAGCGCTCCGGGGAATCCAGCAGCAGCGCCATCCC
CACGCCCGTGCGCGTCAACGGCATGCGGTGCCCCACCCGTGAGCGCATCTCGGCGCCGCGCG
TACCGGGCAGCTTCTCCAGGTggatcc

Templates for Ms1 *in vitro* transcription

Ms1 GeneArt Strings DNA Fragments (Invitrogen)

TACGTAATACGACTCACTATAGGGAAGCTTGGCGAGGCCAAGACCCAGCCGGAAGAGA
AGGCTAGATCTCCCGACCCAAGCTCCTAGCACGGATACCGAGCACCCACGCGGAGCAC
ATGCCGCGGAATAGGCAAAAGTGTTGCGGACCTGCGTAGTTTCGAAAAGCGGACGGCC
ACGACGGCCCTTTGGGTGGGGTTGCAGCCGTAGCGCATCGCAAAGACGCCGAGGTCA
CCCACGCAACCCACATCGCACGCTTGGTCACTCGGGGTCCGTGCTAGCGGGCGGCGA
ACCGGACATTGTCCGGGACGCCGCCCGATTTCTTTT

Ms1notail GeneArt Strings DNA Fragments (Invitrogen)

TACGTAATACGACTCACTATAGGGTAGCACGGATACCGAGCACCCACGCGGAGCACAT
GCCGCGGAATAGGCAAAAGTGTTGCGGACCTGCGTAGTTTCGAAAAGCGGACGGCCAC
GACGGCCCTTTGGGTGGGGTTGCAGCCGTAGCGCATCGCAAAGACGCCGAGGTCACC
CACGCAACCCACATCGCACGCTTGGTCACTCGGGGTCCGTGCTA

Ms1nb GeneArt Strings DNA Fragments (Invitrogen)

TACGTAATACGACTCACTATAGGGAAGCTTGGCGAGGCCAAGACCCAGCCGGAAGAGA
AGGCTAGATCTCCCGACCCAAGCTCCTAGCACGGATACCGAGCACCCACGCGGAGCGT
TGCGGACCTGCGTAGTTTCGAAAAGCGGACGGCCACGACGGCCCTTTGGGTGGGGTT
GCAGCCGTAGCGCATCGCAAAGACGCCGAGGTCACCCACGCAACGCACGCTTGGTCA
CTCGGGGTCCGTGCTAGCGGGCGGCGAACCGGACATTGTCCGGGACGCCGCCCGATT
TCTTTT

T7 promoter is underlined grey nucleotides are added during PCR synthesis

List of Primers

Oligonucleotide name	Sequence	
Oligonucleotide sequences of Ms1 core promoter		
1320/Pms1_CU	CCCTTGCTGTGACTCGGGACACGTAGTACAAAGGAGGCACGGAAGCT	
1321/Pms1_CB	AGCTTCCGTGCCTCCTTTGTACTACGTGTCCCGAGTCACAGCAAGGG	
Primes for PCR amplification of promoter of Ms1		
1322/Pms1_R	AGCTTCCGTGCCTCCTTTGTAC	reverse primer
1323/Pms1_140F	GCCGGTTCGCGCTCTGACG	forward for -131 +9
1324/Pms1_240F	CGTGACCGGTTCCCCGCGC	forward for -231 +9
1325/Pms1_340F	GGTGGGGCACCCCACCGCG	forward for -331 +9
1326/Pms1_500F	TGGTGGTGGAGGACGGCCG	forward for -491 +9
Oligonucleotide sequences of rrnB promoter		
PrrnB Sense	GTCTGACCAGGGAAAATAGCCCTCTGACCTGGGGATTTGACTCCCAGTTTCCAAGGACGTAACTTAT TCCAGGTCAGAGCGACACGGCCCAGA	
PrrnB AntiSense	CTGGGCCGTGTCGCTCTGACCTGGAATAAGTTACGTCCTTGGAAACTGGGAGTCAAATCCCCAGGTC AGAGGGCTATTTTCCCTGGTCAGACA	
Primers for sequencing insert in ScaI site on pSM128		
1335/pSM128-F	AATTGGGGACCCTAGAGGTC	
1336/pSM128-R	ATTCGTAGAGCCTCGTTGCG	
1360/pSM128-F2	CCAGATCTTTGTGGATGACC	
Primers for PCR amplification of modified Ms1 promoter		
1431/Pms1_mut	AGCTTCCGTGCCTCCTTCTGCCTACGTGTCCCG	
1432/Pms1_no(-10)	CCGAGTCACAGCAAGGGCC	
Primers for Ms1-null strain construction		
1386_Ms1_KOb_PstI	TGCCTGCAGGTTAACGAAATCAATCTA	primers to amplify *hyg* from pML1342
1387_Ms1_KOb_XbaI	TCGATCTAGAGAAGTTATCCCGGGGCGT	
1384_Ms1_KOa_HindIII	TGCCAAGCTTGAGGAGATCGTCGCCCCC	primers to amplify left arm (LA) from genomic DNA
1385_Ms1_KOa_PstI	GACCTGCAGCGTGCCTCCTTTGTACTA	
1464/linkerH	CTAGAGCTGTCAAGATCCTG	linker to separate XbaI and BamHI in the pUC18 plasmid; on the left side, XbaI is preserved, on the right side XbaI is cancelled (it allows the cloning of the linker but not subsequent digestion)
1465/linkerB	CTAGCAGGATCTTGACAGCT	
1388_Ms1_KOc_XbaI	CGACTCTAGAGCGGGCGGCGAACCGGACA	primers to amplify right arm (RA) from GeneArt DNA fragment
1389_Ms1_KOc_BamHI	TTACGGATCCACCTGGAGAAGCTGCCCG	
		primers to amplify Ms1 gene and surrounding regions for complemented strain
Primers for templates for *in vitro* transcription		
1254/IVT_GeneString_F	TACGTAATACGACTCACTAT	Forward primer to amplify Ms1, Ms1nb and Ms1notail from GeneArt Strings DNA Fragments (Invitrogen) (Hnilicová *et al.*, 2014)
1255/ IVT_Genestring_Ms1all_R	AAAAGAAATCGGGCGGCGTCCCGGACAATGTCCGG	Reverse primer to amplify Ms1 and Ms1nb

1256/ IVT_Genestring_Ms1notail_R	TAGCACGGACCCCGAGTGAC	Reverse primer to amplify Ms1notail
1281/ 16SrRNA_IVT_F	TACGTAATACGACTCACTATAGGGAGACAG CTCGTGTCGTGAGATGT	Forward primer to amplify 16S rRNA from genomic DNA
1282/ 16SrRNA_IVT_R	CGTTGCTGATCTGCGATTAC	Reverse primer to amplify 16S rRNA from genomic DNA
BsrA_6S_Bs_IVT_F	TACGTAATACGACTCACTATAGGAGAAAAGTCCT GATGTGTTAG	Forward primer to amplify 6S RNA (B.subtilis) from genomic DNA
BsrA_6S_Bs_IVT_R	TAAAGTCCCAATAGTGCC	Reverse primer to amplify 6S RNA (B.subtilis) from genomic DNA
Primers for CRISPR cloning		
2439/CRISPR_PNPase_F	GGGAATCTTTTTCGCGTCGTCACGC	
2440/CRISPR_PNPase_R	AAACGCGTGACGACGCGAAAAAGAT	
2441/CRISPR_RNaseE_F	GGGAGCACGCGCCGACTGGTGGTGC	
2442/CRISPR_RNaseE_R	AAACGCACCACCAGTCGGCGCGTGC	
2443/CRISPR_RNaseJ_F	GGGAACGCCGGGCTCGTCATGTCC	
2444/CRISPR_RNaseJ_R	AAACGGACATGACGAGCCCGGCGT	
2449/ CRISPR_Ms1_F	GGGAGAGGCCAAGACCCAGCCGGA	
2450/ CRISPR_Ms1_R	AAACTCCGGCTGGGTCTTGGCCTC	
2482/CRISPR_ctrl_F	GGGAGGAGACGATTAATGCGTCTCG	
2483/CRISPR_crtl_R	AAACCGAGACGCATTAATCGTCTCC	
Primers for PCR and cloning PNPase		
1470/PNPase_F	ATGG CATATGTCTGTAGTCGAACTTGAAGACGG	
1471/ PNPase_R	AT GCGGCCGC GGCCTCGGCCGGCGTGACATC	
Primers for qPCR (verification of RNA-seq, CRISPR)		
2720/MSMEG_1205 _F	AAACGCCACAGAAATCGAAC	
2721/MSMEG_1205 _R	TCGTTCGACAGGTCGTAGTG	
2728/MSMEG_5540 _F	GCGACACTCGACGAATATGA	
2729/MSMEG_5540 _R	CGACACGATGATCAGGAAGA	
2726/MSMEG_5556 _F	TGTTCGCCGTGTACACCTAC	
2727/MSMEG_5556 _R	GAAGCCGAAGACCATGAGC	
989/ MSMEG_1368_RpoC_F	CGACGAGATCTGGAACACCT	
990/ MSMEG_1368_RpoC_R	GGTGAAGTACTCGCCGTAGC	
987/SigA_F	CCAAGGGCTACAAGTTCTCG	
988/SigA_R	CTTGTTGATCACCTCGACCA	
2712/MSMEG_1367_RpoB _F	AGGGCACCTTCATCATCAAC	
2713/MSMEG_1367_RpoB _R	GGTGGACTTGTCGATGGTCT	
2462/Ms1_F	GCCGGAAGAGAAGGCTAGAT	
2463/Ms1_R	CGTCCGCTTTTCGAAACTAC	
2186/MSMEG_2656_PNPase_F	GTCGTCAAGACCACCGATTT	
2187/MSMEG_2656_PNPase_R	ACCTTCACCACGTCTTCGAC	
2190/MSMEG_4626_RNaseE_F	GGCAGAACCGTAAGATCGAG	
2191/MSMEG_4626_RNaseE_R	GGGCACGTACACCAGATAGC	
2194/MSMEG_2685_ RNaseJ _F	GTACTTCGCGGTGAACCACT	

2195 MSMEG_2685_ RNaseJ _R	GGCAACTGGTCGAGTTTGAT
979/BsrA_6S_Bs_F	ATGGCGTACATGCCTCTTTT
980/BsrA_6S_Bs_R	AATAGTGCCGTTGCAGCTTT

References

Dussurget, O., Timm, J., Gomez, M., Gold, B., Yu, S., Sabol, S.Z., Holmes, R.K., Jacobs, W.R., and Smith, I. (1999) Transcriptional control of the iron-responsive fxbA gene by the mycobacterial regulator IdeR. *J Bacteriol* **181**: 3402-3408.

Hnilicová, J., Jirát Matějčková, J., Šiková, M., Pospíšil, J., Halada, P., Pánek, J., and Krásný, L. (2014) Ms1, a novel sRNA interacting with the RNA polymerase core in mycobacteria. *Nucleic Acids Res* **42**: 11763-11776.

Huff, J., Czyz, A., Landick, R., and Niederweis, M. (2010) Taking phage integration to the next level as a genetic tool for mycobacteria. *Gene* **468**: 8-19.

Klotzsche, M., Ehrt, S., and Schnappinger, D. (2009) Improved tetracycline repressors for gene silencing in mycobacteria. *Nucleic Acids Res* **37**: 1778-1788.

Rock, J.M., Hopkins, F.F., Chavez, A., Diallo, M., Chase, M.R., Gerrick, E.R., Pritchard, J.R., Church, G.M., Rubin, E.J., Sassetti, C.M., Schnappinger, D., and Fortune, S.M. (2017) Programmable transcriptional repression in mycobacteria using an orthogonal CRISPR interference platform. *Nat Microbiol* **2**: 16274.

Triccas, J.A., Parish, T., Britton, W.J., and Gicquel, B. (1998) An inducible expression system permitting the efficient purification of a recombinant antigen from Mycobacterium smegmatis. *FEMS Microbiol Lett* **167**: 151-156.

van Kessel, J.C., and Hatfull, G.F. (2007) Recombineering in Mycobacterium tuberculosis. *Nat Methods* **4**: 147-152.

nature COMMUNICATIONS

ARTICLE

https://doi.org/10.1038/s41467-020-18800-2 OPEN

Bacterial nanotubes as a manifestation of cell death

Jiří Pospíšil[1], Dragana Vítovská[1], Olga Kofroňová[2], Katarína Muchová[3], Hana Šanderová[1], Martin Hubálek[4], Michaela Šiková[1], Martin Modrák[5], Oldřich Benada[2✉], Imrich Barák[3✉] & Libor Krásný[1✉]

Bacterial nanotubes are membranous structures that have been reported to function as conduits between cells to exchange DNA, proteins, and nutrients. Here, we investigate the morphology and formation of bacterial nanotubes using *Bacillus subtilis*. We show that nanotube formation is associated with stress conditions, and is highly sensitive to the cells' genetic background, growth phase, and sample preparation methods. Remarkably, nanotubes appear to be extruded exclusively from dying cells, likely as a result of biophysical forces. Their emergence is extremely fast, occurring within seconds by cannibalizing the cell membrane. Subsequent experiments reveal that cell-to-cell transfer of non-conjugative plasmids depends strictly on the competence system of the cell, and not on nanotube formation. Our study thus supports the notion that bacterial nanotubes are a post mortem phenomenon involved in cell disintegration, and are unlikely to be involved in cytoplasmic content exchange between live cells.

[1] Laboratory of Microbial Genetics and Gene Expression, Institute of Microbiology of the Czech Academy of Sciences, 142 20 Prague 4, Czech Republic. [2] Laboratory of Molecular Structure Characterization, Institute of Microbiology of the Czech Academy of Sciences, 142 20 Prague 4, Czech Republic. [3] Department of Microbial Genetics, Institute of Molecular Biology, Slovak Academy of Sciences, 845 51 Bratislava, Slovakia. [4] Institute of Organic Chemistry and Biochemistry of the Czech Academy of Sciences, 160 00 Prague 6, Czech Republic. [5] Laboratory of Bioinformatics/Core Facility, Institute of Microbiology of the Czech Academy of Sciences, 142 20 Prague 4, Czech Republic. ✉email: benada@biomed.cas.cz; imrich.barak@savba.sk; krasny@biomed.cas.cz

Bacteria are one of the most dominant forms of life on Earth, employing a vast range of strategies to exploit their environments. One of these strategies may involve formation of tubular membranous structures. These structures are termed nanotubes (NTs) in *Bacillus subtilis* and *Escherichia coli*[1,2], nanowires (NWs) in *Shewanella oneidensis*[2–4], nanopods (NPs) in *Delfitia* sp. Cs1-4 and in hyperthermophilic archaea of the genus *Thermococcus*[5–7], or outer membrane tubes (OMTs) in *Myxococcus xanthus*[8]. These structures are composed of cytoplasmic or outer membranes, depending on the species of origin, and may serve different functions in these organisms. The NTs of *B. subtilis* are perhaps the best characterized example. They were reported to frequently occur in exponentially growing cells: ~70% of cells contained NTs and a single cell contained several of them[9].

YmdB, a phosphodiesterase that hydrolyzes cyclic nucleotides such as cAMP[10], and flagellar body proteins[9,11] have been reported to be necessary for NT formation in *B. subtilis*. YmdB was found to localize to NTs[11], though the exact mechanism by which it contributes to NT formation is unknown. The flagellar body proteins required for the flagellar export apparatus, called CORE, function both in flagella and in NT assembly[9,12].

Two classes of *B. subtilis* NTs have been recognized: (i) extending nanotubes (attached to a single cell) and (ii) intercellular nanotubes (connecting two cells)[1,13]. Extending NTs are thought to increase the surface area of the cell and contribute to nutrient uptake. Intercellular NTs can function as conduits for transport of molecules such as metabolites (e.g., amino acids), proteins (including toxins), and even non-conjugative plasmids[1,2,14]. These intercellular tubes can be formed between two cells of a single bacterial species, between cells of two different bacterial species, and even between a bacterium and a eukaryotic host, where the bacterium uses NTs to extract nutrients from its host, as reported for enteropathogenic *E. coli*[15].

NTs appear to be a common phenomenon shaping intra-, and inter-species interactions, with far reaching consequences for our understanding of, and fight against bacterial pathogens[16]. Yet, the number of reports on these structures is relatively small, and models of their functioning are still poorly defined. Therefore, detailed insights into this cellular feature are needed.

Here, we focus on *B. subtilis* NTs and identify genes and conditions required for NT formation. We show that under non-stress conditions, NTs are rare; under stress, the number of NTs increases. Most importantly and surprisingly, these structures are formed when cells are dying or even after cell death and, therefore, they are unlikely to be involved in nutrient uptake or cytoplasmic content exchange as proposed by previous studies. This is demonstrated by the complete absence of non-conjugative plasmid transfer in a Δ*comK* strain, which is still able to form NTs [ComK is essential for bacterial competence and DNA uptake[17]]. The results of this study, therefore, indicate that NTs are an attribute of dying cells and are not involved in the exploitation of the environment by live cells.

Results

Identification of NTs. Initially, we wished to detect NTs in *B. subtilis*. Using a combination of scanning electron microscopy (SEM) and structured illumination microscopy (SIM), we analyzed wt *B. subtilis* cells (BSB1) grown to exponential phase in liquid LB. The electron micrographs revealed that at least two types of filamentous structures were present: (i) numerous thinner filaments (diameter < 30 nm) and (ii) rare thicker filaments (diameter ~70 nm). Since *B. subtilis* can form flagella, we also examined a Δ*hag* strain lacking the gene encoding flagellin, the principal flagellar component[18]. Supplementary Fig. 1a–c clearly shows the disappearance of the numerous thinner filaments in the Δ*hag* strain; we therefore surmised that the remaining thicker filaments were NTs. In a subset of these filaments we observed elongated, flattish terminal structures (Supplementary Fig. 1d, e). The frequency of NTs was rather low: only one NT approximately per 500 cells.

To verify the NT identification, we used SIM to examine a strain bearing a single amino acid substitution in flagellin [hag^{T209C}][19], which allows this protein to be stained with a maleimide derivative of Alexa Fluor 488, thereby distinguishing it from membranous structures stained with Nile Red. Supplementary Fig. 1g shows one cell with a large number of flagella and a single membranous structure, a nanotube, which was the typical number of NTs per cell (when present). The rare terminal structures were also occasionally detected by this method. It is important to note that the SIM approach required no cell fixation (unlike SEM where it is an integral part of the protocol), thereby excluding the possibility that these structures were byproducts of the cell fixation procedure. Nevertheless, the NT-bearing cells displayed patchy staining with Nile Red, which may indicate non-optimal cell conditions. Taken together, we had thus succeeded in identifying NTs, although the frequency of their occurrence was significantly lower than that claimed previously[1,9].

Genetic requirements for NT formation. We next determined which genes were required for NT formation. Although several genes had already been reported, we took a systematic, unbiased approach, and used a number of strains with deletions in one or more sigma factors. These factors associate with RNA polymerase (RNAP), which is responsible for the transcription of DNA into RNA, and provide the holoenzyme with an affinity for specific DNA promoter sequences[20]. Using this approach, we wanted to identify the regulon that contains genes necessary for NT formation. Altogether, we tested deletions of 10 alternative sigma factors [out of the 19 present in *B. subtilis*[21,22]] and monitored NT formation by SEM. Of the 10 tested sigma factors, only SigD[23,24] was required for NT formation (Supplementary Fig. 1h–l). However, due to the extremely low numbers of NTs that can be found by SEM under these conditions, the results were not statistically significant. Nevertheless, the absence of NTs in the Δ*sigD* strain was consistent with the known NT requirement for the CORE proteins, whose genes are SigD-dependent[25].

Conditions under which the majority of cells form NTs. Both SEM and SIM are high-resolution imaging techniques that are best suited for capturing static structures. To gain more detailed insights into the dynamics of NT formation and their potential movements, we therefore used time-lapse imaging with a fluorescence microscope. In Fig. 1a we used 1× phosphate-buffered saline (PBS) agar pads covered with coverslips ("Glass-Agar-Glass"—the GAG method). At times $t = 0$ min and $t = 15$ min, no NTs were detectable in wt *B. subtilis* cells from exponential phase, consistent with the low frequency of NT formation we had observed by SEM and SIM. However, when we used glass slides and coverslips coated with poly-L-lysine and the bacteria in liquid 1 × PBS ("Glass-Liquid-Glass"— the GLG method), a few NTs were detected. We noticed, though, that when we firmly pressed down the coverslip to obtain a monolayer of bacteria (a common technique to prepare samples), the number of NTs increased as opposed to when the coverslip was gently positioned over the sample. Therefore, we applied defined pressure (P; ~80 kPa) on the coverslip (P-GLG), and this resulted in a large number of NTs originating from many cells within 15 min; the number of NTs approached those previously reported (Fig. 1b and Supplementary Movie 1)[9]. The same result was obtained regardless of the wt

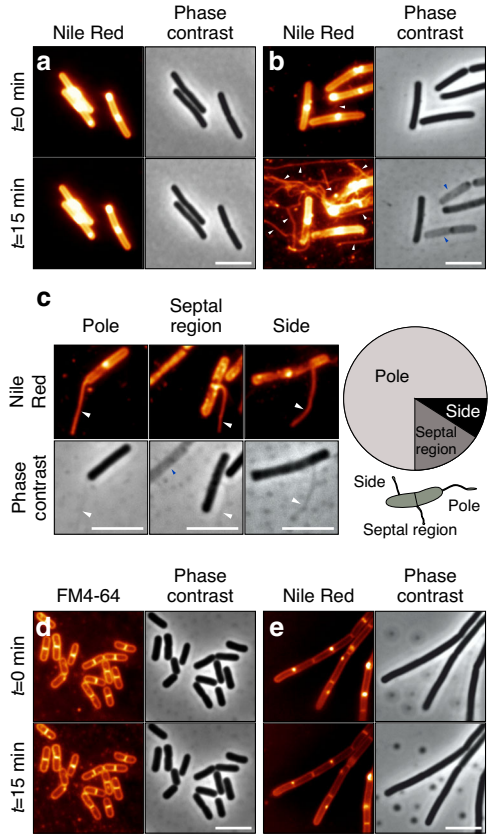

Fig. 1 NT formation in exponential and stationary phase. These images were acquired by fluorescence microscopy; the corresponding phase-contrast images are also shown. For definition of $t = 0$ refer to Mat & Met. **a** Exponentially grown wt *B. subtilis* (LK1432) cells prepared by the GAG method. **b** Exponentially grown wt *B. subtilis* (LK1432) cells prepared by the P-GLG method. **c** One-hundred exponentially growing wt *B. subtilis* (LK1432) cells bearing NTs were analyzed. Most NTs emanated from the cell poles (75 NTs), followed by NTs from the septal region (16 NTs) and the sides (9 NTs). The positions of NT attachment to the rod-shaped cells were not uniformly distributed over the cell surface ($p < 0.001$, custom test —see Quantification and statistical analysis). **d** Stationary phase wt *B. subtilis* (LK1432) cells prepared by the P-GLG method but to stain the membranes, FM4-64 was used instead of Nile Red, as Nile Red poorly stains membranes of cells from this phase (Supplementary Fig. 2d). **e** Exponentially grown Δ*sigD* (LK1873) cells prepared by the P-GLG method. The images were taken at 0 and 15 min time points. White arrows indicate NTs, blue arrows indicate ghost cells in the phase-contrast images. The membrane stain (false colored glow, FM4-64 or Nile Red) is indicated above the images. Scale bar = 5 µm. All experiments (**a**–**e**) were conducted in at least three biological replicates with similar results.

strain used: PY79 behaved like BSB1 (Supplementary Fig. 2a–c). The positions of NT attachment to the rod-shaped cells were not random: the majority of NTs (75%) originated from the cell poles, 16% from septal regions and 9% from other regions (Fig. 1c, *p*-value < 0.001). Moreover, in the phase-contrast images we noticed that the NTs were in some cases attached to gray cells (Fig. 1b, right hand panel, and Supplementary Fig. 2a–c). These cells are characterized by a decrease in phase-contrast due to the efflux of cytoplasmic contents. This is typically associated with cell death[26–28] and we refer to such cells as ghost cells.

In parallel, we performed experiments with wt stationary phase cells using the P-GLG experimental setup. These cells did not produce NTs within the 15 min time course (Fig. 1d). The absence of NTs from wt stationary phase cells might be due to the thicker and more ordered cell wall of non-dividing cells[29], presenting a stronger barrier to NT extrusion. We also viewed exponential phase Δ*sigD* cells using the same approach, and these also produced no NTs within the 15 min time course (Fig. 1e). We then speculated that other genes from the SigD regulon besides the CORE genes might also be involved in NT formation. Obvious candidates are autolysins - peptidoglycan hydrolases that open meshes in the peptidoglycan net allowing the insertion of newly synthesized material for surface expansion and cell separation[30]. LytE and LytF are major *B. subtilis* cell wall hydrolases that localize to the septal regions and the cell poles[31]. Consistent with the hypothesis, Δ*lytEF* deletion strain arranged cells into chains, but only during exponential phase (Supplementary Fig. 3a, b). In stationary phase, other autolysins must be responsible for cell separation. Supplementary Fig. 3c shows that exponential phase Δ*lytEF* cells behave like Δ*sigD* cells within the 15 min time-lapse experiment, consistent with the hypothesis that the weakening of peptidoglycan that occurs during its remodeling may be instrumental in NT extrusion. A mass spectrometry comparison of the membrane fractions of wt and Δ*sigD* cells subsequently confirmed that the two strains differed in the presence of autolysins, including LytF (Supplementary Fig. 3d).

Taken together, the experiments performed thus far indicated that the frequency of NT formation depended on (i) the genetic background of the cell, (ii) the method of sample preparation, and (iii) the growth phase of the culture. Intriguingly, phase-contrast images indicated that some of the NT containing cells (ghost cells) might be dying.

Therefore, we added the SYTOX Green stain (SYTOX) to the cells and prepared the samples by the GLG or P-GLG method. SYTOX penetrates into the cells with compromised/permeabilized membranes where it stains nucleic acids and indicates cell death[32]. Figure 2a shows respective SEM and fluorescence microscopy images. The SEM images illustrate the severe damage caused to cells by the P-GLG experimental setup. Subsequent analysis revealed that NTs were associated exclusively with SYTOX-stained cells (Fig. 2b, c). Moreover, the P-GLG method resulted in larger amounts of dying cells and NTs than the GLG method (Fig. 2b, c, $p < 0.001$ [numbers of dying cells between P-GLG and GLG], two-sided, $z = 10$, 95% CI OR = 11–37 and $p = 0.04$, two-sided, $z = 2.05$, 95% CI OR = 1.2–16 [numbers of NTs between P-GLG and GLG]; both GLM [Generalized Linear Model], two-sided; Supplementary Fig. 4a). To further confirm this, we examined those areas where the cells were partially under the coverslip and partially only under the immersion oil. We detected a clear boundary: the cells under the coverslip (the P-GLG method) were frequently SYTOX-stained whereas cells in their immediate vicinity but not under the coverslip were mostly SYTOX-free (Supplementary Fig. 4b). This also shows that poly-L-lysine, which was previously reported to negatively impact bacterial growth[33], is not a major factor causing SYTOX permeability. We also noted that over time, as the cells were progressively losing their contents, including DNA, the SYTOX signal decreased or even disappeared as the SYTOX-stained DNA leaked out of the dead cell.

NTs are formed from dying cells. Next we asked whether NTs form before or after cell death. To answer this, we performed a detailed study of the kinetics of NT formation using cells from exponential phase and the P-GLG experimental setup. Figure 3a, c shows that NTs are formed from wt cells within seconds after SYTOX entry. The decrease in signal density in the phase-contrast panel should also be noted. The order of events (SYTOX green penetration, formation of NTs, DNA release, and ghost cell appearance) is shown in a time-lapse microscopy movie

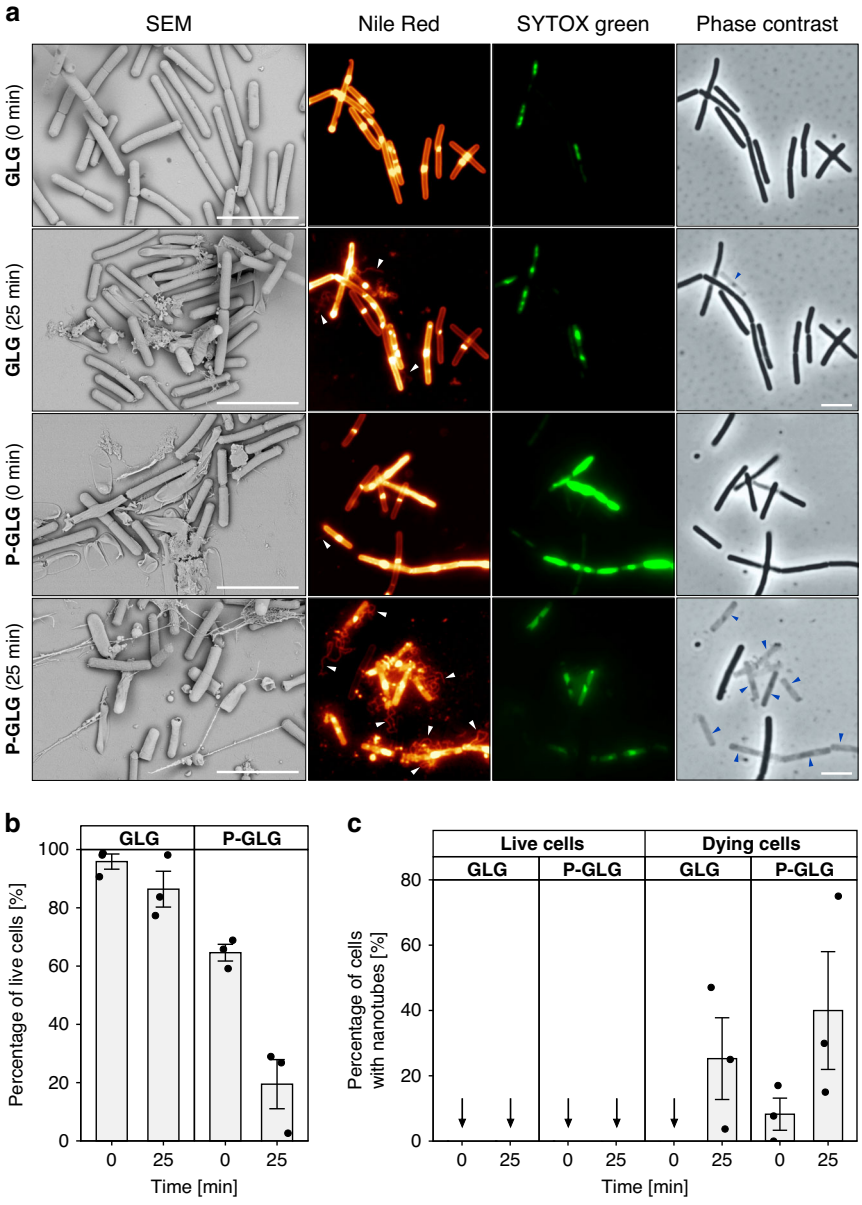

Fig. 2 Effect of coverslip pressure on NT formation. a SEM-exponentially growing *B. subtilis* Δ*hag* (LK1966) cells spotted on an uncoated glass slide and covered with a poly-L-lysine coverslip. The coverslips were either gently positioned over the sample (the GLG method) or pressed down (the P-GLG method). $t = 0$, the coverslip, after being positioned over the sample, was immediately removed (for SEM), or the sample, still with the coverslip, was immediately imaged (fluorescence microscopy); $t = 25$, the same with $t = 0$ but the coverslip was left over the sample for 25 min. Before SEM, bacteria were fixed. For fluorescence microscopy, non-fixed living bacteria (LK1432-wt) were observed. White arrows indicate NTs, blue arrows indicate ghost cells. Membranes were stained with Nile Red (false colored glow). Dying cells were monitored with SYTOX green (green). Scale bars in all images represent 5 μm. All experiments were conducted in three biological replicates with similar results. **b** Effect of sample preparation methods on bacterial viability. Low pressure (GLG) and high pressure (P-GLG) methods were compared at two different time points ($t = 0$ and $t = 25$ min). Live and dying cells were quantified according to the presence or absence of the SYTOX signal within the cells. We note that among live cells may be also those that are actually dead and intact, impenetrable to SYTOX. Significantly fewer live cells were observed by P-GLG (at both times) than by GLG ($p < 0.001$, GLM, two-sided, $z = -10$, 95% CI OR = 0.02–0.08) and at the later time points for both methods ($p < 0.001$, GLM, two-sided, $z = -4$, 95% CI OR = 0.12–0.45). For both conditions, a total of 400 cells from three independent experiments were analyzed (the black dots represent individual replicates). The bars are averages and error bars ± SEM. **c** The presence/absence of NTs in samples that were prepared by two different methods (GLG or P-GLG method). Quantification of NTs was based on the Nile Red signal. The percentage of NTs is expressed relative to the number of dying (SYTOX positive) or live (SYTOX negative) cells, which was set as 100% (e.g., out of the 10% of dying cells, 20% formed NTs—that is 2% of the total number of cells). The P-GLG method of sample preparation (compared to GLG) resulted in larger amounts of dying cells with NTs at both time points ($p = 0.04$, GLM, two-sided, $z = 2.05$, 95% CI OR = 1.2–16). No NTs were detected in live cells. For both conditions, 400 cells from three independent experiments were analyzed (the black dots represent individual replicates). The vertical arrows in the chart indicate values "zero". The bars are averages and error bars ± SEM (standard error of the mean).

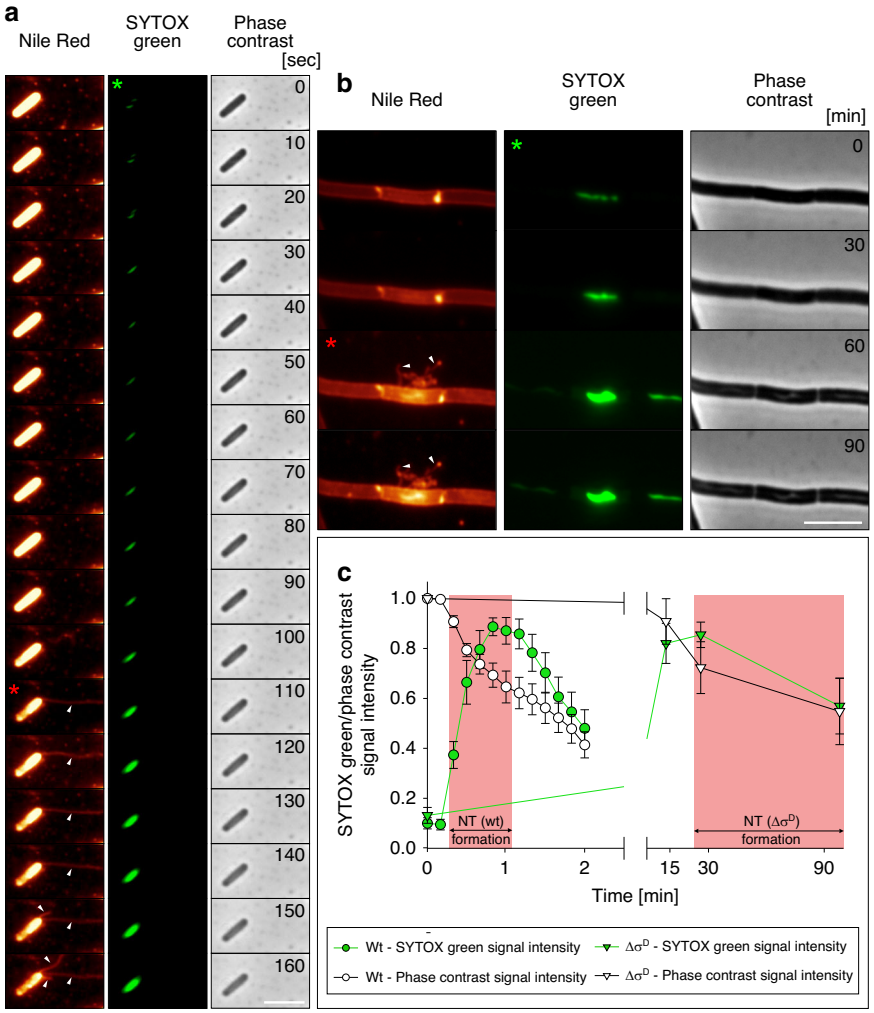

Fig. 3 Correlations between NT formation and cell death. a Exponentially growing wt *B. subtilis* (LK1432) cells stained with Nile Red (false colored glow) and SYTOX green (green). Bacteria were prepared by the P-GLG method. The cells were observed every 10 s. Three channels of the same cell are shown: Nile Red, SYTOX green, and phase-contrast. White arrows indicate NTs. The numbers in the phase-contrast panels are seconds. Notice the progressive loss of phase-contrast of the cells as the time advances. In panels **a**, **b** the green asterisk indicates the time when SYTOX green was inside the cell (i.e., the cell was dying). The red asterisk indicates the start of NT formation. **b** Δ*sigD* (LK1873) cells were prepared in the same manner as wt in **a**. White arrows indicate NTs. Numbers in the phase-contrast panels are minutes. Scale bar = 5 µm. **c** Kinetics of NT formation and in wt (LK1432) and Δ*sigD* (LK1873) strains. NT formation occurs in dying cells of both strains, however, the kinetics of SYTOX green penetration and NT formation differs between these strains; it takes ~30x longer in Δ*sigD*. Symbol definitions are shown below the graph. The pink area marks the time limits of NT formation for the two strains. The data represent three biological replicates (a total of 12 cells for wt and 11 cells for Δ*sigD* strain were analyzed) ± SEM.

of wt *B. subtilis* cells (Supplementary Fig. 5 and Supplementary Movie 2).

In the Δ*sigD* strain, SYTOX penetration displayed slower kinetics than in wt cells and the dying cells took longer to form NTs (Fig. 3b, c). Moreover, the frequency of NT formation in Δ*sigD* (at 90 min) was lower than in wt (at 25 min) (Supplementary Fig. 6a, b compared to Fig. 2c, $p < 0.001$, GLM, two-sided, $z = -10$, 95% CI OR = 0.10–0.22). This validated our initial genetic screen based on SEM (Supplementary Fig. 1l). We further analyzed the Δ*lytEF* strain and found that it also formed NTs less frequently than wt (Supplementary Fig. 6c–e compared to Fig. 2c, $p < 0.001$, GLM, two-sided, $z = -9$, 95% CI OR = 0.01–0.04).

The signal arising from the Nile Red membrane stain that appeared in the newly formed NTs (ca. 25%) quantitatively corresponded with the decrease in the signal coming from the cell envelope (Supplementary Fig. 7a, b). This correlated with the amount of the newly created NT surface (Supplementary Fig. 7c), implying that the cell membrane was rapidly and aggressively utilized for NT formation.

We also asked, whether cells killed by other means (antibiotics) but grown without pressure in frames (Gene frames, Thermo Scientific) containing LB agar covered with coverslips would form NTs. Supplementary Fig. 8a–c shows that even in the control experiment under these conditions in the absence of any antibiotic a small fraction of the cells died, although no NTs were detected. Using ampicillin, which inhibits a transpeptidase involved in bacterial cell wall biosynthesis[34], led to death of majority of the cells and induced NT formation from dying cells although not as frequently as the P-GLG method (Supplementary Fig. 9a–c, $p < 0.001$, GLM, two-sided, $z = -8$, 95% CI OR = 0.01–0.05). Interestingly, NTs now originated mostly from the cell sides, to a lesser degree from the septal regions and not at all from cell poles (Supplementary Fig. 10). We also tested chloramphenicol, which inhibits the peptidyl transferase activity of the ribosome[35]; even though chloramphenicol is bacteriostatic, the concentration used did result in some dying cells and we detected a single NT at 90 min (Supplementary Fig. 11a–c). A similar result was also obtained using the RNAP-targeting rifampicin[36,37] (Supplementary Fig. 12a–c).

NTs do not transfer non-conjugative plasmid DNA. Previously, protein transfer was claimed to occur through NTs[1]. Using SIM we, indeed, detected both membrane-targeted GFP and cytoplasmic ZsGreen in NTs (Supplementary Fig. 13).

So far, we had observed NT formation solely from dying *B. subtilis* cells. However, we could not exclude the possibility that occasionally NTs might be formed from living (though likely highly stressed) cells, and we had not been able to detect these presumably extremely rare events. The presence of ZsGreen in NTs indicated that if NTs did connect two cells, then they could function to transport various molecules, and this might be of biological relevance as previously proposed. The best way to test this was to use the reported non-conjugative plasmid transport as the readout for the transfer. The advantage of this approach over, e.g., monitoring the transport of proteins or mRNA or metabolites is its extreme sensitivity. Even a single plasmid transfer among millions of cells can be detected.

Initially, we used an already published protocol[9,38], using a non-conjugative plasmid, pCPP31-Y1[39], bearing a chloramphenicol resistance gene. We incubated donor (containing the plasmid) and recipient (bearing chromosomally encoded macrolides (MLS) resistance gene) strains for four hours in LB. We then plated serially diluted cultures on LB containing various antibiotic combinations. Figure 4a shows that bacterial growth on the combination of both antibiotics was observed only at the highest cell density, suggesting that the transfer might, indeed occur, though rarely. Subsequent tests revealed that the resulting strain contained both antibiotic resistance genes, one chromosomally encoded and the other plasmid-borne.

Next, we wished to determine whether the bacterial growth on both antibiotics was due to DNA transfer through NTs or to DNA uptake by the competence system that allows a bacterial culture to bind and take up high-molecular-weight exogenous DNA. The master regulator of competence in *B. subtilis* is the ComK transcription factor[17]. We began with the same donor and recipient strains as in the previous experiment and made several genetic alterations to them: (i) Δ*sigD*; (ii) Δ*comK*; and (iii) $P_{hyperspank}$-*comK*—a strain overproducing ComK [strains (ii) and (iii) also form NTs, Supplementary Fig. 14a, b]. Finally, we also examined each of these strains with or without DNase I treatment to remove any DNA originating from lysed cells. Figure 4b shows that all transfer that was observed in the absence of DNase I for each strain was abolished when DNase I treatment was included. Furthermore, the Δ*comK* strain showed no transfer even without DNase I treatment. Conversely, ComK overproduction greatly increased plasmid transfer. In the Δ*sigD* genetic background, the plasmid transfer was decreased. In the genetic backgrounds (i)–(iii), the transfer was quantitatively correlated with the expression of the *comK* gene (Fig. 4c). Moreover, it was previously reported that the absence of the strictly SigD-dependent *hag* gene decreases competence[40]. Subsequent analysis then revealed that it was plasmid and not chromosomal DNA that was transferred under these experimental conditions (Supplementary Fig. 14c). We note that a previous study showed the ability of *B. subtilis* to be transformed in LB, albeit with low efficiency, and this efficiency increased when *comK* was overexpressed, similar to our results[41]. Taken together, we conclude that NTs are unlikely to serve as conduits for non-conjugative plasmid DNA transfer between *B. subtilis* cells.

Formation of NTs in different bacterial species. Finally, we investigated how other bacterial species form NTs. We used (i) the gram-positive *Bacillus megaterium*, an industrially important organism and a relative of *B. subtilis*, (ii) the gram-positive *Deinococcus radiodurans*, an extremophile capable of surviving high doses of radiation[42], and (iii) the gram-negative model bacterium *E. coli*. Figure 5 shows that all these species formed NTs to various degrees under the P-GLG setup. The NTs from *B. megaterium* were most similar to those from *B. subtilis*. *D. radiodurans* extruded a high number of NTs from each cell. *E. coli* reacted mostly by forming blebs, or vesicles, and occasionally also NTs. In all cases, NTs were formed only from dying cells.

Discussion

Our study indicates that the bacterial membranous tubular structures, often called nanotubes, are formed when the cells are dying, or after cell death, as a consequence of the compromised cell wall and (likely) excess internal pressure (Fig. 6). Importantly, these NTs do not serve as channels through which non-conjugative plasmids can be transported. Instead, they are a sign of disintegrating cells, and we believe it is debatable whether they have a physiological role.

Our initial experiments were aimed at defining the genetic requirements for NT formation. We identified the SigD regulon as important for this process and this correlated with the known involvement of the CORE element (*fliOPQR*, *flhBA*)[9]. The loss of the CORE element genes leads to inactivation of SigD by preventing export and proteolysis of FlgM, the anti-SigD factor[43]. Further, a mutant strain lacking the autolysins LytE and LytF, of which the latter is SigD-dependent, proved to be similarly deficient in NT formation. As LytE and LytF localize to cell poles and Δ*sigD* or Δ*lytEF* mutant cells remain in chains and do not separate into single cells, the blockage of the cell poles/absence of cell wall degradation by LytE and LytF might have caused the delay in the appearance of NTs. Moreover, it was very recently reported that a Δ*lytBC* mutant displays reduced NT production[38]. Both these genes also belong to the SigD regulon.

In our experiments, NTs were formed exclusively from dying cells. Cell death was monitored by SYTOX. In some instances, NTs that were detached from dying cells could be occasionally associated with living cells, creating thus a misleading illusion (Supplementary Fig. 15). When observed by time-lapse microscopy, NT formation was a rapid process, in the order of seconds, during which the NTs used the cell plasma membrane for their extrusion. Occasionally, NTs contained terminal structures (see also Supplementary Movie 3); these were also detected in a previous study[9], but not commented upon.

We used various types of stress to cause cell death (pressure, different antibiotics); regardless of the stress applied, NTs were always detected associated with dying cells, though their relative amounts varied. The greatest number of NTs was formed in samples prepared by P-GLG method where pressure was applied to the coverslip (Figs. 2 and 3 and Supplementary Movie 1). Mechanistic details of the process and identification of forces involved therein will be addressed by a future study.

How, then, are NTs formed? We propose that, as the cells are dying and start disintegrating, weak spots in the cell wall may serve as channels through which NTs are extruded to release the intracellular pressure[44]. This is again consistent with the reported requirement for the CORE element in NT formation. The same components that are required for flagella to be assembled and traverse the cell wall likely create weak spots in the cell envelope that may serve as channels through which NTs can be extruded. Typically, NTs emerge from the cell poles. The appearance of NTs from other parts of the cell (sides) in, e.g., ampicillin-treated cells might stem from region-nonspecific structural damage to the cell wall. The tubular nature of NTs may then depend on the lipid composition of the membrane. Cardiolipin in combination with the PmtA protein from the phytopathogenic bacterium *Agrobacterium tumefaciens* was previously reported to promote

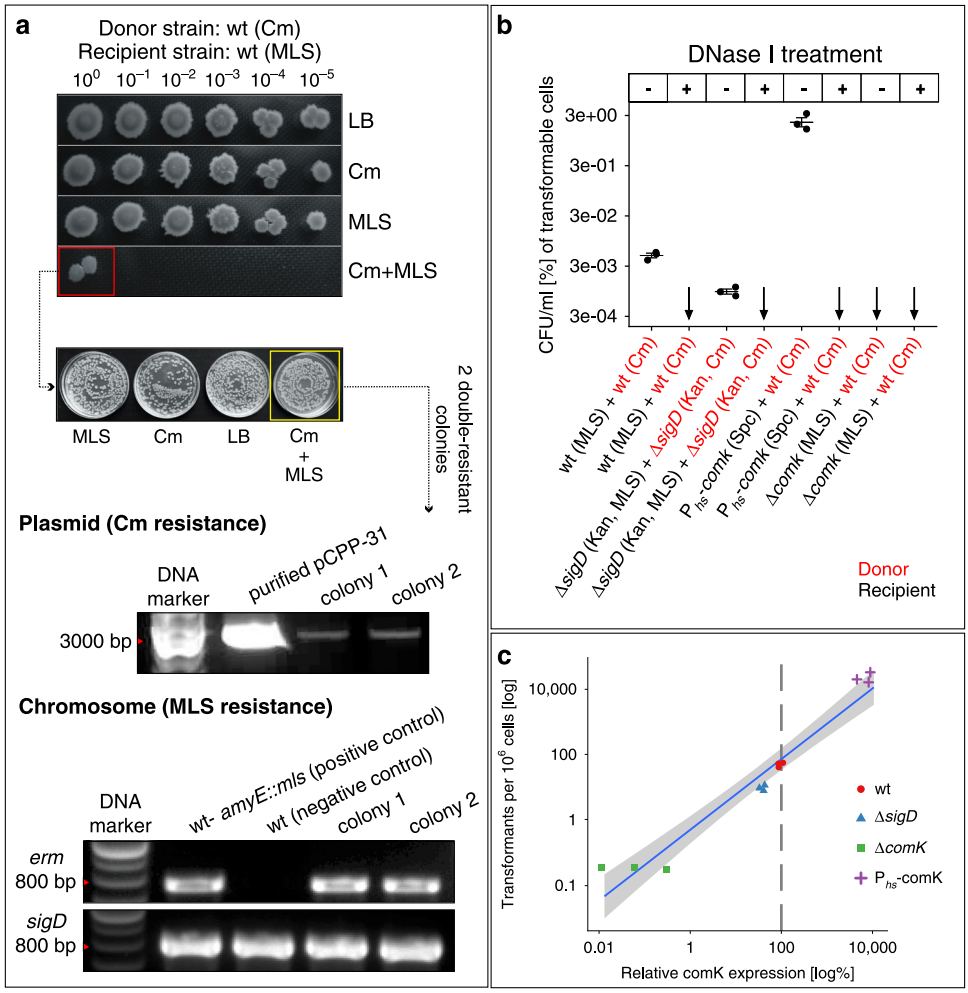

Fig. 4 Non-conjugative plasmid DNA transfer. a The donor (LK1925, wt containing the Cm resistance gene on plasmid pCPP31-Y1) and recipient (LK1922, wt harboring the MLS resistance gene on chromosomal DNA) strains were grown separately overnight. The following day, both strains were diluted to an initial $OD_{600} = 0.05$, mixed 1:1, and cultivated for 4 h at 37 °C. The mixture was then serially diluted into fresh LB medium and 2 µl were spotted on LB agar (control) and LB agar containing appropriate antibiotics (Cm-donor selection, MLS-recipient selection, Cm+MLS-cells with both antibiotic resistance genes). The cells were allowed to grow for 18 h at 37 °C. Only the mixture with the highest initial density then produced double-resistant cells. This colony was subsequently diluted into fresh LB medium to $OD_{600} = 0.05$ and 100 µl were plated on LB agar dishes with or without Cm, MLS or Cm + MLS. We detected many double-resistant colonies on the Cm + MLS agar dish (yellow square) and for two of them we confirmed the presence of the two resistance genes by plasmid isolation (the dominant supercoiled form of the plasmid is shown) and PCR of the chromosomally-located *erm* (MLS) resistance gene (primers against the *sigD* gene were used as a control). As the DNA marker we used GeneRuler DNA Ladder Mix (Thermo Scientific). All experiments were conducted in three biological replicates with similar results. **b** Donor (LK1925-wt or LK1944-Δ*sigD*) and recipient (LK1925-wt; LK2317-P_{hs}-*comK* [hs, hyperspank]; LK1940-Δ*sigD* or LK2380-Δ*comK*) strains were grown separately overnight, then diluted to an initial $OD_{600} = 0.05$, treated or not treated with DNase I, and mixed in a 1:1 ratio. The mixtures were inoculated into fresh LB medium (to an initial $OD_{600} = 0.05$) without antibiotics and gently shaken. After 4 h, bacteria were harvested and diluted to an $OD_{600} = 0.5$. 100 µl of each mixture was plated on LB agar dishes with appropriate antibiotic combinations, based on antibiotic resistance genes in donor/recipient. The combinations are specified in parenthesis after each strain below the graph. The dishes were incubated overnight at 37 °C and then CFU/ml were counted. Data are presented as mean values ± SEM, $n = 3$ biological replicates per condition shown as individual dots. Black arrows indicate zero values in all three biological replicates. All differences between DNAase(-) and DNase(+) conditions in wt, Δ*sigD* and P_{hs}-*comK* are statistically significant as well as all pairwise differences between the DNase(-) conditions (all $p < 0.001$, ANOVA adjusted with Tukey's HSD, two-sided). **c** Correlation between the number of transformants per 10^6 cells and *comK* expression (determined by RT-qPCR). For display purposes we added 1 to all raw transformation counts. The blue solid line is the maximum likelihood linear fit, the shaded gray area represents the 95% confidence interval of the fit. The vertical dashed line indicates the wt expression against which the samples were normalized (100%).

formation of tubular structures in vitro[45,46]. Cardiolipin is an integral part of the *B. subtilis* membrane and might play a role in NT formation.

We have also noticed that the amounts of NTs (or filamentous, NT-like structures in the case of SEM) observed by SIM and/or SEM are sensitive to growth conditions (solid or liquid media) and the conditions used for preparation of the microscopic sample. Supplementary Figs. 16 and 17 illustrate this issue. Cells grown in liquid media and visualized by SIM or SEM display few NTs (Supplementary Fig. 16a–d). Cells grown on solid media and visualized by SIM form no NTs under the conditions tested in our study (Supplementary Fig. 16e, f, h) and we assume that this is due to the minimal manipulation required for this imaging method. To the contrary, when we used two previously published sample preparation protocols for solid media-grown cells, we detected many NT-like structures by SEM (Supplementary

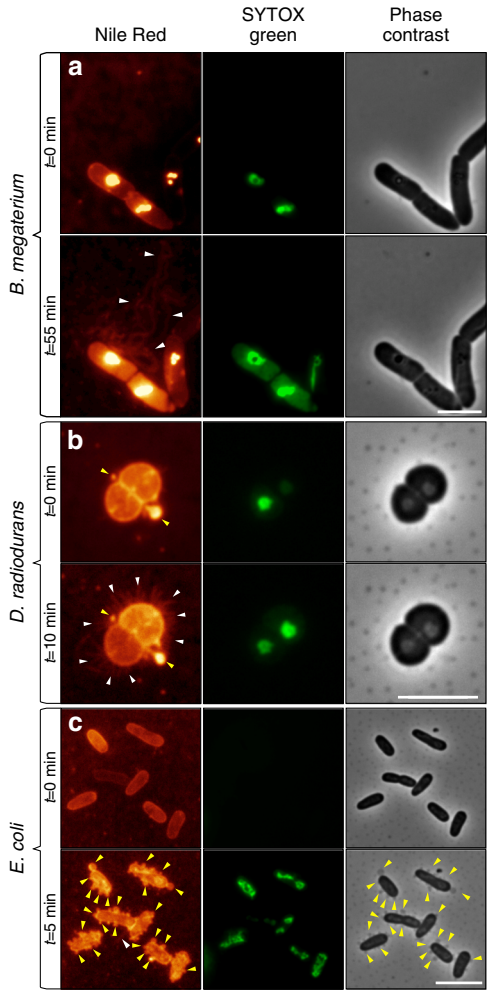

Fig. 5 Formation of NTs from selected bacterial species. a *Bacillus megaterium* (LK1780) was grown to exponential phase. The microscopic samples for this and other organisms shown in this Figure were prepared as in Fig. 3 (the P-GLG method). After 55 min under the coverslip, the cells formed NTs that were similar to those of *B. subtilis*. **b** Exponentially growing cells from the extremophile bacterium *Deinococcus radiodurans* (LK1553). **c** Exponentially growing cells of gram-negative *E. coli* (LK1133). In all samples, membranes were stained with Nile Red (false colored glow) and SYTOX green (green); the third column shows phase-contrast images. All experiments were performed three times. Yellow arrows indicate membranous blebs and vesicles, white arrows indicate NTs. Scale bar = 5 μm.

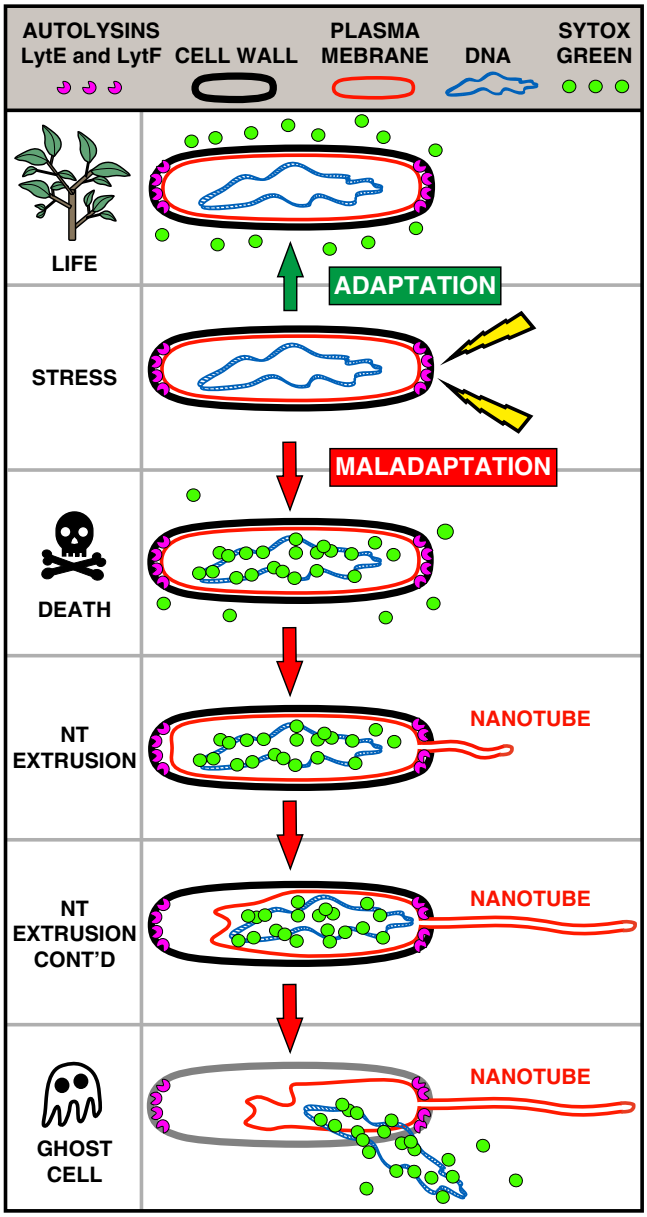

Fig. 6 Model of NT formation. The figure depicts NT formation: stressed cells (e.g., pressure, ampicillin treatment) either adapt or when the stress is too severe, die. During cell death, the plasma membrane becomes compromised and membranous tubular structures are extruded from dying cells. Autolysins LytE and LytF that localize at the cell poles weaken the cell wall and facilitate NT extrusion. Eventually, the cell contents are emptied and a hollow husk—the ghost cell—remains. No physiological role for these NTs has been detected.

Figs. 16e, g, h and 17c–f). What do these NT-like structures consist of? Apparently, they are not made of membranes as shown in the SIM images (Supplementary Figs. 16b and 17b). We speculate that they might be derived from the disrupted extracellular matrix. The disruption is likely caused by imprinting of the bacteria on EM grids and/or subsequent manipulations with the grids (Supplementary Fig. 17c–f). Consistently, cells grown on cellophane positioned on LB agar and imaged by SEM without the requirement for EM grid imprinting display undisrupted extracellular matrix (Supplementary Fig. 17a). To summarize this part: the more gentle the conditions (Supplementary Fig. 17a, b), the fewer (if any) filaments detected.

A most pressing question then is whether NTs in fact have any physiological roles. Although we did not detect any NTs associated with live cells by microscopy, we screened for their potential to serve as channels for transferring non-conjugative plasmids. Our screen revealed that this transfer was exclusively dependent on the cell ability to take up exogenous DNA, thereby ruling out any NT involvement. Moreover, although NTs were reported to connect cells and in some of our images we detected such cell pairs, we believe that these connecting NTs are artifacts of the microscopy techniques—the NTs likely emanate from one cell and their entanglement with other, nearby cells creates the illusion of a connection. In any case, the occurrence of NTs is rare and these connecting NTs are even less frequent. Furthermore, NTs were previously reported to transport metabolites such as amino acids and this phenomenon was contact (i.e., NT)-dependent[2,14]. In light of the evidence presented here, it seems more likely that the metabolites taken up by the auxotrophic cells in these studies were released from nearby lysed cells.

In addition to *B. subtilis*, we also observed membranous tubular structures emerging from dying cells of other bacterial species (*B. megaterium, D. radiodurans, E. coli*). The literature contains several reports of membranous tubular structures emerging from still other bacterial species; interestingly, some type of stress typically induces these structures. An example is *Myxococcus xanthus* where these structures are termed outer membrane tubes (OMTs). OMTs were found to contain outer membrane (OM) proteins and lipids but no other cytoplasmic material. Massive OMT formation induced by stress (lack of oxygen; addition of metabolic inhibitors) then blocks the intercellular transfer of OM proteins, suggesting that the OM protein transfer between cells is not mediated by OMTs. Rather, the transfer depends on the TraAB system and direct cell-to-cell contact[8,47,48]. Furthermore, Wei et al.[8] published phase-contrast images, suggesting that it is predominantly ghost cells that are associated with OMTs. Although these authors discussed that OMT formation was caused by cell stress they did not explore the possibility that some cells were dying[8]. Finally, OMTs were also found in the pathogens *Francisella novidica* and *Francisella tularensis* where OMTs were stimulated by stress conditions induced by amino-acid deprivation or during macrophage infection[49,50]. Nevertheless, these structures, being formed from the outer membrane, do not have to cross the cell wall and, therefore, the mechanism of their formation is likely different from that one of *B. subtilis* NTs. Finally, NT-like structures were formed by *D. radiodurans* when challenged with mitomycin C[51].

Various types of tubular structures have also been reported for eukaryotic cells and mitochondria. In some cases, the formation of these structures was induced by the presence of bacteria. Tunneling nanotubes (TNTs) of macrophages are an example[52,53]. TNTs are long-range membranous F-actin-containing tubes that are classified into two types based on their thickness and the presence or absence of microtubules[54]. TNTs, e.g., help spread the HIV-1 virus and their formation is stimulated by coinfection with *Mycobacterium tuberculosis*[55]. TNTs, however, appear to be distinct from bacterial NTs by the presence of a proteinaceous scaffold and appear to be bona fide channels for cell-to-cell communication.

We conclude that *B. subtilis* nanotubes are a hallmark of dying cells, or cell death, and are involved in the final cell disintegration. In other bacterial species, similar structures should be studied with utmost care before attributing physiological roles to them.

Methods

Media and growth conditions. *B. subtilis, B. megaterium*, and *E. coli* strains were grown at 37 °C in Luria-Bertani (LB) media, supplemented, when needed, with ampicillin (Amp, 100 µg/ml), spectinomycin (Spc, 100 µg/ml), chloramphenicol (Cm, 5 µg/ml), tetracycline (Tet, 10 µg/ml), kanamycin (Kan, 10 µg/ml), and MLS (lincomycin 25 µg/ml and erythromycin 1 µg/ml). One milimolar IPTG (isopropyl-D-thiogalactopyranoside, Amresco) was added where indicated. *D. radiodurans* was grown in TGY medium (1% Bacto Tryptone; 0.5% yeast extract; 0.1% glucose).

Bacterial strain construction. Bacterial strains are listed in Supplementary Table 1, and primers used for the validation of gene deletions are listed in Supplementary Table 2. Genomic DNAs (gDNAs) were isolated using the High Pure PCR Template Preparation Kit (Roche) and PCR reactions were carried out using an Expand High Fidelity PCR System (Roche).

SEM procedure. Sample preparation and processing were carried out essentially as in[56] but with some modifications. In brief, exponential cultures of *B. subtilis* strains (OD_{600} ~ 0.6) were pre-fixed with 3% glutaraldehyde in culturing media at room temperature (RT), washed with cacodylate buffer and fixed with 3% glutaraldehyde in cacodylate buffer at 4 °C overnight. These extensively washed cells were then sedimented onto poly-L-lysine-treated circular glass coverslips at 4 °C in a Petri-dish moist chamber for 42 h. The cells attached to the coverslips were washed three times and postfixed in 1% OsO_4 for one hour at room temperature and again washed three times. The coverslips were dehydrated in a graded ethanol series (25, 50, 75, 90, 96 100, and 100%) followed by absolute acetone and critical point dried in a K850 Critical Point Dryer (Quorum Technologies Ltd, Ringmer, UK). The dried samples were sputter-coated with 3 nm of platinum in a Q150T Turbo-Pumped Sputter Coater (Quorum Technologies Ltd, Ringmer, UK). The final samples were examined in a FEI Nova NanoSEM scanning electron microscope (FEI, Brno, Czech Republic) at 3 or 5 kV using ETD, CBS, and TLD detectors and using SEM software Helios NanoLab. The beam deceleration mode was used when sample charging occurred[57].

SIM procedure. For membrane staining, Nile Red was added to 1 ml of exponentially growing culture at a final concentration of 10 µg/ml. After 10 min of incubation at RT, bacteria were pelleted and washed once with 1× PBS. For staining of flagella, Alexa Fluor 488 maleimide conjugate (5 µg/ml, final concentration) was added and samples were washed twice with 1× PBS, then stained with Nile Red. The bacteria were subsequently re-suspended in 1× PBS, spotted on a coverslip covered with a thin agarose pad (1.5% agarose in 1× PBS supplemented with 10× diluted LB medium). Alternatively, for pressure experiments, samples were spotted on poly-L-lysine glass slides and covered with a poly-L-lysine coated coverslip. The samples were observed using a DeltaVision OMX™ equipped with a 60× 1.42, PlanApo N, oil immersion objective and softWoRx™ Imaging Workstation software. ZsGreen and GFP-tagged protein or Alexa Fluor maleimide conjugate were imaged using 488 nm excitation; Nile Red was imaged using 568 nm excitation.

Time-lapse fluorescence microscopy. To visualize the membrane structures, 1 ml of exponentially growing bacterial culture was stained by Nile Red (10 µg/ml) or by FM4–64 (1 µg/ml), washed twice with 1× PBS and re-suspended in 1× PBS containing 1 µM SYTOX green. The sample was then immediately either spotted onto a poly-L-lysine glass slide and covered with a poly-L-lysine coverslip (GLG method or P-GLG method when pressure ~80 kPa was applied for 10 s) or spotted on a 1× PBS agarose pad covered with a non-coated coverslip (GAG method). Pictures were obtained at the indicated time points ($t = 0$ is the start of microscopy, typically 30 s after coverslip addition) using a Olympus BX63 fluorescence microscope equipped with a Andor Zyla 5.5 sCMOS camera (alternatively, an Olympus IX81 microscope equipped with Hamamatsu Orca/ER camera was also used). Olympus CellP imaging software or Olympus Image-Pro Plus 6.0 software was used for image acquisition and analysis.

MS analysis of cytoplasmic membrane fractions. Cytoplasmic membrane fractions from the *B. subtilis* wt (LK1432) and Δ*sigD* (LK1873) strains were prepared following a previously described protocol with some modifications[11]. Briefly, cells were gently shaken and grown until they reached exponential phase (OD_{600} = 0.6) and then pelleted (6000 × *g*, 10 min at 4 °C). Samples were re-suspended in 20 ml of 1× P buffer (35% NaCl; 35% Na_2HPO_4; 10% glycerol; v/v) containing 3 mM 2-mercaptoethanol and 1 mM serine protease inhibitor PMSF (phenylmethylsulfonyl fluoride) and sonicated on ice for 10× 10 s, with probe amplitude 0.5, (Hielscher sonicator, UP 200 s). The lysates were then centrifuged (6000 × *g*, 20 min at 4 °C), the supernatants were transferred to clean ultracentrifuge tubes, and the membranes were collected by centrifugation at 100,000 × *g* for 45 min at 4 °C. The supernatants were subsequently discarded and the pellets containing the membrane fractions were dissolved in 1× P buffer and analyzed by MS.

The proteins were analyzed by trypsin filter digestion in the form of an eFASP (enhanced Filter-aided sample preparation) method[58]. Briefly, the samples were reduced, alkylated and digested by trypsin on YM-10 Microcon filters (Merck). The resulting peptides were then desalted on a C18 SPE column (PepClean, Thermo). The peptides were separated during LC-MS/MS using a nano-LC system (Ultimate 3000 RSLC nano, Dionex) on an Acclaim PepMap C18 column (75 um Internal Diameter, 250 mm length) by applying a 125 min acetonitrile elution gradient in 0.1% formic acid. The chromatographic column was connected via nanoESI to a tandem mass spectrometer (TripleTOF 5600, Sciex). We collected data for the identification and the quantification of the proteins in one measurement sequence. Employing two methods using the same chromatographic parameters but different mass spectrometric data collection setups [the first: the data-dependent analysis (DDA) method; the second: the data independent method (DIA)—SWATH[59]], we measured the samples in a sequence of two consecutive runs of each sample (the first run aimed at collecting the DDA data to identify the proteins; the second aimed at collecting the DIA data for to quantify them). All resulting DDA spectra were searched together using Protein Pilot 4.5 (Sciex) against the Uniprot *B. subtilis* reference protein database (downloaded 8th of October 2015), thus creating the library used for SWATH processing in PeakView 2.2 (Sciex). In the SWATH analysis the retention time was aligned in all the samples by selecting the peptides common across the retention time range for all the samples. For quantification purposes, we allowed up to 30 peptides per protein, 6 transitions per peptide, a peptide confidence of 95% and a false-discovery rate threshold of 1%. The processing steps produced an intensity of transitions, peptides and proteins. The final protein table was processed in MarkerView (Sciex) in order to create a statistical evaluation. The Student's *t*-test was performed on the monitored groups.

Spotting assay—non-conjugative plasmid transfer. Donor [LK1925, wt containing the Cm resistance gene on plasmid pCPP31-Y1)[39]] and recipient (LK1922, wt harboring the MLS resistance gene on chromosomal DNA) strains were grown

separately overnight. Next day, the strains were mixed (equal numbers of cells), diluted to an initial $OD_{600} = 0.05$ and cultivated for 4 h at 37 °C with shaking. The mixtures, serially diluted, were spotted on LB agar (without antibiotics) and LB agar containing appropriate antibiotics (Cm for donor selection, MLS for recipient selection, Cm+MLS for recipients that acquired the non-conjugative plasmid). After 18 h, the dishes were photographed and double-resistant colonies were inoculated into LB to $OD_{600} = 0.05$. 100 µl of bacterial suspensions were plated on LB agar with or without antibiotics (the same as above). Double-resistant colonies were inoculated into LB medium with antibiotics (Cm + MLS) and grown overnight at 37 °C. On the following day, their genomic (High Pure PCR Template Preparation Kit) and plasmid (see: *B. subtilis* plasmid isolation) DNAs were extracted. The presence of the *erm* gene (MLS^r) in double-resistant strains was verified by PCR (Expand High Fidelity PCR System).

***B. subtilis* plasmid isolation**. Two milliliter of overnight culture was pelleted (5 min, 13,200 × *g* at 4 °C) and washed twice with 500 µl of TES (0.02 M, Tris-HCl pH 8; 5 mM, EDTA; 0.1 M, NaCl). The supernatant was discarded and 40 µl of lysozyme-containing buffer (30 mM, Tris-HCl pH 8; 50 mM, EDTA; 50 mM, NaCl; 25%, sucrose; lysozyme 500 µg/ml) was added. After 15 min at 37 °C, the sample was placed on ice. 160 µl of SDS buffer (2 ml of 10% SDS; 2 ml of 0.5 M EDTA pH 8; 12 ml of TES buffer) was mixed with 50 µl of 5 M NaCl and added to the sample, gently mixed and left on ice for 60 min. The mixture was subsequently centrifuged (30 min, 13,200 × *g* at 4 °C) and the supernatant containing the plasmid DNA was transferred to a clean micro centrifuge tube. Finally, the plasmid DNA was precipitated with ethanol and analyzed on an agarose gel.

Non-conjugative plasmid transfer. Donor (harboring plasmid pCPP31-Y1, Cm^r) and recipient (containing MLS^r in genome) strains were grown separately overnight. The next day, cultures were pelleted (9000 × *g*, 3 min at RT) and dissolved in 1× DNAse I buffer diluted in 1× PBS. DNAse I was then added (or not for the negative control) and samples were incubated for 20 min at 37 °C. Donor and recipient strains were then mixed (or each strain was grown separately) at a 1:1 ratio at an initial $OD_{600} = 0.05$ into fresh LB medium without antibiotics. Cultures were gently shaken for 4 h at 37 °C. Subsequently, bacteria were diluted to $OD_{600} = 0.5$ and 100 µl were plated on LB agar dishes with appropriate antibiotics (MLS-recipient selection; Cm + MLS—selection for double-resistant bacteria). CFU/ml were counted on the following day. The efficiency of plasmid receipt by recipient cells was expressed as the ratio of double-resistant cells (those able to grow on Cm + MLS) to all recipient cells in the mixture that grew in the presence of MLS.

Quantitative PCR. Two milliliters of exponentially growing cells (LB medium with 200 µM IPTG, gentle shaking) [wt (LK1432), Δ*sigD* (LK1873), Δ*comK* (LK2380), P_{hs}-*comK* (LK2317); OD_{600} ~0.8] were treated with RNAprotect Bacteria reagent (QIAGEN), pelleted and immediately frozen. Their total RNA was isolated with the RNeasy Mini Kit (QIAGEN). Prior to RNA extraction, recovery marker RNA was added [a fragment of 16 s rRNA from *M. smegmatis* (amplified by primers nos. LK1281 and LK1282, see Supplementary Table 2)]. Finally, RNA was DNase treated (TURBO DNA-free™ Kit, Invitrogen). Five micrograms of total RNA was reverse transcribed to complementary DNA with reverse transcriptase using random hexamers as primers (SuperScript™ III Reverse Transcriptase, Invitrogen). This was followed by qPCR in a LightCycler 480 System (Roche Applied Science) containing LightCycler® 480 SYBR Green I Master and 0.5 µM of each primer. The primers were designed with Primer3 software and their sequences are given in Supplementary Table 2. The data were normalized to the recovery marker and the number of cells.

Growth of *B. subtilis* in the presence of antibiotics. One milliliter of *B. subtilis* exponential culture was stained with Nile Red (final concentration 10 µg/ml) for 10 min at RT and washed once with 1× PBS. LB agarose containing 1 µM SYTOX green and an appropriate antibiotic (Amp, 500 µg/ml; Cm, 5 µg/ml; Rif, 50 µg/ml) was prepared inside a gene frame (Invitrogen). For time-lapse experiments, it was necessary to create a narrow agarose strip (~2.5 mm) in the middle of the gene frame (by removing agar from its sides) to allow oxygen to efficiently diffuse through the sample. The Nile Red-stained culture was then spotted on agarose and covered with a coverslip that was held by the gene frame (no pressure) and placed in a chamber at a constant 37 °C temperature. Pictures were taken with an Olympus CellR IX81 detection and analysis system equipped with a Plan-Apochromat 100×/1.45 NA oil objective and an EMCCD Hamamatsu camera.

Diverse methods for high-resolution bacterial culture observation. Exponential bacterial culture ($OD_{600} = 0.6$) was diluted to low density ($OD_{600} = 0.05$) and spotted on cellophane lying on an LB agar dish and grown for 4 h. In all, 4 × 2 cm cellophane strips containing bacteria were carefully taken and mounted onto glass slides using Scotch tape. The slides were placed into a glass desiccator with a small container of 2% OsO_4 in double-distilled water (ddH_2O) and the cells were allowed to fix at room temperature for several days[60]. The fixed cellophane strips were then cut into pieces in size of standard SEM mounts (12.5 mm) and mounted with conductive tape onto aluminum mounts (SPI). The samples were then sputter-coated with 3 nm of platinum. The SEM analysis was essentially done as described above.

As an alternative to the cellophane SEM experiment, we used a SIM-based approach. Here, instead of cellophane, a thin ~1 mm 1× PBS agarose pad was used. The pad was positioned on an LB agar dish containing 10 µg/ml Nile Red. After 4 h, the agarose pad was removed, covered with a coverslip and observed by SIM (see: SIM procedure).

Subsequently, two previously published protocols for observing NTs were used with minor changes[1,9,11]. First, bacterial cells were grown directly on LB agar dishes for 4 h at 37 °C and then imprinted onto glow-discharge activated EM grids[61]. The grids were fixed with drops of 2.5% glutaraldehyde in sodium cacodylate buffer in Petri-dish for 20 min[1]. The fixed grids were washed three times with ddH_2O and dehydrated in a graded ethanol series (25, 50, 75, 90, 96, 100, and 100%), and air-dried directly from 100% ethanol. Finally, the grids were sputter-coated with 3 nm of platinum and mounted into a transmission electron microscopy grid table for SEM examination. A FEI Nova NanoSEM scanning electron microscope (FEI, Brno, Czech Republic) at 5 kV using ETD, CBS, and TLD detectors in beam deceleration mode was used for SEM analysis.

Second, exponentially growing cells were spotted at $OD_{600} = 0.05$ onto glow-discharge activated formvar/carbon film coated EM grids placed on a nitrocellulose membrane[11]. These grids were taken after 4 h of cultivation (at 37 °C) on an LB agar dish and fixed with drops of 3% glutaraldehyde in a petri-dish most chamber. The fixed grids were subsequently processed as described above.

Image analysis. The final adjustment of the fluorescent images was done using Fiji ImageJ or the Analysis 3.2 Pro software suite (Sis GmbH; Olympus, now EMSIS GmbH) for SEM images. The free software Gimp (https://www.gimp.org/) and Inkscape (https://inkscape.org/) were also used for final image plate setup.

NTs vs. cell membrane signal calculation. Measurement of the membrane signal in the time-lapse images was done following bleaching correction. NT and cell membrane signals were measured at each time point. The background value was subtracted from the NT and cell membrane signal, yielding the final signal intensity.

SYTOX green penetration. The SYTOX green signal was measured at each time point in the time-lapse images. The background was subtracted and the highest value was normalized to 1. Combination with the membrane staining signal allowed the NT formation time point to be detected.

Quantification and statistical analysis. For each experiment we had at least three biological replicates. Averages of individual cells from different replicas are reported. The number of analyzed cells is given in the charts and figures. NT quantification was done manually. MS Excel and SigmaPlot were used for all statistical analyses, data processing, and presentation. For testing uniformity of distribution of NTs over cell we assumed the auxiliary hypothesis that poles cover <50% of cell surface. *p*-value for this joint hypothesis was computed using quantiles of the Beta distribution. Comparison of cell counts was performed with a binomial generalized linear model using the `glm` function in R[62] and—as an additional check—the `stan_glm` function from the RStanArm package[63]. Analysis of plasmid transfer and relative expression was performed on the log scale using a linear model with the `lm` and `cor.test` functions in R. Where applicable, contrasts and multiple testing corrections were performed with the `TukeyHSD` function. The difference of spatial distributions of NTs between wild type and Ampicilin-treated bacteria was assessed with Chi-squared test using the `chisq.test` function in R. Where applicable, we used models with full interactions. Whenever multiple model formulations were considered, we have reported the *p*-value least favorable to our conclusions. See "Code availability" for details regarding code for the statistical analysis.

Reporting summary. Further information on research design is available in the Nature Research Reporting Summary linked to this article.

Data availability

Original microscopic images are available upon request. All data generated or analyzed during this study are included in this published article and its supplementary files, or available upon request. Source data are provided with this paper.

Code availability

Full code for the statistical analysis can be found at Zenodo (https://doi.org/10.5281/zenodo.3999744).

Received: 24 March 2020; Accepted: 3 September 2020;
Published online: 02 October 2020

References

1. Dubey, G. P. & Ben-Yehuda, S. Intercellular nanotubes mediate bacterial communication. *Cell* **144**, 590–600 (2011).
2. Pande, S. et al. Metabolic cross-feeding via intercellular nanotubes among bacteria. *Nat. Commun.* **6**, 6238 (2015).
3. Barchinger, S. E. et al. Regulation of gene expression in *Shewanella oneidensis* MR-1 during electron acceptor limitation and bacterial nanowire formation. *Appl. Environ. Microbiol.* **82**, 5428–5443 (2016).
4. Subramanian, P., Pirbadian, S., El-Naggar, M. Y. & Jensen, G. J. Ultrastructure of *Shewanella oneidensis* MR-1 nanowires revealed by electron cryotomography. *Proc. Natl Acad. Sci. USA* **115**, E3246–E3255 (2018).
5. Marguet, E. et al. Membrane vesicles, nanopods and/or nanotubes produced by hyperthermophilic archaea of the genus Thermococcus. *Biochem. Soc. Trans.* **41**, 436–442 (2013).
6. Shetty, A. & Hickey, W. J. Effects of outer membrane vesicle formation, surface-layer production and nanopod development on the metabolism of phenanthrene by Delftia acidovorans Cs1-4. *PLoS ONE* **9**, e92143 (2014).
7. Shetty, A., Chen, S., Tocheva, E. I., Jensen, G. J. & Hickey, W. J. Nanopods: a new bacterial structure and mechanism for deployment of outer membrane vesicles. *PLoS ONE* **6**, e20725 (2011).
8. Wei, X., Vassallo, C. N., Pathak, D. T. & Wall, D. Myxobacteria produce outer membrane-enclosed tubes in unstructured environments. *J. Bacteriol.* **196**, 1807–1814 (2014).
9. Bhattacharya, S. et al. A ubiquitous platform for bacterial nanotube biogenesis. *Cell Rep.* **27**, 334–342 e310 (2019).
10. Diethmaier, C. et al. The YmdB phosphodiesterase is a global regulator of late adaptive responses in *Bacillus subtilis*. *J. Bacteriol.* **196**, 265–275 (2014).
11. Dubey, G. P. et al. Architecture and characteristics of bacterial nanotubes. *Dev. Cell* **36**, 453–461 (2016).
12. Kubori, T. et al. Purification and characterization of the flagellar hook-basal body complex of Bacillus subtilis. *Mol. Microbiol.* **24**, 399–410 (1997).
13. Mamou, G., Malli Mohan, G. B., Rouvinski, A., Rosenberg, A. & Ben-Yehuda, S. Early developmental program shapes colony morphology in bacteria. *Cell Rep.* **14**, 1850–1857 (2016).
14. Stempler, O. et al. Interspecies nutrient extraction and toxin delivery between bacteria. *Nat. Commun.* **8**, 315 (2017).
15. Pal, R. R. et al. Pathogenic *E. coli* extracts nutrients from infected host cells utilizing injectisome components. *Cell* **177**, 683–696 e618 (2019).
16. Baidya, A. K., Bhattacharya, S., Dubey, G. P., Mamou, G. & Ben-Yehuda, S. Bacterial nanotubes: a conduit for intercellular molecular trade. *Curr. Opin. Microbiol.* **42**, 1–6 (2018).
17. van Sinderen, D., ten Berge, A., Hayema, B. J., Hamoen, L. & Venema, G. Molecular cloning and sequence of comK, a gene required for genetic competence in *Bacillus subtilis*. *Mol. Microbiol.* **11**, 695–703 (1994).
18. Turner, L., Ping, L., Neubauer, M. & Berg, H. C. Visualizing flagella while tracking bacteria. *Biophys. J.* **111**, 630–639 (2016).
19. Blair, K. M., Turner, L., Winkelman, J. T., Berg, H. C. & Kearns, D. B. A molecular clutch disables flagella in the Bacillus subtilis biofilm. *Science* **320**, 1636–1638 (2008).
20. Paget, M. S. Bacterial sigma factors and anti-sigma factors: structure, function and distribution. *Biomolecules* **5**, 1245–1265 (2015).
21. Burton, A. T., DeLoughery, A., Li, G. W. & Kearns, D. B. Transcriptional regulation and mechanism of SigN (ZpdN), a pBS32-encoded sigma factor in *Bacillus subtilis*. *MBio* **10**, https://doi.org/10.1128/mBio.01899-19 (2019).
22. Nicolas, P. et al. Condition-dependent transcriptome reveals high-level regulatory architecture in Bacillus subtilis. *Science* **335**, 1103–1106 (2012).
23. Mirel, D. B. & Chamberlin, M. J. The Bacillus subtilis flagellin gene (hag) is transcribed by the sigma 28 form of RNA polymerase. *J. Bacteriol.* **171**, 3095–3101 (1989).
24. Sevim, E., Gaballa, A., Belduz, A. O. & Helmann, J. D. DNA-binding properties of the Bacillus subtilis and Aeribacillus pallidus AC6 sigma(D) proteins. *J. Bacteriol.* **193**, 575–579 (2011).
25. Albertini, A. M., Caramori, T., Crabb, W. D., Scoffone, F. & Galizzi, A. The flaA locus of Bacillus subtilis is part of a large operon coding for flagellar structures, motility functions, and an ATPase-like polypeptide. *J. Bacteriol.* **173**, 3573–3579 (1991).
26. Reuter, M. et al. Mechanosensitive channels and bacterial cell wall integrity: does life end with a bang or a whimper? *J. R. Soc. Interface* **11**, 20130850 (2014).
27. Lee, S. et al. Dynamic analysis of pathogen-infected host cells using quantitative phase microscopy. *J. Biomed. Opt.* **16**, 036004 (2011).
28. Mohamed, Y. F. & Valvano, M. A. A Burkholderia cenocepacia MurJ (MviN) homolog is essential for cell wall peptidoglycan synthesis and bacterial viability. *Glycobiology* **24**, 564–576 (2014).
29. Li, K. et al. Atomic force microscopy of side wall and septa peptidoglycan from *Bacillus subtilis* reveals an architectural remodeling during growth. *Front. Microbiol.* **9**, 620 (2018).
30. Smith, T. J., Blackman, S. A. & Foster, S. J. Autolysins of *Bacillus subtilis*: multiple enzymes with multiple functions. *Microbiology* **146**, 249–262 (2000).
31. Yamamoto, H., Kurosawa, S. & Sekiguchi, J. Localization of the vegetative cell wall hydrolases LytC, LytE, and LytF on the *Bacillus subtilis* cell surface and stability of these enzymes to cell wall-bound or extracellular proteases. *J. Bacteriol.* **185**, 6666–6677 (2003).
32. Roth, B. L., Poot, M., Yue, S. T. & Millard, P. J. Bacterial viability and antibiotic susceptibility testing with SYTOX green nucleic acid stain. *Appl. Environ. Microbiol.* **63**, 2421–2431 (1997).
33. Katsu, T., Tsuchiya, T. & Fujita, Y. Dissipation of membrane potential of *Escherichia coli* cells induced by macromolecular polylysine. *Biochem. Biophys. Res. Commun.* **122**, 401–406 (1984).
34. Izaki, K., Matsuhashi, M. & Strominger, J. L. Biosynthesis of the peptidoglycan of bacterial cell walls. 8. Peptidoglycan transpeptidase and D-alanine carboxypeptidase: penicillin-sensitive enzymatic reaction in strains of *Escherichia coli*. *J. Biol. Chem.* **243**, 3180–3192 (1968).
35. Svetlov, M. S. et al. High-resolution crystal structures of ribosome-bound chloramphenicol and erythromycin provide the ultimate basis for their competition. *RNA* **25**, 600–606 (2019).
36. Calvori, C., Frontali, L., Leoni, L. & Tecce, G. Effect of rifamycin on protein synthesis. *Nature* **207**, 417–418 (1965).
37. Campbell, E. A. et al. Structural mechanism for rifampicin inhibition of bacterial rna polymerase. *Cell* **104**, 901–912 (2001).
38. Baidya, A. K., Rosenshine, I. & Ben-Yehuda, S. Donor-delivered cell wall hydrolases facilitate nanotube penetration into recipient bacteria. *Nat. Commun.* **11**, 1938 (2020).
39. Krasny, L., Vacik, T., Fucik, V. & Jonak, J. Cloning and characterization of the str operon and elongation factor Tu expression in *Bacillus stearothermophilus*. *J. Bacteriol.* **182**, 6114–6122 (2000).
40. Holscher, T. et al. Impaired competence in flagellar mutants of *Bacillus subtilis* is connected to the regulatory network governed by DegU. *Environ. Microbiol. Rep.* **10**, 23–32 (2018).
41. Rahmer, R., Morabbi Heravi, K. & Altenbuchner, J. Construction of a super-competent *Bacillus subtilis* 168 using the P mtlA -comKS inducible cassette. *Front. Microbiol.* **6**, 1431 (2015).
42. Daly, M. J. et al. Protein oxidation implicated as the primary determinant of bacterial radioresistance. *PLoS Biol.* **5**, e92 (2007).
43. Calvo, R. A. & Kearns, D. B. FlgM is secreted by the flagellar export apparatus in *Bacillus subtilis*. *J. Bacteriol.* **197**, 81–91 (2015).
44. Whatmore, A. M. & Reed, R. H. Determination of turgor pressure in *Bacillus subtilis*: a possible role for K+ in turgor regulation. *J. Gen. Microbiol.* **136**, 2521–2526 (1990).
45. Beltran-Heredia, E. et al. Membrane curvature induces cardiolipin sorting. *Commun. Biol.* **2**, 225 (2019).
46. Danne, L. et al. Membrane remodeling by a bacterial phospholipid-methylating enzyme. *MBio* **8**, https://doi.org/10.1128/mBio.02082-16 (2017).
47. Ducret, A., Fleuchot, B., Bergam, P. & Mignot, T. Direct live imaging of cell-cell protein transfer by transient outer membrane fusion in Myxococcus xanthus. *Elife* **2**, e00868 (2013).
48. Pathak, D. T. et al. Cell contact-dependent outer membrane exchange in myxobacteria: genetic determinants and mechanism. *PLoS Genet.* **8**, e1002626 (2012).
49. McCaig, W. D., Koller, A. & Thanassi, D. G. Production of outer membrane vesicles and outer membrane tubes by Francisella novicida. *J. Bacteriol.* **195**, 1120–1132 (2013).
50. Sampath, V., McCaig, W. D. & Thanassi, D. G. Amino acid deprivation and central carbon metabolism regulate the production of outer membrane vesicles and tubes by Francisella. *Mol. Microbiol.* **107**, 523–541 (2018).
51. Li, T. et al. Deinococcus radiodurans toxin-antitoxin MazEF-dr mediates cell death in response to DNA damage stress. *Front. Microbiol.* **8**, 1427 (2017).
52. Hanna, S. J. et al. Tunneling nanotubes, a novel mode of tumor cell-macrophage communication in tumor cell invasion. *J. Cell Sci.* **132**, https://doi.org/10.1242/jcs.223321 (2019).
53. Birmingham, C. L., Jiang, X., Ohlson, M. B., Miller, S. I. & Brumell, J. H. Salmonella-induced filament formation is a dynamic phenotype induced by rapidly replicating Salmonella enterica serovar typhimurium in epithelial cells. *Infect. Immun.* **73**, 1204–1208 (2005).
54. Drab, M., Stopar, D., Kralj-Iglic, V. & Iglic, A. Inception mechanisms of tunneling nanotubes. *Cells* **8**, https://doi.org/10.3390/cells8060626 (2019).
55. Souriant, S. et al. Tuberculosis exacerbates HIV-1 infection through IL-10/STAT3-dependent tunneling nanotube formation in macrophages. *Cell Rep.* **26**, 3586–3599 e3587 (2019).
56. Sikova, M. et al. The torpedo effect in *Bacillus subtilis*: RNase J1 resolves stalled transcription complexes. *EMBO J.* e102500, https://doi.org/10.15252/embj.2019102500 (2019).
57. Gao, E., Zhang, C. & Wang, J. Effects of budesonide combined with noninvasive ventilation on PCT, sTREM-1, chest lung compliance, humoral

immune function and quality of life in patients with AECOPD complicated with type II respiratory failure. *Open Med. (Wars.)* **14**, 271–278 (2019).
58. Erde, J., Loo, R. R. & Loo, J. A. Enhanced FASP (eFASP) to increase proteome coverage and sample recovery for quantitative proteomic experiments. *J. Proteome Res.* **13**, 1885–1895 (2014).
59. Gillet, L. C. et al. Targeted data extraction of the MS/MS spectra generated by data-independent acquisition: a new concept for consistent and accurate proteome analysis. *Mol. Cell Proteom.* **11**, O111 016717 (2012).
60. Boubakri, H. et al. The absence of pupylation (prokaryotic ubiquitin-like protein modification) affects morphological and physiological differentiation in *Streptomyces coelicolor*. *J. Bacteriol.* **197**, 3388–3399 (2015).
61. Benada, O. & Pokorny, V. Modification of the Polaron sputter-coater unit for glow-discharge activation of carbon support films. *J. Electron Microsc. Tech.* **16**, 235–239 (1990).
62. R-Core-Team. *R: A Language and Environment for Statistical Computing. Version 3.6.2*. https://www.R-project.org/ (2019).
63. Goodrich, B., Gabry, J., Ali, I. & Brilleman, S. *rstanarm: Bayesian Applied Regression Modeling Via Stan. R Package Version 2.19.3*. https://mc-stan.org/rstanarm (2020).

Acknowledgements

This work was supported by Czech Science Foundation-Grant No. 19-12956S (to L.K.), Ministry of Education, Youth, and Sports of the Czech Republic-project LO1509 (to O.K. and O.B.) and ELIXIR_CZ project LM2018131 (to M.M.), VEGA–Grant No. 2/0007/17 from the Slovak Academy of Sciences (to I.B.), a Grant from the Slovak Research and Development Agency under contract APVV-14-0181 and APVV-18-0104 (to I.B.), Czech Ministry of Health (Grant No. 17-29680A to L.K.). We thank C. Condon and J. Bauer for critically reading the manuscript.

Author contributions

J.P., L.K., I.B. conceptualized the project. J.P., I.B., K.M., D.V., M.H., O.B., O.K., M.Š., H.Š. performed the experiments. M.M. performed statistical analyses. L.K., J.P., I.B., and O.B. wrote the first draft of the manuscript. All authors read and contributed to the final version.

Competing interests

The authors declare no competing interests.

Additional information

Supplementary information is available for this paper at https://doi.org/10.1038/s41467-020-18800-2.

Correspondence and requests for materials should be addressed to O.B., I.B. or L.K.

Peer review information *Nature Communications* thanks the anonymous reviewers for their contribution to the peer review of this work. Peer reviewer reports are available.

Reprints and permission information is available at http://www.nature.com/reprints

Publisher's note Springer Nature remains neutral with regard to jurisdictional claims in published maps and institutional affiliations.

SUPPLEMENTARY INFORMATION

Bacterial nanotubes are a manifestation of cell death

Pospíšil *et al*.

Supplementary Figures 1-17

Supplementary Tables 1-4

Supplementary Information References

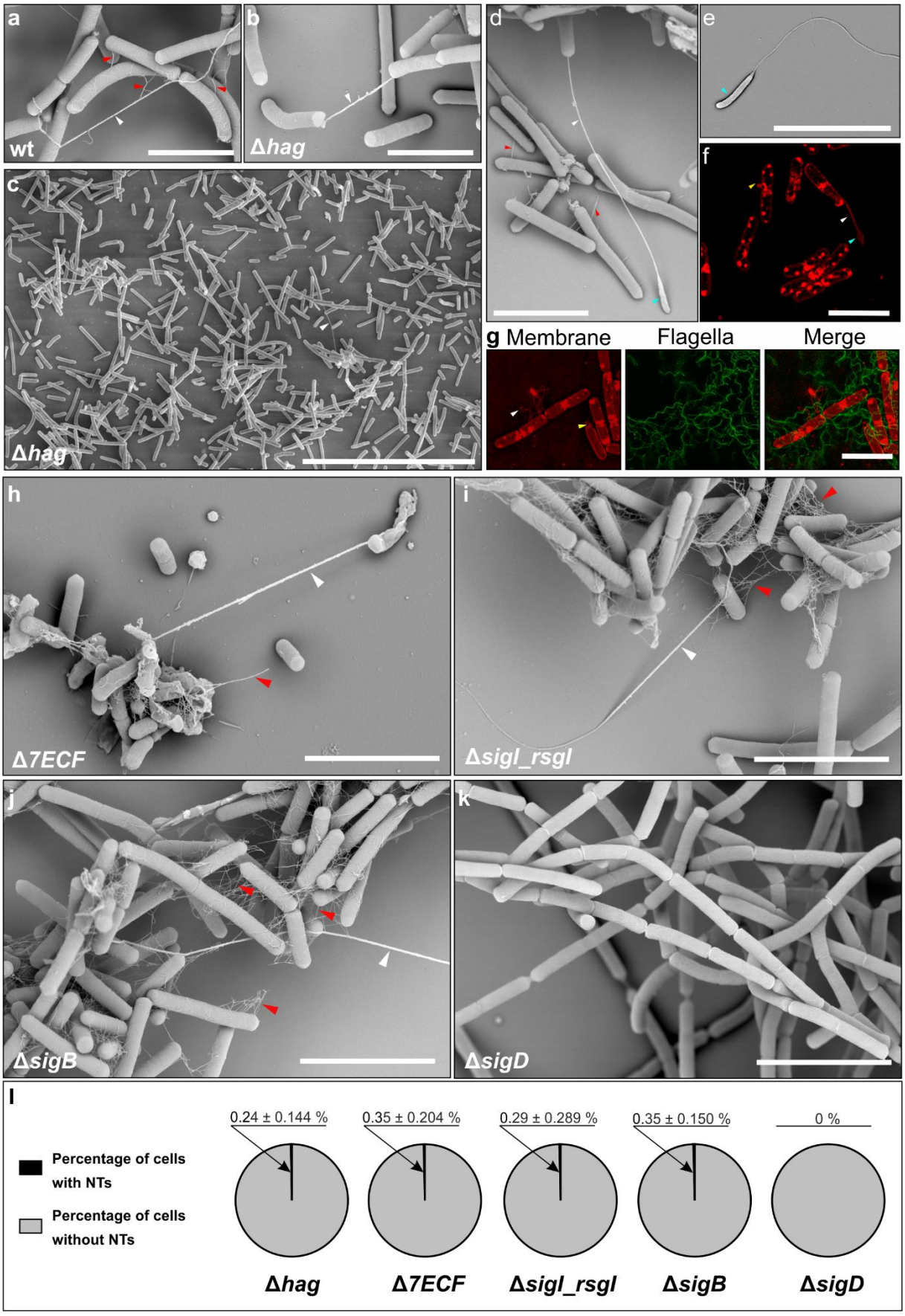

Supplementary Figure 1 | NT morphology, discrimination from flagella and identification of a sigma factor responsible for their formation.

SEM (Scanning Electron Microscopy) analysis of *B. subtilis* cells from the exponential phase of (**a**) wt (LK1432) and (**b**) Δ*hag* (LK1966) strains growing in liquid medium. White arrows indicate NTs; Red arrows indicate flagella. The scale bar=5 µm.

(**c**) A SEM image of the Δ*hag* strain showing the typical numbers of observed NTs for such image fields. The white arrow indicates the only NT in the field. Scale bar=30 µm.

(**d**-**e**) SEM images of the terminal structures of wt *B. subtilis* (LK1432) NTs. Scale bar=5 µm.

(**f**) A SIM image of a terminal structure of a wt *B. subtilis* NT. White arrows indicate NTs; Red arrows indicate flagella; Yellow arrows indicate membrane vesicles; Cyan arrows indicate terminal structures. Scale bar=5 µm.

(**g**) SIM microscopy of the hag^{T209C} (LK2052) strain containing a mutated *hag* gene[1]. The flagella are visualized using AF488-maleimide (green), membranes are stained by Nile red (red). White arrows indicate nanotubes; Yellow arrows indicate membrane vesicles. Scale bar=5 µm.

(**h**-**k**) SEM analysis of cells from exponential phase. Wt (LK1432) and deletion strains of various sigma factors (BSU2007 – Δ7ECF; LK2218 - Δ*sigB*; LK1550 - Δ*sigI*; LK1873 - Δ*sigD*) were imaged as described in Mat & Met. White arrows indicate nanotubes; Red arrows indicate flagella. Only the Δ*sigD* (LK1873) strain did not form NTs (it also did not form flagella). The scale bar=5 µm. All experiments (panels a-k) were conducted in at least three biological replicates (except for experiments in panel j, where two biological replicates were carried out).

(**l**) Quantification of NTs based on SEM analysis. Thick tubular structures (marked with white arrows in other panels) were counted as NTs. For each strain, ca 500 cells were analyzed for NT presence. The cell images used for the analysis were from three independent biological replicates, except for the Δ*sigB* strain where two biological replicas were used but the number of analyzed cells was 1,000. The pie chart represents 100%. Grey, cells without NTs; Black, cells with NTs (this percentage including ±SEM [Standard Error of the Mean] is indicated above each chart). The difference between wt and the mutant strains was not statistically significant. Nevertheless, the difference between wt and Δ*sigD* is highly significant $p<0.001$ when a different microscopic technique is used (Fig. 2c [wt] versus Supplementary Fig. 6b [Δ*sigD*]).

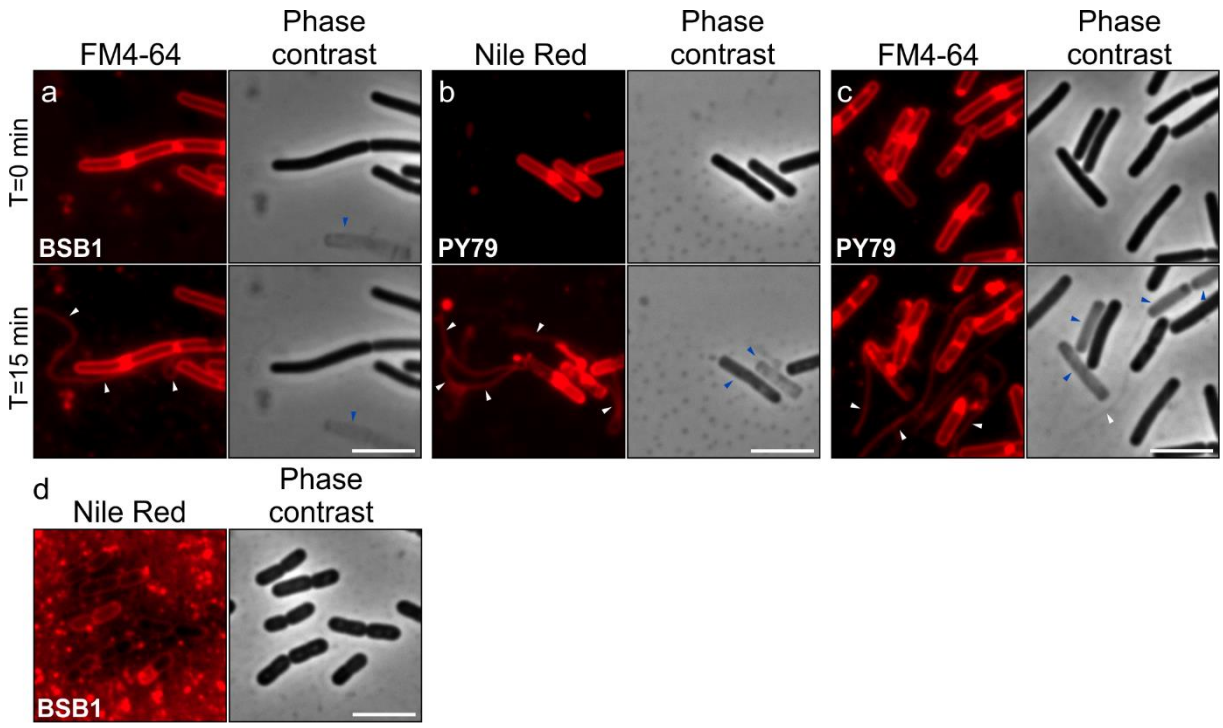

Supplementary Figure 2 | Comparison of the membrane staining of *B. subtilis* BSB1 and PY79 strains with Nile Red and FM4-64.

Fluorescence microscopy of exponentially grown *B. subtilis* BSB1 (LK1432) and PY79 (LK1629) strains. Bacteria were stained with Nile Red or FM4-64 (both in red) and samples were prepared by the P-GLG method. Pictures were taken at the indicated time points. White arrows indicate NTs; Blue arrows indicate ghost cells. Scale bar=5 µm. All experiments (panels a-d) were conducted in three biological replicates.

(**a**) The BSB1 strain stained with FM4-64.

(**b**) The PY79 strain stained with Nile Red.

(**c**) The PY79 strain stained with FM4-64.

(**d**) Example of incomplete staining of stationary phase *B. subtilis* cells with Nile Red.

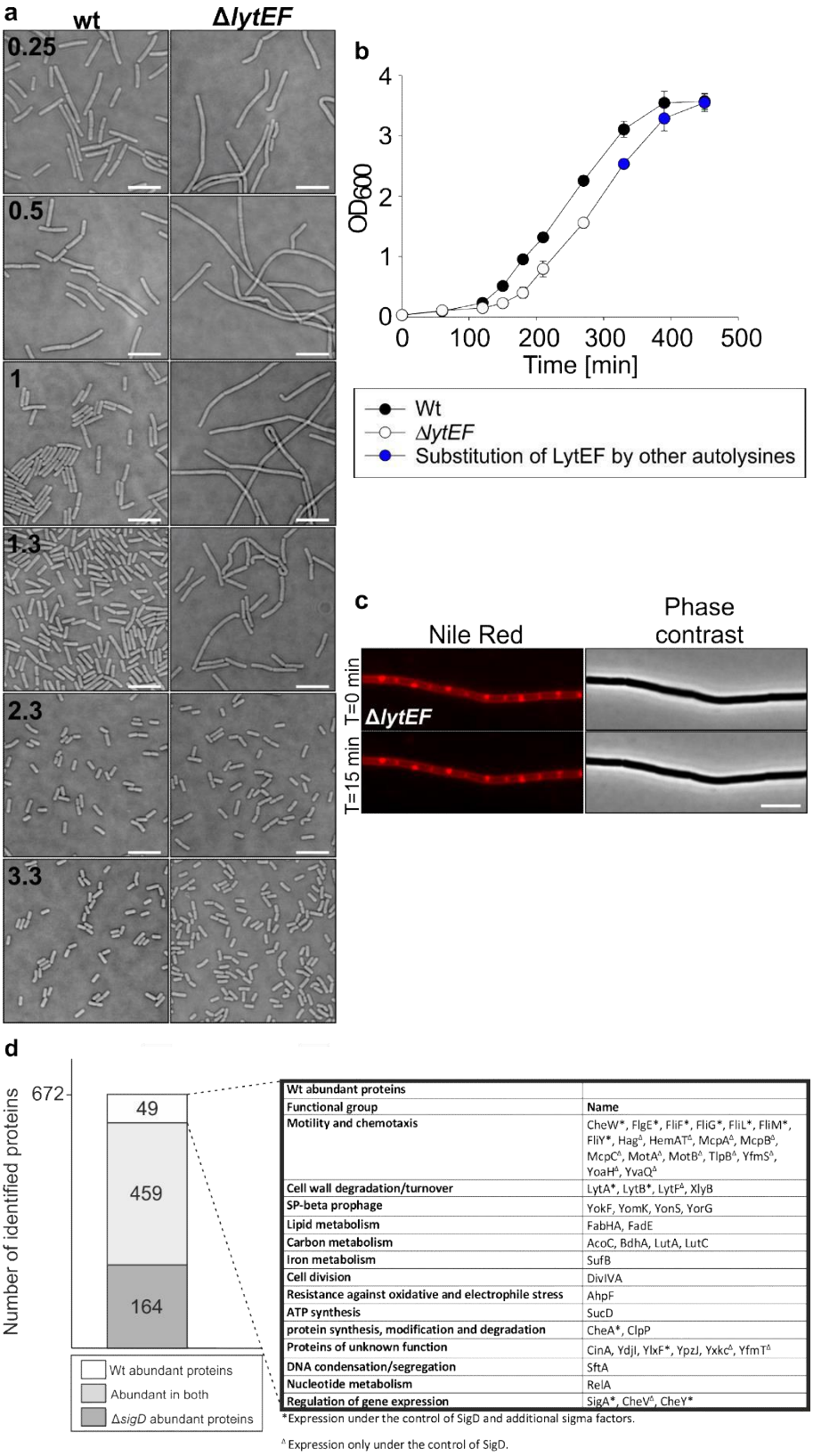

Wt abundant proteins	
Functional group	**Name**
Motility and chemotaxis	CheW*, FlgE*, FliF*, FliG*, FliL*, FliM*, FliY*, Hag$^{\Delta}$, HemAT$^{\Delta}$, McpA$^{\Delta}$, McpB$^{\Delta}$, McpC$^{\Delta}$, MotA$^{\Delta}$, MotB$^{\Delta}$, TlpB$^{\Delta}$, YfmS$^{\Delta}$, YoaH$^{\Delta}$, YvaQ$^{\Delta}$
Cell wall degradation/turnover	LytA*, LytB*, LytF$^{\Delta}$, XlyB
SP-beta prophage	YokF, YomK, YonS, YorG
Lipid metabolism	FabHA, FadE
Carbon metabolism	AcoC, BdhA, LutA, LutC
Iron metabolism	SufB
Cell division	DivIVA
Resistance against oxidative and electrophile stress	AhpF
ATP synthesis	SucD
protein synthesis, modification and degradation	CheA*, ClpP
Proteins of unknown function	CinA, YdjI, YlxF*, YpzJ, Yxkc$^{\Delta}$, YfmT$^{\Delta}$
DNA condensation/segregation	SftA
Nucleotide metabolism	RelA
Regulation of gene expression	SigA*, CheV$^{\Delta}$, CheY*

*Expression under the control of SigD and additional sigma factors.

$^{\Delta}$ Expression only under the control of SigD.

Supplementary Figure 3 | Morphology of the LytE and LytF autolysin deletion mutant in exponential phase and MS analysis of wt and Δ*sigD* membrane fractions.

(**a**) Wt *B. subtilis* (LK1432) and Δ*lytEF* (LK2290) strains were grown in liquid LB and cell morphology was observed by bright field microscopy at the indicated optical densities (OD_{600}) during culture growth. Scale bar=5 µm. The experiment was conducted in 3 biological replicates with similar results.

(**b**) Growth curves of the wt and Δ*lytEF* strains. Blue points indicate times when the functions of LytE and LytF are taken over by other autolysins. Data represent 3 biological replicates, shown as averages, the error bars indicate ±SEM [Standard Error of the Mean].

(**c**) Exponentially growing culture of the Δ*lytEF* strain was stained with Nile Red and prepared by the P-GLG method. Pictures were taken at the indicated time points. Scale bar=5 µm. Experiment was performed in 3 biological replicates with similar results.

(**d**) Protein mass spectrometry analysis of the wt (LK1432) and Δ*sigD* (LK1873) membrane fractions. The graph shows the number of genes sorted according to the membrane fractions in which they were found. The table lists those proteins that were enriched in the wt compared to Δ*sigD* (t-value ≥ 2, according to student's t-test). See Supplementary Tables 3 and 4 for the lists of proteins found in the other two fractions.

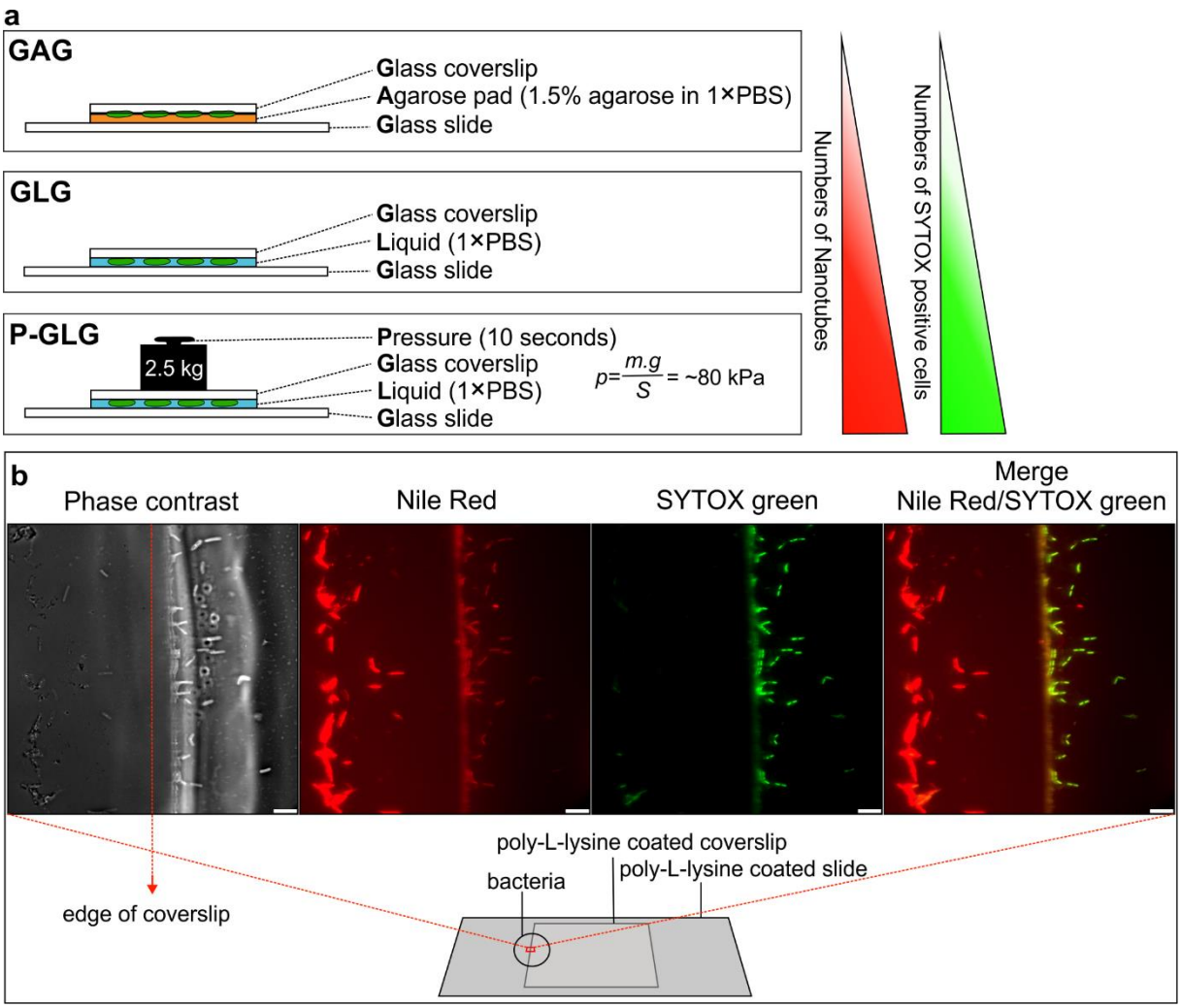

Supplementary Figure 4 | Different methods of sample preparation and death under the coverslip.

(**a**) Scheme of different methods of sample preparation. Red and green triangles indicate the trends in NT formation and the numbers of dying cells (monitored by SYTOX green).

(**b**) Exponentially grown wt (LK1432) cells were spotted on a poly-L-lysine coated glass slide and partially covered with a poly-L-lysine coverslip. Pressure was then applied on the coverslip as in the P-GLG method. The area around the edge of the coverslip was observed as indicated in the drawing. Membranes were stained with Nile Red (red) and cell death was determined by SYTOX green (green). Scale bar=5 µm. The experiment was conducted in 2 biological replicates with similar results.

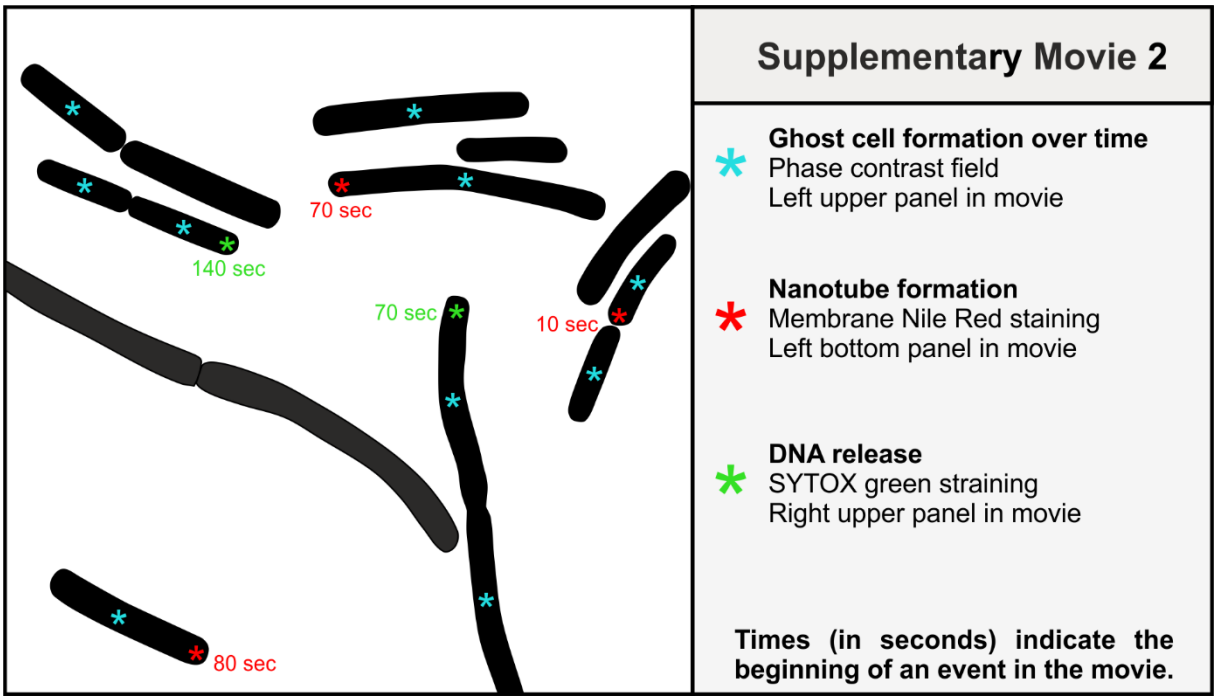

Supplementary Figure 5 | *B. subtilis* time-lapse fluorescence microscopy movie. Supplementary Movie 2 description.

This Supplementary Movie shows events occurring in dying cells under the P-GLG experimental setup. Colored asterisks indicate specific events (see legend next to the scheme). Seconds beside the asterisks indicate times at which these events begin.

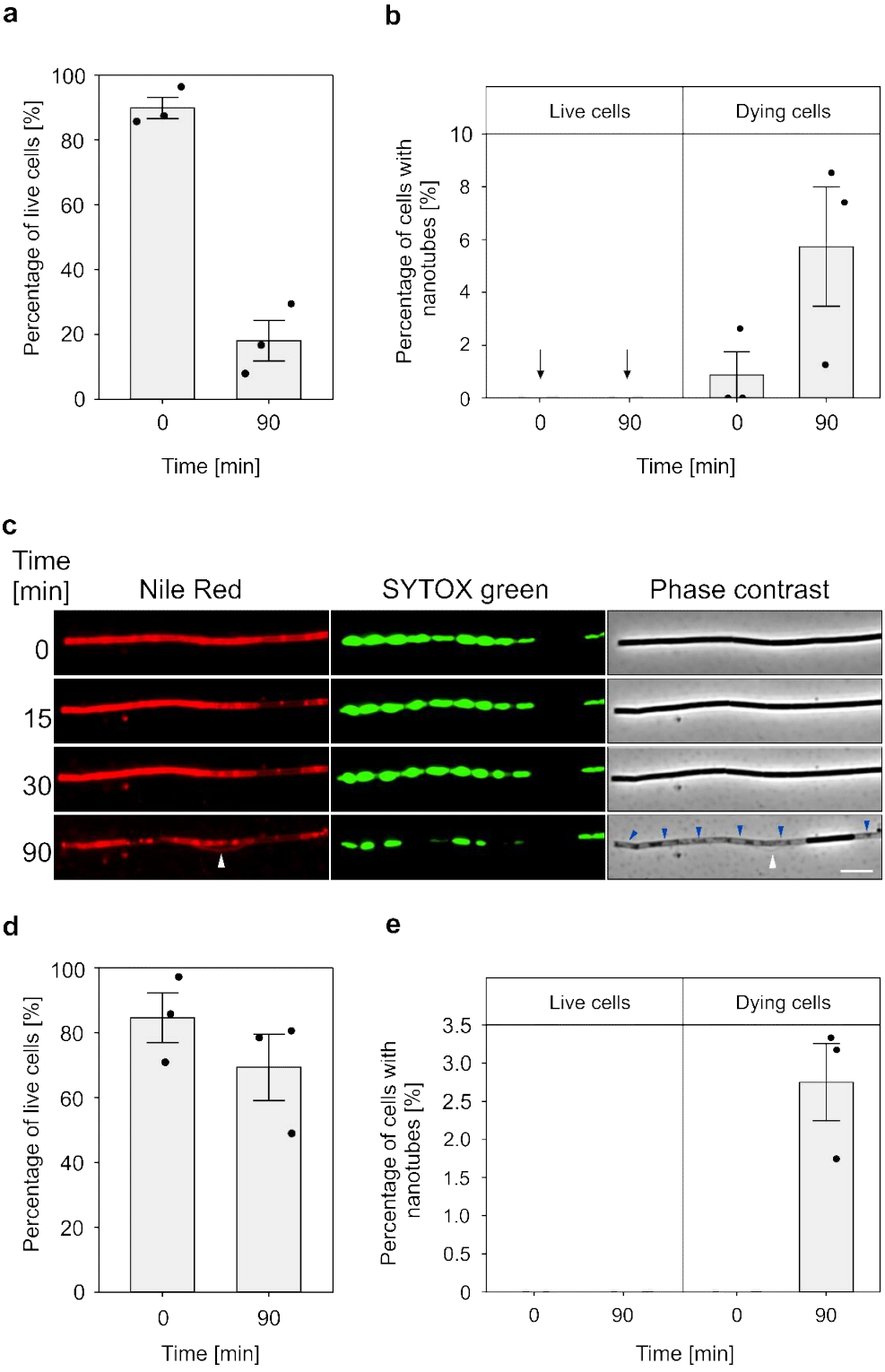

Supplementary Figure 6 | Delay in NT formation in the Δ*sigD* and Δ*lytEF* strains.

(**a**) Quantifications of live/dying Δ*sigD* (LK1873) cells were done based on the absence/presence of the SYTOX signal inside cells (sample was prepared by P-GLG method). The decrease in live cells numbers from t=0 to t = 90 is statistically significant ($p < 0.001$, GLM, two sided, $z = -24$, 95% CI OR = 0.02 – 0.03). 500 cells from 3 independent experiments were analyzed. The bars are averages and error bars ±SEM. The dots in this and other bar graphs represent individual experiments.

(**b**) Quantifications of the presence/absence of Δ*sigD* NTs were based on the Nile Red signal. The percentage of NTs is expressed relative to the number of dying (SYTOX positive) or live (SYTOX negative) cells, which was set as 100% (*e. g.* if out of 10% of dying cells, 20% formed NTs, then this would represent 2% of the total number of cells). 500 cells from 3 independent experiments were analyzed. The difference between the amounts of NTs formed by dying and live cells at t = 90 is statistically significant (p = 0.03, GLM, two sided, z = -2.2, 95% CI OR = 0.06 – 0.7). The bars are averages and error bars ±SEM. The vertical arrows in the graph indicate zero values.

(**c**) Exponentially grown *B. subtilis* Δ*lytEF* (LK2290) cells were stained with Nile Red (red), SYTOX green (green) and observed at the indicated time points (sample was prepared by the P-GLG method). The third column shows phase contrast images. White arrows indicate NTs. Blue arrows indicate ghost cells in the phase contrast fields. Scale bar=5 µm. Experiment was conducted in 3 biological replicates with similar results.

(**d**) Quantifications of live/dying Δ*lytEF* (LK2290) cells were done based on the absence/presence of the SYTOX signal inside cells (sample was prepared by P-GLG method). The decrease in live cells numbers from t = 0 to t = 90 is statistically significant (p < 0.001, GLM, two-sided, z = -7, 95% CI OR = 0.3 – 0.5). 500 cells from 3 independent experiments were analyzed. The bars are averages and error bars ±SEM.

(**e**) Quantification of the presence/absence of Δ*lytEF* NTs was based on the Nile Red signal. The percentage of NTs is expressed relative to the number of dying (SYTOX positive) or live (SYTOX negative) cells, which was set as 100% (e. g. out of the 10% of dying cells, 20% formed NTs – that is 2% of the total number of cells). 500 cells from 3 independent experiments were analyzed. The difference between the percentage of dying and live cells forming NTs at t = 90 is statistically significant (p = 0.007, GLM, two-sided, z = -2.6, 95% CI OR = 1.7 - 27). The bars are averages and error bars ±SEM. The vertical arrows in the graph indicate zero values.

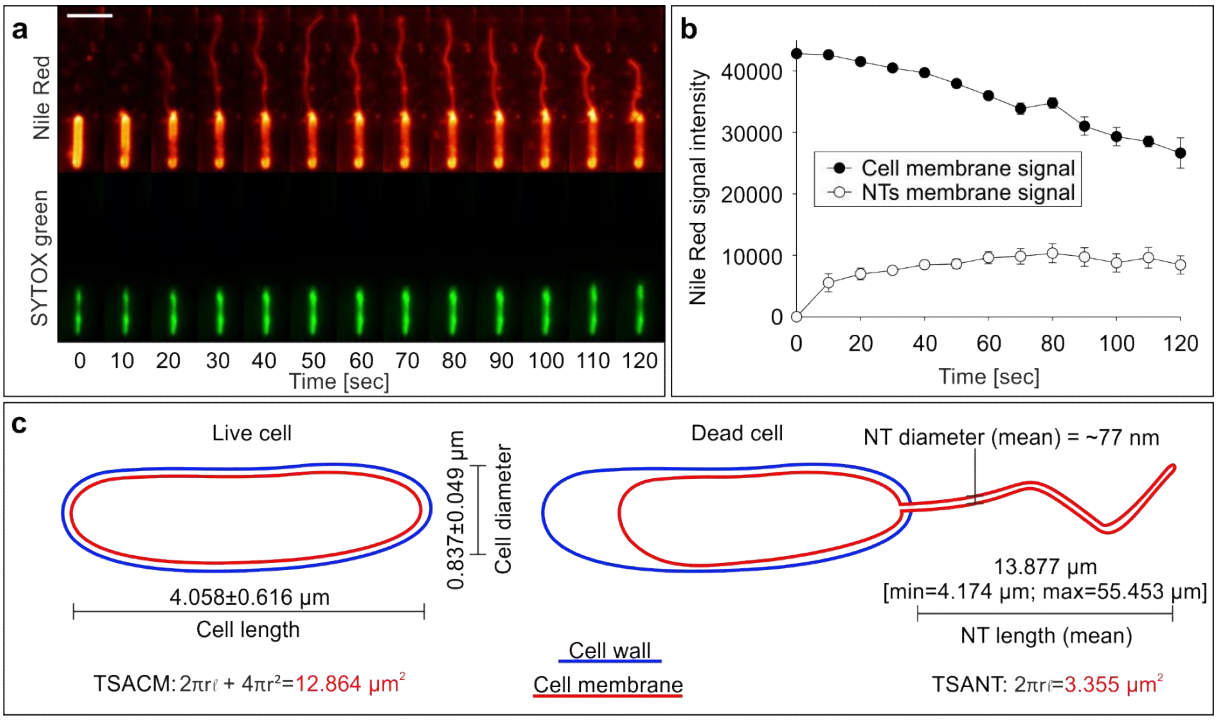

Supplementary Figure 7 | NTs are formed using the existing plasma membrane.

(**a**) Wt (LK1432) cells were prepared as in Figure 3 (main text). The primary data show time lapse (10 sec intervals) of a representative cell. The upper panel shows membrane stain Nile Red (false colored glow), the lower panel shows SYTOX (green). Note the decrease in the Nile red intensity in the cell area, concomitant with NT extrusion. Scale bar=5 µm. Experiment was conducted in 3 biological replicates with similar results.

(**b**) Quantification of the Nile Red signal in the cell area (closed circles) and in the NT area (open circles). After bleaching and background-subtraction corrections, the Nile red signal was quantified from 5 different NT-forming cells from one representative experiment. The error bars indicate ±SEM.

(**c**) Calculations of the **T**otal **S**urface **A**rea of the **C**ell **M**embrane (TSACM) and **T**otal **S**urface **A**rea of the **NT** (TSANT). After cell death, the NT is built from the cell's membrane. The length (l) and diameter (2r) of the Nile Red-stained cells (the membrane envelope dimensions) were measured in SIM images (from 100 exponentially growing cells). NT lengths were measured from fluorescence microscopy images. NT diameters were measured from SEM micrographs (10 NTs) because fluorescence microscopy does not have sufficient resolution for this and NT movement in SIM images may cause this parameter to be overestimated.

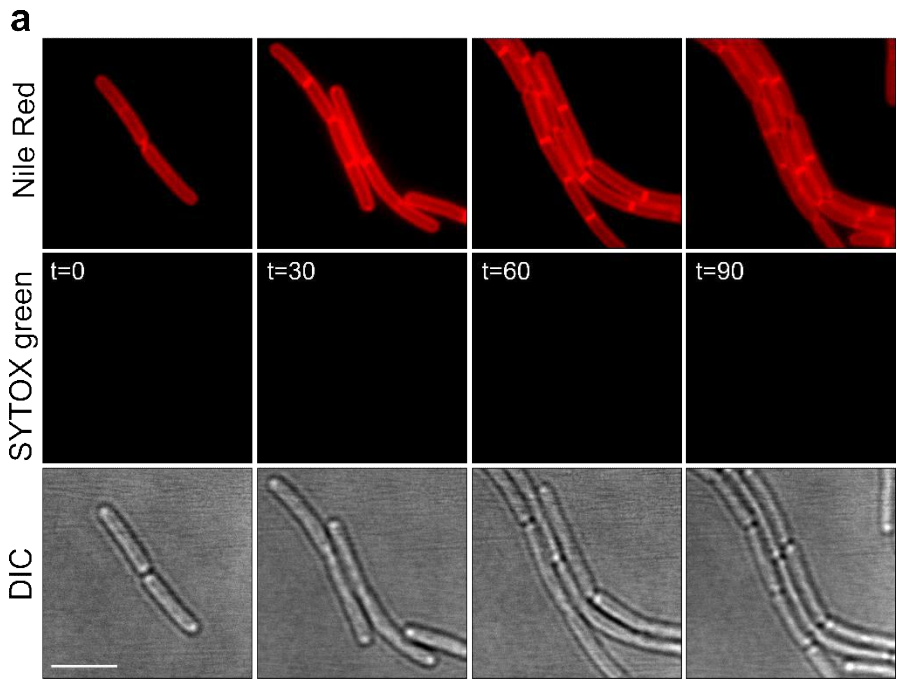

Time [min]	0	30	60	90
Live/Dying cells	159/0	262/7	557/9	1245/23
Live/Dying cells NTs	0/0	0/0	0/0	0/0

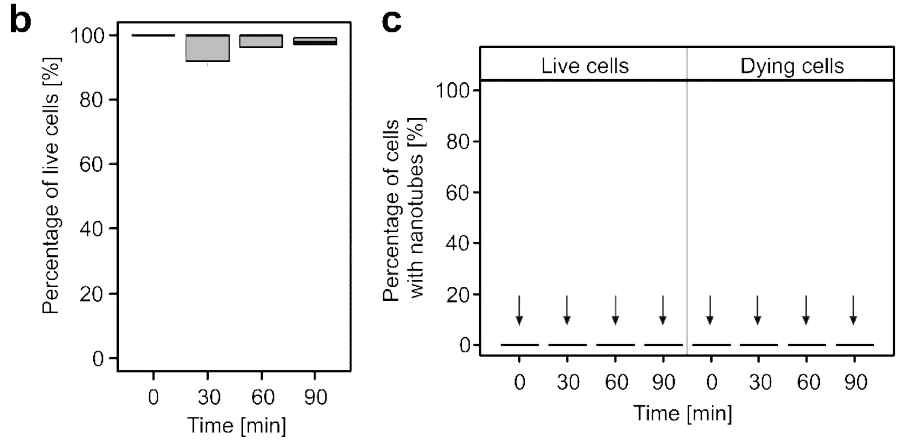

Supplementary Figure 8 | Time-lapse images of *B. subtilis* cells grown in frames on LB agarose without antibiotic supplementation at 37 °C.

(**a**) Exponentially growing wt cells (LK1432) were stained with Nile Red (red) and spotted on LB agar in gene frames (*i.e.* 'no pressure' conditions) containing SYTOX green (green). Pictures were taken every 30 minutes and the numbers of live/dying cells and the numbers of NTs emerging from live/dying cells were counted and are shown below the images (summary of 3 independent biological repeats). Scale bar=5 µm.

(**b**) Box plot shows the percentage of live cells at indicated time points. The differences are not statistically significant. The data are from 3 biological replicates.
Box plots were plotted with default R setting: center line = median; vertical size of the boxes = interquartile range (IQR); box limits = upper and lower quartiles; whiskers = 1.5x interquartile range (1.5×IQR).

(**c**) Quantification of the presence/absence of NTs at the indicated time points. Quantification of NTs was based on the Nile Red signal. The values are in all cases 0 as no NTs were detected with this technique. The vertical arrows in the graph indicate zero values in all replicates. Data represent 3 biological replicates. Box plots are defined as in chart b.

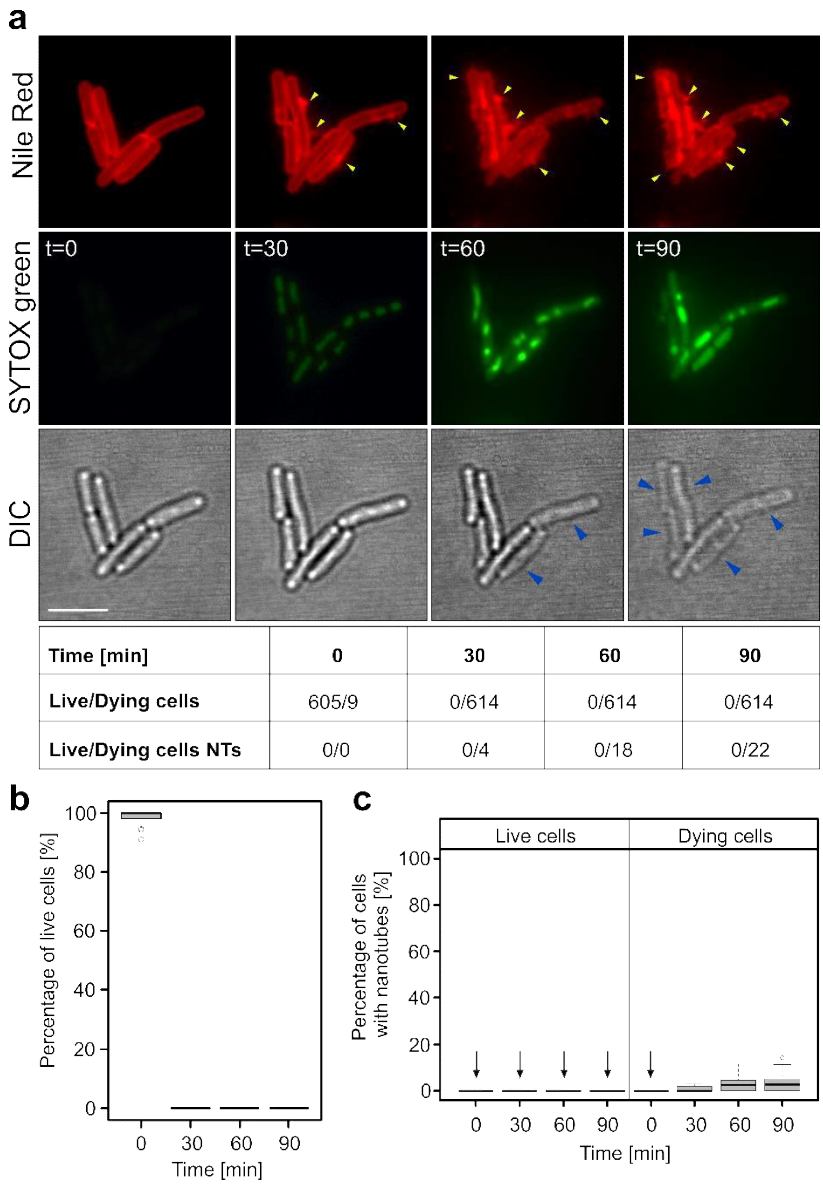

Time [min]	0	30	60	90
Live/Dying cells	605/9	0/614	0/614	0/614
Live/Dying cells NTs	0/0	0/4	0/18	0/22

Supplementary Figure 9 | Time-lapse images of *B. subtilis* cells grown in frames on LB agarose supplemented with ampicillin at 37 °C.

(**a**) Exponentially growing wt cells (LK1432) were stained with Nile Red (red) and spotted on LB agar containing ampicillin (500 µg/ml) and SYTOX green (green) in gene frames (*i.e.* 'no pressure' conditions). Pictures were taken every 30 minutes and the numbers of live/dying cells and the numbers of NTs emerging from live/dying cells were counted and are shown below the images (summary of 3 independent biological repeats). Yellow arrows indicate membrane blebs and vesicles. Dark blue arrows indicate dying cells in DIC images. Scale bar=5 µm. The data are from 3 biological replicates.

(**b**) Box plot shows the percentage of live cells at indicated time points, decreasing over time ($p < 0.001$, GLM, two-sided, $z = -24$, 95% CI OR = 0.01 – 0.03). Box plots were plotted with default R setting: center line = median; vertical size of the boxes = interquartile range (IQR); box limits = upper and lower quartiles; whiskers = 1.5x interquartile range (1.5×IQR); points (open circles) = outliers.

(**c**) Quantification of the presence/absence of NTs at the indicated time points. Quantification of NTs was based on the Nile Red signal. The percentage of NTs is expressed relative to the number of dying (SYTOX positive) or live (SYTOX negative) cells, which was set as 100% (e. g. out of the 10% of dying cells, 20% formed NTs – that is 2% of the total number of cells). The percentage of NTs of dying cells increases over time ($p = 0.001$, GLM, two-sided, $z = 3.2$, 95% CI OR = 1.3 – 2.8). The vertical arrows in the graph indicate zero values in all replicates. Data represent 3 biological replicates. Box plots are defined as in chart b.

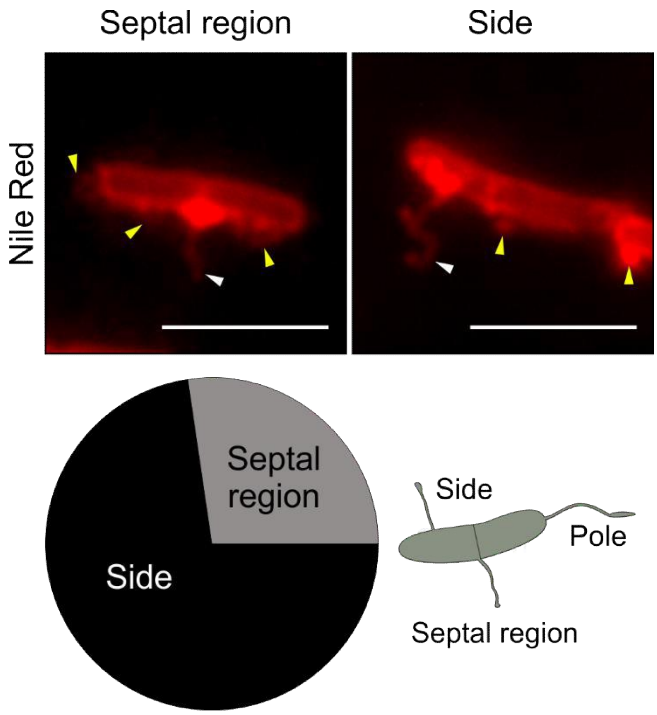

Supplementary Figure 10 | Quantification of the sites of NT origin after ampicillin treatment.

Dying wt cells (LK1432) containing NTs were analyzed with respect to the position on NT attachment (polar, septal, from sides). The cells were stained with Nile Red to visualize membranous structures. White arrows indicate NTs. Yellow arrows indicate membrane blebs. Scale bar=5 µm. A total of 22 cells were analyzed, selected from 3 biological replicates, with similar results in each replicate. The overall trend is shown in the pie chart: No NTs emanating from the cell poles were found. NTs originating from the sides prevailed (16 NTs) over NTs formed from septa (6 NTs).

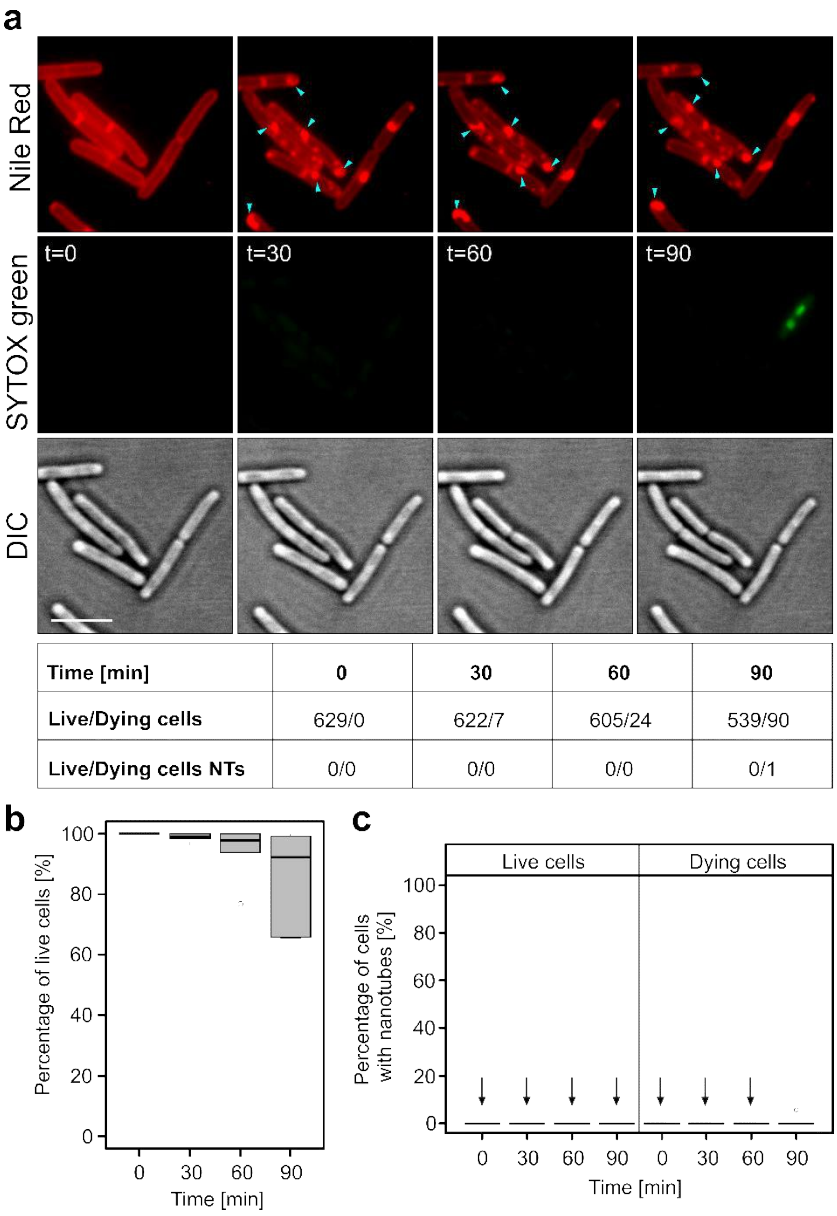

Time [min]	0	30	60	90
Live/Dying cells	629/0	622/7	605/24	539/90
Live/Dying cells NTs	0/0	0/0	0/0	0/1

Supplementary Figure 11 | Time-lapse images of *B. subtilis* cells grown in frames on LB agarose supplemented with chloramphenicol at 37 °C.

(**a**) Exponentially growing wt cells (LK1432) were stained with Nile Red (red) and spotted on LB agar containing chloramphenicol (5 µg/ml) and SYTOX green (green) in gene frames (*i.e.* 'no pressure' conditions). Pictures were taken every 30 minutes and the numbers of live/dying cells and the numbers of NTs emerging from live/dying cells were counted and are shown below the images (summary of 3 independent biological repeats). Light blue arrows indicate dying cells in DIC images. Scale bar=5 µm.

(**b**) Box plot shows the percentage of live cells at indicated time points, decreasing over time ($p < 0.001$, GLM, two-sided, $z = -9$, 95% CI OR = 0.16 – 0.30). Box plots were plotted with default R setting: center line = median; vertical size of the boxes = interquartile range (IQR); box limits = upper and lower quartiles; whiskers = 1.5x interquartile range (1.5×IQR); points (open circles) = outliers. The data are from 3 independent biological replicates.

(**c**) Quantification of the presence/absence of NTs at the indicated time points. Quantification of NTs was based on the Nile Red signal. The values are in all but one case 0 as no NTs were detected at these time points. The only exception is the last time point (dying cells) where a single NT was detected. The vertical arrows in the graph indicate zero values in all replicates. Data represent 3 independent biological replicates. Box plots are defined as in chart b.

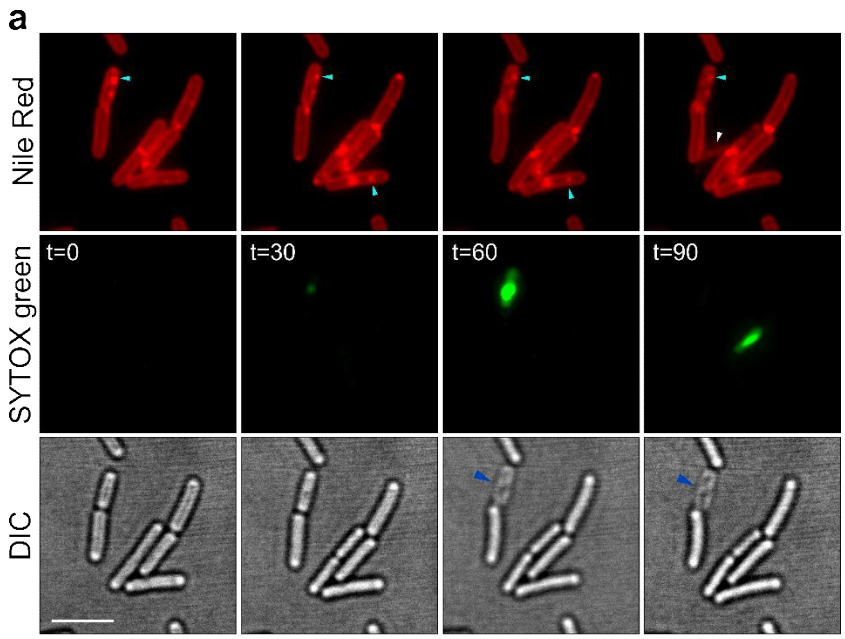

Time [min]	0	30	60	90
Live/Dying cells	749/0	739/10	729/20	693/56
Live/Dying cells NTs	0/0	0/0	0/0	0/1

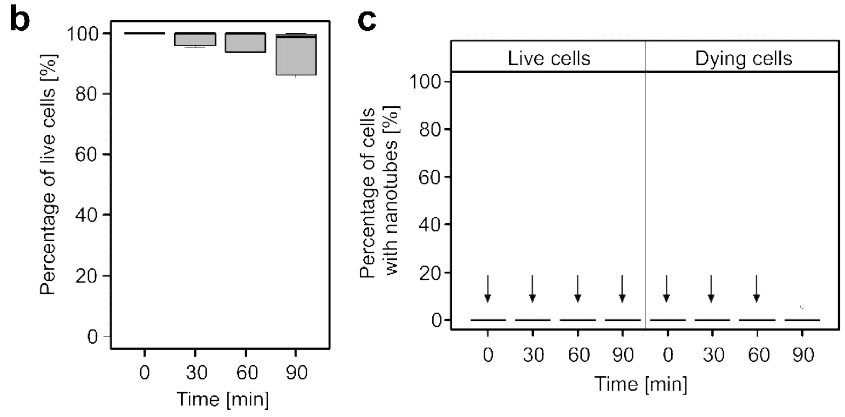

Supplementary Figure 12 | Time-lapse images of *B. subtilis* cells grown in frames on LB agarose supplemented with rifampicin at 37 °C.

(**a**) Exponentially growing wt cells (LK1432) were stained with Nile Red (red) and spotted on LB agar containing rifampicin (50 µg/ml) and SYTOX green (green) in gene frames (*i.e.* 'no pressure' conditions). Pictures were taken every 30 minutes and the numbers of live/dying cells and the numbers of NTs emerging from live/dying cells were counted and are shown below the images (summary of 3 independent biological repeats). Light blue arrows indicate impaired membranes, white arrow indicates nanotube, dark blue arrows indicate dying cells in DIC images. Scale bar=5 µm.

(**b**) Box plot shows the percentage of live cells at indicated time points, decreasing over time ($p < 0.001$, GLM, two-sided, $z = -7$, 95% CI OR = 0.24 – 0.43). The data are from 3 independent biological replicates. Box plots were plotted with default R setting: center line = median; vertical size of the boxes = interquartile range (IQR); box limits = upper and lower quartiles; whiskers = 1.5x interquartile range (1.5×IQR).

(**c**) Quantification of the presence/absence of NTs at the indicated time points. Quantification of NTs was based on the Nile Red signal. Quantification of NTs was based on the Nile Red signal. The values are in all but one case 0 as no NTs were detected at these time points. The only exception is the last time point (dying cells) where a single NT was detected. The vertical arrows in the graph indicate zero values in all replicates. Data represent 3 independent biological replicates. Box plots are defined as in chart b; the point (open circle) = outlier.

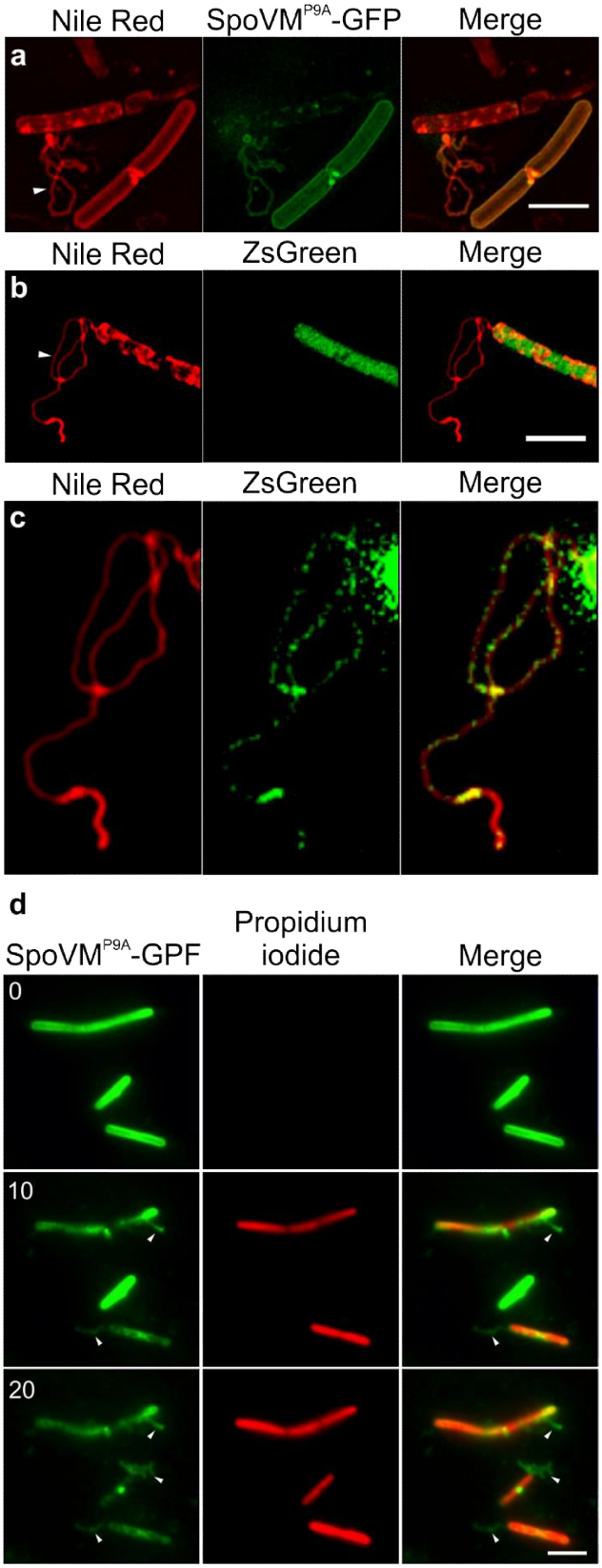

Supplementary Figure 13 | SpoVM^{P9A}-GFP and GFP localize to NTs.

(**a-c**) Exponentially growing *B. subtilis* cells prepared by the P-GLG method and observed by SIM. Membranes were stained with Nile Red (red), ZsGreen and SpoVM^{P9A} (green). White arrows indicate NTs. Scale bar=2.5 µm.

(**a**) Strain LK2525 harboring a mutated variant of the SpoVM protein (SpoVM^{P9A}) that binds indiscriminately to cell membranes[2].

(**b**) Strain LK2375 producing free cytosolic ZsGreen (green fluorescence protein[3]. The brightness and contrast in panels **a** and **b** are identical. At these settings, free GFP was not detected in the NT.

(**c**) Brightness was adjusted relative to panel **b** to visualize ZsGreen in the NT.

(**d**) Fluorescence microscopy. The SpoVM^{P9A}-GFP (LK2525) strain was grown in the presence of 1mM IPTG into exponential phase. Cells were harvested and re-suspended in 1× PBS containing Propidium iodide. The sample was prepared by the GLG method. Pictures were taken after 0, 10 and 20 minutes. Propidium iodide (red) revealed that the bacterial population began to die after 10 minutes. Dying cells formed tubular structures (white arrows) that were full of the SpoVM^{P9A}-GFP (green) membrane protein. Interestingly, we again observed SpoVM^{P9A}-GFP signal decay in cell during NT production, which suggests that SpoVM^{P9A}-GFP is extruded into the extracellular space together with (bound to) the membrane. Scale bar=5 µm.

Experiments in panels a-d were conducted in 3 biological replicates with similar results.

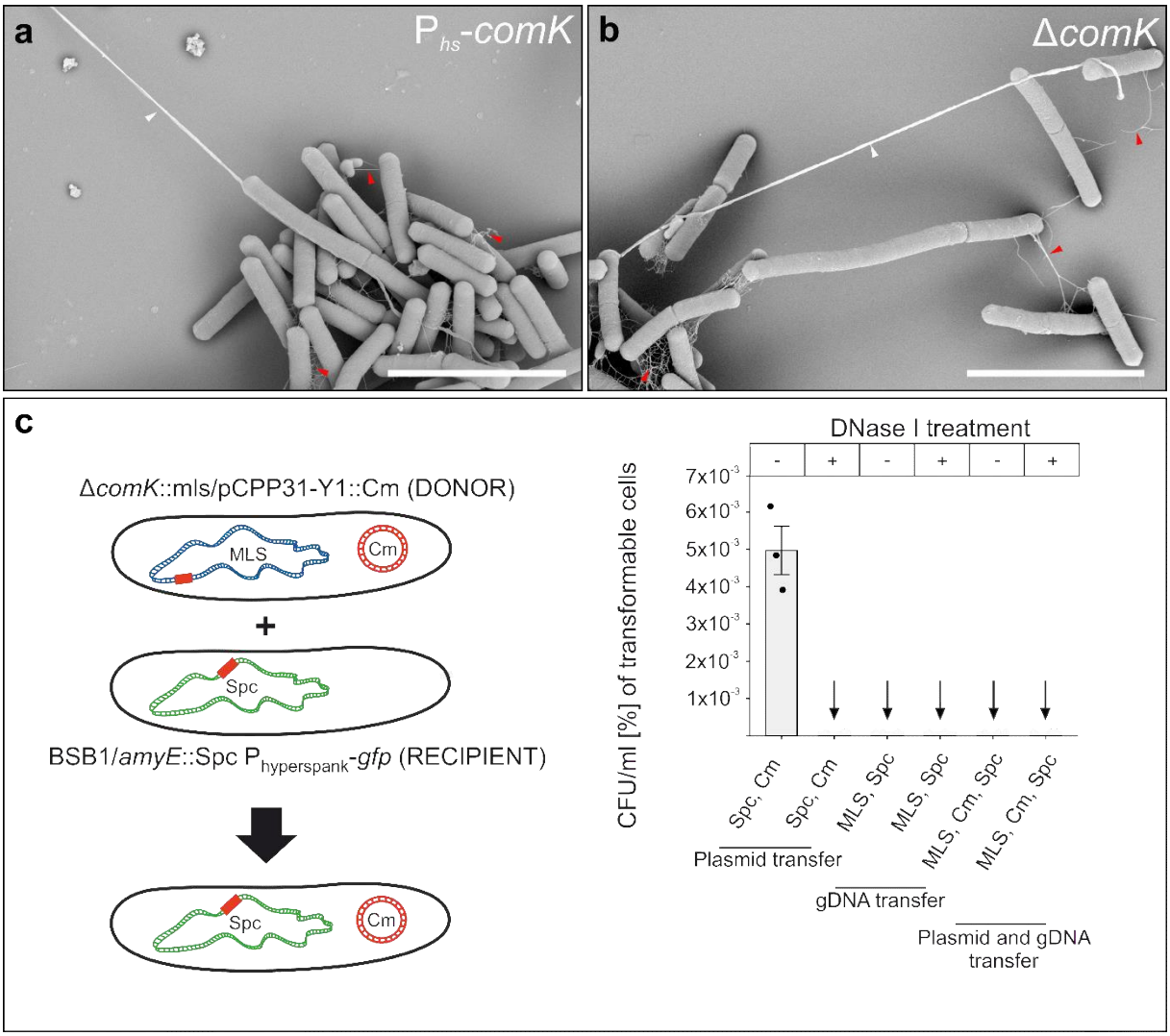

Supplementary Figure 14 | Distinguishing plasmid transfer from gDNA transfer.

(**a**-**b**) A SEM analysis of $P_{hyperspank}$-*comK* and Δ*comK* exponentially growing cells reveal that NTs formed by these strains were the same as those formed by wt. White arrows indicate nanotubes; Red arrows indicate flagella. The scale bar=5 µm. The experiment was conducted in 2 biological replicates with similar results.

(**c**) The donor strain (LK2392, Δ*comK*::mls/pCPP31-Y1::cm) was cocultivated with recipient strain (LK2398, *amyE*::Spc $P_{hyperspank}$-*gfp*) for 4 hours in LB without antibiotics. Double-resistant colonies were selected on LB agar plates containing appropriate antibiotics. We did not obtain any colonies on LB supplemented with MLS+Cm+ Spc or MLS+Spc. Double resistant colonies were obtained only on LB with Spc+Cm, which suggests non-conjugative plasmid transfer but not gDNA transfer. Importantly, the DNA transfer was abolished by DNase I treatment. The difference between Spc+Cm in the DNase- condition and all other conditions is statistically significant ($p < 0.001$). The bars are averages from three biological replicates and error bars show ±SEM.

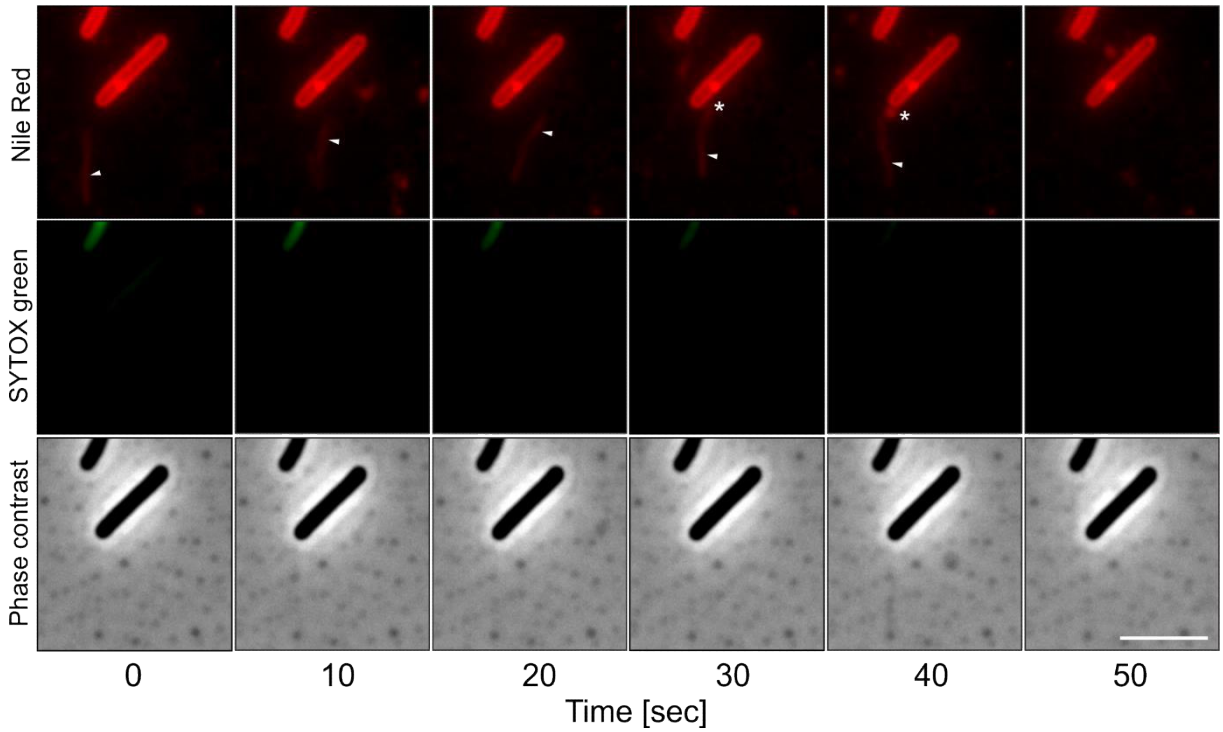

Supplementary Figure 15 | Nanotubes 'connected' to a living cell.

Time-lapse images of wt *B. subtilis* (LK1432) prepared by the P-GLG method. In some cases, after NT formation tubules are torn apart and dragged around by the capillary forces within the sample liquid. This NT fragment can be captured by a living cell, creating the illusion of an NT extruded from a living cell (white asterisk). The white arrows indicate the moving NT. Scale bar=5 µm. Experiment was conducted in at least 3 biological replicates with similar results.

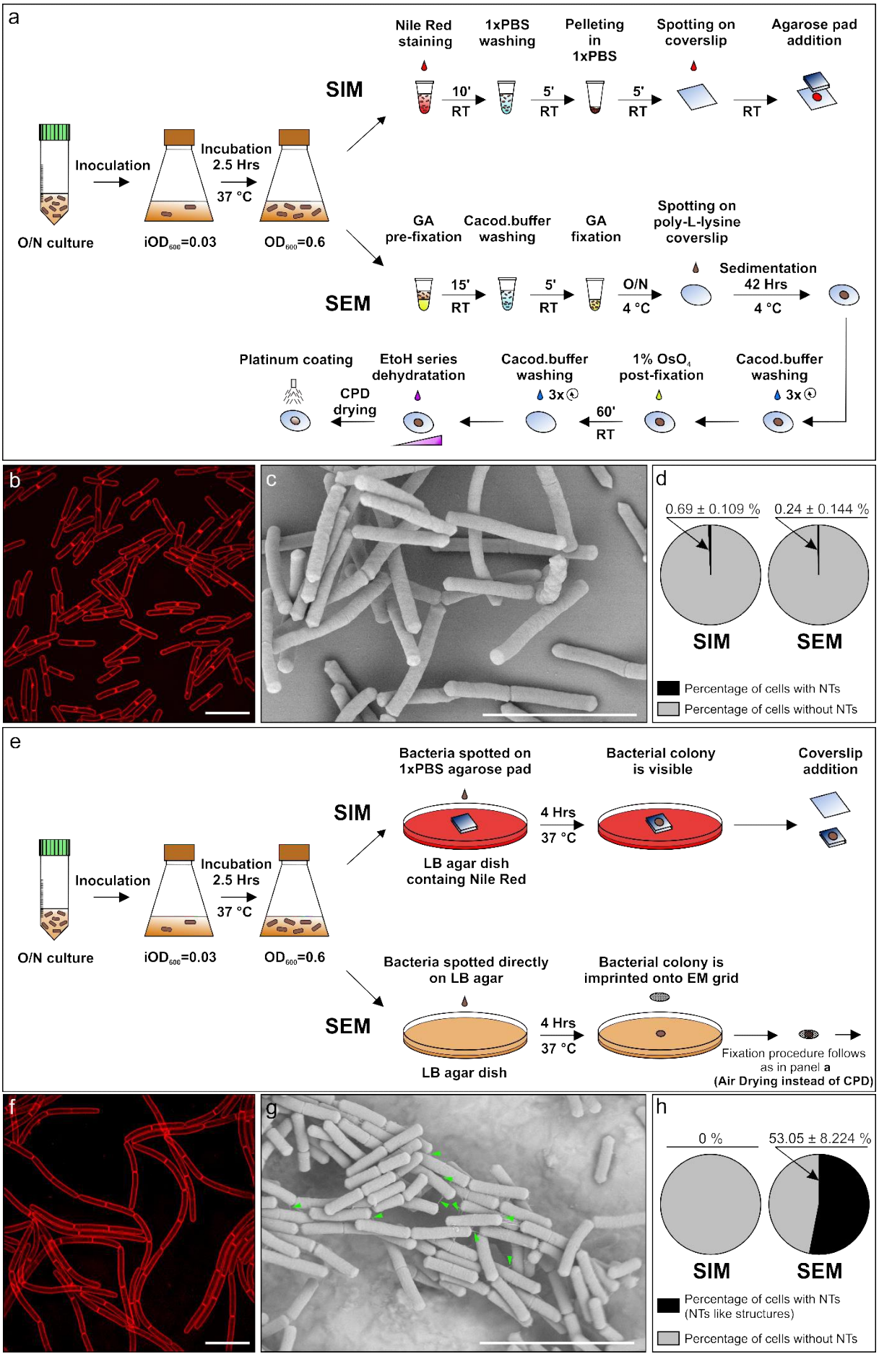
a
Nile Red staining
1xPBS washing
Pelleting in 1xPBS
Spotting on coverslip
Agarose pad addition
SIM
10' RT
5' RT
5' RT
RT
Inoculation
Incubation 2.5 Hrs 37 °C
O/N culture
iOD600=0.03
OD600=0.6
GA pre-fixation
Cacod.buffer washing
GA fixation
Spotting on poly-L-lysine coverslip
SEM
15' RT
5' RT
O/N 4 °C
Sedimentation 42 Hrs 4 °C
Platinum coating
EtoH series dehydratation
Cacod.buffer washing 3x
1% OsO4 post-fixation
Cacod.buffer washing 3x
CPD drying
60' RT
b
c
d
0.69 ± 0.109 %
0.24 ± 0.144 %
SIM
SEM
Percentage of cells with NTs
Percentage of cells without NTs
e
Bacteria spotted on 1xPBS agarose pad
Bacterial colony is visible
Coverslip addition
SIM
4 Hrs 37 °C
LB agar dish containg Nile Red
Inoculation
Incubation 2.5 Hrs 37 °C
O/N culture
iOD600=0.03
OD600=0.6
Bacteria spotted directly on LB agar
Bacterial colony is imprinted onto EM grid
SEM
4 Hrs 37 °C
LB agar dish
Fixation procedure follows as in panel a (Air Drying instead of CPD)
f
g
h
0 %
53.05 ± 8.224 %
SIM
SEM
Percentage of cells with NTs (NTs like structures)
Percentage of cells without NTs

Supplementary Figure 16 | Sample preparation of bacteria grown in liquid media or on solid media.

(**a**) Scheme of sample preparation of bacteria grown in liquid media. Bacteria were inoculated from glycerine stocks into 10 ml of LB media with appropriate antibiotics and grown overnight (O/N). Next day, bacteria were inoculated at **i**nitial **O**ptical **D**ensity 0.03 (iOD_{600}) into 10 ml of fresh LB media without any antibiotic. The cultures were grown until mid-logarithmic phase (OD_{600}=0.6). For **SIM**, 1 ml of the bacterial culture was withdrawn and Nile Red was added at a final concentration of 10 µg/ml. After 10 minutes of incubation at room temperature (RT), bacteria were pelleted by centrifugation (6,000× g, 5 min at RT) and washed once with 1× PBS. Subsequently, bacteria were pelleted again a resuspended in 50 µl of 1× PBS. 3 µl of cell suspension were spotted on an uncoated coverslip and covered with a thin (ca 3 mm) 1× PBS agarose pad. The coverslip was placed into a holder and the sample was observed using DeltaVision OMX™. Alternatively - for **SEM** - cells were grown in the same way but immediately fixed. 0.5 ml of exponentially growing cells was added to 0.5 ml of 6% glutaraldehyde (GA pre-fixation). After 15 minutes of incubation at RT, bacteria were pelleted (6,000× g, 5 min at RT) and washed once with cacodylate buffer. Then, the sample was pelleted again, resuspended in 0.5 ml of 3% glutaraldehyde (GA fixation) and kept at 4 °C, O/N. Next day, the sample was spotted on a poly-L-lysine-treated circular glass coverslip and sedimented at 4°C in a Petri-dish moist chamber for 42 h. The cells attached to the coverslip were washed three times with the cacodylate buffer and postfixed in 1% OsO_4 for one hour at room temperature and subsequently washed three times with the cacodylate buffer. The coverslips were dehydrated through a graded ethanol series (25%, 50%, 75%, 90%, 96%, 100% and 100%) followed by absolute acetone and critical point-dried (CPD) in a K850 Critical Point Dryer. The dried samples were sputter-coated with 3 nm of platinum. The sample was observed using a FEI Nova NanoSEM scanning electron microscope.

(**b**) Membrane stained planktonic cells display few, if any, NTs. This large SIM field of Nile Red stained wt *B. subtilis* (LK1432) represents a typical picture. No NTs are visible in this field. Scale bar=5 µm. For examples of NTs that were identified by SIM see Supplementary Data Fig. 1f-g and Fig. 13. The experiment was conducted in at least 3 biological replicates with similar results.

(**c**) Planktonic culture of *B. subtilis* analyzed by SEM. Δ*hag* (LK1966, non-flagellated strain) cells were used to simplify interpretation. As in SIM, few, if any, tubular structure were detected. The picture represents a typical SEM field and contains no tubular structures. In rare cases, however, tubular structures were detected. Scale bar=5 µm. To view a larger field (in terms of cells) that also contains a single NT, see Supplementary Data Fig. 1c. The experiment was conducted in at least 3 biological replicates with similar results.

(**d**) Quantification of NTs based on SIM and SEM methods. For each method, ca 1,000 cells (from three independent replicates) were analyzed for NT presence. For SIM, NTs were detected based on the Nile Red fluorescence signal and thus only membranous tubular structures were strictly quantified. For SEM, “thick” (ca 77 nm – see Supplementary Data Fig. 6c) tubular structures (marked with white arrows in SEM figures) were counted as NTs. The pie chart represents 100%. Grey, cells without NTs; Black, cells with NTs (this percentage including ±SEM is indicated above each chart; the difference between the percentages is not statistically significant).

(**e**) Scheme of sample preparation of bacteria grown on solid media. Bacteria were inoculated from glycerine stocks into 10 ml of LB media with appropriate antibiotics and grown O/N. Next day, bacteria were inoculated at initial optical density 0.03 (iOD_{600}) into 10 ml of fresh LB without any antibiotics. Then, the culture was grown until mid-logarithmic phase (OD_{600}=0.6). For SIM, an exponential culture was 10x diluted in 1× PBS and 2 µl were spotted on a 1× PBS agarose pad lying on LB agar containing Nile Red (final conc. 20 µg/ml). Cells were then incubated at 37 °C for 4 hours in dark. Subsequently, the agarose pad containing the bacterial colony (that grew from the spotted culture) was removed from the dish and covered with an uncoated coverslip. The coverslip was placed into a holder and the sample was observed using DeltaVision OMX™. Alternatively - for SEM - cells were grown in the same way but bacteria were spotted directly on LB agar (without Nile Red). After four hours, a bacterial colony was imprinted onto a Electron microscopy (EM) grid. The following fixation procedure was identical as in panel a, except for the drying technique (air drying was used instead of CPD drying).

(**f**) SIM analysis of wt *B. subtilis* (LK1432) grown on solid media and stained by Nile Red. No NTs were detected. Scale bar=5 µm. The experiment was conducted in at least 3 biological replicates with similar results.

(**g**) SEM analysis of *B. subtilis* (LK1966, non-flagellated strain) grown on solid media. Numerous structures were identified between cells (green arrows). However, these structures were not identified by membrane staining (SIM) and thus they are unlikely to be made of membranes. Scale bar=5 µm. The experiment was conducted in at least 3 biological replicates with similar results.

(**h**) Quantification of NTs (or NT-like structures) emerging from cells cultured on solid medium and observed with SIM and SEM methods. For each method, ca 300 cells (from three independent replicates) were analyzed for NT presence. For SIM, no NTs were detected based on Nile Red fluorescence signal. For SEM, tubular filamentous structures were quantified (marked with green arrows in panel g). We stress that all these structures are unlikely to be NTs as this method is unable to distinguish between tubular structures of different origin (hence the term 'NT-like'). The pie chart represents 100%. Grey, cells without NTs; Black, cells with NTs/NT-like structures (this percentage including ±SEM is indicated above each chart; the difference between the SIM and SEM results is statistically significant [$p < 0.001$, GLM, two-sided, $z = 8$, 95% CI OR = 47 - 516]).

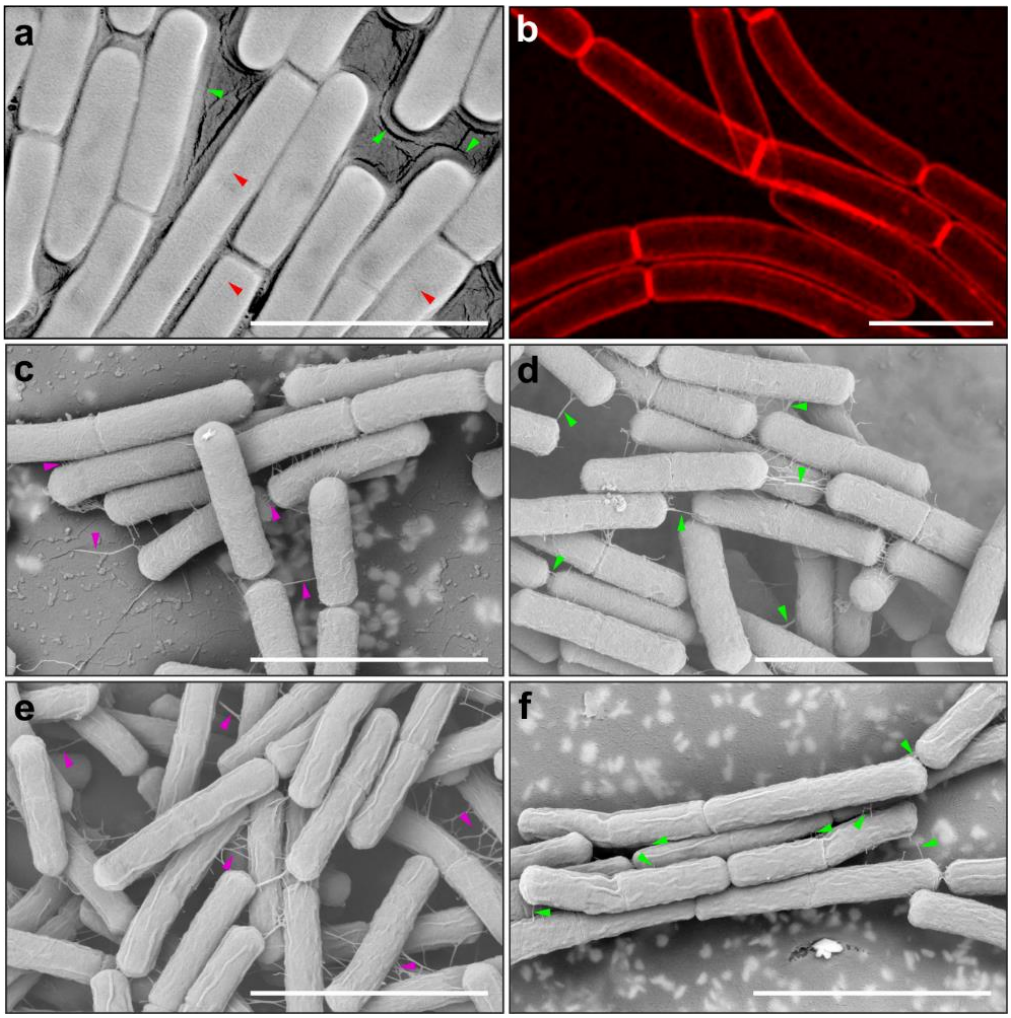

Supplementary Figure 17 | Comparison of various methods for observing bacteria.

(**a**) wt *B. subtilis* (LK1432) grown on LB agar covered with cellophane for 4 hours at 37 °C. The cellophane containing bacteria was carefully removed and fixed and coated for SEM. An intact layer of extracellular matrix (green arrows) and likely flagella (red arrows) are clearly visible. Scale bar=3 µm.

(**b**) wt *B. subtilis* (LK1432) grown on a thin layer of a 1× PBS agarose pad lying atop LB agar containing Nile Red for 4 hours. The 1×PBS agarose pad was covered with a coverslip and observed by SIM. Membranes were stained with Nile Red (red). No membranous structures were observed in the extracellular space. Scale bar=3 µm.

(**c**) wt *B. subtilis* (LK1432) grown in the same way as for SIM analysis. After 4 hours, bacteria were imprinted on EM grids, fixed and coated. SEM showed tubular structures – flagella and possibly filaments made of extracellular matrix (magenta arrows). Scale bar=3 µm.

(**d**) Δ*hag* (LK1966) grown and imaged in the same way as in panel **c**. As the strain lacks flagella, the green arrows show likely filaments made of disrupted extracellular matrix. Scale bar=3 µm.

(**e**) wt *B. subtilis* (LK1432) grown for 4 hours on nitrocellulose membrane-supported EM grids. After 4 hours, bacteria were fixed and coated. As in panel **c**, SEM showed tubular structures – flagella and possibly filaments made of extracellular matrix (magenta arrows). Scale bar=3 µm.

(**f**) Δ*hag* (LK1966) grown and imaged in the same way as in panel **e**. As the strain lacks flagella, the green arrows show likely filaments made of disrupted extracellular matrix. Scale bar=3 µm.

All experiments (panels a-f) were conducted in 3 biological replicates.

Supplementary Table 1 | List of strains used in this study

Experimental Models: Organisms/Strains	**Source**
LK1432 (*B. subtilis* BSB1 wt-derivative 168 trp$^+$)	[4]
LK1629 (*B. subtilis* PY79 wt-derivative 168 trp$^+$)	[5]
LK1780 (*B. megaterium* wt CCM3380)	Czech Collection of Microorganisms (CCM)
LK1553 (*D. raidodurans* R1 wt ATCC-BAA816)	[6]
LK1133 (*E. coli* wt K12 KW72)	[7]
GP902 (*B. subtilis* 168 trpC2-Δ*hag::tet*)	[8]
LK1966 (LK1432 was transformed with WN1237 gDNA-Δ*hag::tet*)	This study
DS1895 (*B. subtilis* PY79-*amyE::*P*hag-hag^{T209C}::spc*)	[1]
LK2052 (LK1432 was transformed with DS1895 gDNA-*amyE::Phag-hag^{T209C}::spc*	This study
WN1237 (WN716-Δ*sigD::kan*)	[9]
LK1873 (LK1432 was transformed with WN1237 gDNA-Δ*sigD*::*kan*)	This study
LK1550 (*B. subtilis* BSB1-Δ*sigI* Δ*rsgI::spc*)	[10]
QB5344 (*B. subtilis* 168 trpC2-Δ*sigB::cat*)	J. Stülke
LK2218 (LK1432 was transformed with QB5344 gDNA – Δ*sigB::cat*)	This study
BSU2007 (*B. subtilis* 168 trpC2 Marburg-*ΔsigY* Δ*sigZ* Δ*sigV* Δ*ylaC* Δ*sigX* Δ*sigM* Δ*sigW*)	[11]
1A771 (*B. subtilis* MO1099 trpC2 pheA1- *amyE::ery*)	[12]
LK1922 (LK1432 was transformed with 1A771 gDNA-*amyE::ery*)	This study
LK1925 (LK1432 harboring pCPP31-Y1::*neo, cat*)	This study
LK2317 (LK1432 *amyE::Phyperspank-comK::spc*)	This study
BKE1042 (*B. subtilis* 168 trpC2-Δ*comK::ery*)	[13]
LK2380 (LK1432 was transformed with BKE1042 gDNA-Δ*comK::ery)*	This study
LK1940 (LK1873 Δ*sigD::kan* transformed with 1A771 gDNA-*amyE::ery*)	This study
LK1944 (LK1873 Δ*sigD::kan* harboring pCPP31-Y1::neo, cat)	This study
LK2392 (LK1925 was transformed with BKE1042 gDNA-Δ*comK::ery*)	This study
SB444 (*B. subtilis* PY79-*amyE::*P*hyperspank-gfp::spc*)	[14]
LK2078 (LK1432 was transformed with SB444 gDNA- *amyE::*P*hyperspank-gfp::spc*)	This study
KR318 (*B. subtilis* PY79-*amyE::*P*hyperspank-spoVM^{P9A}-gfp::spc*)	[2]
LK2525 (LK1432 was transformed with KR318 gDNA- *amyE::*P*hyperspank-spoVM^{P9A}-gfp::spc*)	This study

LK2375 (LK1432 harboring pHY300-P*veg-ZsGreen-term*)	This study
DS1447 (*B. subtilis* 3610- Δ*lytF::tet*)	[15]
LK2125 (LK1432 was transformed with DS1447 gDNA- Δ*lytF::tet*)	This study
BKE09420 (*B. subtilis* 168 trpC2-*ΔlytE::ery*)	[13]
LK2290 (LK2125 Δ*lytF::tet* was transformed with BKE09420 gDNA-Δ*lytE::mls*)	This study
Recombinant DNA (plasmids)	
pCPP31-Y1 (Cm^r, Neo^r)	[16]
pHY300 (P*veg*-ZsGreen-term, Tet^r)	[3]
pDR111 (P*hyperspank-comK*, Amp^r, $Spec^r$)	[17]

Supplementary Table 2 | List of primers used in this study.

No.	SEQUENCE (5'-3')	USAGE
Primers for verification of genes deletion		
LK1010	GGGAATTCCATATGCAATCCTTGAATTATGAAGATC	verification of Δ*sigD*
LK1011	CCGCTCGAGTCATTATTGTATCACTTTTTCC	verification of Δ*sigD*
LK1004	GGAATTCCATATGACACAACCATCAAAAAC	verification of Δ*sigB*
LK1005	CCGCTCGAGTCATTACATTAACTCCATCGA	verification of Δ*sigB*
LK1164	GGAATTCCATATGGTGAAACCAGTGCTTAGCC	verification of Δ*sigI*
LK1165	CCGCTCGAGTCATGAGTGCAGCACCCC	verification of Δ*sigI*
LK2322	AGCGCTTAACACACTGAACCGTTTGTCTTC	verification of Δ*hag*
LK2323	TTGAAGTACGTTTTGCGGCTGTTGGTTTGC	verification of Δ*hag*
LK2490	GTTACCTCGGTGCGAAAAGATTCTAA	verification of Δ*lytE*
LK2491	ATGAAAAAGCAAATCATTACAGCTACG	verification of Δ*lytE*
LK2680	ATGAAAAAGAAATTAGCAGCAGGG	verification of Δ*lytF*
LK2681	TTAGAAATATCGTTTTGCACCGAG	verification of Δ*lytF*
LK2826	AGTCAGAAAACAGACGCACCTTTAGAATCG	verification of *comK* integration into *amyE* site
LK2827	CTAATACCGTTCCCCGAGCTCACGCAAAAT	verification of *comK* integration into *amyE* site
LK3172	ATGAACGAGAAAAATATAAAACAC	verification of *erm* gene in *amyE* site
LK3173	TTACTTATTAAATAATTTATAGCT	verification of *erm* gene in *amyE* site
Primers for qPCR: SEQUENCE (5'-3')		
LK1281	TACGTAATACGACTCACTATAGGGAGACAGCTCGTGTCGTGAGATGT	Preparation of recovery marker
LK1282	CGTTGCTGATCTGCGATTAC	Preparation of recovery marker
LK2910	GAAGTGAACGGCGCAACAAT	*comK* qPCR
LK2911	CTGTCGACAATTTGCAGCGG	*comK* qPCR
LK2618	TCATGTTGCCAGCACGTTAT	recovery marker qPCR
LK2619	AAGGGGCATGATGACTTGAC	recovery marker qPCR

Supplementary Table 3 | Proteins identified by MS analysis as part of the group 'Enriched proteins in Δ*sigD* strain' (t-value ≤ -2).

Enriched proteins in Δ*sigD* strain	
Functional group	Name
ABC Transporters	BmrA, YhaP, MetP, MntA, MntB, YtrE, FtsX, OppA, OppF, RbsC, TcyB, TcyC, YwjA, OpuAA, OpuAC, OpuD, ArtQ, YbaE, YclO, YclP, YclQ, YwrB, YrhG, GltT, CopA, MgtE, GlpF, GlpT, NupC, MleN, PutP, Mdr, AlsT
ATP synthesis	AtpB, AtpC, AtpH, AtpE, Pgk, Pyk
Biosynthesis of cofactors	NadE, MenH, HemQ
Lipid metabolism	PgsA, PlsY
Biosynthesis/ acquisition of amino acids	GlnA, CysK, GlyA, CysE
Biosynthesis/ acquisition of nucleotides	GuaA, GuaB
Carbon metabolism	PfkA, CitB, FbaA, PdhB, PdhC, Eno, Pta, Tkt, Mdh, Pgi
Cell division	SepF, RasP, DivIB
Cell envelope stress proteins (controlled by SigM, V, W, X, Y)	YteJ, YqfB
Cell shape	RodZ, MreC
Cell wall degradation/ turnover	GamP, LytE
Cell wall synthesis	PgcA, TagG, TagV, MurAA, MurD
Cell wall/ other	WalK, YycH
DNA condensation/ segregation	Hbs, Soj
DNA repair/ recombination	RuvA, PnpA
Electron transport/ other	TrxA, Fer
General stress proteins (controlled by SigB)	YitT, SodA
Chaperones/ protein folding	GrpE, GroES
Membrane dynamics	FloT
Metabolism of signaling nucleotides	CdaR, GdpP
Motility and chemotaxis	YcdA, MotP
Proteins of unknown function	YfmQ, YbfF, YrbF, YvbI, YjhA, YxaI, YneF, YpmS, YwnC, YheA, YerA, YukB, YukE, YugP, YhbJ, YlmG, YdjN, YtkA, YqfF, YvfG, YukC
Phage-related functions	YueB
Phosphate metabolism	PhoR
Phosphorelay	YaaT
Phosphotransferase systems	NagP, SacP, PtsG, TreP, BglP, FruA
Protein modification	Lgt
Protein secretion	SecDF, SecG, SecY, SipS, SipT, SpoIIIJ, LspA, YacD
Regulators of electron transport	ResE
Resistance against oxidative and electrophile stress	Tpx
Respiration	QoxB, NarH, QcrB
RNA chaperones	CspD

Regulation of gene expression	AbrB, Abh, YhcB, RsiX
Sporulation proteins	YlbC
Translation	GatA, YlaG, Tgt, YtpR, RplC, RplL, RplT, RplU, GltX, TyrS, MetS, IleS, Frr, LysS
Utilization of amino acids	AnsB, Bcd, Ald, Pdp
Utilization of specific carbon sources	YtsJ, GlpK, RbsK, MleA

Supplementary Table 4 | Proteins identified by MS analysis as part of the group 'Membrane fraction proteins in both wt and Δ*sigD*' (t-value [2,-2]).

Membrane fraction proteins in both wt and Δ*sigD*	
ABC Transporters	ArtP, EcsA, FeuA, FhuC, FhuD, FtsE, MetN, MetQ, MsmX, OppC, OpuAB, PstBA, PstS, RbsA, RbsB, RbsD, SufC, TcyA, YbxA, YckB, YdbJ, YfiY, YfmC, YfmM, YhaQ, YhcH, YhfQ, YknW, YknX, YkpA, YtrB, YtrF, YusV, YvgL, YvrC, YxeB, YybJ, ZnuA, ZnuC
Electron transport and ATP synthesis	AckA, AtpA, AtpD, AtpF, AtpG, SucC, Rex, ResD, EtfA, YumC, YojN, YutJ
Biosynthesis of cofactors	GsaB, HemB, HemY, HepT, LipA, MenB, PanB, PdxK, PdxS, RibH
Lipid metabolism	AccA, AccB, AccC, AccD, AcpA, FabG, FabI, FabL, GpsA, IspG, PlsC, PlsX, Psd
Biosynthesis/ acquisition of amino acids	AroA, AsnB, AspB, DapA, DapG, MetK, MtnA, MtnK, ProA, Prs, SerA
Biosynthesis/ acquisition of nucleotides	Adk, Dra, Gmk, Ndk, NrdF, PupG, PurA, PyrAB, PyrG, PyrH, Tmk, Udk, Upp
Carbon metabolism	CggR, CitG, CitZ, GapA, GapB, GlpX, GndA, Icd, OdhA, OdhB, PckA, PdhA, PdhD, Pgm, PycA, SdhA, SdhB, SdhC, Tpi, YqfL, YwjH, Zwf, AcoA, AcoB, AcoL, AcsA, FruC, GalE, GalK, GlpD, GntZ, IolS, LicH, LutB, MalK, MalR, TreA
Cell division	EzrA, FtsA, FtsH, FtsZ, GpsB, MinD, Noc
Cell envelope stress proteins (controlled by SigM, V, W, X, Y)	PspA, YaaN, YdbS, YebC, YoaF, YobJ, YpuA
Cell shape	Mbl, MreB
Cell wall degradation/ turnover	IseA, LytC, LytG
Cell wall synthesis	DacA, Ddl, DltA, DltC, DltD, GgaB, GlmM, GlmS, GtaB, LtaS, MurB, MurC, MurG, PatA, PbpA, PbpB, PbpC, PbpD, PbpX, PonA, RacE, TagD, TagE, TagF, TagH, TagT, TagU, YfnI, YkuQ, PdaC, WalR, WapA, WprA, YodJ
Coping with hypo-osmotic stress	MscL
RNA synthesis and degradation	CshA, CshB, CspB, RnjA, RnjB, Rny, NusA, NusG, Rho, RpoA, RpoB, RpoC, RpoE, SigH, SigW, SigX, CodY, DegU, SalA, YmcA, RsiW, YhdL
DNA condensation/ segregation	GyrB, ParE, Spo0J, SpoIIIE
DNA repair/ recombination	MutSB, PcrA, PolA, RecA
DNA replication	DnaA, DnaI, DnaN, PolC, TopB, YpcP
DNA restriction/ modification	YdiS
General stress proteins (controlled by SigB)	CsbB, YacL, YceC, YceD, YceE, YceH, YtxG, YtxH, YwsB
Genetic competence	BdbD, Med, Nin, Rok, YvcJ
Chaperones/ protein folding	DnaJ, DnaK, GroEL, HtpG, PpiB, Tig
Iron metabolism	SufD, SufS
Membrane dynamics	FloA, FabF
Miscellaneous metabolic pathways	SpeE, SrfAA, SrfAB, SrfAC, SrfAD
Motility and chemotaxis	FlhA, FlhF, TlpC

Proteins of unknown function	DhaS, LepA, MraW, YaaK, YccF, YcnI, YddK, YdeO, YdjG, YeaC, YerC, YerH, YfhC, YgaE, YhaH, YhdP, YheB, YhgE, YjlC, YkaA, YkyA, YkzS, YlbA, YlbL, YloU, YloV, YoxD, YpmB, YqeG, YqeY, YqgA, YqhL, YqhY, YqiW, YqjE, YqzC, YqzD, YrhD, YrhE, YrkA, YrrL, YrvD, YsbA, YshE, YtsP, YubF, YueD, YugI, YutD, YutI, YvbJ, YvrP, YwhC, YwtE, YxiF, YxkD, YxxG, YyaF, YydB
Phosphate metabolism	PpaC
Phosphotransferase systems	ManP, MtlA, PtsH, PtsI
Protein modification	McsB, RsbW
Protein secretion	Ffh, FtsY, PrsA, SecA, SppA
Proteolysis	ClpC, ClpX, ClpY, CtpA, HtpX, HtrB
Resistance against oxidative and electrophile stress	AhpC, KatA
Resistance against toxins/ antibiotics	SunI, SwrC, YokG
Respiration	CccA, CccB, CtaC, NarG, Ndh, QcrA, QoxA
SP-beta prophage	YqaP, YokE, YonB, YonC, YopQ
Sporulation	Spo0M
Sulfur metabolism	CymR
Translation	AlaS, AsnS, AspS, EngA, Era, FolD, FusA, GatB, GidA, GlyS, InfA, InfB, InfC, KsgA, LeuS, Obg, PheT, PrfA, ProS, QueA, QueC, RbfA, RbgA, RplA, RplB, RplD, RplE, RplF, RplJ, RplK, RplM, RplN, RplO, RplP, RplQ, RplR, RplS, RplV, RplW, RplX, RpmA, RpmC, RpmD, RpmI, RpsB, RpsC, RpsD, RpsE, RpsF, RpsG, RpsH, RpsI, RpsJ, RpsK, RpsL, RpsM, RpsN, RpsO, RpsP, RpsR, RpsS, RpsU, SerS, ThdF, ThrS, TrmB, Tsf, TufA, YloN, YmcB, YpfD, YqeH, YqeI, YqeT, YqeV
Transporters/ other	DctP, KtrC, LutP, MdtP, MrpG, SteT, YbeC, YclF, YcnJ, YutK, YvsH, YwbM, YwbN, ZosA
Utilization of amino acids	AnsA, BkdB, GudB, Kbl, LpdV, RocD, SdaAA, SdaAB, Tdh

Supplementary Information References:

1 Blair, K. M., Turner, L., Winkelman, J. T., Berg, H. C. & Kearns, D. B. A molecular clutch disables flagella in the Bacillus subtilis biofilm. *Science* **320**, 1636-1638, doi:10.1126/science.1157877 (2008).

2 Ramamurthi, K. S., Lecuyer, S., Stone, H. A. & Losick, R. Geometric cue for protein localization in a bacterium. *Science* **323**, 1354-1357, doi:10.1126/science.1169218 (2009).

3 Toyofuku, M. *et al.* Prophage-triggered membrane vesicle formation through peptidoglycan damage in Bacillus subtilis. *Nat Commun* **8**, 481, doi:10.1038/s41467-017-00492-w (2017).

4 Nicolas, P. *et al.* Condition-dependent transcriptome reveals high-level regulatory architecture in Bacillus subtilis. *Science* **335**, 1103-1106, doi:10.1126/science.1206848 (2012).

5 Youngman, P., Perkins, J. B. & Losick, R. Construction of a cloning site near one end of Tn917 into which foreign DNA may be inserted without affecting transposition in Bacillus subtilis or expression of the transposon-borne erm gene. *Plasmid* **12**, 1-9, doi:10.1016/0147-619x(84)90061-1 (1984).

6 Lin, J. *et al.* Whole-genome shotgun optical mapping of Deinococcus radiodurans. *Science* **285**, 1558-1562, doi:10.1126/science.285.5433.1558 (1999).

7 Trotochaud, A. E. & Wassarman, K. M. 6S RNA function enhances long-term cell survival. *J Bacteriol* **186**, 4978-4985, doi:10.1128/JB.186.15.4978-4985.2004 (2004).

8 Diethmaier, C. *et al.* A novel factor controlling bistability in Bacillus subtilis: the YmdB protein affects flagellin expression and biofilm formation. *J Bacteriol* **193**, 5997-6007, doi:10.1128/JB.05360-11 (2011).

9 Nicholson, W. L. Increased competitive fitness of Bacillus subtilis under nonsporulating conditions via inactivation of pleiotropic regulators AlsR, SigD, and SigW. *Appl Environ Microbiol* **78**, 3500-3503, doi:10.1128/AEM.07742-11 (2012).

10 Ramaniuk, O. *et al.* sigma(I) from Bacillus subtilis: Impact on Gene Expression and Characterization of sigma(I)-Dependent Transcription That Requires New Types of Promoters with Extended -35 and -10 Elements. *J Bacteriol* **200**, doi:10.1128/JB.00251-18 (2018).

11 Asai, K., Ishiwata, K., Matsuzaki, K. & Sadaie, Y. A viable Bacillus subtilis strain without functional extracytoplasmic function sigma genes. *J Bacteriol* **190**, 2633-2636, doi:10.1128/JB.01859-07 (2008).

12 Guerout-Fleury, A. M., Frandsen, N. & Stragier, P. Plasmids for ectopic integration in Bacillus subtilis. *Gene* **180**, 57-61, doi:10.1016/s0378-1119(96)00404-0 (1996).

13 Koo, B. M. *et al.* Construction and Analysis of Two Genome-Scale Deletion Libraries for Bacillus subtilis. *Cell Syst* **4**, 291-305 e297, doi:10.1016/j.cels.2016.12.013 (2017).

14 Dubey, G. P. & Ben-Yehuda, S. Intercellular nanotubes mediate bacterial communication. *Cell* **144**, 590-600, doi:10.1016/j.cell.2011.01.015 (2011).

15 Chen, R., Guttenplan, S. B., Blair, K. M. & Kearns, D. B. Role of the sigmaD-dependent autolysins in Bacillus subtilis population heterogeneity. *J Bacteriol* **191**, 5775-5784, doi:10.1128/JB.00521-09 (2009).

16 Krasny, L., Vacik, T., Fucik, V. & Jonak, J. Cloning and characterization of the str operon and elongation factor Tu expression in Bacillus stearothermophilus. *J Bacteriol* **182**, 6114-6122, doi:10.1128/jb.182.21.6114-6122.2000 (2000).

17 Maamar, H. & Dubnau, D. Bistability in the Bacillus subtilis K-state (competence) system requires a positive feedback loop. *Mol Microbiol* **56**, 615-624, doi:10.1111/j.1365-2958.2005.04592.x (2005).